Additive Manufacture of an in vitro Neuron Biosensor.

By Benjamin Templeton Paul

Supervised by: Christopher Tuck, Ricky Wildman and Noah Russell

Abstract

Two photon polymerisation is presented as a fabrication technique for advancing *in vitro* neuron biosensors, primarily by coordinating the topology of the cultured neurons but also by developing microstructures capable of monitoring the soluble environment of the cultured neurons. A substrate treatment protocol was developed to facilitate the adhesion of an *in vitro* neural culture in the presence of two photon polymerised microstructures of a commercially available organically modified ceramic (Ormocer), called OrmoComp. A method for promoting the adhesion of neurons to gold rather than glass was developed using a thiol containing cyclical peptide motif known for promoting cell adhesion, arginine glycine aspartate (cRGD). The two photon polymerisation of OrmoComp was optimised by developing a modular design and performing parameter optimisation sweeps on a single unit of the design, allowing for larger neural guidance structures to be made by two photon polymerisation than previously possible. Dissociated rat hippocampal neurons were seeded, cultured and imaged in the presence of OrmoComp microstructure designs to coordinate their structural and functional topology. Although phase contrast micrographs suggested that the culture had been successfully coordinated, calcium imaging and scanning electron microscopy indicated that the microculture of neurons within the microstructure were functionally connected to the surrounding macroculture. Hydrogel microstructures containing a combination of fluorophores capable of ratiometrically measuring the pH of the solution were produced using a polyethylene glycol diacrylate and a water soluble two photon compatible photoinitiator. This thesis integrated existing processes from a wide range of disciplines ranging from cell culture, chemical synthesis and manufacturing engineering. The progress made applying two photon polymerisation to neuron biosensors was underpinned by advancements in the implementation of two photon polymerisation through improvements in software, hardware and photochemistry. This thesis concludes that the continued development of two photon polymerisation will provide the neuron biosensor community, and the wider tissue engineering community, with new tools to build and monitor artificial tissue.

Acknowledgements

To my supervisors for access to the facilities I required to perform the experimental portion of this work and the finances they supported with me to attend buy reagents and attend conferences. Particular thanks to Noah Russell for his kind concern for my wellbeing throughout the thesis.

To incorporate the pH sensitive fluorophores the two dyes were conjugated to a N-(3-aminopropyl) methacrylamide linker by collaborator Veeren Chauhan. To support the collaboration with Veeren Chauhan an interdepartmental collaboration grant was acquired from the University of Nottingham's Interdisciplinary Centre for Analytical Science (UNICAS).

To all the fellow PhD students, researchers and technicians across departments whose advice, discussions and camaraderie made this an enjoyable and educational experience.

To my friends for listening to my obsessions and fears and distracting me from them.

To my family for their support, inspiration and love which gave me the resilience to push through difficult experiments and endless editing.

To grapes for helping me survive malaria at the beginning of this thesis and my uncle Bill for ensuring that I was equipped with a malarial treatment and diagnosis kit.

To my grandmother who passed away during this thesis, whose strength and dedication to helping others I will endeavour to emulate through the implementation of the skills I learnt in this thesis.

To my cat, Mushroom Magee, whose unconditional love and cuddles gave me and my family strength in difficult times and passed away as I came to the last weeks of this long journey.

Contents

ABSTRACT **2**

ACKNOWLEDGEMENTS **3**

TABLE OF FIGURES **9**

1 INTRODUCTION **16**

1.1 OVERVIEW **16**

1.2 MOTIVATION **21**

1.3 THE IMPORTANCE OF NEURAL NETWORKS IN THE CONTEXT OF NEURON BIOSENSORS. **26**

1.4 NEURAL INTERFACES, MICROELECTRODE ARRAYS AND THE NECESSITY OF NEURAL PATTERNING **32**

1.5 ENGINEERING *IN VITRO* CULTURES USING SURFACE CHEMISTRY AND MICROFABRICATION **37**

1.6 PATTERNING CELL CULTURE USING TWO PHOTON POLYMERISATION. **48**

1.7 INCORPORATING PH SENSORS INTO HYDROGELS FOR THE PRODUCTION OF EMBEDDED SENSORS. **55**

1.8 THESIS SUMMARY **59**

2 SUBSTRATE TREATMENTS FOR *IN VITRO* NEURAL CULTURE ADHESION. **62**

2.1 OVERVIEW **62**

2.2 METHODOLOGY **63**

2.2.1 TWO PHOTON POLYMERISATION 63

2.2.2 NEURAL CELL CULTURE 64

2.2.3 Time of flight secondary ion mass spectroscopy 64

2.3 Experimental 65

2.3.1 Two photon polymerisation using the custom built rig 65

2.3.2 Preparing substrates for cell seeding 67

2.3.3 Seeding of rat hippocampal cultures on substrates 67

2.3.4 Time of flight secondary ion mass spectroscopy 68

2.4 Results 69

2.4.1 Optimisation of OrmoComp development protocol to support neural cell adhesion 69

2.4.2 Selective adhesion of neurons on gold and not glass. 72

2.5 Discussion 77

3 OPTIMISING THE TWO-PHOTON POLYMERISATION OF ORMOCOMP MICROSTRUCTURES. 82

3.1 Overview 82

3.2 Methodology 83

3.2.1 Comparison of Two Photon Polymerisation Rigs. 83

3.2.2 Dip-in vs standard writing configuration on the Nanoscribe 89

3.2.3 Computer assisted design and manufacture 91

3.3 Experimental 94

3.3.1 Ormocomp substrate preparation 94

3.3.2 Ormocomp substrate preparation 94

3.3.3 Optimisation sweeps 95

3.3.4 Scanning electron microscopy 95

3.4 RESULTS 96

3.5 DISCUSSION 108

4 CHARACTERISING THE GROWTH OF NEURONS CULTURED ON MICROSTRUCTURED SUBSTRATES. 112

4.1 OVERVIEW 112

4.2 METHODOLOGY 115

4.2.1 DESIGNS FOR PATTERNING NEURONS. 115

4.2.2 CALCEIN-ACETOMETHYL STAINING 120

4.2.3 CALCIUM IMAGING 120

4.3 EXPERIMENTAL 121

4.3.1 CELL DISSECTION, DISSOCIATION AND SEEDING 121

4.3.2 CALCEIN STAINING AND IMAGING 121

4.3.3 DYNAMIC CALCIUM IMAGING 121

4.3.4 SCANNING ELECTRON MICROSCOPY 122

4.4 RESULTS 123

4.5 DISCUSSION 137

5 PRODUCTION OF PH SENSITIVE HYDROGEL FLUORESCENT MICROSENSORS 143

5.1 OVERVIEW 143

5.2 METHODOLOGY 146

5.2.1 TWO PHOTON PHOTOINITIATION 146

5.2.2 Self assembled monolayer for promoting adhesion 147

5.3 Experimental 149

5.3.1 6-Bis(4-(dimethylamino)benzylidene)-4-methylcyclo- hexanone synthesis 149

5.3.2 Nuclear Magnetic Resonance 149

5.3.3 Mass spectrometry 150

5.3.4 PEGDA: PETA resin formulation 150

5.3.5 PEGDA:Water resin formulation 150

5.3.6 Coating of substrate with trimethoxysilylmethacrylate 150

5.3.7 Calibration of pH sensors using ratiometric measurements 151

5.3.8 Production of tape based microfluidic device 152

5.4 Results 153

5.4.1 Nuclear Magnetic Resonance 153

5.4.2 Mass Spectroscopy 153

5.4.3 Formulation of PEGDA photoresist 154

5.4.4 Calibration of pH microsensors 155

5.4.5 Incorporation of pH microsensors into microfluidic device 158

5.5 Discussion 160

6 CONCLUSION 163

BIBLIOGRAPHY 167

APPENDIX 177

NUCLEAR MAGNETIC RESONANCE SPECTRA OF PHOTOINITIATOR E3..... 177

INFRARED SPECTRA OF PHOTOINITIATOR E3..... 178

DESCRIBE FABRICATION CODES 179

TOF-SIMS POSITIVE ION SPECTRA OF CRGDFC MODIFIED GLASS AND GOLD SUBSTRATES. 185

Table of Figures

Figure 1 The transition from animal spirits to electricity in neuroscience 17

Figure 2 First Contact Guidance Experiments 19

Figure 3: Imaging the the strucutrual morphology of neural tissue from Golgi method to Brainbow. 23

Figure 4 Hodgkin and Huxley's circuit diagram of a neuron. 27

Figure 5 A biohybrid chemical detector. 28

Figure 6 Basic structure of the growth cone. 30

Figure 7 The variety of patch clamping techniques available for interrogating the electrophysiological properties. 33

Figure 8 Utah intra-cortical microelectrode array for in vivo neural interfacing. 35

Figure 9 Microelectrode detecting different neuronal membrane depolarisations. 36

Figure 10 Phase contrast image of first published in vitro dissociated neural cultures. 37

Figure 11 Patterning neurons with photolithographically defined self-assembled monolayers. 39

Figure 12 Patterning neurons with photolithographically defined self-assembled monolayers. 40

Figure 13 The Campenot chamber: Early microstructured growth substrate for compartmentalisation of neuronal soma. 41

Figure 14 Stripe assay for interrogating contact guidance molecules in axon guidance. 42

Figure 15 Microfluidic Taylor device for the study of axonal regeneration. 44

Figure 16 III tubulin stained hippocampal cells cultured for 6 days in the NeuroArray PDMS stencil. 45

Figure 17 Scanning Electron Micrograph of the Neurocage Design. 46

Figure 18 Multistep photolithography for the fabrication of the Neurocage. 47

Figure 19 Two photon vs one photon excitation of a fluorophore. 49

Figure 20. Achieving two photon absorption through the spatial and temporal compression of photons. 50

Figure 21 Patterning cells using two photon polymerisation. 51

Figure 22 Neuron-like cell line growing on parallel lines produced through two photon polymerisation. 53

Figure 23. Human embryonic stem cells cultured on two photon polymerised OrmoComp microstructures. 54

Figure 24 Fluorescent imaging the pH of Caernohditis Elegens digestive tract after ingesting pH sesnitve fluorescent Nanoparticles. 57

Figure 25 Overview diagram of thesis showing aims and objectives. 61

Figure 26 Schematic of time of flight secondary ion mass analyser. 65

Figure 27 Optical Micrograph of a multielectrode array outline fabricated using the two photon polymerization custom rig in automatic mode. 69

Figure 28 Primary hippocampal culture after two days in vitro grown in the presence of OrmoComp microstructures developed with original protocol from Microchem ltd. 70

Figure 29 Primary hippocampal neural culture adhering to an OrmoComp modified substrate developed with optimised protocol. 71

Figure 30 Ion intensities of cRGDfC treated glass and gold substrate for both the gold coated and uncoated regions of the substrate. Normalised to total ion intensity. 74

Figure 31 Phase contrast micrographs of neural culture on glass and gold substrates treated with cRGDfC. 76

Figure 32 Comparison of the state of art in patterning neurons using two-photon polymerisation. . 79

Figure 33 Sandwich configuration implemented on custom rig. 84

Figure 34 Equation of optcial dose which is proportional to the dwell time and the laser power. 86

Figure 35 Standard and dip-in orientations for direct laser writing. 90

Figure 36 Describe simulation depicting exposed volume at four time points during the build of a single unit of the grid structure for patterning neurons in vitro. 91

Figure 37 Preparing a file for use on the Nanoscribe: Layer thickness, line spacing, shell thickness and scaffold density. 92

Figure 38 Describe simulation direct laser writing process and build. 93

Figure 39 Describe simulation of four identical designs with different line spacing. 97

Figure 40 Scanning electron micrographs of the different classes of microstructures produced by the parameter sweep array. 98

Figure 41 Parameter optimisation Sweep work flow. 99

Figure 42 Scanning electron micrograph of an optimisation array. 101

Figure 43 Coarse parameter sweep optimisation array. 102

Figure 44 Maximum speed and Processing range depending on line spacing 104

Figure 45 High resolution parameter sweep optimisation array. 105

Figure 46 Workflow aiming to pattern neurons using two photon polymerised microstructures. Red arrows indicate normal progress with grey arrows indicating data informing alterations to previous steps. 113

Figure 47 Hexagonal design 117

Figure 48 High definition microelectrode array design 118

Figure 49 Describe simulation of large area array 119

Figure 50 Hexagonal array surrounded by outer wall. 124

Figure 51 Hexagonal array without outer walls. 125

Figure 52 Cells moving between the internal compartments of the hexagonal microstructure. 126

Figure 53 Array designed to fit on a high density microelectrode 5 x 6 array. 128

Figure 54 Extracted traces from calcium imaging of neurons cultured on direct laser written microstructures. 129

Figure 55 Delayed onset of calcium wave of neurons positioned further inside the grid. 130

Figure 56 Comparison of quiescent cell traces. 131

Figure 57 The power of suggestion: Diverting neurites instead of containing them. 132

Figure 58 Calcein-AM and phase contrast images of large area microstructures for patterning neurites. 133

Figure 59 SEM of neural processes passing through the channels in the grid. 134

Figure 60 Neurites aligning on a second level. 135

Figure 61 Aligning microstructures to multielectrode array. 136

Figure 62 Growing out of the intended pattern visible in fluorescent micrographs of patterned neurons. 139

Figure 63 Overview of direct laser written pH sensor development. 145

Figure 64 Schematic demonstrating the bipolar structure of a self assembled monolayer. 148

Figure 65 FITC and TRITC filter cube emission and excitation spectra. 151

Figure 66 PEGDA:PETA formulation compared to PEGDA:Water. 155

Figure 67 Collage of fluorescent intensity images taken of two photon polymerised hydrogel microstructures in a range of different pH buffers. 156

Figure 68 Calibration curve displaying ratiometric measurements of fluorescence intensity in response to a range different pH buffers. 157

Figure 69 Neurons cultured in the presence pH sensitive microstructures. 158

Figure 70 Fluorescent intensity images of two photon polymerised microstructures incorporated into microfluidics channel. 159

Figure 71 Proton Nuclear Magnetic Resonance Spectra of Photoinitiator E3. 177

Figure 72 Infrared spectra of synthesised photoinitiator E3. 178

Figure 73 Total Time of Flight secondary positive ion mass spectra of whole area of the cRGDfC modified glass and gold substrates. 186

Figure 74 Total Time of Flight secondary positive ion mas spectra of the gold region of the cRGDfC modified glass and gold substrates. 187

Figure 75 Total Time of Flight secondary positive ion mas spectra of the glass region of the cRGDfC modified glass and gold substrates. 189

Figure 76 Time of Flight secondary positive ion mass spectra of Si on the whole area of the cRGDfC modified glass and gold substrates. 190

Figure 77 Time of Flight secondary positive ion mass spectra of Si on the gold region of the cRGDfC modified glass and gold substrates 191

Figure 78 Time of Flight secondary positive ion mass spectra of Si on the glass region of the cRGDfC modified glass and gold substrates 192

Figure 79 Time of Flight secondary positive ion mass spectra of CH_4N on the whole are of the cRGDfC modified glass and gold substrates. 193

Figure 80 Time of Flight secondary positive ion mass spectra of CH_4N on the gold region of the cRGDfC modified glass and gold substrate. 194

Figure 81 Time of Flight secondary positive ion mass spectra of CH_4N+ on the glass region of the cRGDfC modified glass and gold substrates 195

Figure 82 Time of Flight secondary positive ion mass spectra of CH_3N_2+ on the whole area of the cRGDfC modified glass and gold substrates 196

Figure 83 Time of Flight secondary positive ion mass spectra of CH_3N_2+ on the whole area of the cRGDfC modified glass and gold substrates 197

Figure 84 Time of Flight secondary positive ion mass spectra of CH_4N+ on the glass region of the cRGDfC modified glass and gold substrates 198

Figure 85 Time of Flight secondary positive ion mass spectra of CHS+ on the gold region of the cRGDfC modified glass and gold substrates 199

Figure 86 Time of Flight secondary positive ion mass spectra of CHS+ on the glass region of the cRGDfC modified glass and gold substrates 200

Figure 87 Time of Flight secondary positive ion mass spectra of CHS+ on the whole area of the cRGDfC modified glass and gold substrates. 201

Figure 88 Time of Flight secondary positive ion mass spectra of $C_3H_6NO_2$+ on the whole area of the cRGDfC modified glass and gold substrates 202

Figure 89 Time of Flight secondary positive ion mass spectra of $C_3H_6NO_2$+ on the gold region of the cRGDfC modified glass and gold substrates 203

Figure 90 Time of Flight secondary positive ion mass spectra of $C_3H_6NO_2$+ on the glass region of the cRGDfC modified glass and gold substrates 204

Figure 91 Time of Flight secondary positive ion mass spectra of $C_8H_{10}N$+ on the whole area of the cRGDfC modified glass and gold substrates 205

Figure 92 Time of Flight secondary positive ion mass spectra of $C_8H_{10}N+$ on the gold region of the cRGDfC modified glass and gold substrates 206

Figure 93 Time of Flight secondary positive ion mass spectra of $C_8H_{10}N+$ on the glass region of the cRGDfC modified glass and gold substrates 207

Figure 94 Time of Flight secondary positive ion mass spectra of Au+ on the whole area of the cRGDfC modified glass and gold substrates 208

Figure 95 Time of Flight secondary positive ion mass spectra of Au+ on the gold region of the cRGDfC modified glass and gold substrates 209

Figure 96 Time of Flight secondary positive ion mass spectra of Au+ on the glass region of the cRGDfC modified glass and gold substrates 210

1 Introduction

1.1 Overview

Additive manufacturing, building objects through the addition of material, gives a freedom and flexibility to design that more established subtractive manufacturing techniques lack which decreases the number of steps in the production of an existing object or in some cases to produce objects which would have been impossible to build using subtractive techniques. Two photon polymerisation is an additive manufacturing technique which is capable of producing microstructures with sub-micron resolution. Two photon polymerisation systems are generally a diffraction-limited, meaning the theoretical resolution limit is half the wavelength of the excitation source used. By combining two photon polymerisation with techniques from super resolution microscopy, such stimulated emission depletion[1], it is possible to produce microstructures with a feature size of 50 micron and a resolution of 120 micron, well beyond the distraction limit[2]. By exploiting the flexibility and design freedom two photon polymerisation offers at the microscale, novel microstructures can be produced to meet challenges facing the field of *in vitro* neuron biosensors.

in vitro neuron biosensors consist of a neural network cultured *in vitro* either for investigating neural network dynamics or exploit the function of the nervous system to monitor a physiochemical variable. Although the technique developed in this thesis may be applied to a range of *in vitro* neuron biosensors the focus will be particularly on a platform which interrogates neural network dynamics. Neural network dynamics are essentially the pattern of electrophysiological activity an interconnected community of neurons performs which underpins a particular function. Records of electrophysiological phenomena date back as far as ancient Egyptian observations of the electric organ discharge of a River Nile Catfish[3]. From the time of the ancient Greeks' the therapeutic potential of such electric fish species was documented and attempted although with no evidence to suggest an awareness or understanding of the phenomena[3]. The ability of nerves in controlling movement and sensation was considered to be due to their role as conduits for animal spirits, a theory which had

several manifestations from Galen through Descartes to Newton[4]. An early challenger of the animal spirit theory was Jan's Swammerdam's neuromuscular preparation of a frog thigh which utilised a brass ring with a silver wire leading to the excitation, or "irritation" as it was referred to, of the explant muscle. Although the electrical nature of the Swammerdam's stimulation is difficult to prove it could represent the first electrophysiological experimentation[5].

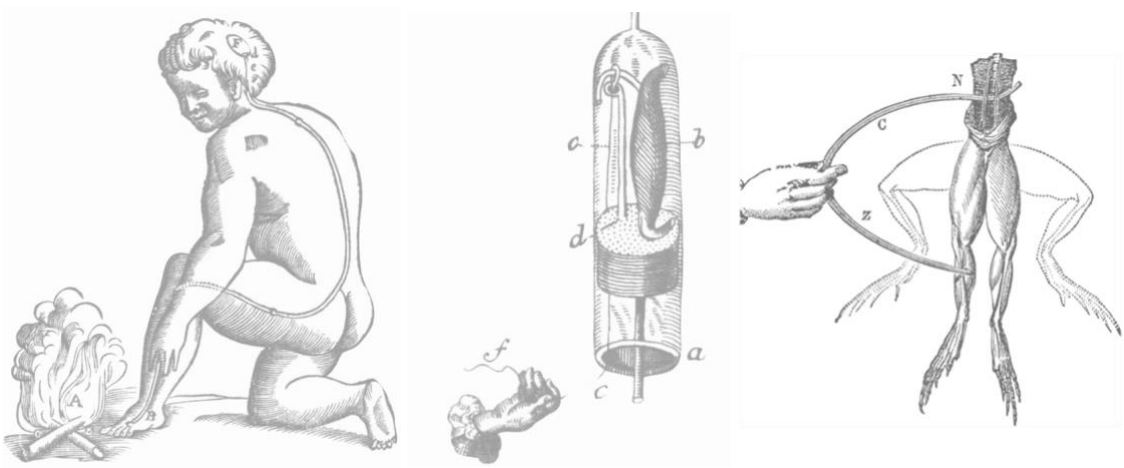


Figure 1 The transition from animal spirits to electricity in neuroscience

Left) Descartes illustration of nerves transmitting sensation to the brain via the flow of animal spirits. Centre) Jans Swammerdam's early neuromuscular preparation of the frog thigh muscle. As external stimulation or irritation lead to contraction animal spirits are not responsible for the control of nerves on muscles. Right) Galvani's Demonstration of the intrinsic excitability of nervous and muscle tissue on a frog muscle. Leg outlines indicate the twitching of the legs in response to electrical stimulation.

It was not until 1776 that John Walsh, in a letter to Benjamin Franklin, described a visible light flash as a result of the discharge of an electric organ that stands as the first experimental evidence of the electrical nature of biological tissue[6] and can be also be considered as the initiation of the field of electrophysiology[3]. Later in the 18th century Luigi Galvani demonstrated the intrinsic electrical activity of tissue in a frog's leg, initiating the discussion of an investigation into how electrical signals are involved in the physiology of living organisms[7].

The role of electric fields and flux in living cells has much developed since the time of Walsh and Galvani but the role of electrical currents in the circuitry of the human brain which underpin many neurological processes is still not fully understood. The density and shear number of the cells within the human brain makes investigating these neural network processes difficult to decipher yet

promises to help develop treatments for neurological diseases which are still poorly understood e.g. Bipolar disorder. This research is motivated by the potential impact that neuron biosensors offer to a wide a range of fields; from drug discovery to chemical detection but particularly as a platform for investigating neural network dynamics, the underlying workings of the human brain[8,9]. The structure of a neuronal network is considered to, like many biological tissues, to underpin its function. Being able to control the structure of a neural network within a neuron biosensors is a challenge that, despite being attempted for over thirty years, has still not been definitively solved[10,11].

This thesis presents an approach to coordinate a cultured neural network's structural and functional topology by advanced two photon polymerised microstructures. This approach is based on the ability of the growth substrate to exert influence on the growth of cells in vitro, a process known as contact guidance. The phenomenon of contact guidance was first observed in 1912 when it was observed that the presence of a solid support was necessary for the outgrowth or migration of certain cell types from cultured embryonic tissue[12]. The term contact guidance was not coined however until the first attempt to coordinate the growth of neurons *in vitro* in 1945[13]. Paul Weiss at the University of Chicago made fine scratches on mica substrates and then cultured embryonic chick spinal ganglion on the scratches and observed a strong preference for the neurite outgrowth to align with the grooves formed by the scratches on the substrate surface [13]. With the advent of microfabrication technology from the microelectronics industry *in vitro* models of contact guidance became popular for investigating the mechanisms underpinning axonal guidance in embryogenesis. The stripe assay is used to investigate the effect of surface bound molecules on the growth of neurons *in vitro* [14] and will be discussed further in the section on Engineering *in vitro* Neural Networks with Surface Chemistry and Engineering (Section 1.3). The synergistic effect of surface bound molecules and the aspect ratio of topographical grooves, e.g. vitronectin, was also demonstrated using microfabricated substrates for neural culture [15].

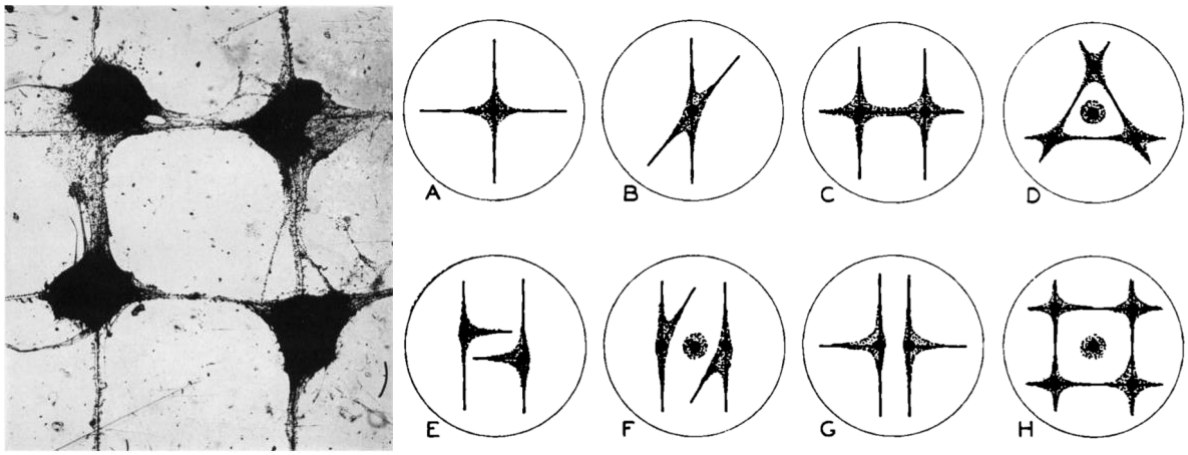


Figure 2 First Contact Guidance Experiments

Left) Four spinal ganglion from 14-day chick embryos grown on lamellae mica with two pairs of parallel scratches intersecting each other at right angles (see pattern labelled H without centre piece). Cultured for four days in Serum and Tyrodes solution (1:4) with a trace of embryo extract. 30x magnification. Right) Various other patterns produced using embryonic chick spinal ganglions grown on scratched mica.

Coordinating the neural network's topology will allow for more repeatable and controlled investigations into neural network dynamics as well as allowing for the network's structural topology to be used as an experimental variable which will influence the neural network dynamics.

Many factors influence the growth of neurons *in vitro* such as soluble gradients of biochemical guidance molecules (neurotropic molecules) [16] and substrate anchored biochemical or mechanical cues (contact guidance)[14,15]. Most of the approaches which exploit contact guidance to coordinate the growth of neural networks *in vitro* have been produced using photolithographic patterning as it can produce features with sub-micron resolution. Photolithography is limited in what three dimensional geometries can be produced and a new sequence of etching and deposition has to be developed for the majority of changes made to a three dimensional design[17,18]. The necessity to have a bespoke fabrication sequence for each design restricts the flexibility to experiment with new designs or rapidly reconfigure the design of the structure as an experimental variable.

Two photon polymerisation has been previously used to influence the growth of neurons *in vitro*, but the control achieved was limited due to the design of the structures used [19,20]. The fidelity of the pattern was also greatly reduced due to the poor adhesion of the neurons to the substrate, an issue which will be addressed in Chapter 2 on the development of surface treatment protocols for

promoting neuronal adhesion. Advancements made in the processing of two photon polymerised microstructures have allowed for increased design size and complexity which will be discussed at length in Chapter 3. In addition to controlling the structural topology of neural networks *in vitro*; controlling the physiochemical milieu is also of great importance, as it is not only essential for the survival of the culture but can influence the culture's topology.

Microfluidic devices constrain liquid in microvolumes where precise manipulation of the fluids is possible often with low energy expenditure. This microscale manipulation of fluids can take shape in the formation of microdroplets or gradients[9,21]. Culturing neurons within microfluidic devices is an increasingly popular platform for controlling the physiochemical milieu that neurons are exposed to for example generating gradients of axon guidance factors[9], physically segregating neurons[22–24] and culturing neurons at low area densities by reducing the volume density[25]. The reduction in volume, and therefore increase in cell density, in a microfluidic device compared to an open bath culture makes the need for real time monitoring when maintaining the balance of nutrient replenishment and waste removal yet more delicate. As such having a way to monitor the physiochemical variables in real time would be of great benefit to the culturing of neurons within microfluidic devices. As a demonstration of how fluorescent molecules sensitive to physiochemical variables can be incorporated within two photon polymerised gels to provide real time monitoring within microfluidic devices pH sensitive gels will be produced using two photon polymerisation and incorporated into microfluidic devices.

The state of the art in coordinating *in vitro* neural networks, detecting the pH of micro-environments and a detailed summary of the research will be presented in this introduction. The bulk of this thesis comprises primarily of four experimental Chapters covering the development of surface treatments (Chapter 2), the optimisation of the two-photon polymerisation process (Chapter 3), the characterisation of neurons growing in the microstructures (Chapter 4) and the implementation of microstructures to detect pH within microfluidic devices (Chapter 5). The findings of these sections will be discussed in the context of the state-of-the-art literature and used to inform suggestions of the

future direction two photon polymerisation may have in the field of neuron biosensors. What developments in two photon polymerisation would allow for better application to neuron biosensors will also be discussed.

1.2 Motivation

Human brains are some of the most complex structures in the universe and as such the least understood aspect of human physiology. Improving our understanding of the human brain is necessary to meet many of the challenges faced by the modern world. Such challenges include the development of preventative and non-symptomatic treatments to neurological disease, the advancement of computational and predictive software and the creation of brain-machine interfaces for the rehabilitation of the physically disabled. The increase in lifespan in modernised societies has led to an increase the burden neurodegenerative diseases have on society [26]. Currently many neurological conditions are treated symptomatically as the precise mechanisms of their pathologies have yet to be resolved, such as multiple sclerosis[27]. Although much research is directed towards these fields, relatively little progress has been made as the mechanisms of the normal working brain remain unclear. Although progress at many levels of neuroscience is required for such challenges to be met, developing an understanding of how a population of neurons are organised into a network to collectively process information is a key step. To effectively interrogate such network dynamics, it is important to use an experimental model where the activity of all the cells connected to the network can be recorded at single cell resolution. Although many events contribute to the activity of a single neuron in a neural network it can still be considered the basic unit of a network. Being able to monitor the activity of a network at the resolution of the network's basic unit should allow for meaningful information about the dynamics of the network underpinning its function to be discerned.

Modern psychological approaches have a history stretching back to the 19th century [28] and have done much to categorise and analyse human behaviour from a top down approach by observing and analysing human behaviour. In the late 20th century the advent of neuroimaging and cognitive

psychology have brought have brought together the fields of neuroanatomy and psychology to neuropsychology [29] however the first observations that regions of the brain were associated to particular aspects of behaviour may date as far back as 2700 BC to the legendary grand vizier of ancient Egypt, Imhotep [30]. Modern neuropsychology, however, relies on the resolution of neuroimaging techniques, such as functional magnetic resonance imaging, which is currently limited to >1 mm^3 [31]. This volume contains hundreds to thousands of cells making such a technique incapable of investigating how groups of cells are organised into functional networks for processing information. Single neurons were first imaged in 1894 by Ramon y Cajal [32] using Golgi's method in dead tissue slices. Advanced immunohistochemical techniques such as the "Brainbow" exploit advanced immunohistochemical staining to resolve adjacent cells due to the combinatorial expression of multiple fluorophores creating many distinct hues within the tissue [33] Figure 3. Although characterising the structural morphology of neural architecture is still underway to improve our understanding of the brain it is necessary to characterise the functional morphology of neural architecture.

Fluorescent dye techniques using calcium sensitive dyes can be used to image the action potentials solicited by neurons and as such visualise the functional morphology of the neuronal network. Optical techniques to monitor neural activity have a limited field of view due to the necessity to have high numerical aperture objectives in order to high resolve individual cells, ~300 $micron^2$. Additionally, optical monitoring of neural activity is limited to penetration depth, ~1 mm, due to scattering and absorption of incident and emitted light and imaging time due to photobleaching and phototoxicity. Similarly, electrophysiological techniques such as patch clamping or microelectrode arrays (MEAs) are able to record from or stimulate at single cell resolution but can only record from between tens and hundreds of cells *in vivo*. *In vivo* electrophysiological monitoring of neural tissue is also traumatic to the cells or tissue leading to the technique being only possible for a limited time. For patch clamping this is due to the leaking of cytoplasmic contents out of the cell as the membrane must be punctured, a lethal procedure for the cell. penetrating microelectrode arrays are often encapsulated in fibrous

material, reducing their ability to record or stimulate neurons, due to a foreign body response being initiated by the host immune system leading to scarification [34].

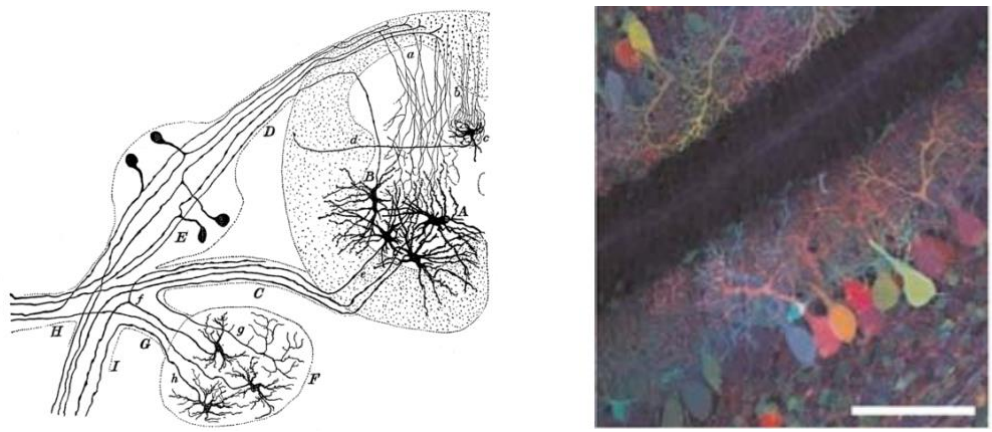


Figure 3: Imaging the the strucutrual morphology of neural tissue from Golgi method to Brainbow.

Imaging the structural morphology of *in vivo* neural networks has developed through time but the need for functional characterisation is still lacking. Left: Dorsal root ganglion stained using the Golgi Method showing individual cells. This image will have been the reconstruction of multiple stains and does not show all the cells in the tissue. The fact that it does not show all the cells in the tissue is what allows individual cells to be identified and this is due to the randomised selective uptake of the Golgi stain. Right: Brainbow multiple fluorescent stained mice neurons in the hippocampus; scale bar 100 *micron*. [32,33]**.**

As an alternative to the *in vivo* techniques for studying neural network dynamics, culturing neurons *in vitro* on microelectrode arrays can provide a more accessible platform. One of the main criticisms of *in vitro* neural networks is their lack of validity, as they are generally two dimensional unstructured cultures which do not resemble *in vivo* neural architecture [10,35–37]. Although there are many examples of three dimensional neural cultures *in vitro* the methods of interfacing with them are, e.g. with microelectrode arrays, are primarily two dimensional as producing dense three dimensional electrode arrays are still beyond the ability of the microelectronics industry. Some three dimensional *in vitro* neural interfaces have utilised fluorescent imaging techniques but are subject to the disadvantages relating to fluorescent imaging that are discussed above and still lack fine control over the structural morphology of the network [38].

The uncontrolled growth of two dimensional neural cultures makes them almost impossible to reproduce making it difficult to draw significant conclusions. The undefined placement of the neurons and their tendency to aggregate over time often leads to a single electrode, which detects field potentials, recording the summated activity of up to tens of proximal neurons [39,40]. Although some techniques have looked at constraining the number of neurons and coordinating their neurite outgrowth on an electrode array most have been based on chemical coatings patterned using photolithography [10,11]. Photolithography has high resolution but is inflexible in design, requiring a new mask to be produce for each new design making it an expensive and time consuming process to experiment with pattern design. Due to the non-specific adsorption of secreted biomolecules, surface coating techniques have yet been able to control the growth of the neural culture longer than 90 days [10,35]. By exploiting the high-resolution additive manufacturing technology, two photon polymerisation, this thesis aimed to improve the reproducibility of these *in vitro* neural interfaces by constraining the placement of cell somas and coordinating the outgrowth of neurites using microstructures. Other attempts to use three dimensional structures to pattern the growth of neurons *in vitro* will discussed at greater length in section 1.5 Engineering *in vitro* cultures using surface chemistry and microfabrication.

A major issue with neural interfaces is the long-term maintenance of the neural cell culture's viability. Much work has been done to optimise the solute and growth factor composition of neural cell culture media. However, over time the culture influences this composition through the uptake of metabolites and the secretion of waste products, e.g., oxygen, carbon dioxide, glucose and amino acids. It is important to tightly regulate the culture's physiochemical milieu as it is key to the viability of the culture as well as influencing the excitability and neurophysiological behaviour of the cells. Although this can be regulated approximately with the replenishment of media it is an inaccurate and time-consuming task. The move towards automated cell culture maintenance is a potential advantage of the microfluidic lab-on-a-chip revolution. Developing techniques for non-destructively monitoring key physiochemical variables may enable closed-loop control over the physiochemical environment within

microdevices. As the microchannels in cell bioreactors become yet smaller it is increasingly difficult to monitor changes in the physiochemical environment as sampling the media destructively is not possible due to the minute volume. Approaches to achieving this is may be through the incorporation of microsensors or the embedding of sensors into the structural material of the microdevices. This is of particular importance for three dimensional tissue constructs where the interior of the culture will need to be monitored, potentially in a dense environment of cells and scaffold material. Embedding pH sensitive fluorophores into two photon polymerised microstructures would enable non-destructive, real-time monitoring of key physiochemical parameters such as pH.

This pH monitoring approach would serve as an example for future methods of monitoring other key physiochemical variables through the incorporation of fluorophores sensitive to the other key variables, e.g. temperature or glucose. The development of these pH sensors highlights that although this thesis focused on developing technologies specifically for *in vitro* neuron biosensors, it both draws upon and contributes to the techniques for the wider tissue engineering community where automated maintenance of the cell culture environment is highly desirable.

1.3 The Importance of Neural Networks in the Context of Neuron Biosensors.

The term biosensor refers to a device which interrogates a biological system for a physiochemical or biological analyte. *in vivo* biosensors can range from monitoring the level of oxygen in the blood using a smart phone [41], to measuring the electrical activity of the central nervous system using implanted electrode arrays to control a robotic arm [42]. *In vitro* cellular biosensors are used for detecting and investigating the effects of biologically relevant compounds such as herbicides and drugs [43,44].

The nervous system is one of the primary pharmaceutical targets for many pathologies that effect a wide range of tissues including neural tissue. Advanced neural culture based biosensors allow for greater access for many analytical techniques compared with *in vivo* investigations. The greater access provided by *in vitro* platforms can help identify and decipher the mechanisms of pharmaceuticals acting on the nervous system. Such biosensors may therefore facilitate high throughput screening and more thorough characterisation in a wide range of therapeutic scenarios. For many neuropsychological diseases large pharmaceutical companies have decreased funding in recent years due to the lack of valid animal models and the complications and restrictions associated with human test subjects [45]. This highlights the need for novel approaches, such as more sophisticated *in vitro* neuron biosensors which accurately mimic the human nervous system, for the study of therapeutics on neuropsychological disease. Drugs which target the central nervous system for the treatment of neuropsychological and neurodegenerative diseases are often well characterised in terms of the pharmacology and cell biology, such as which receptors the drug binds to and which signal cascade it activates. An example of this is chlorpromazine for the treatment of schizophrenia has been shown to inhibit the calmodulin activation of cyclic phosphodiesterase since 1985 however how this contributes to its effects on higher level cognitive function and why this effect is so variable between patients is poorly understood [46,47]. Similarly, the regions of the brain associated with such diseases and therapeutics are also reasonably well characterised through the wide range of brain imaging techniques now available [48]. However, how individual cellular and molecular events contribute to the

increased activity of brain regions to produce various behavioural, physiological and pathological phenotypes is very rarely well established. Establishing this link is key to moving from treatments discovered through trial and error to treatments which are developed based on a mechanistic understanding of the pathology and action of the drug. It is therefore key to the development of valid experimental models for investigating neuropsychological therapeutics that those models consider how neural cells interact as a network. Before characterising how pathological and pharmacological perturbations effect a system it is first necessary to establish a benchmark understanding of the physiological function of the system. Previously, *in vitro* neuron biosensors have been used to model, interrogate and greatly advance our knowledge of neurophysiology and neurobiology. An early example of this was the giant squid axon experiments of Hodgkin and Huxley which inspired an accurate description of the neurophysiological events which underpin the current understanding of an action potential [49]. By measuring the excitability of the giant squid axon in a range of different salt solutions, Hodgkin and Huxley produced a model describing a neuron as a circuit of electrical components, e.g., where the cell membrane is described as a capacitor (Figure 4). They described other structures responsible for generating a current or acting as resistors, these were late identified as ion pumps and voltage gated ion channels respectively.

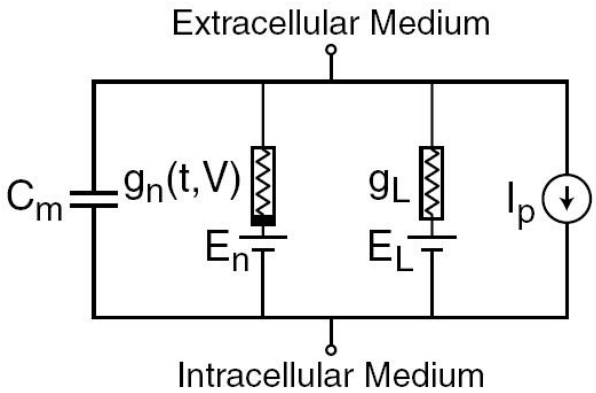


Figure 4 Hodgkin and Huxley's circuit diagram of an excitable cell.

The C_m represents the cell membrane as a capacitor. The g_n and g_L are linear and non-linear conductance representing voltage gated and leaky ion channels respectively. The E_n and E_L are batteries which represent the electrochemical gradient which drives the flow of ions. I_p represents an ion pump which maintains and establishes the electrochemical gradient. [49]

This model is still used today as the basis of many mathematical models of neural networks used as adaptive and forecasting software for a range of signal processing applications from optics to weather [50]. In developmental neurobiology *in vitro* models have been useful in identifying and studying the action of diffusible and matrix bound molecular cues involved in axon guidance, necessary for the wiring up of the nervous system [16,51]. Despite these examples, *in vitro* neural models are fraught with validity issues, certainly when trying to model higher level brain function or diseases which impair higher level cognitive function. To utilise *in vitro* neuron biosensors as models of the human brain, previously mentioned as one of the most complex known structures, a great deal more structural complexity is required than an uncoordinated two dimensional culture of disassociated neurons. Combining microfabrication and microfluidic techniques to precisely control the physiochemical and biochemical environment in order to produce more valid models of *in vitro* cell culture platforms has been the focus of much research in the last decade [25,52–55].

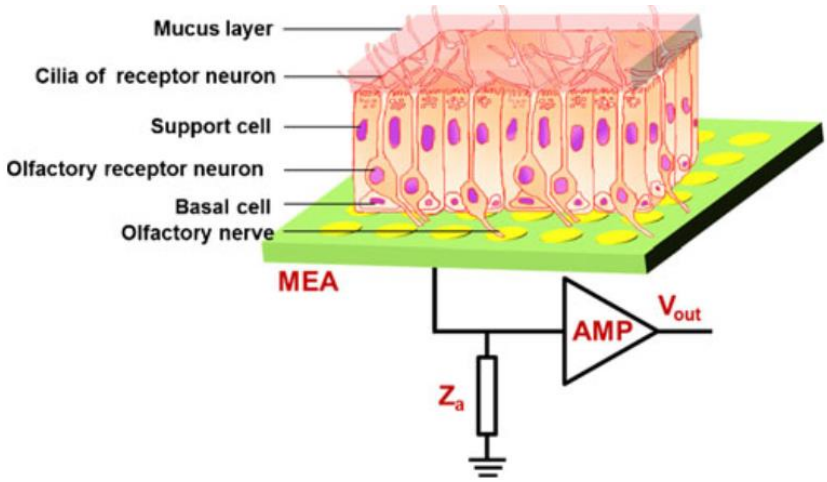


Figure 5 A biohybrid chemical detector.

Exploiting the sensitivity of neural detection through a bio-hybrid chemical detector based on interfacing a micro electrode array with olfactory neurons in an explanted olfactory epithelium. (Liu et al., 2012).

Neuronal based cell biosensors also offer potential for the development of devices which are not focused at investigating the function of the nervous system but exploit the power and sensitivity of the nervous system, e.g. for the detection of environmental variables [8]. As an ectoderm derived tissue, the nervous system is primarily an interface between an organism and its environment. Many

neuronal subtypes are therefore specialised for the detection of environmental analytes making them well suited as the basis of cell based detectors. However, the strength of neural systems does not come from the sensitivity of an individual receptor or cell but from the integration of information at several hierarchical levels. The olfactory bulb will detect a single odorant as a profile of the frequency of activation of many neurons [56]. The relative strength of the odorant profiles is modulated in a top down way from higher brain regions such as the amygdala and neocortex in order to reduce the transmission strength of chronic background odorants and sensitising to emotionally associated odorants [57]. Therefore, to most effectively exploit neural cultures as detectors, and in other forms of biohybrid devices, it may be necessary to be able to coordinate multiple neurons into hierarchical networks capable of integrative information processing.

In vivo, neural cells are differentiated and spatially organised during embryonic development, like most other cells, through carefully regulated overlapping gradients of soluble paracrine, extracellular matrix bound and cell to cell differentiation factors [58,59]. The factors a cell is exposed to will determine its cell fate which in turn determines how it will respond to the environmental cues which guide neurites to their synaptic partners. This is achieved by regulating the expression of receptors on the growth cone, a dynamic structure dependent on the regulation of cytoskeletal elements by membrane bound receptors. The growth cone is made up of undulating lamellipodia and filopodia which, via membrane receptors and cytoskeletal elements respond to a wide range of biochemical and physical cues [60,61]. It is these highly organised and sensitive processes which allow for such complex biological structures to be formed and are responsible for the foetal sensitivity to environmental factors which leads to developmental disease [62] and the immense challenge that tissue engineers, specifically in neural engineering face.

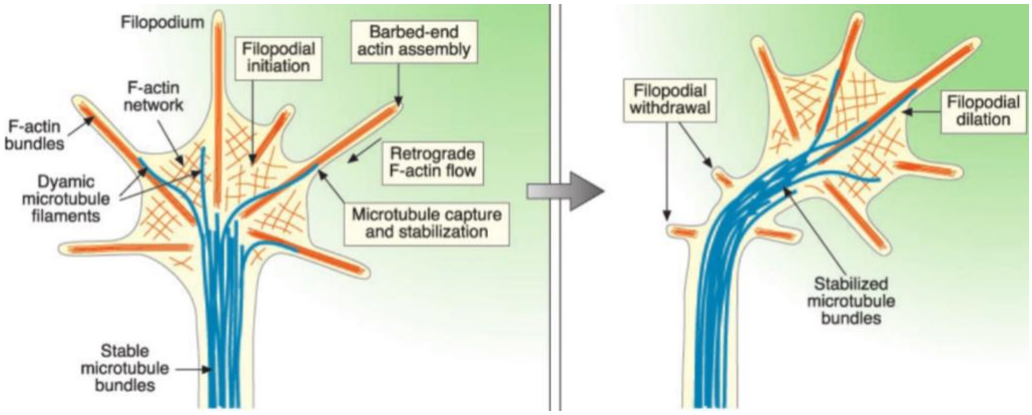


Figure 6 Basic structure of the growth cone.

A growth cone is the dynamic structure which guides neurites through a complex three dimensional landscape made up of overlapping gradients of diffusible molecules, green, and substrate bound biochemical cues to locate its synaptic partner. Contact with guidance cues will either prompt the cytoskeleton of the growth to stabilise or destabilise altering its direction [58].

In the case of primary dissociated neural cultures, the cells are nurtured and directed in the embryo, a tightly regulated environment, up until they are explanted where they are then exposed to an alien environment. Engineering this environment is essential for producing viable cultures but also offers an opportunity for manipulating the subsequent growth of the cells [9,23,36,63,64]. Cells at different time points during development vary in their ability to adapt to the novel artificial environmental of tissue culture. In the later stages of prenatal mammalian development, the neuroprogenitors in the foetal brain undergo differentiation, neuritogenisis and synaptogenesis generating a loosely interconnected network which is not possible to dissociate whilst maintaining high cellular viability. In order to keep the cells in a natural environment for as long as possible and get the highest yield of cells through dissociation, hippocampal neurons for *in vitro* network cultures are normally dissociated at a late prenatal stage or early postnatal stage., e.g. E18 – P03 in rat[65]. Post-natal harvesting however can lead to undesirably high proportions of neural progenitors differentiating into glia[65].

Thereafter it is the cell culture substrate, media and paracrine signalling of the dissociated culture which influence the development of the *in vitro* network. Optimising and experimenting with the physiochemical environment of *in vitro* cell cultures was initially required to facilitate the first *in vitro* neural culture [36]. Since then however the sensitivity of these explanted cell cultures to their environment has provided an opportunity to explore the factors which influence their growth and differentiation. This thesis aims to exploit the sensitivity of *in vitro* cultured neurons to microstructures to coordinate the structure of the resultant network for improving the efficacy of a microelectrode based *in vitro* neural interface.

1.4 Neural interfaces, microelectrode arrays and the necessity of neural patterning

To investigate neural network dynamics or exploit *in vitro* neural networks in novel biohybrid devices it is necessary to interface the neurons with a computer, this a form of cell culture brain computer interface (BCI). Neurons are excitable cells which, upon excitation, transmit a signal down their main extension, their axon, via a flux of ions across the membrane known as an action potential. The flow of ions across the membranes can be detected and stimulated using electromagnetic techniques, for example transcranial magnetic stimulation[66], electroencephalogram (EEG)[67], electroconvulsive therapy[68], etc. These approaches have been found as useful methods for diagnosing and treating neural pathology, e.g. the use of EEG in the diagnosis of epilepsy[69], as well as for investigating the mechanisms of neural function. EEG can be said to be a direct measurement of neural activity by measuring summated excitatory presynaptic potentials. functional Magnetic Resonance Imaging (fMRI) could be considered an indirect measurement of neural activity as it measures fluctuations in metabolic variables associated with neural activity, e.g. blood oxygenation[70]. As both fMRI and EEG monitor a population of cells, they lack the resolution to discern the activity of individual cells in a network. Being able to monitor the activity of all neurons in the network is key to understanding neural network dynamics. The same can be said for the imprecise stimulation modalities of transcranial magnetic stimulation and electroconvulsive therapy which effect the entire brain.

Techniques capable of recording from single neurons often rely on making direct contact with the cells via implantable electrodes. Patch clamping uses a glass micropipette filled with an electrolyte solution and can be used to record and stimulate a single cell. It is even possible to record from single receptors from either side of the cell membrane (Figure 7). However, the invasive nature of this technique is destructive to the tissue and gaining access to the cytosol by puncturing the membrane is eventually lethal to the cell. Patch clamping is not only limited by a short time window of several hours but also to the number of cells that can be recorded from at any one time. Even with specialised set ups and computer guided and automated patch clamping a total of twelve cells was patch clamped *in vitro* [71].

For studying the role of network dynamics involved in brain function interfacing with every cell in the network over a period of weeks to months and ideally longer is required so that changes in the network dynamics in response to stimulation be measured. This adaptation in response to stimulation is known as neural plasticity and is considered to be key to the brain's ability to learn responses to environmental stimuli [72].

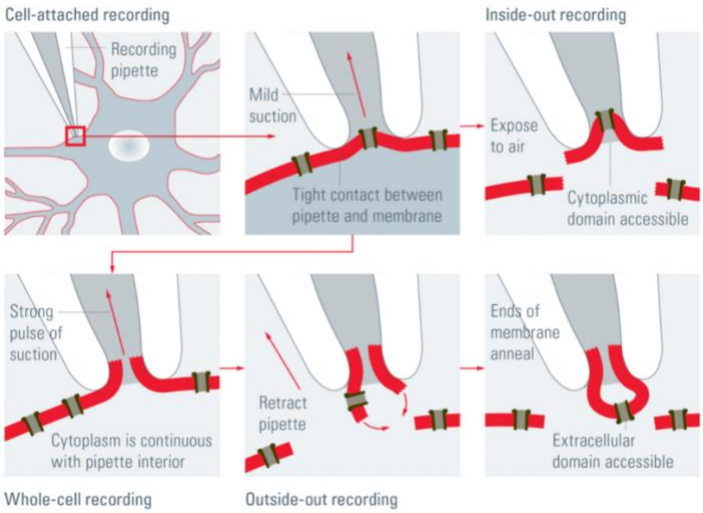


Figure 7 The variety of patch clamping techniques available for interrogating the electrophysiological properties.

The versatility of the technique allows for recording and stimulating a range of electrophysiological entities from whole cells, by attaching and puncturing the cell membrane, down to single receptors by removing a minute section of the membrane and sealing the end of the pipette with it. The technique is demanding on both time and skill of the experimenter and ultimately lethal to the cell in question and as such not suited to recording from many cells in parallel for long term plasticity studies.[73]

Biophotonic approaches to interface with neurons have the potential to provide high resolution without direct, destructive, contact with the cells of interest, making it particularly relevant for monitoring three dimensional networks where introducing an electrode to every cell is infeasible. Stimulating or suppressing action potentials in neurons using light is becoming routine using optogenetics where a genetically encoded photosensitive ion channel, e.g. channelrhodopsin, opens upon exposure to a specific waveband of light [74]. For monitoring neural activity optically fluorescent microscopy based approaches, such as calcium imaging, are well suited to small transparent animals

or cell culture but lack the penetration depth for *in vivo* studies of mammalian central nervous systems. Developments in two photon imaging and adaptive optics are improving the penetration depth of *in vivo* calcium imaging however such techniques are still vulnerable to the major disadvantage of these fluorescent techniques which is photobleaching. Every fluorescent excitation event can undergo a probabilistic intersystem crossing potentially leading to the bleaching of the dye and its conversion to a reactive free radical. The bleaching will ultimately limit the lifetime of the dye, but the free radicals will also kill the cells, a phenomenon known as phototoxicity. This limits any long term experiments where fluorescent dyes are used. Although research into non-dye based photonic methods, such as surface plasmon resonance or ring resonators, for monitoring neural activity is underway to date no established protocol exists.

Microelectrode arrays (MEAs) were first used in 1972 with myocytes[75] but were not widely adopted until advances in photolithography in the early 1990s which made both the devices, and the computer power required, to process the resultant data more accessible[76]. MEAs designed for *in vivo* use have recently been advanced partially due to their potential for restoring function in tetra- and para-plegics by bypassing a damaged or dysfunctional peripheral nervous system [42]. Using the Utah array, a three dimensional MEA, a tetraplegic patient was able to control a robotic arm through wireless transmitted signals from the MEA implanted in her motor cortex to a computer controlling the arm [42]. *In vivo* MEAs have received interest from the Defence Advanced Research Program Agency (DARPA) for their Revolutionising Prosthetics programme and more recently from Glaxo-Smith-Kline who are interested in interfacing with the peripheral nervous system to treat chronic conditions based on organ dysfunction, e.g. asthma[77]. However, the cell density of most neural tissue, especially the mammalian cortex, exceeds the capabilities of modern implantable electrodes limiting the efficacy of microelectrode arrays for investigating neural networks (Figure 8).

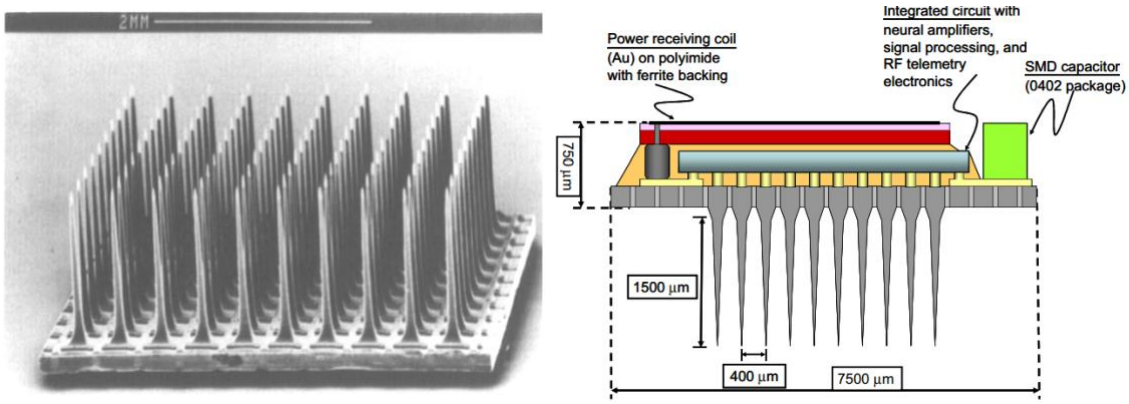


Figure 8 Utah intra-cortical microelectrode array for in vivo neural interfacing.

Left: Scanning electron micrograph of original Utah array, note that the electrode tips are all in a single plane. Having all the electrodes in a single plane neglects the fact that the neural tissue is a three dimensional structure and as such many cells in the tissue are not interfaced with. Right: Schematic of telemetric Utah array for wireless *in vivo* neural interfacing, note the spacing of 400 *micron* between electrodes, a distance in which many cells would reside [78].

Microelectrode arrays for interfacing with *in vitro* neural cultures are capable of recording from multiple cells at high spatial resolution and for up to three months. *In vitro* MEAs have so far been utilised to correlate synaptic connectivity with electrical activity during the growth of the culture up to 28 days [39]. Using a high density microelectrode array allows for somewhat improved interfacing and combined with spatiotemporal filtering and cross-correlative analysis it is possible to determine the connectivity of some of the neurons within the culture [40]. The spatial resolution of MEAs has been further advanced by the development of Complementary Metal-oxide Semiconductor (CMOS) microelectrode arrays where the number of electrodes available in a single array is now in the tens of thousands [37,79,80]. However, as these microelectrodes detect field potentials they have the potential to record from multiple cells at the same time [81,82]. Microelectrode arrays tend to primarily detect larger peri somatic depolarisations, caused by the summation of many dendritic excitatory post synaptic potentials (Figure 9).

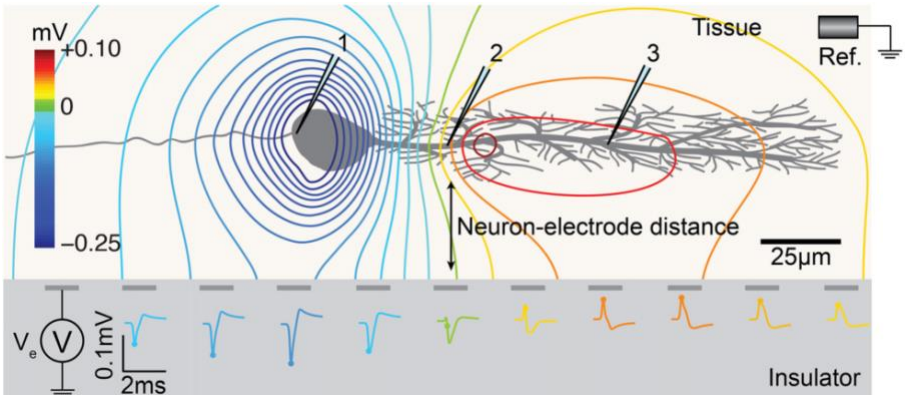


Figure 9 Microelectrode detecting different neuronal membrane depolarisations.

Note the greatest voltage change is at in the peri somatic regions where the excitatory post synaptic potentials of many dendritic branches summate. [83]**.**

One theory is that neurons tend to aggregate as they prefer to bind to each other rather than the substrate surface, possibly due to the denaturing of secreted extracellular matrix proteins on the surface. Once the neuronal soma in the culture have aggregated it is difficult to record from individual cells in the culture as the soma are denser than the microelectrodes. One approach to reduce aggregation has been to encourage neurons to adhere to the surface with a variety of coatings, discussed in the following section, however somatic aggregation and neurite fasciculation are still common occurrences in the relatively high density cultures normally used for *in vitro* microelectrode area experiments [84]. It has also been shown that aggregates of cells are less susceptible to nanoscale contact guidance cues[23]. As such, developing a technique which is capable of preventing soma aggregation and restricting a single soma to a single microelectrode is a key requirement when coordinating the topology of the network. Attempts to constrain soma to microelectrodes have utilised both surface chemistry and microfabrication and will described in more detail in the following section, Engineering in vitro Cultures using Surface chemistry and Microfabrication. Guiding the growth of neurites has also been an aim attempts at coordinating the topology of neural networks *in vitro*[10,35]. This is not only important for making *in vitro* neural interfaces a reproducible experimental platform but also to provide researchers with the opportunity to exploit network topology as an experimental variable.

1.5 Engineering *in vitro* Cultures using Surface Chemistry and Microfabrication.

In order to keep explanted tissue in a functioning state it must be stored in an environment which provides certain physiochemical variables, and as such, optimising culture media and growth substrate functionalisation have underpinned many major advances in cell culture such as the introduction of ringer's solution as a cell culture medium[85]. Adherent cells, such as neurons, must be able to bind to the substrate surface to survive. The first viable *in vitro* neural culture adhered to a glass petri dish coated via the chemisorption of poly-l-lysine (PLL)[36] (Figure 10). The pendent chains of PLL are terminated in an amine group which can ionically interact with the negatively charged membrane proteins of neurons to facilitate adhesion[86]. The positively charged amino coated surface also promotes secreted proteins adsorb to the substrate in a more native configuration than hydrophobic glass which tends to interact with the hydrophobic core of the proteins interfering with entropic protein folding[87]. Having proteins adhere to the substrate in a native conformation c encourages closer adherence to the surface which can improve microelectrode recordings by reducing the neuron to electrode distance[87]. Encouraging adherence to the cell surface also helps to prevent the somatic aggregation mentioned in the previous section.

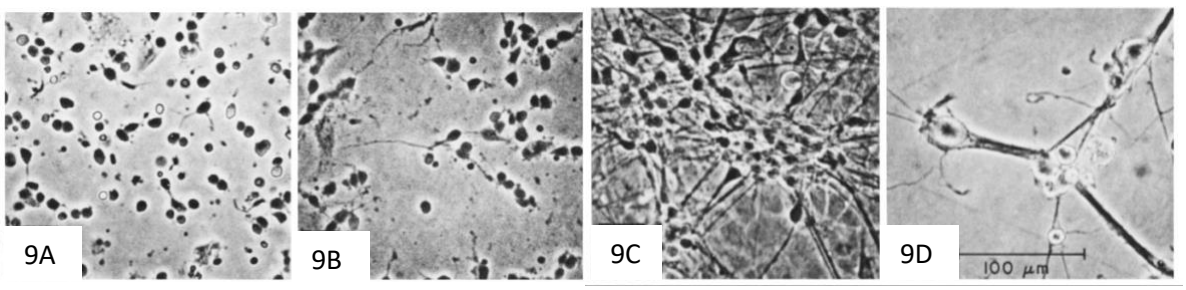


Figure 10 Phase contrast image of first published in vitro dissociated neural cultures.

Primary mouse hippocampal neurons seeded onto poly-L-lysine coated glass substrates. 9A: After 2 hours small processes begin to sprout neurites. 9B: After 24 hours longer, processes can be seen, and the cells begin to aggregate. 2C: After four days *in vitro* there is extensive neurite outgrowth and soma being to aggregate. 2D: After 6 days tight aggregates of cells from and are linked by thick fascicles of neurites [36].

To further encourage the adsorption of correctly folded proteins to glass substrates amino terminated silanes can be covalently bond to the substrate, producing a positively charged self-assembled monolayer[10]. Silanes have a bipolar chemistry, with one end of the molecule forming a covalent bond with a glass surface and the other facing away from the surface and therefore altering the chemical properties of the surface[88]. Silanes have the advantage of being covalently bound and are therefore more stable and resistant to solvent washes and baking for sterilisation than chemisorbed polymers such as PLL. More biomimetic approaches to improving soma and neurite adhesion to the substrate have employed coatings of cell adhesion proteins, e.g. laminin, or their active peptide motifs, e.g., Arginine Glycine Aspartate[89]. Proteins, or their active motifs, exploit existing endogenous pathways of adhesion, the RGD motif binding to an integrin receptor, and could be seen as a more valid form of facilitating adhesion than an amino coated surface. Exploiting cell adhesion pathways through substrate bound molecular cues has also been used to influence neural progenitor differentiation[53,90]. This demonstrates the important role the extracellular matrix plays in embryonic development and how it mimics this *in vitro* can be used to interrogate and exploit developmental process for the creation of more biologically sophisticated models of neural tissue. Even neuronal cultures which adhere well to the substrate with little aggregation are still subject to random placement and migration of cells. The number and identity of cells on an individual electrode is therefore likely to vary between samples and over time making prolonged or repeatable investigations into neuronal network dynamics at single cell resolution unattainable.

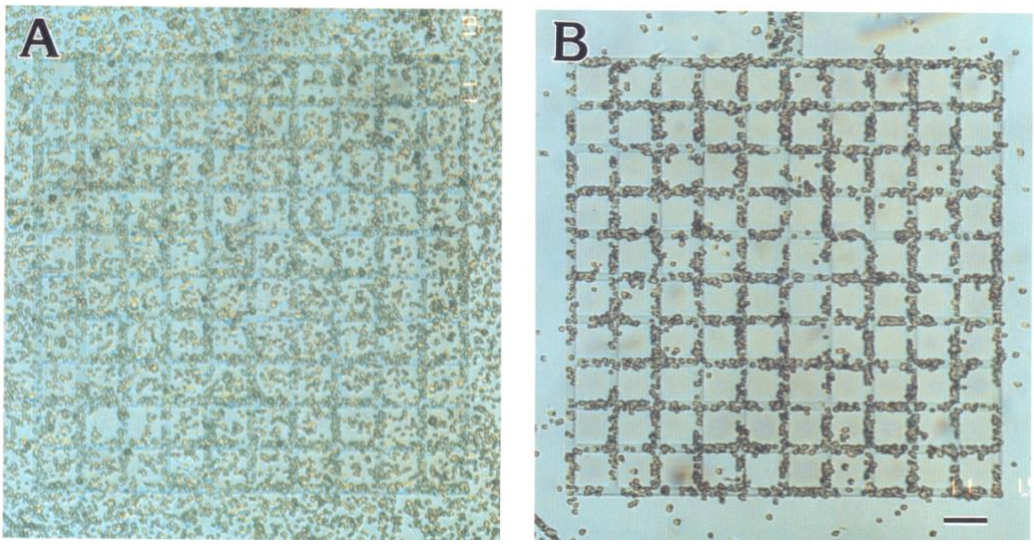


Figure 11 Patterning neurons with photolithographically defined self-assembled monolayers.

***Left: Immediately post seeding Right: 70 minutes after plating and 10 minutes after media has been exchanged to remove cells which have not adhered*[10].**

The first approach to control the distribution of neural cells *in vitro* was based on patterning, using photolithography, silanes which either increased or decreased the surface energy of the substrate to either promote or demote cell adhesion (Figure 11)[10]. Although this surface chemistry approach prevented early adhesion to certain regions after two weeks the pattern would begin to break down, due to a build-up of secreted proteins. As the culture becomes electrically active at 2 weeks[38] this approach is limited in its application to neural network dynamic investigations. This approach also appears to promote aggregation, potentially due to inefficient space for the cells to occupy, this is also apparent when a similar approach was attempted twenty five years later (Figure 12)[35]. In this later approach it is possible to observe the pattern breaking down as fascicules between aggregates contract detaching aggregates from their position in the pattern (Figure 12).

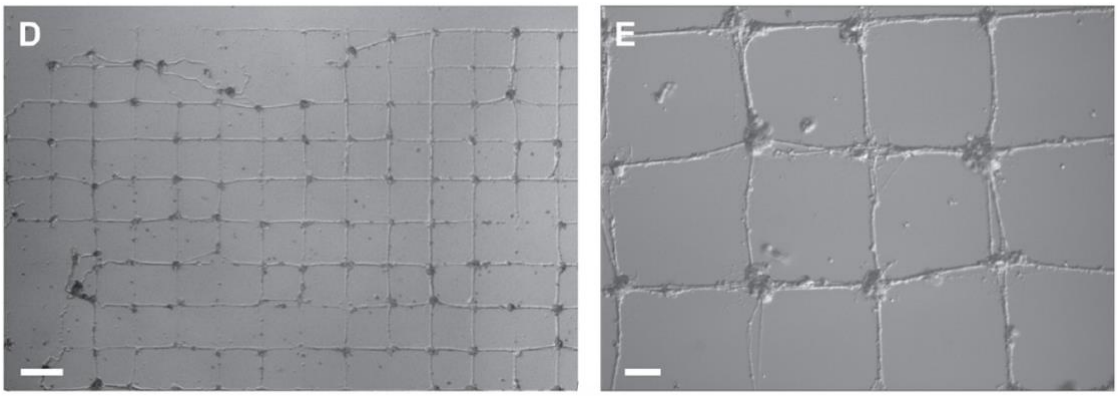


Figure 12 Patterning neurons with photolithographically defined self-assembled monolayers.

Cultures patterned on silane patterned substrate for 2 weeks. Note how it is primarily the cells at the edge of the grid that seem to be pulled off of their patterned position leading to the breakdown of the patterned culture. Scale bars: Left, 100 micron; Right,: 25 micron[11]***.***

To pattern biological molecules, such as cell adhesion proteins, photolithographic patterning is not necessarily suitable as the biological molecules can be denatured or degraded in the high temperatures and strong solvents utilised in the removal of photoresists. In order to pattern proteins and other biological molecules microcontact printing is used or multiple step complex surface chemistry protocols have to be employed[91–93]. Microcontact printing is a type of soft lithography which exploits the resolution of photolithography in the fabrication of masters which are then used as moulds to produce stamps, often out of polydimethoxysiloxane (PDMS)[94–97]. A disadvantage of any photolithographic based patterning technique is that it requires the fabrication of a new mask for any change of pattern which can be expensive and, in this context, limits the ease at which the topology of a neural network could be used as an experimental variable. In terms of microcontact printing the process to adapt the pattern is even more time consuming due to the additional necessity of producing new moulds and stamps. Instead of two dimensionally patterning coatings to control the adhesion of neurons another approach is to build microstructures for controlling the neurons. Using microstructures to pattern the culture has the potential for patterning in three-dimensions and increase the pattern's longevity as they will not be made redundant by the adsorption of screted biomolecules as in the sase of a hydrophobice silane coating[10]. However, many microfabrication

approaches rely on photolithography and suffer from the aforementioned disadvantages of this technique.

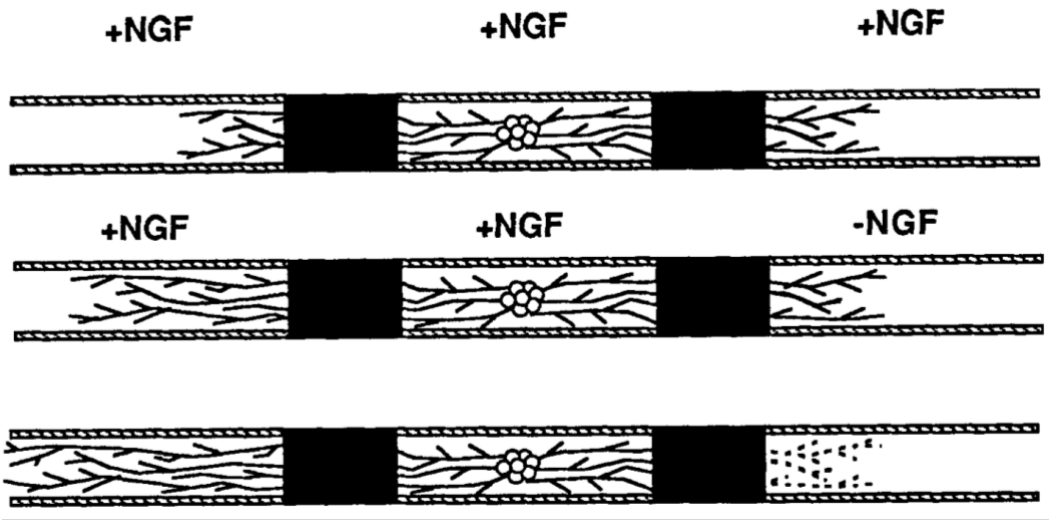


Figure 13 The Campenot chamber: Early microstructured growth substrate for compartmentalisation of neuronal soma.

The Campenot chamber allows for compartmentalisation of diffusible growth factors, e.g. neural growth factor (NGF) to demonstrate the local neurotrophic effect on the distal ends of neurites, as demonstrated by the degeneration of neurites in the -NGF chamber [16]***.***

Microstructures have been exploited by researchers to influence the growth *in vitro* neural cultures and to investigate a range of processes in developmental neurobiology [9,14,16] and for patterning neurons when investigating network dynamics [11,17,18]. Microstructures used for culturing neurons *in vitro* have been fabricated by a wide range of techniques including multi step photolithographic deposition and etching [17], soft lithography [18,22], electrospinning [23] and additive manufacturing techniques such as two photon polymerisation [19,20,96]. In developmental neurobiology microstructured *in vitro* platforms have been used to interrogate the spatially dependent effects of diffusible and substrate bound growth factors. An early example of this is the Campenot chamber which partially separates a central soma containing chamber from two adjacent empty chambers [16]. The separation is partial as the base of the partition is perforated with micron diameter channels. These channels permit the passage of neurites but not somas, considered to be due to the inability of the nucleus to

deform less than two or three micron. Prospective neurotropic factors can then be added to one of the two adjacent chambers of the Campenot chamber. The neurites then preferentially infiltrate the chamber containing a neurotrophic factor, Neural growth factor (NGF) was used in the original experiment, demonstrating the diffusible and attractive nature of the molecule (Figure 13). A stripe assay is used to demonstrate contact guidance and short range diffusive effects of various extracellular matrix components, membrane bound cues and cell adhesion molecules have on both axon guidance and cell migration[14]. Initially one of the guidance cues of interest will be sucked onto a Nucleopore filter, this will form a striped pattern as the suction is applied through microchannels in a silicone matrix under the filter paper. The space between these stripes is then filled with a second guidance cue by sucking through the filter paper, not restricted by a microchannels[98]. Originally the stripe assay used to determine the cues used in mapping the rewiring of the retina to the tectum in the chick embryo, the stripe assay has also been combined with biochemical techniques, such as quantitative polymerase chain reaction to determine the signal cascade events downstream of the substrate bound guidance cues. This helps to determine how gene expression, in conjunction with transcriptional regulation at the growth cone, coordinates the cells response to substrate bound guidance cues [99].

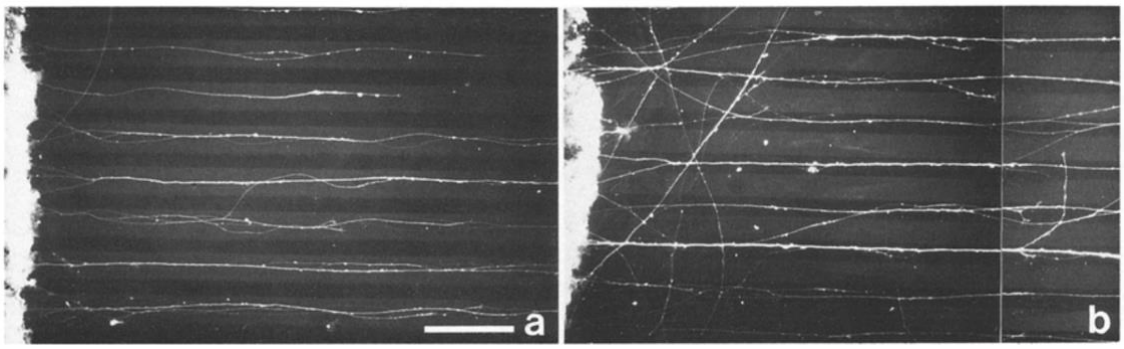


Figure 14 Stripe assay for interrogating contact guidance molecules in axon guidance.

Explanted embryonic retina on the left of each image. Right: Lentil lectin immobilised on the lighter stripes and Haemoglobin on the thin stripes. Left: The haemoglobin and lectin have been swapped over and the neurites change over. Neurites exhibit preference for growing on lentil lectin [14]***.***

Microfluidic devices can provide even greater control over the soluble environment than the previous examples of stripe assay and Campenot chamber[9,54]. For cell culture these microdevices have the potential to provide automated culture maintenance, fine control over the soluble environment and compartmentalisation of cells for patterning the growth of cultures and co-cultures[23,53,100,101]. An early example of controlling the growth of neuronal cultures within microfluidic devices was developed for investigating the axon specific effect of certain growth factors on axon regeneration [22]. This device, the Taylor Device, has since been commercialised and is now for sale amongst other variations of the design (Xona Microfluidics ltd). This commercialisation emphasises how the growing neuroscience research field is a market with increasing demand for advanced *in vitro* models. This device, much like the Campenot chamber, exploits the 1-3 micron window through which neurites can fit but, due to the nucleus being only partially deformable, the soma cannot. The cells are seeded in the one chamber and their neurites grow through the microgroove barrier and across a central fluidic chamber. To ensure axons are isolated from dendrites the gap between the proximal and distal chambers, i.e. the width of the fluidic channel, must be longer than dendrites tend to grow *in vitro*, greater than 900 micron (Figure 13)(Xona Microfluidics ltd.). The central fluidic chamber is therefore only populated by neurites and isolated from the somas allowing the axon specific effect of drugs, toxins and growth factors to be resolved. Additionally, isolating the axons allows for axotomy to be performed in the distal chamber using vacuum aspiration whilst maintaining the viability of the culture based in the seeded chamber. Fluidically isolating axons and somas has, much like the stripe assay, enabled investigations into the mechanisms by which molecular events at the axon growth cone effects expression in the nucleus. This was used to elucidate micro-RNA mediated effects of chondroitin sulphate, an important extracellular matrix molecule in axonal guidance, has on the regeneration neurons in a damaged region of the brain[102].

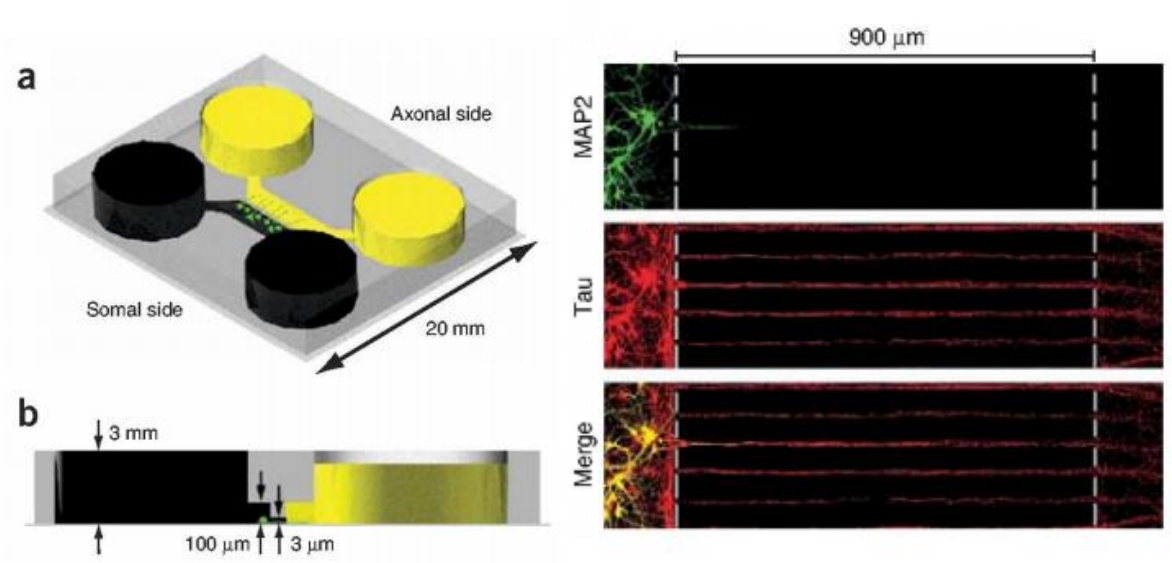


Figure 15 Microfluidic Taylor device for the study of axonal regeneration.

Left images: show schematic of the device and its dimensions. Note the 3 micron high channels for thee neurites to pass through. Yellow and black demonstrates the fluidic isolation with neurons in green. Right: image showing how dendrites (MAP2, green) are confined to the soma chamber whereas the axons extend to the opposite chamber [22]***.***

The NeuroArray is a PDMS device, fabricated using multi-step photolithography and focused on constraining soma placement rather than influencing neurite[18]. three micron high pedestals are fabricated on the bottom of a PDMS block, which is perforated with a homogenous pores, in order to provide sufficient space for neurites to spread underneath the block. Neurons are seeded from above, fall through the pores to attach on the surface underneath the PDMS block. Excess neurons are washed off the PDMS block which, uncoated, does not support the attachment of neurons. Although the publication claims this technique has confined the neuronal soma to the pore of entry however there is no evidence directly to this effect as the fluorescent images in the paper are largely obscured by the PDMS stencil (Figure 16). Additionally, there is no reason to suspect that the neurons would remain where they initially adhered to the substrate as there is at least three microns of clearance in the z axis and much more clearance in the x and y axes for a neuron soma to migrate through. Some images, particularly with the 30 micron holes, appear to show soma underneath sealed regions of the PDMS, as visible by the dim fluorescence in between the holes which is in rounded soma shapes as opposed to purely neurite-like extensions. By varying the size of the holes in the stencil the researchers

were able to vary the average number of cells in each pore. And although they claim only one cell per hole in the 10 micron pore stencil this is again difficult to see clearly as the images provided show only a single fluorescent circle is visible and no discerning features to count cells, and no nuclear stain has been performed to identify the number of nuclei present in each pore (Figure 16). The functional and structural characterisation of their network suggests that they are able to influence the signal propagation through the patterned network according to the patterning stencil. The link between the order of activation and the topology however seems strained as the fluorescent images provided in conjunction with the calcium imaging data are only 5 days *in vitro* and as such yet to become a fully connected electrically active network. This work highlights the need to thoroughly characterise the patterning architecture, the structural network topology and signal propagation before concluding that neural circuitry has been successfully patterned and a *"Neuron Diode"* created[18].

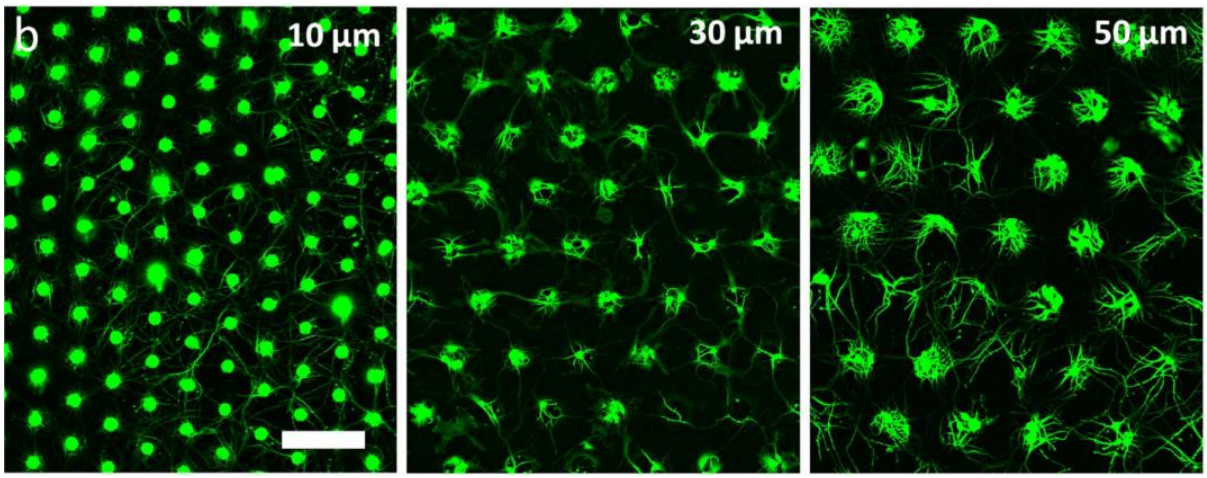


Figure 16 III tubulin stained hippocampal cells cultured for 6 days in the NeuroArray PDMS stencil.

Note the inability to see the cell morphology through the stencil and inability to determine number of cells in the 10 micron holes. Scale bar: 100 micron[18].

Microstructures fabricated by multi-step photolithographic deposition and etching have been implemented to restrict neuronal somas to single electrodes on microelectrode arrays. Four micron high rings (Figure 17) were built using a multistep photolithographic process, including both etching and depositing, in which the microelectrodes were also produced (Figure 18)[17]. The resultant *neurochip* produced at least one culture that had one to one interfacing between an electrode and

each neuron in the culture as demonstrated by stimulating each cell and correlating their activity using voltage sensitive dyes[17]. Although the majority of soma primarily remained with the rings some did escape, making the technique less reliable. Neurites grew to an unpredifined geometry, limiting the reproducablity of any single experiment and preventing network topology being used as an experimental variable. To ensure neurons were only seeded within the *Neurocages* a glass micropipette and a micromanipulator was used to manually place neurons individually into each *Neurocage*. However, to ensure there was a sufficient volume density of cells to produce the concentrations of neurotrophic factors required to support the micro culture, a macro culture of neurons was plated around the edge of the substrate. Neuronal viability depends on paracrine signalling factors, neurotrophic factors, a deficiency of which will cause the culture to undergo apoptosis. To maintain the micro culture in (Figure 17) a neuronal macro culture is cultured in the same dish to provide a cellular volume density sufficient to maintain the concentration of paracrine secreted neurotrophic factors required to maintain the culture's viability.

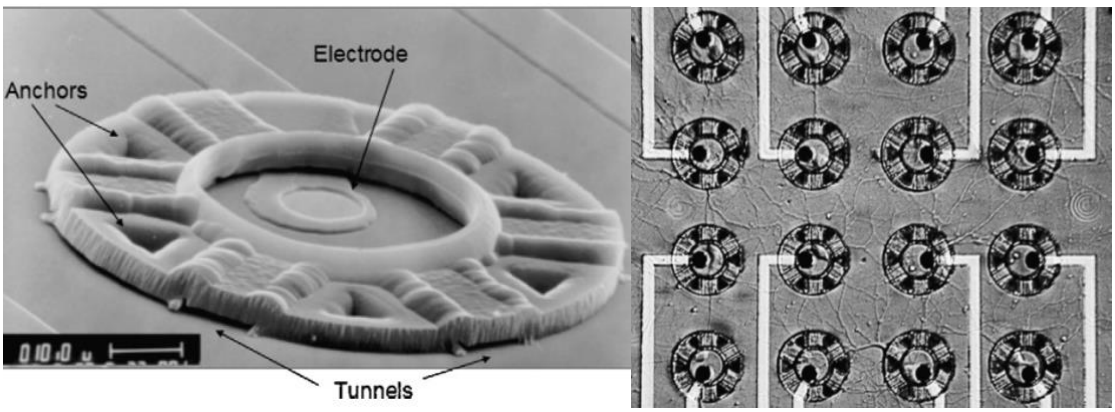


Figure 17 Scanning Electron Micrograph of the Neurocage Design.

A neuron is placed in the central chimney region, near the electrode. Axons and dendrites are free to grow though the tunnels to synapse with other neurons. The cage is made out of 4-parylene, a biocompatible polymer. Low-stress silicon nitride insulates the gold electrode and leads. Scale bar: 10 micron.[17]

Fabricating electrodes and microstructures for patterning the culture using the same process has advantages for scaling up and commercialisation. The process however, is time consuming and importantly is fraught with design constraints. The process of etching and depositing photoresists and

metal microstructures is limited in its ability to build three dimensional structures, much like other subtractive manufacturing approaches, e.g. moulding and milling. A possible alternative is the high-resolution additive manufacturing technique, two photon polymerisation whose free form fabrication ability offers design freedom and flexibility.

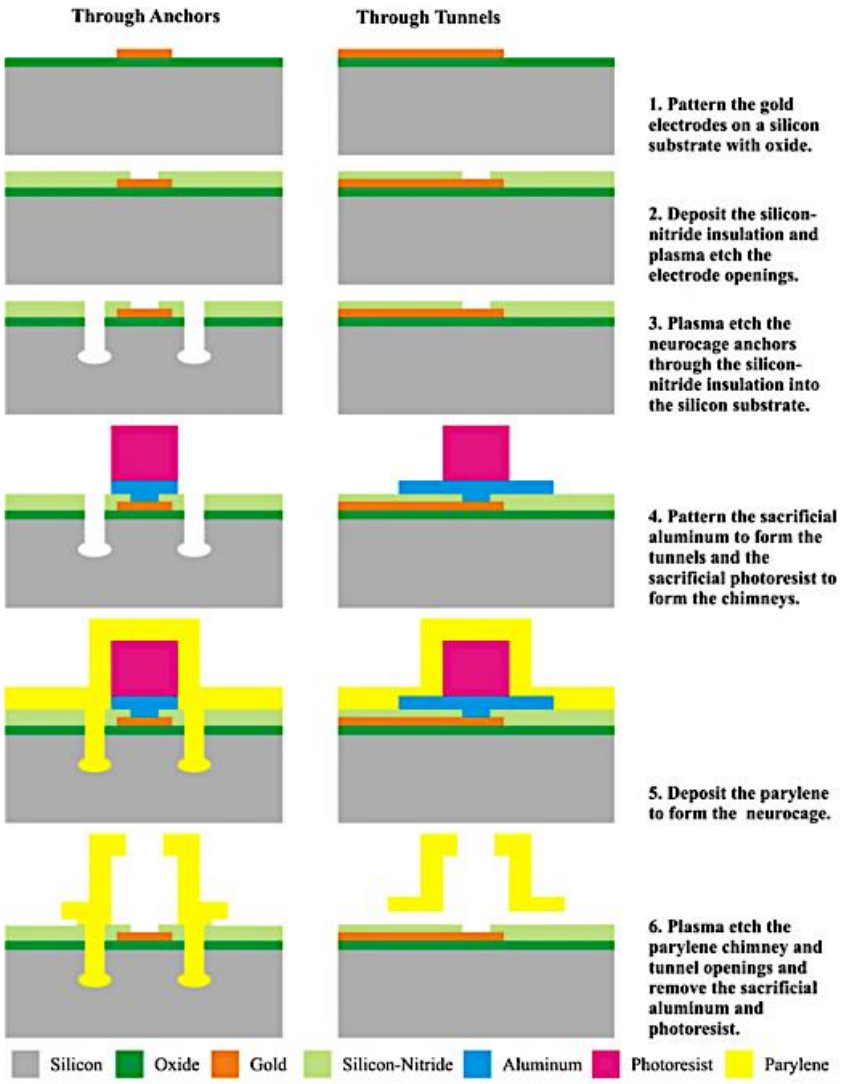


Figure 18 Multistep photolithography for the fabrication of the Neurocage.

Note how the many steps make a single substrate time consuming to fabricate and also how the changing the structure morphology would require adapting multiple steps. [17]

1.6 Patterning Cell Culture using Two Photon Polymerisation.

Additive manufacturing is "the process of joining materials to make objects from three dimensional model data, usually layer upon layer, as opposed to subtractive manufacturing methodologies where material is removed to produce the desired form. One of the most significant advantages of additive manufacture is free form design. As material is built up and not removed the geometry is not dependent on what material is possible to remove. Geometries which would normally take multiple steps to fabricate, such as the Neurocages discussed in the previous section, can more easily be built in a single step using additive manufacturing. Additive manufacturing techniques can still suffer from design restrictions depending on the material used. Producing overhangs sometimes requires the use of a sacrificial support material which is removed after the deposition of material as a secondary step, and as such are susceptible to disadvantages associated with subtractive manufacturing.

E-beam lithography is more flexible than a photolithographic process and does have some three dimensional capabilities although mainly by utilising ablation, a subtractive manufacturing approach. E-beam lithography has a very high resolution limit, in the tens of nanometres, but requires the use of an ultra-high vacuum and is therefore expensive and incompatible with living cells. Inkjet printing [103,104] offers flexible geometries and often ambient conditions, however, its resolution is above the size of a single cell making it useful for coarse patterns but not for patterning cultures at the resolution of single cells or single neurites. Two photon polymerisation is capable of three dimensional freeform fabrication at ambient conditions to two orders of magnitude smaller than a cell, hundreds of nanometres generally, in the XY axes and one order of magnitude smaller in the Z axis[20,105]. The low fabrication speed, limiting total structure size, is a limitation of two photon polymerisation. Recent advances in the application of the technology, introduced by the commercial system Nanoscribe GT (Photonics Professional Ltd), have helped to reduce the obstacle of speed allowing for structures up to several millimetres high to be produced with sub-micron resolution. The approaches implemented by the Nanoscribe GT to quicken the process will be discussed in more depth

in the methodology section of Chapter 3, Optimising the Two Photon Polymerisation of OrmoComp Microstructures.

Two photon polymerisation is a photochemical process, it exploits energy from light to initiate a chemical process. Most photochemical processes, i.e. photosynthesis, fluorescence, free radical photopolymerisation and metal halide photoreduction, require a high energy photon to bump up an electron into an excited state. The electron then either returns to the ground state and releases a photon with lower energy than of the one which had been absorbed, also known as fluorescence, or it undergoes intersystem crossing which probabilistically, depending on the quantum yield, leads to the production of a free radical capable of initiating polymerisation. This phenomenon has been utilised in inkjet printing and stereolithography to solidify a layer of liquid resin through U.V. initiated photopolymerisation. The most similar technique to two photon polymerisation is one photon stereolithography which involves a laser being scanned across the top of a bath of liquid and then lowers the solidified material further into the bath. The U.V. laser then scans again to produce a second layer of polymerised material and the process is repeated to produce a three dimensional structure. Compared to one photon excitation, such as in the case of stereolithography, two photon excitation has a much higher resolution is the excitation is confined to the focal spot not the entire beam (Figure 19).

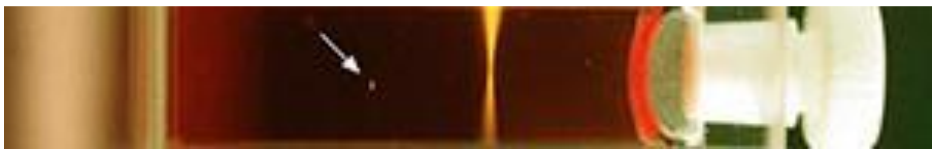


Figure 19 Two photon vs one photon excitation of a fluorophore.

The left-hand spot indicated by the white arrow shows the excitation volume is constrained to the focal spot when using two photon excitation whereas the beam on the right hand is one photon excitation. Image courtesy of Brad Amos.

In 1931 it was predicted in the doctoral thesis of Maria Goeppert-Mayer[106] that two photons at a certain wavelength could cause the same effect as a single photon with half the wavelength (Figure 20). A photochemical process which requires a single ultraviolet photon of 400 nanometres to excite

an electron into an excited state can alternatively be initiated with two near infrared photons with a wavelength of 800nm, this phenomenon is known as two photon absorption. Two photon absorption requires the second photon to arrive before the energy from the first photon has dissipated which requires extremely high intensities of photons to overcome the low probability of such an event. To achieve such a high intensity of photons an ultrafast mode locked laser, e.g. a titanium sapphire laser, and a high numerical aperture objective lens are used to temporally and spatially compress the photons respectively (Figure 20)[107]. It is also necessary for the molecule absorbing the photons to have a high two photon cross section at the wavelength of excitation. The two photon absorption of a molecule is expressed in Goeppert-Mayer (GM or 10^{-50}cm^{4}s photon^{-1}) which describes the product of the two areas available (cm^4) for each photon to arrive at the same time (s) per photon and a scaling factor (10^{-50}) to simplify the values for conventional dyes. The high resolution of the process is due to the induced photochemical reaction being confined to the focal spot of the beam as only this region exceeds the photon intensity threshold of two photon absorption, and the photon intensity decays quadratically from the focal spot sue to the spatial focusing from the high numerical aperture objective lens[107]. The high resolution of two photon absorption has been exploited in fluorescence microscopy as only the dye molecules in the focal volume are excited reducing background excitation. Reducing the background excitation is responsible for unnecessary photo bleaching, phototoxicity and noise associated with background fluorescence (Figure 19).

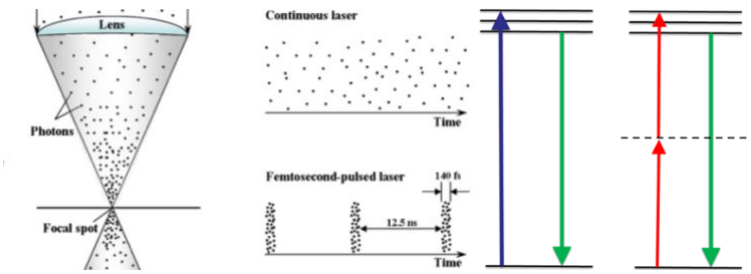


Figure 20. Achieving two photon absorption through the spatial and temporal compression of photons.
Left: Spatial compression of photons using a high numerical aperture lens. Centre: Temporal compression of photons using a mode-locked ultrafast Ti:Sa laser. Right: Jablonski diagram demonstrating one photon vs. two photon absorption [107]

After its prediction in 1931 two photon absorption was initially demonstrated in 1965 with the advent of the laser, by inducing photopolymerisation with multiple photons[108]. Two photon polymerization became a useful microfabrication technique after the invention of mode locked lasers in the 1990s when structures with feature sizes close to the diffraction limit of light were realized[109,110]. Two photon polymerization has been used for biological scaffolds using biocompatible materials, including hydrogels and sol-gels[105,111,112]. The high resolution of two photon polymerisation lends this technique to microstructuring cell scaffold environments for tissue engineering or micropatterning 2D cultures as features an more than an order of magnitude smaller than a cell, <1 micron (Figure 21)[105,113–115]. During a two photon polymerisation build the focal point of laser is translated through the photoresist, exciting a photoinitiator which in turn polymerised the monomer, facilitating a liquid to solid transition. To date, a wide range of polymers have been successfully polymerised using two photon polymerisation such as organically modified ceramics, protein-based biomaterials and several hydrogels[19,113,114,116,117].

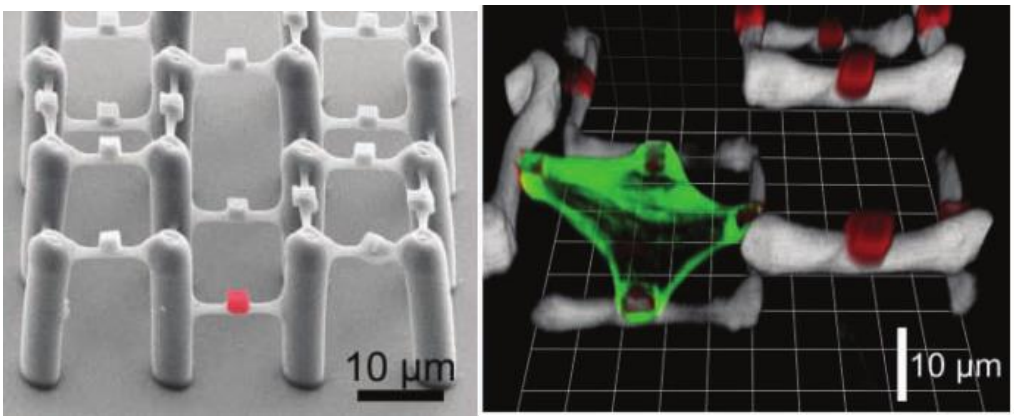


Figure 21 Patterning cells using two photon polymerisation.

Left) OrmoComp microcubes (red) attached to a PEGDa scaffold. Right) Fibroblast adhering to adhesive OrmoComp blocks[111].

The high resolution and ambient processing conditions of two photon polymerisation have seen the technique applied in a variety of tissue engineering contexts, either for producing scaffolds for the production of artificial tissues or for studying the adhesion of cells in a three dimensional space. An early example of two photon polymerisations applications to cell culture was for studying fibroblast adhesion and utilised two materials, OrmoComp, an organically modified ceramic, and polyethylene glycol diacrylate (PEGDA), a hydrophilic polymer capable of forming a hydrogel. The OrmoComp blocks provided adhesion points for the cells whereas the PEGDA microstructures provided a non-adhesive support for the OrmoComp blocks (Figure 21). The technique, in combination with fluorescence microscopy showed how cytoskeletal elements adapt to different distributions of adhesion points. Cells have also been patterned *in situ* using two photon polymerisation. This *in situ* patterning of cells involved encapsulating the cells in a gel and then irradiating the gel with a femtosecond laser to selectively induce photocleavage, photoconjugation or photodegradation[118]. Making such photoconjugation reactions reversible has helped develop the technique into four-dimensional patterning as the patterning can not only be induced in the three dimensions of space but also over time[119].

Several studies have looked at the interaction of two photon polymerised microstructures on the growth of neurons *in vitro*[19,20,96]. The first example showed the potential of the technique to make fiducial fluorescent markers for assisting with microscopy calibration and imaging in the presence of cell culture[96]. A study into the mechanobiology of axons involved culturing cell lines resembling neurons and neuron progenitors on two photon polymerised parallel stripes of OrmoComp (Figure 22)[20]. The neurites grew longer in the presence of the mechanical cues and a greater proportion of the progenitor like SH-SYS5 cells expressed a neuronal marker, microtubule associated protein 2 (MAP2) showing further differentiation towards a neuronal state. The growing axons also deformed ridges which, after quantifying the force required using scanning probe deformation measurements, gave an indication of the strength a growing axon adheres to the substrate[20].

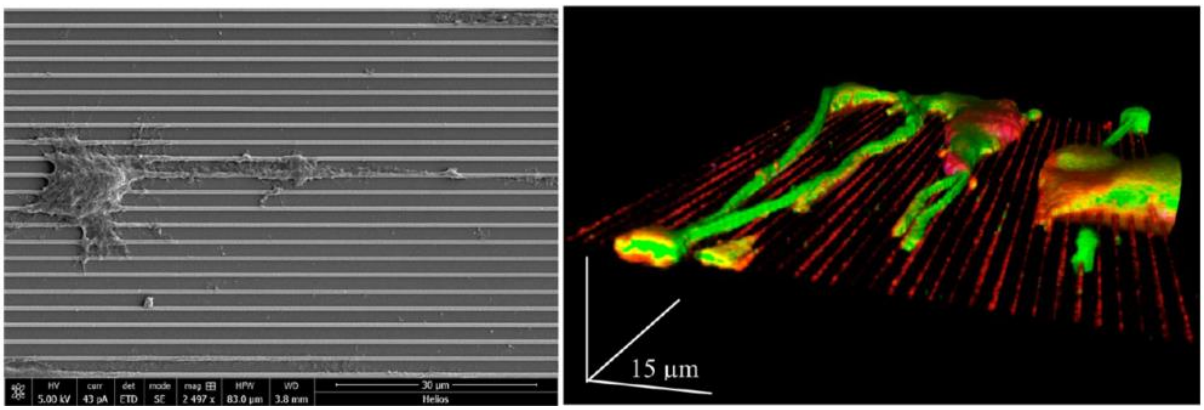


Figure 22 Neuron-like cell line growing on parallel lines produced through two photon polymerisation.

Neuron-like PC12 cells produced more and longer neurites on the patterned substrates than on the control glass[20].

The first attempt at patterning the organisation of a network of neurons with two photon polymerisation utilised a custom built two photon fabrication rig to produce microstructures out of OrmoComp[19]. Structural deformations, during development, primarily due to surface tension and overly slender walls, can be seen in the form of broken walls (Neurocage 4, Figure 23.) The deformation was reduced by replacing the commercial developer, OrmoDev (50:50 vol:vol, Isopropanol: methyl pentanone) with a lower surface tension solvent, hexamethyldisilazane for development. In conjunction with the two photon microstructures a selective surface coating was attempted using a glass micropipette to place a drop of laminin within the microstructure. Some guidance effects are observed with neurites tending to grow parallel to the microstructures however somatic growth appears not to be confined to or even within the structure. The out of focus cell bodies colocalising with the microstructures suggests that the cells preferred to grow on top of the wall as opposed to either side of it, see *Neurocages 1 and 2* (Figure 23). The aggregation of cells visible on day 5 is indicative of a culture which is not adhering well to its substrate and cells preferentially migrate to grow on top their neighbouring cells, Neurocages 1 and 2. The poor cell adhesion suggests that the micro pipetting of laminin used may not be suitable for producing surfaces which strongly promote adhesion for the human mesenchymal stem cell derived neurons used in this study (Figure 23). Additionally, when coated in laminin the mechanical presence of these microstructures alone was not sufficient to restrict the migration of somas. Neurocages 3 and 4 however demonstrate, partially

through their own defects, that a neurite will preferentially grow through a gap and along a walled channel rather than over it. Further experimentation with designs of OrmoComp microstructures may have the potential for patterning neurons at single cell and neurite resolution[19]. This thesis describes the use two photon polymerised OrmoComp microstructures to confine neuronal soma as well as coordinate the growth of their neurites.

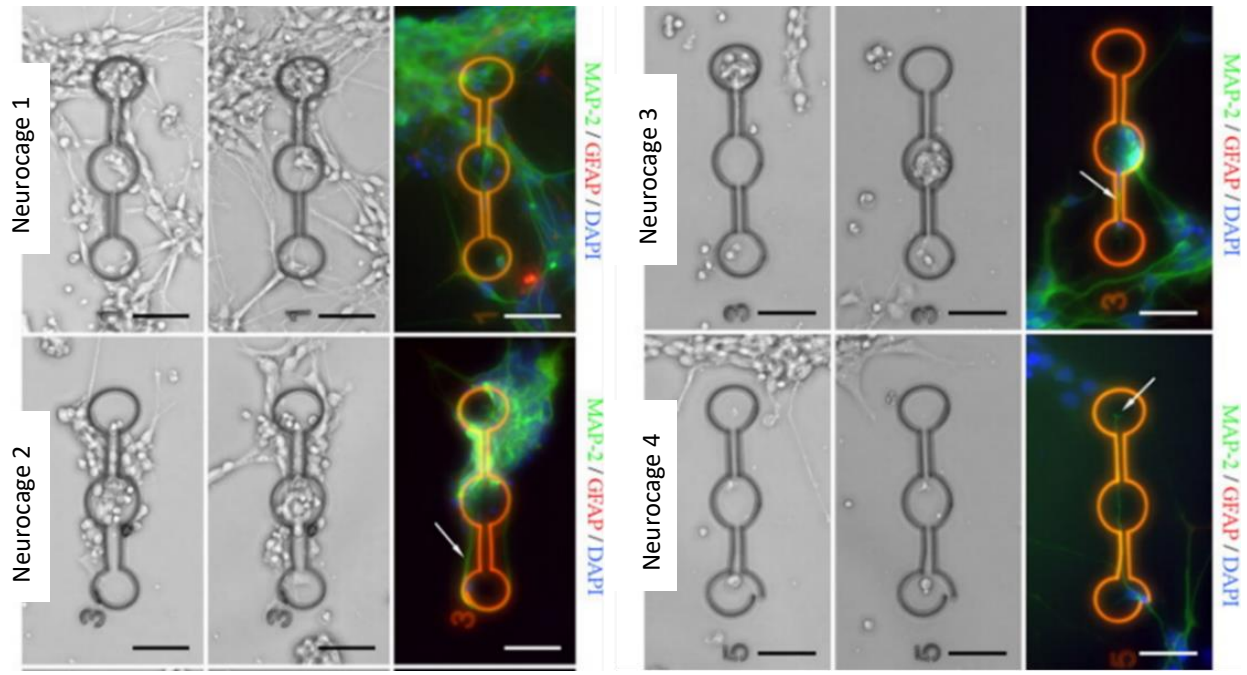


Figure 23. Human embryonic stem cells cultured on two photon polymerised OrmoComp microstructures.

Day 2 and 3 are imaged with bright field and day 5 is imaged with fluorescent immunohistochemically stained of microtubule associated protein 2 (MAP2, Green). Note the heavy aggregation in Neurocages 1 and 2. Note on day 5 in Neurocages 3 and 4 the single neurite passing through the structures central tunnel. Scale bar 50 micron [19]***.***

1.7 Incorporating pH sensors into hydrogels for the production of embedded sensors.

Microstructures can provide more than just mechanical guidance cues to facilitate advancements in biohybrid devices. Cells require a fine-tuned biochemical and physiochemical environment for long term viability and the growth of complex architecture. Being able to maintain the correct physiochemical environments is viewed as a key challenge in the tissue engineering field where diffusion alone is not enough to meet the metabolic demands of a three dimensional construct [120]. The feature and volume size of artificial tissue structures, e.g. vasculature or nerve fascicles, complicates the monitoring of cells *in vitro* using destruction methods or methods which rely on imbedded electrodes. It is therefore useful, not only to neuron biosensors but to the tissue engineering community as a whole, to develop sensors which are embedded within microfabricated growth substrates and capable of non-destructive and non-invasive monitoring of physiochemical variables key to the survival of the *in vitro* neural cultures.

Due to their similarity to biological tissue hydrogels are well suited as *in vitro* cell growth substrates. Hydrogels are hydrophilic polymer networks with water molecules dispersed throughout their polymer lattice, this makes them well suited as both biological growth substrates and as a support matrix for embedded sensors due to the free movement of soluble metabolites or analytes. Hydrogels can be used to detect the concentration of a chemical analyte either directly[121,122] or indirectly where the hydrogel provides the structural support for another molecule which provides the sensory functionality[123]. Direct hydrogel sensors are influenced mechanically by various physiochemical variables, the temperature or the concentration of different ions in their aqueous environment. Measuring this mechanical change, in a controlled environment, will give a signal proportional to the change in analyte concentration. Additionally a hydrogel can be tuned to release encapsulated molecules when a threshold of an environmental variable is exceeded[124]. There are, however, many variables which can impact a hydrogel's mechanical properties making it difficult to make specific measurements with a smart hydrogel in the complex chemical environment of cell culture media.

S*mart* hydrogels have been made more specific by the introduction of crosslinkers which are formed or broken through the binding of a specific chemical. For example specific ion chelators have been used to allow hydrogels to measure the concentration of the ion[121]. However, this approach is limited to one sensory function per gel. Additionally, as the role of hydrogels as guidance cues depends on both mechanical properties, having a sensing modality that alters those properties may be conflicting. Indirect sensing with hydrogels where the hydrogel provides a support for the direct sensory pathway decouples the mechanical and sensory functions of the hydrogel and as such is a much more suitable choice for an embedded sensor which may play both a structural and sensory role and detect/monitor multiple environmental variables.

Indirect sensing with hydrogels can be achieved using the hydrogel as supporting lattice for molecules with sensing capabilities. Fluorophores are molecules which upon excitation with one wavelength of light emit a second photon of a slightly lower energy, and therefore higher wavelength of light. The fluorescent emission intensity of some fluorophores is strongly altered by a particular physiochemical variable, such as temperature or pH. These physiochemically sensitive fluorophores can be used to provide high resolution imaging of a particular physiochemical variable[125,126]. Two dyes with distinctive emission spectra are used in ratiometric sensing, one sensitive to the physiochemical parameter of interest and one insensitive to that physiochemical parameter. The sensitive dye provides a signal proportional to the analyte concentration whilst the other provides a reference signal allowing for normalization of the measurement, preventing the production of an artefact due to heterogeneous dye distribution[125,127]. This ratiometric measurement however requires recalibration for each microstructure, unless the ratio of the two dyes remains fixed. Entrapping such dyes in a matrix prevents excited dyes interacting with cellular components which damages cells and reduces the lifetime of the dye[125].

By entrapping Oregan Green and Fluorescein isethionate dextran (FITC-d), pH sensitive dyes, and 5-(and-6)-carboxyte-tramethylrhodamine (TAMRA-D), a pH insensitive dye, in a matrix of

polyacrylamide, pH sensitive nanosensors have been used to make *in vivo* and *in vitro* measurements (Figure 24) [125]. Nanosensors have been encapsulated in gels in order to increase their biocompatibility and their *in vivo* life time by preventing them reacting with cellular components when in an excited state [123]. By incorporating similar dyes into a hydrogel photoresist compatible with two photon polymerisation this thesis will endeavour to produce microsensors capable of monitoring pH within microfluidic devices. Although the microstructures in this thesis will only be capable of detecting one physiochemical parameter, the fact that multiple dyes will be used to perform ratiometric measurements will provide proof of concept that this approach can produce microstructures capable of incorporating multiple sensory dyes. As multiple sensory dyes can be incorporated and monitored, there is the potential that dyes sensitive to different physiochemical variables could be incorporated into a single microstructure facilitating multimodal sensing.

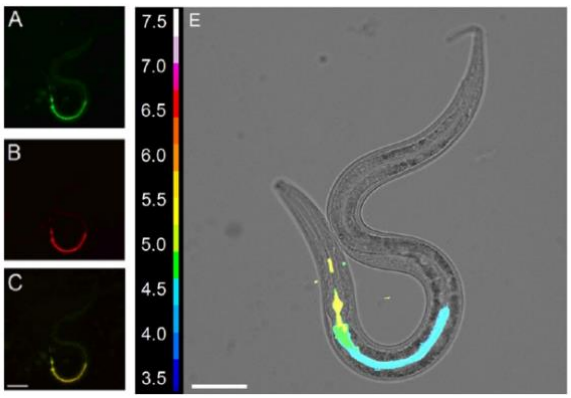


Figure 24 Fluorescent imaging the pH of Caenorhabditis Elegans digestive tract after ingesting pH sesnitve fluorescent Nanoparticles.

Right) The three fluorescent images, (A,B,C) required for the extended range ratiometric sensing, two sensory dyes and one reference dye. Left) Ratiometric image calculated to give a bleaching independent measurement of the pH. Importantly the pH can be measured within a closed microvolume noninvasively[126].

Hydrogels are particularly relevant for sensing in biological contexts as the natural habitat of most adherent cells, such as neurons, is a hydrogel made of fibrous proteins, glycoproteins and saccharides, the extracellular matrix[128]. Naturally derived and synthetic polymers have been used to make hydrogels for cell scaffolds as they have high water content and tissue like elasticity[105,129–131]. The high water content allows diffusion of waste products and nutrients[132,133]. Natural polymers such as chitosan, collagen and fibrin have been used for hydrogel cell scaffolds as they promote cell adhesion and are biodegradable, e.g. they contain metalloprotease cleavage sites[134–136]. Some synthetic polymer hydrogels, such as polyethylene diacrylate (PEGDA), are both non-biodegradable and are non-fouling as well as having tuneable mechanical and chemical composition[134]. Both mechanical and chemical composition have been shown to influence cell function and differentiation[129,137]. The non-degradable nature of PEGDA, its compatibility with two photon polymerisation make it suitable to be the bulk monomer in the formulation of the embedded pH microsensors [116,138]. pH sensitive and pH insensitive fluorophores FAM-D and TAMRA-D were incorporated into a two photon polymerised hydrogel in this thesis in order to produce embedded pH microsensors.

1.8 Thesis Summary

This thesis had four aims, each comprised of several objectives (Figure 25) whose completion would be determined by deliverables, mainly in the form of micrographs or spectra. The Second Chapter details the development of surface treatment protocols to facilitate the adhesion of the *in vitro* neural culture, the first aim of the thesis. The first objective was to develop a surface treatment protocol that ensured the substrates which had undergone the process of producing and developing OrmoComp microstructures were adhesive to neurons. Developing a chemistry which facilitated the adhesion of neurons to gold but not to glass was the second substrate preparation objective. This would be utilised to ensure neurons preferentially adhered to electrode contact pads to optimise the electromagnetic coupling between the electrode and the neuron. The Third Chapter will describe how the aim of optimising the production of OrmoComp microstructures was completed. This initially involved completing the objective of developing a modular design which allowed for rapid redesigning of the structure and high throughput optimisation arrays of processing parameters. The high throughput optimisation arrays allowed for the fastest parameters settings capable of producing a stable structure to be identified, the final objective of this Chapter.

The Fourth Chapter of this thesis covers the characterisation of *in vitro* neural cultures growing in two photon polymerised microstructures of OrmoComp and to test the hypothesis that two photon polymerised structures are well suited as guidance cues for *in vitro* neural cultures. Neurons were seeded onto a substrate supporting a microstructure, first objective of this aim, that was designed to isolate a microculture from the surrounding macroculture, compartmentalise individual somas and guide the growth of neurites between such somatic compartments. The growth of neurons in two photon polymerised microstructure would first be assessed structurally, the second objective of this aim, using phase contrast microscopy, fluorescence microscopy and scanning electron microscopy. The Fourth Chapter also characterised the functional topology of the culture grown in the presence of the two photon polymerised microstructures using calcium imaging.

The Fifth Chapter of this thesis describes the use two photon polymerisation to produce hydrogel microstructures capable of monitoring pH within a microfluidic environment. This final Chapter covers the synthesis of a suitable photoinitiator and its incorporation into a photoresist containing PEGDA and fluorophores to achieve the first objective of using pH sensitive PEGDA microstructures. The next objective was to incorporate the microstructures within a microfluidic device. Neurons were also cultured in the presence of the microstructures to provide an initial indication of the microsensors' biocompatibility and suitability for monitoring neuronal cultures within microfluidic devices.

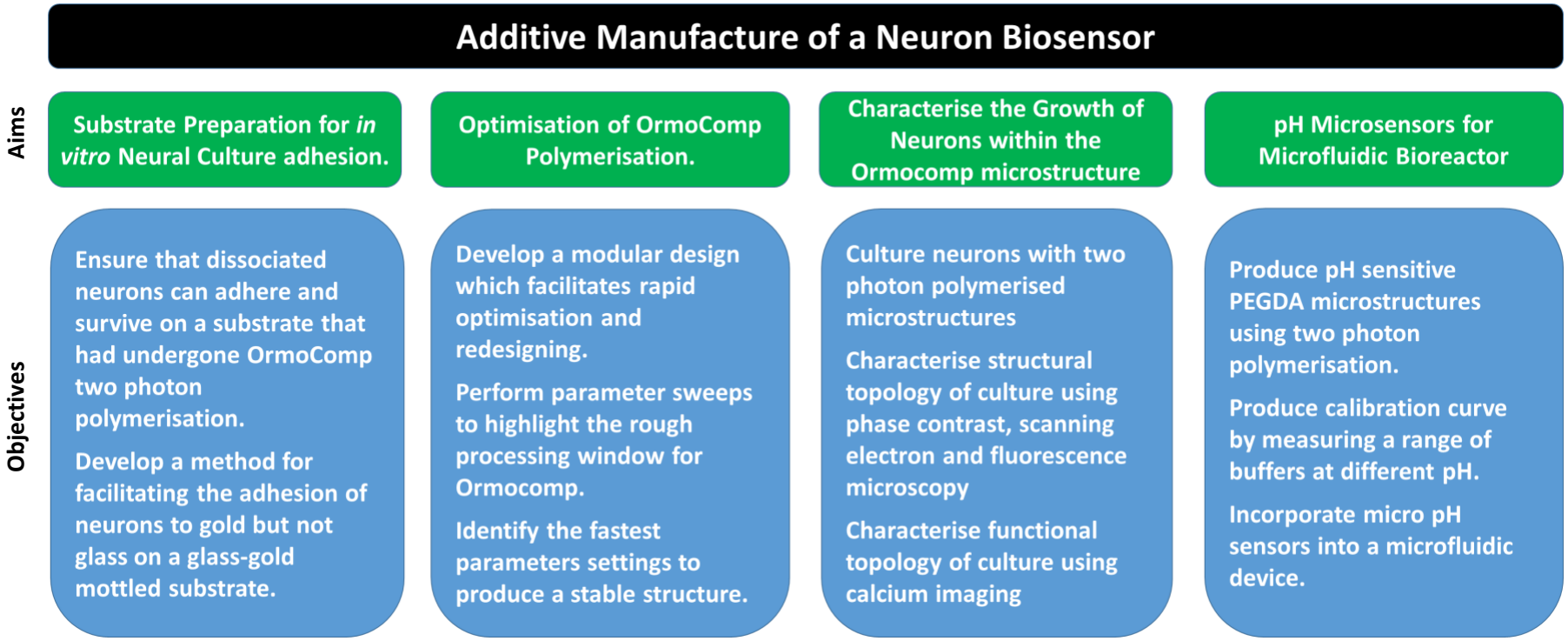


Figure 25 Overview diagram of thesis showing aims and objectives.

2 Substrate treatments for *in vitro* neural culture adhesion.

2.1 Overview

Neurons, as an adherent cell type, must adhere to the substrate surface in order to form a viable culture[36]. Two surface treatment strategies were developed for promoting and coordinating the adhesion of neurons to the surface of the substrate. The first surface treatment strategy was to ensure that the neurons could adhere to glass substrates which had been exposed to the OrmoComp resin and the OrmoDev developer, containing methyl-pentanone and isopropanol. As discussed in the introduction close adhesion of a neuronal soma to the electrode surface is important for monitoring and stimulating neurons. Poor adhesion often leads to the aggregation of neuronal soma, which not only makes it impossible to interface with single neurons but encourages neurons to grow over mechanical guidance cues, such as two photon polymerised microstructures[19]. OrmoComp microstructures were built on glass coverslips using the custom two photon polymerisation rig, which will be described in detail in Chapter 3, on the optimisation of the two-photon polymerisation process. The microstructures were then developed and treated with poly-L-lysine, a polymer with cationic pendent side groups. Neurons were then cultured on the substrates and the response of the neurons to the substrate was characterised using phase contrast microscopy. This process was then repeated with variations to the development process until closer adhesion and increased viability were observed.

The second substrate treatment strategy aimed to promote selective adhesion of neurons to gold over glass, with the aim of selectively promoting adhesion to the gold contact pads of a microelectrode array. Primarily this was to ensure close contact of the neurons to the microelectrodes in the array. This strategy was also to augment the patterning influence of the microstructures by leaving them non-adhesive by not treating them with any adhesion promoting coating. The tripeptide moiety arginine glycine aspartate (RGD), from the cell adhesion protein fibronectin, was used as the adhesion promoting molecule. RGD is one of the key molecules involved in cell adhesion *in vivo* and has been

utilised *in vitro* in a variety of contexts [139–142]. A cyclic variation of the RGD molecule (cRGD) was used as it has been shown to promote adhesion *in vitro* more effectively than a linear version of the molecule, theoretically due to its closer mirroring of the motif's native state[140,143]. By using a peptide motif which not only contained the cRGD sequence but also a cysteine molecule it was hypothesised that the thiol group of the cysteine would bind to a solvent cleaned gold surface. Gold and glass mottled substrates were produced by sputter coating a glass coverslip that had been patterned with a photoresist. To ascertain if the cRGD molecule had selectively bound to the gold surface Time of Flight Secondary Ion Mass Spectroscopy (ToF-SIMS) was used. The spectra from the gold and glass regions of the substrate were compared for the presence of daughter ions which were representative of the amino acids in the cRGD moiety. Once it was confirmed that the cRGD had selectively bound to the gold regions of the substrate, neurons were cultured on substrates which had undergone the same treatment. Phase contrast analysis of the cultures showed poor cell adhesion to the glass regions compared to the gold regions suggesting the selective promotion of cell adhesion using a cysteine containing cRGD moiety had been successful.

2.2 Methodology

2.2.1 Two Photon Polymerisation

A key requirement of a two photon polymerisation rig is being able to create a photon intensity that exceeds the threshold of two photon absorption in a molecule capable of, once excited, initiating a polymerisation reaction. This is achieved by temporally compressing photons in time using a mode-locked laser which releases its energy in pulses and spatially compressing photons using a high numerical aperture objective lens. The laser and the objective lens represent the beginning and end of the fixed optical apparatus. After exciting the laser aperture, the beam is first expanded to fill the back of the objective lens to maximise the spatial focusing and therefore the photon intensity at the focal spot and subsequently the resolution. After expansion, the beam then passes through a variable neutral density filter to attenuate the power of the laser. A high-speed shutter controls whether the

sample is being exposed to the laser beam. If let through the shutter, the beam is then focused by the microscope objective lens and subsequently passes through immersion oil and a glass coverslip before reaching the sample. The oil and the coverslip's refractive index are matched to the objective lens to minimise the loss of spatial frequencies due to diffraction of photons when passing across a refractive index interface.

2.2.2 Neural cell culture

Primary neuron progenitors were dissociated from embryonic rat hippocampi as it is a region well studied for its role in learning and memory consolidation through structural and functional plasticity as well as being extensively grown *in vitro*. Cells were collected at embryonic stage 18 as at this stage most proliferation has occurred, so there is the maximum number of cells to be harvested per embryo, but differentiation into glial lineages is still minimal[144]. The cells were dissociated both through enzymatic digestion of their extracellular matrix and mechanically by pipetting the material repeatedly. After dissociation, the cells are plated on adhesion coated glass coverslips which presented amino groups which are commonly found in the active motifs of cell adhesion proteins and facilitate the adhesion of proteins in a native conformation[87]. Once adhered to the substrate the cells differentiate into a co-culture of neurons and various glia, prominently astrocytes. The neurons begin to extend neurites and then over the following week begin to form synapses and start firing action potentials[36]. All the neural cells begin secreting extracellular matrix molecules over the first few days[145]. After 14 days a culture, with approximately 100,000 cells per millimetre squared, will be electrically active and therefore ready for electrophysiological analysis.

2.2.3 Time of flight secondary ion mass spectroscopy

A beam of primary ions, in this case bismuth, was used to dislodge and sputter secondary ions from species on the surface (Figure 26). Both positive and negative secondary ions are sputtered, each of which were detected separately. Sputtered secondary daughter ions are then accelerated towards a mass analyser where they arrive at different time intervals, depending on their charge to mass ratio,

producing a mass spectrum (Figure 26). By analysing the combination of different fragments, daughter ions, it is possible to infer information pertaining to the molecular composition of the surface. ToF-SIMS therefore can be used to confirm if the correct molecules have been deposited in the right place, especially as this technique has lateral resolution of <100 nanometre and depth resolution of <1 nanometre. It can also help determine the location and composition of any contaminants on the surface. Daughter ions previously associated with the amino acids contained in the cRGD molecule were used to identify the presence and localisation of the peptide on the surface[146]. The localisation of the peptide was then compared to the localisation of both glass and gold signals to determine whether the peptide had preferentially adsorbed to the gold.

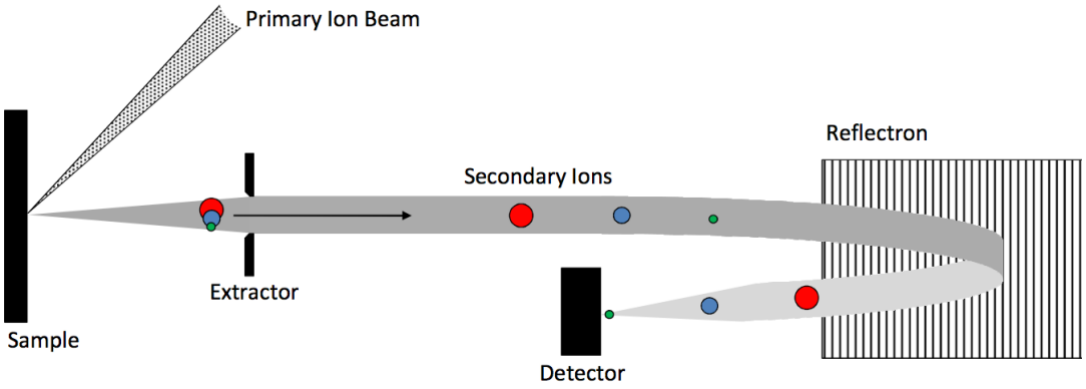


Figure 26 Schematic of time of flight secondary ion mass analyser.

A high energy ion beam, the primary beam, sputters fragment ions from the sample. The fragments then pass through a field free drift tube which separates the ions based on their velocity, as a function of their charge to mass ratio. Red, blue green represent ions of increasing charge to mass ratio. [147]**.**

2.3 Experimental

2.3.1 Two photon polymerisation using the custom built rig

The custom rig used the sandwich configuration of two photon polymerisation, for a more detailed discussion of the merits of this configuration see Chapter 3 on the optimisation of two photon polymerisation of OrmoComp microstructures. The sample sandwich is constructed by attaching a bespoke inkjet printed coverslip holder to a glass microscope slide using adhesive tape. To clean the coverslip, it was rinsed with acetone and then isopropanol and subsequently dried with a nitrogen

stream to ensure that no residue is left on the surface. The cleaned coverslip was then placed into the coverslip holder. A bespoke inkjet printed 180 micron thick spacer which lines the edge of the coverslip holder cavity was placed on top of the coverslip. A small drop (~20-40 microlitres) of OrmoComp resin was then placed in the centre of the coverslip and a second coverslip placed on top of the spacer as lid. The second coverslip was then secured using adhesive tape. The sample sandwich was placed on the hotplate at 80 degrees Celsius for two minutes to relax the intermolecular forces of the photoresist, facilitating the wetting of the sample and efficient diffusion-mediated photopolymerization. The sample sandwich was then fixed onto the piezoelectric stage by three screws that threaded through the bespoke coverslip holder. A drop of immersion oil was placed on top of the coverslip and the microscope objective lowered into the immersion oil using the manually operated dial. For both the automatic and manual use of the rig the power was set to 30 milliwatts, and the translation speed of the stage was set at 60 micrometre per second. For the manual use of the machine the shutter was manually operated whilst the piezoelectric stage was set to translate a set distance. For the automated use of the custom rig a binary image was loaded into the LabView software developed by Meisam Askari. Each black pixel in the binary image was then exposed point by point by opening or closing of the shutter at each coordinate in the image. The shutter speed was set to 400 milliseconds for each exposure and the step size of the piezoelectric stage set to 1 micron. Post-exposure the sample was placed on a hotplate at 130 degrees Celsius for 2 minutes to improve the solubility of the uncured resin in the OrmoDev developer. The sample sandwich was then carefully dismantled, and the sample placed into 10 millilitres of the OrmoDev developer for 2-3 minutes. The sample was then rinsed in isopropanol and dried with a nitrogen stream. For the final hard bake, which cures any uncured photoresist, the sample is placed onto the hotplate for another 3 hours at 130 degrees Celsius.

2.3.2 Preparing substrates for cell seeding

After the samples had been developed, they were taken from the hotplate directly to the laminar flow cell culture hood, in order to maintain sterility. Each coverslip was then placed in a well in a six well plate (Thermofisher). 500 micolitre of Poly-l-lysine (PLL) (Sigma) was then deposited onto each substrate. For structures with high aspect ratio wells air pockets would often be trapped within the structure preventing the deposition of the PLL on the surface within the microstructure. To remove the air bubbles the well plate was placed in a plastic airtight chamber attached to a vacuum pump. The pump was then turned on to reduce the pressure within the chamber causing the trapped air to swell into larger bubbles and escape into the surrounding chamber over a period of about fifteen minutes. The substrates were then removed from the airtight chamber and left in the PLL solution for an hour. Most of the PLL was then pipetted off and the whole well washed three times with two millilitres of distilled and autoclaved water. In order to completely dry the substrates, the lid of the well plate was left ajar and the well plate was left at the back of the laminar flow hood overnight. The PLL was thoroughly washed away as unbound PLL is toxic to the cells.

2.3.3 Seeding of rat hippocampal cultures on substrates

All disassociation and dissection of rat hippocampi was performed by Mrs Dhurma Thakker. The primary neural cultures were isolated from E18 rat foetuses, the hippocampus and cortex were removed and enzymatically dissociated separately in 2 millilitres of 20mM 2-[4-(2-hydroxyethyl) piperazin-1-yl] ethane sulfonic acid buffered Hanks balanced salt solution containing 200 microlitre of 1 percent trypsin and 20 microlitres of 0.5 percent DNAse at 37 degrees Celsius. Foetal bovine serum dissolved in Eagle's Basal Medium was used to inactivate the trypsin, due to the naturally occurring protease inhibitors. Mechanical dissociation was performed using a flame-polished Pasteur pipette by gently triturating the tissue in the presence of DNAse. The dissociated cells were then pelleted in a centrifuge for 5 minutes at 1200 rounds per minute. 10 millilitres of B27 supplement was then added to 475 millilitres of neurobasal culture medium and 0.5mM glutamine (Sigma). The pellet was then re-

suspended in the serum free Neurobasal media containing the B27 supplement. The cell concentration of the suspension was calculated using a haemocytometer. A haemocytometer works by placing 1 microlitre of cell suspension on the entry hole of the haemocytometer and then, under a microscope at 10x magnification, the number of cells in contained in the grid inside the haemocytometer is counted. The number of cells is present is the same as the number of cells in 1 microlitre and as such the concentration of the cell suspension has been calculated and any necessary dilutions can be calculated and made. To produce a culture with 100,000 cells per millimetre squared the suspension was diluted to a concentration of 300,000 cells per millilitre. 750 microlitres of this solution was then pipetted onto each substrate and left to adhere for thirty minutes. After thirty minutes the majority of cells had adhered, and the well was flooded with an additional 1250 microlitres of Neurobasal and B27 media. The cultures were then stored in a 5 percent humidified CO_2 atmosphere at 37 degrees Celsius except when being imaged with phase contrast microscopy when they were briefly kept at ambient atmospheric conditions.

2.3.4 Time of flight secondary ion mass spectroscopy

The time of flight secondary ion mass spectroscopy (ToF-SIMS) measurement was performed by either Dr David Scurr or Dr Adam Celiz using a TOF-SIMS IV (ION-TOF GMBH). The primary ion source was operated in high current bunched mode with a pulse width of 10.2 nanoseconds and was composed of Bismuth (+3) ions. To compensate charging of the surface the sample was showered with low energy electrons by an electron flood gun. Analysis was performed using ION-MEASURE software. The spectra were calibrated to small hydrocarbon ions and salts, e.g. CH^+ and NA^+, the cRGD molecule was localised and identified by the presence of daughter fragments associated with the cRGD's constituent amino acids.

2.4 Results

2.4.1 Optimisation of OrmoComp development protocol to support neural cell adhesion

The first objective of this chapter was to ensure neurons could adhere to and survive on a substrate which had undergone the processes required to produce two photon polymerised microstructures, primarily exposure to the photoresist and the developer. The microstructures were produced out of OrmoComp using the custom built two photon polymerisation rig. The first structures produced on this rig used the automation software developed by Meisam Askari (Figure 27) the point-by-point exposure used by this software meant an overnight build was required to produce a structure only one layer high. To speed up the process and produce the multiple samples required for cell culture, samples were produced through manual operation of the rig.

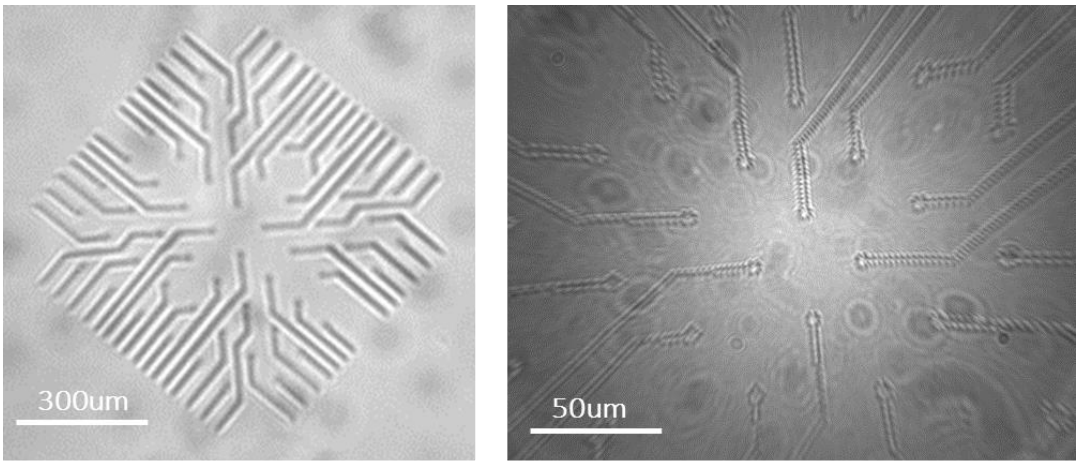


Figure 27 Optical Micrograph of a multielectrode array outline fabricated using the two photon polymerization custom rig in automatic mode.

Left) Micrograph of whole OrmoComp microstructure taken pre-development on a glass substrate built on the custom rig. (10x magnification) Right) view of microstructure through the objective used for fabrication, the live feed, also pre-development. (100x magnification).

After the sample was developed it was coated in poly-l-lysine (PLL), see experimental section above. The structures were approximately two micron high and 500 nanometres wide. All substrates which had undergone two photon polymerisation showed greatly reduced neuronal adhesion with only very few cells adhering (Figure 28). Some cells that did adhere however were found to be in close proximity to the OrmoComp microstructures (Figure 28), suggesting that it was not the presence of the

microstructures themselves which were the source of the poor adhesion. Some neurites were observed growing in parallel to the microstructures, along straight edges and around corners, as well as squeezing, almost imperceptibly through small gaps at the junction of two OrmoComp walls. Interacting with the structures in this way suggested that the microstructures have the potential to guide the cultures growth as mechanical guidance cures. There is a distinction between a culture which adheres to the substrate and later dies and a culture which does not adhere in the first place. When a culture is unable to adhere to a substrate, very few cells will be on the surface and the majority will be floating within the cell media. The lack of cells on the substrates with two photon polymerised microstructures suggests a surface contaminant had interfered with the deposition of the cell adhesive coating PLL.

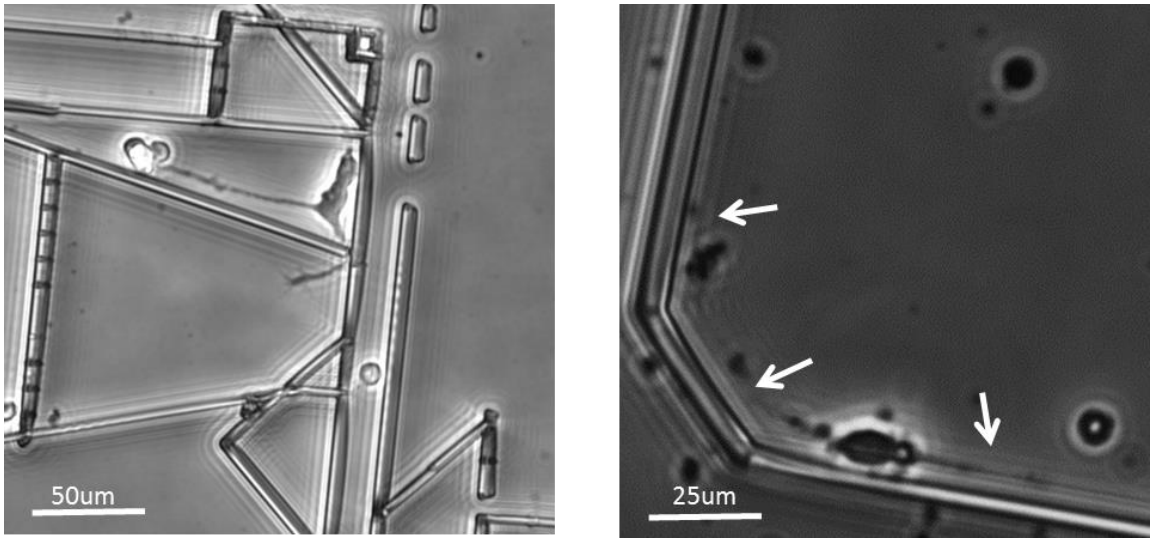


Figure 28 Primary hippocampal culture after two days in vitro grown in the presence of OrmoComp microstructures developed with original protocol from Microchem ltd.

Notice the lack of adhered cells in both images but how the cells which have adhered grow in close proximity to the microstructures. In the left image it can be seen that a neurite with a large growth cone has passed through an almost imperceptible gap in the microstructure wall. In the right image it is just possible to make out, although slightly obscured by the microstructures halo, the neurites running parallel to the microstructure

The poor of adhesion of the neurons suggests that the process of producing and developing the OrmoComp microstructure had prevented the adhesion of neurons to the surface. As the PLL surface

treatment was successful on control glass which had not undergone exposure to OrmoComp it could suggest that residual OrmoComp or developer may be present on the substrate and interfere with the PLL coating and the subsequent neuronal adhesion. This was also prompted by the presence of a visible watermark at the edges of the substrate. To investigate if a more thorough development process could improve the adhesion of the neurons to the substrate the number of washes and rinses in both the developer, OrmoDev, and isopropanol were increased from once, as sighted in the materials protocol, to thrice, a number of washes routinely used to increase the thoroughness of rinsing e.g. in immunohistochemistry.

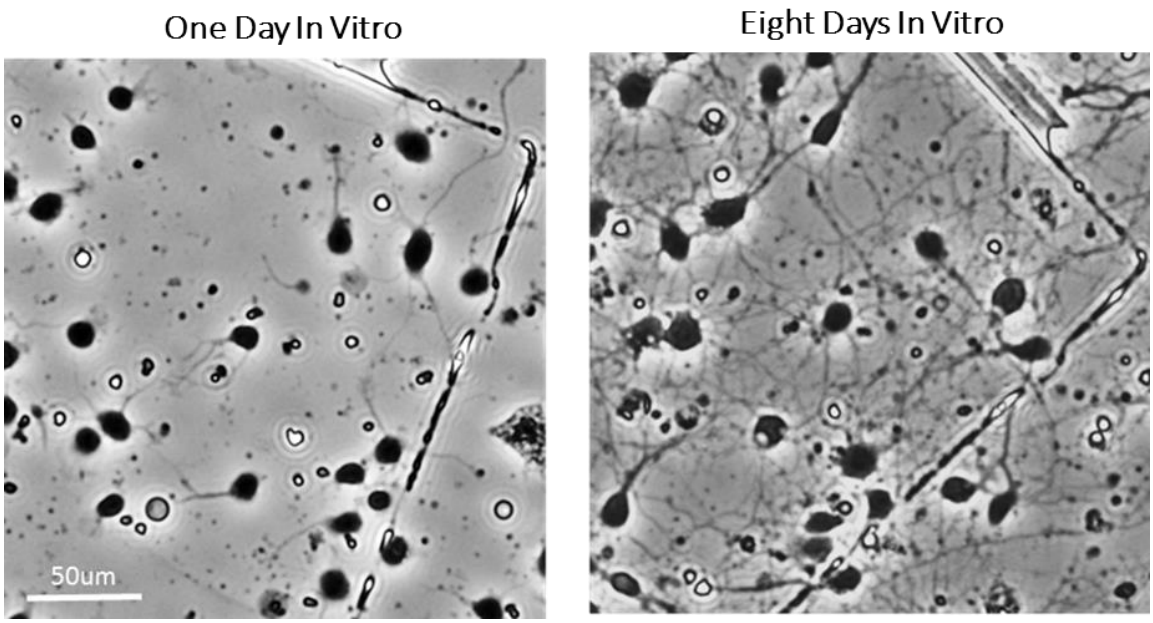


Figure 29 Primary hippocampal neural culture adhering to an OrmoComp modified substrate developed with optimised protocol.

Many neurons adhere to the substrate in comparison to the initial attempts (Figure 28) although there is numerous dead cells, visible as white specks smaller than the black viable cells. Note similar phenomenon of neurites preferentially growing through gaps in the two photon polymerised microstructure.

Increasing the repetitions of the development process increased the cell adhesion to the substrate. This allowed for the culture to survive for longer, up to a month, and to observe neurites preferentially growing through the gaps in the microstructure, an observation used to inform later designs. A large number of dead cells can be seen, visible as small white specks, suggesting a toxic effect of the

OrmoComp microfabrication process. As proximity to the microstructures did not correlate with cell viability it was theorised that the toxic factor in question was soluble, potentially a residue from the developer. To test if the viability could be improved by removing toxic residues from the substrate the 3 hour hard bake at 150 degrees Celsius, normally for finalising any remaining crosslinking, was increased to overnight at the same temperature. The new development procedure decreased the number of dead cells allowing neural cultures to grow on a variety of designs, see Chapter Four.

2.4.2 Selective adhesion of neurons on gold and not glass.

The second aim of the substrate treatment Chapter of this thesis was to use a coating which selectively promoted the adhesion of neurons to gold but not glass. A glass and gold, approximately 100 nanometre thick, mottled substrate produced using photolithography was solvent cleaned and then immersed for three hours in a solution of cyclic Arginine-Glycine-Aspartate-Phenylalanine-Cysteine (cRGDfC) and distilled water solution. cRGDfC contains the cell adhesion motif cRGD from the extracellular matrix protein fibronectin and also a thiol containing cysteine residue which facilitates preferential adsorption to gold[141,148] To assess if the cRGDfC had selectively bound to the gold and not the glass the sample was analysed using TOF-SIMS. The peaks for ionized silicon and gold identified the surface as glass and gold respectively (Figure 30). The regions of the intensity image which had a high intensity for either gold or glass were then demarked as regions of interest. The contrast in the intensity of certain ions between the gold and glass regions is an indication of a molecule preferentially binding to one material over the other.

Specific ion fragments, some of which are listed in Figure 30, have previously been identified as daughter fragments from specific amino acids and therefore markers of the presence of those amino acids[146]. The ion intensity of the fragment ions that indicate the presence of the amino acids which make up the cRGDfC peptide moiety were compared between the glass and gold regions of interest. Any individual one of these ions would be not necessarily be clear indication of the presence of the cRGDfC molecule as other molecules may fragment into similar sized daughter ions as those used as

markers for specific amino acids. Identifying a marker for some of the amino acids in the cRGDfC chain increases the probability that their spatial distribution is representative of the cRGDfC molecule itself. All the ion fragments markers for the cRGDfC molecule had a higher intensity in the gold region of the substrate than in the glass region, demonstrated by both the ion intensity images (Figure 30, next page). These findings suggest that the cRGDfC preferentially bound to the gold instead of the glass, as hypothesised would happen due to the presence of the thiol group in the cysteine molecule.

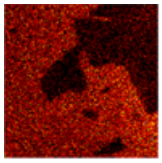
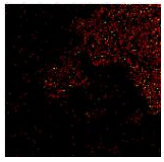
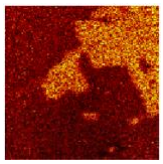
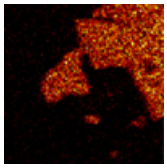
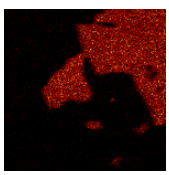
Positive Ions	Parent Material	Ion Intensity Image	Normalized Ion intensity ($x10^{-5}$)		
			Whole Sample	Gold region	Glass region
Si	**Glass**		326	78	4667
Au	**Gold**		19	33	5
CH_4N	**Glycine**		192	5976	382
CH_3N_2	**Arginine**		201	3127	460
CHS	**Cysteine**		949	1053	942
$C_3H_6NO_2$	**Aspartate**		1397	314	22
$C_8H_{10}N$	**Phenyl-alanine**		171	936	-

Figure 30 Ion intensities of cRGDfC treated glass and gold substrate for both the gold coated and uncoated regions of the substrate. Normalised to total ion intensity.

As the ToF-SIMs results had indicated that the cRGDfC had preferentially bound to the gold regions of the substrate, more samples were produced for assessing their influence on the growth of neural cultures. The samples were sterilised and seeded, as described above in the experimental section of this Chapter, and the growth of the resultant cultures monitored using phase contrast microscopy. After one day *in vitro* there appeared to be slightly more aggregation on the glass than the gold but not a dramatic or overt distinction (Figure 31, top image, next page). The contrast between the two surfaces became more clearly apparent after six days *in vitro* when virtually all cells on the glass had aggregated into tight clumps whilst all the cells on the gold remained more evenly distributed despite some aggregation (Figure 31, Bottom). The white grainy appearance of the aggregates on the glass after six days *in vitro* suggest the majority of the cells in the aggregate have undergone cell death. The cells on the gold, despite some aggregation, retain a solid dark appearance in the phase contrast micrographs indicating viable cells adhering well to the gold substrate, suggesting it was successfully coated in cRGDfC.

The ToF-SIMS data indicated that the cRGDfC had selectively bound to the gold regions of the substrate and the neurons also bound preferentially to this region suggesting the substrate selective surface coating is an effective method of patterning the adhesion of neurons. The aggregation visible on the gold surface will be likely to increase as the culture matures and is an issue to address if this strategy is to be utilised as an approach for preferentially promoting adhesion to gold contact pads on microelectrode arrays. The optimisation of the OrmoComp development protocol successfully facilitated the adhesion of neurons to substrates functionalised with OrmoComp microstructures.

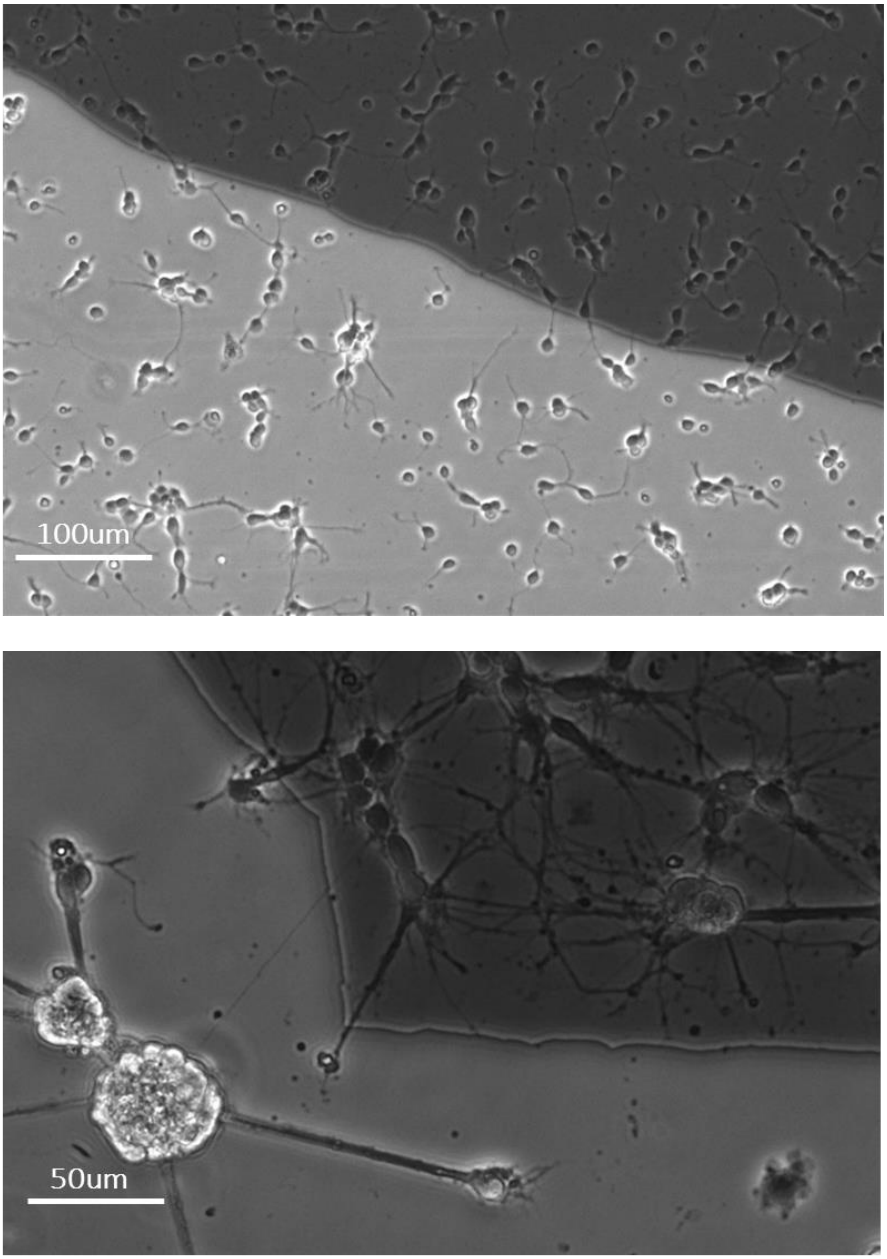


Figure 31 Phase contrast micrographs of neural culture on glass and gold substrates treated with cRGDfC.

Top) After one day in vitro the neurons on the glass and gold appeared relatively similar with slightly more aggregation visible on the glass (10x magnification). Bottom) After six days in vitro the neurons on the glass have formed a tight aggregate with several thick fascicles leading to other aggregates. The neurons growing on the gold although showing some signs of aggregation have a more even distribution with a significantly more surface coverage of neurites than on the gold. The white, grainy appearance of the aggregates on the glass is also in sharp contrast to the darker solid appearance of the neurons growing on the gold. The white and grainy appearance is indicative of cell death whereas the dark and solid appearances is associated with healthy cells adhering well to surface (20x magnification).

2.5 Discussion

In this section two substrate treatment protocols were developed for promoting neuronal adhesion. The first protocol that was developed enabled neurons to adhere to a substrate that had been functionalised with two photon polymerised microstructures, an essential step in characterising the growth of neurons in response to such structures, see Chapter 4. The second protocol selectively promoted adhesion on to gold opposed to glace surfaces and as such could be used to promote the growth of neuronal soma onto gold electrode pads.

Close adhesion of neurons to the substrate surface is necessary for close electromagnetic coupling between the neurons and for the efficacy of contact guidance cues on the growth of neurons. To ensure a microstructured substrate could support the close substrate adhesion and viability of an *in vitro* neural culture a substrate treatment protocol was developed, see experimental section of this Chapter. To improve the initially poor cell adhesion to the substrate, iterations of the post-development protocol were performed with varying extents of washing and baking steps. Increasing the washing and baking steps of the development treatment improved adhesion and viability of the cell cultures to a comparable level with control cultures. This development protocol was facilitated the growth and characterisation of neurons in the presence of microstructures in Chapter Four.

As discussed in the introduction, patterning chemicals on a substrate surface has been used as a way of coordinating the growth of neurons, combining this with contact guidance may allow for greater control than a single technique. A protocol was developed to selectively promote the growth of neurons on gold instead of glass or OrmoComp microstructures. Promoting the growth on gold was to ensure the neuronal soma would attach to the electrode pads and enhance the microstructures guiding influence by presenting both a mechanical and a chemical obstacle. The selective functionalisation was performed by using a thiolated variation of the cell adhesion peptide moiety cRGD. To assess whether the cRGD bound selectively to the glass a mottled gold and glass substrate which had been exposed to the cRGD was analysed using TOF-SIMS. Fragments relating to cRGD

colocalised with the gold (Figure 30) suggesting the selective functionalised was successful. Culturing neurons revealed preferential adherence to the cRGD functionalised gold over the surrounding glass Figure 31) suggesting the selective functionalisation was an effective method for selectively promoting the adhesion of neurons on gold electrodes.

As initially the adhesion of the culture was very low the number of washes performed in the development of the resist, of both the developer solution (OrmoDev) and the rinse solution (isopropanol) was greatly increased. The increased washes successfully improved cell adhesion suggesting that the poor adhesion had been due to residual resist or developer residue being left on the substrate. Despite the increase in adhesion many dead cells, visible as small white dots in the phase contrast images, were present (Figure 29). The viability of cultures seeded on the microstructured substrates was improved by increasing the hard baking step from three hours to overnight, potentially due to the removal of toxic residues. This step also allowed for simultaneous sterilisation of the substrate. Even if a culture adheres enough to survive, poor adhesion can encourage cell aggregation and neurite fasciculation, both of which can be deleterious to the effects of mechanical guidance cues[19]. Aggregates give greater Z height and encourage the cells to ignore mechanical guidance cues such as can be observed by a previous attempt at patterning neurons using two photon polymerised microstructures of OrmoComp (Figure 32)[19].

A protocol for selectively promoting neuron adhesion on gold rather than glass is presented here as a method for ensuring close coupling between the neuron soma and the electrode contact pad. A protocol which improves the adhesion of neurons to the substrate surface of OrmoComp functionalised substrates was also developed. As the adhesion of neurons to the surface is also key to them recognising mechanical cues improving the adhesion of neurons in the presence of OrmoComp microstructures is an advancement of the state of art in patterning neurons *in vitro* (Figure 32).

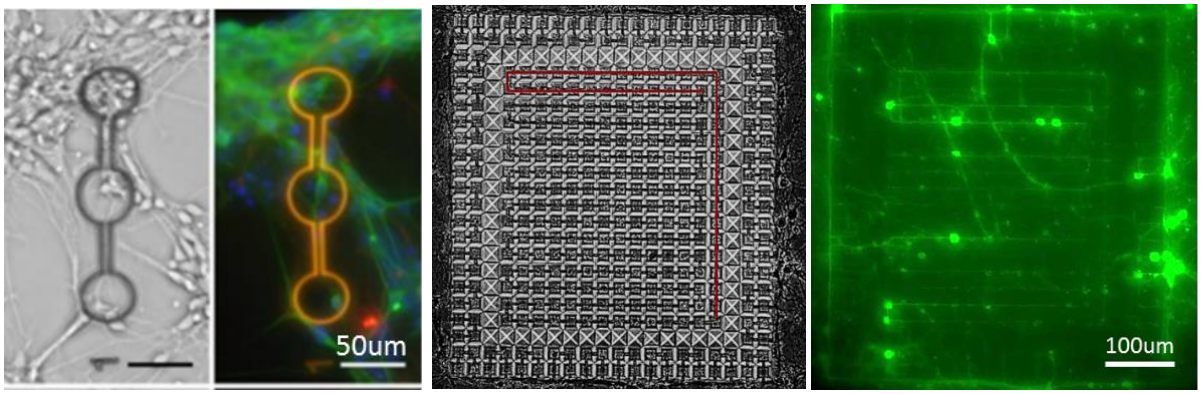


Figure 32 Comparison of the state of art in patterning neurons using two-photon polymerisation.
Left: Phase contrast and fluorescent micrographs of human embryonic stem cell derived neurons culture in the presence of OrmoComp microstructures. The Microstructures were built using an in house two photon rig and treated with a droplet of aqueous laminin to promote adhesion. Note how the human embryonic stem cell derived neural culture primarily disregards the presence of the microstructures and the cells form large aggregates[19]. Right: Phase contrast and fluorescent micrographs of rat primary hippocampal rat neurons cultured in the presence of OrmoComp microstructures built using a Nanoscribe GT and treated with Poly-L-lysine to promote adhesion. Note how there is less aggregation, particular in within the structure and how the majority of the neurites follow the track laid out by the channels in the microstructure. The microstructure produced in this thesis also span a much larger area than the previous attempt.

Close adhesion of neuronal soma to the electrode pads is essential when monitoring the initiation of action potentials as well as ensuring all neurons in the network are being monitored. Recording action potentials from all the neurons connected to the neural network is necessary for investigating neural network dynamics as discussed in the introduction of this thesis. This Chapter aimed to selectively promote the adhesion of neurons to gold electrodes over the silicon oxide insulator. Gold electrodes on a silicon oxide or glass substrate offers a clear material distinction between the electrodes and the surrounding area. Using a molecule with high affinity binding to gold, in this case a thiol, makes it possible to bind a molecules selectively to the gold and not the surrounding non-gold substrate. Having a cell adhesion peptide attached to the gold selective group allows the gold to be selectively coated with cell adhesion promoting molecules. A thiolated cRGD peptide moiety was used to selectively coat the gold regions on a glass substrate mottled with a gold thin film coating. The selective coating of the gold was confirmed using TOF-SIMS analysis demonstrating co-localisation of the gold and daughter ions corresponding to the range of amino acids present in the cRGD (Figure

30)[146]. Neurons cultured on the selectively coated substrates demonstrated preferential adhesion on the gold surfaces with the few neurons which did successfully adhere to the formed aggregates and fascicles over the first days in culture, this is generally associated with poor adherence to surface due to lack of a positively charged surface or the lack of cell adhesion promoting peptides or proteins. The simple immersion of a glass and gold substrate in water-based solution of cRGDfC allowed for the gold specific adhesion of neurons cultured *in vitro* based on the selective adhesion of the thiolated cRGDfC binding to the gold as confirmed by TOF-SIMS.

The simplicity of this substrate-selective coating is due to the use of the pre-defined pattern of the gold on the glass to pattern the adhesion chemicals, removing the need for photolithography to define the chemical micropattern as many previous attempts at producing high resolution *in vitro* neuronal pattern have required[10,11,94]. The use of substrate selective molecules to pattern the adhesion of neurons does, however, lack the ability to pattern the growth of neurites between electrode pads as this would lead to the contact pads being linked by the conductive gold tracks, effectively shorting the circuit and rendering them unable of detecting action potentials. To pattern the growth of neurites between the contact pads microstructures will be produced using two photon polymerisation. The materials used for producing the microstructures will not contain gold and as such, like glass, will not be coated by the thiolated cRGDfC and facilitate the adhesion of neither neurons or neurites. Preventing neurites growing over the microstructures would improve the degree of coordination the microstructures impose upon the neural culture.

The optimal chemical patterning approach for neural patterning would be free form and three dimensional as the two-photon polymerisation of the microstructures so that the adhesion of the culture to the three dimensional microstructure could be varied with chemical patterning. Two photon absorption can be used to initiate photoconjugation or photocleavage reactions[118]. This approach has been used to convey cell adhesion and degradability to scaffolds for culturing the growth of various cell types including neurons[118,119,131]. This approach allows for the adhesion of the neurons to be

patterned in three dimensions, however this currently has limited use in *in vitro* neural interfacing as the *in vitro* MEAs are predominantly two dimensional with three dimensional MEAs generally being designed for *in vivo* neural interfacing[149,150]. The technologies being developed for *in vivo* neural interfaces could be repurposed for *in vitro* allowing for patterned three dimensional neural cultures to be recorded and stimulated from. An alternative is to use light as the medium for recording and stimulating neurons, by using optogenetics and calcium imaging respectively. These optical techniques are limited by the penetration depth of the light but that can be over a millimetre and have been applied to three dimensional neural cultures *in vitro*[38]. A major drawback of neural interfacing with light is the total length of time available for recording. Calcium imaging dyes bleach over time leading to a loss of signal as well as cell death due to phototoxicity caused by the dye undergoing intersystem crossing to become a free radical[151]. Development of a long-term three dimensional neural interfacing technology in combination with three dimensional patterning of the growth of cultured neurons would mark a disruptive step in the development of *in vitro* neural biosensors by allowing for more valid models of neural circuitry to be produced and tested.

By developing protocols for promoting the adhesion of neurons to an OrmoComp modified substrate and the selective adhesion of glass over gold this Chapter will enable the culturing of neurons on substrates functionalised with two photon polymerised microstructures. Before the effect of the microstructures on the growth of the culture can be characterised, in Chapter 4, the production of OrmoComp microstructures must first be optimised and is the subject of the subsequent Chapter, Chapter 3.

3 Optimising the two-photon polymerisation of OrmoComp microstructures.

3.1 Overview

As discussed above two photon polymerisation has a range of attributes that potentially make it well suited for patterning neurons *in vitro*. Previous attempts at exploiting two photon polymerisation for patterning neurons emphasised a need for more sophisticated designs to more successfully influence the culture. The sophistication of their designs appears to have been hindered by both the capabilities of the apparatus they used and the structural integrity of the structures they produced [19]. This chapter will first assess what capabilities can be incorporated into a two photon polymerisation device to improve its applicability in this context. The desired capabilities will be assessed through a technical comparison of the two different two photon polymerisation rigs used in this thesis, a custom built rig and the commercially available Nanoscribe GT. The chapter will then detail the parameter optimisation sweep used to maximise structural both structural stability and fabrication speed.

The first step of the parameter optimisation sweep was to develop a modular design which could be built from repeats of geometrically similar structures one piece at a time. By having the same base repeat structure, with different orientations of channels, it is possible to rapidly reconfigure the neurite path within the microstructure as well as varying the size and shape of the total array to be easily reconfigured for various microelectrode array designs, without the use of a computer aided design suite. Being able to reduce the structure to a small single repeat unit also provided a short build file which was then used to optimise critical build parameters such as, line spacing, scan speed and laser power. The parameter optimisation was achieved by building the same identical structure many times whilst sweeping through different combinations of scan speed, laser power and line spacing. The resultant arrays were then imaged using scanning electron microscopy and each structure was then qualitatively classed depending based on its visual appearance. This process was first used to

identify a coarse processing parameter window for OrmoComp. The coarse processing parameter window was then swept through in smaller increments to find the optimal combination of settings to produce a structure which is a stable, accurate reproduction of the design in as short a time as possible. Minimising the fabrication speed is essential for scaling up the design and producing the number of repeat samples necessary for cell culture and subsequent characterisations such as fluorescent imaging and scanning electron microscopy.

3.2 Methodology

3.2.1 Comparison of Two Photon Polymerisation Rigs.

To assess what capabilities are desirable for a two photon polymerisation rig the two different two photon polymerisation rigs used to produce microstructures in this thesis will be compared in this Section. The different rigs were a custom-built system and the commercially available Nanoscribe GT from Photonics Professional ltd. The custom rig was used for producing simple two photon polymerised microstructures similar to those used previously for patterning neurons *in vitro*[19] and was also used for optimising the protocol for preparing the samples for cell culture (see Chapter 2). The larger microstructures used for patterning neurons (see Chapter 4) were produced using the Nanoscribe GT for reasons highlighted through the comparison of the two rigs in this Section.

A key disadvantage of the custom rig for patterning neurons *in vitro* was that the total size of the structures it can produce are much smaller than the total size the Nanoscribe is capable of. The size was limited on the custom rig due to both software and hardware limitations. For translating the beam through the resin, the custom rig was equipped with a *Nano positioner* piezoelectric stage (physik instruments), 7 nanometre repeatability, with a maximum of translation of 400 micron in X, Y and Z. As the rig has no large, or coarse, automated translation stage the maximum translation distance represents the upper size limit of any structure produced in a single build. As the custom rig was set up in the sandwich configuration (Figure 29) the maximum Z height was further restricted to the working distance of the oil immersion objective, 180 micron. The sandwich configuration involves

trapping resin between two glass coverslips separated by a 150 micron thick spacer ring to position the substrate within the working distance of the objective lens. The immersion oil was then placed on the top surface of the sandwich and the objective lowered into the oil. The oil is necessary to maintain a constant refractive index throughout the beam path of the laser. Maintaining a constant refractive index in the beam path minimises the loss of spatial frequencies due to diffraction caused by passing from a medium of one refractive index, e.g. air, to a medium of another, e.g. glass. Maximising the spatial frequencies present in the beam is necessary for optimising resolution in any optical set up. Achieving a photon intensity high enough to breach the threshold of two photon absorption is dependent on maximising the focusing of light and making it essential to minimise the loss of spatial frequencies to diffraction [110].

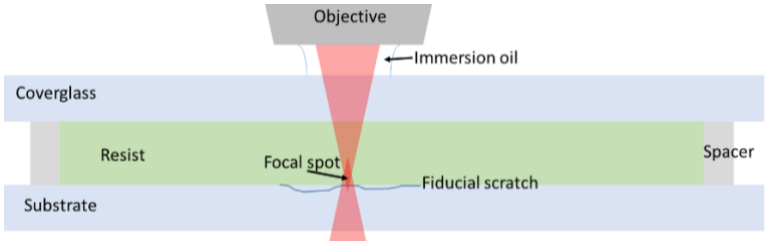


Figure 33 Sandwich configuration implemented on custom rig.

Resist is sandwiched between two glass coverslips separated by a 150 micron space. Immersion oil is placed between the top coverslip and the objective to minimise refraction caused by passing between mediums of different refractive indices. A fiducial scratch is made using a diamond pen for approximate focusing of the focal point on the substrate.

The thickness of the spacer and the maximum translation of the *Nano positioner* piezoelectric stage impose a theoretical limit on the structure's total Z height, but the time taken for these structures to be produced limits the feasible size of structures. The stage's maximum speed of translation is 100 microns/s which, at 0.5 micron line and layer spacing, would take over three hundred hours to raster scan the 400 micron by 400 micron by 180 micron volume. The microstructures built in this thesis did not exceed fifty micron in height but did cover areas up to two millimetres square which would take hundreds of hours to build, which is unfeasible when multiple samples are required for cell culture experiments.

The Nanoscribe greatly exceeds the size and speed limitations of the custom rig through a combination of hardware and software developments. This makes it much more suitable for patterning neurons on microelectrode arrays as it is possible to build structures up to several millimetres squared in X and Y and hundreds of microns in Z height in several hours. One key hardware development of the Nanoscribe, which greatly increases the potential Z height of the structure that can be produced, is the option for *dip-in* configuration instead of standard or sandwich configuration. *Dip-in* configuration uses an objective that does not require immersion oil but has an adjustable refractive index that allows it to be immersed into a variety of resins of differing diffractive indices. Aberrations can be caused by passing through highly mismatched refractive index interfaces, such as that between the air and the lens of the high numerical aperture objective mounted on the Nanoscribe. To avoid these aberrations, a layer of immersion oil is used to fill the space between the glass coverslip and the objective lens. This approach is implemented in the standard configuration of the Nanoscribe GT. The standard configuration has limitations in three dimensional fabrication as the beam has to pass through previously built layers which causes structural distortion, limiting the fabrication height to approximately 40 micron. The sandwich approach gets around this but by building away from the surface it builds on but is ultimately limited to the width of the sandwich, 180 micron.

The Nanoscribe can build to a maximum height limited by the maximum translation of the stage in the Z axis which is 1 centimetre. Much like with the custom rig however, it is translation speed which is the practical limitation on the total size of the structure produced.

The Nanoscribe can produce structures much faster than the custom rig, partially because it is equipped with galvanometric scanning mirrors. The Nanoscribe's galvanometric scanning mirrors are capable of translating the focal point of the laser beam up to 100 millimetres per second, three orders of magnitude faster than the translation speed of the piezo stage on the custom rig. For the Nanoscribe it is the maximum power of the laser which is the limiting factor on scan speed as the optical dose, the amount of energy delivered to an exposed region of resist, decreases proportionally

with the dwell time of the laser. The dwell time is inversely proportional to the scan speed of the laser (Figure 34). The highest speed recommended by Photonics Professional Ltd, the manufacturers of the Nanoscribe GT, is 30 millimetres per second for their in-house resins. Above 30 millimetres per second the galvanometric scanning mirrors produce a structure that has less fidelity to the original design due to aberrations induced when the mirrors change the direction of the beam at such speeds. To raster scan the maximum traversable volume of the custom rig's piezoelectric stage (400 micron x 400 micron x 180 micron) at the top speed of the Nanoscribe GT, 30 millimetres per second, it would take about one hour as opposed to the 320 hours it would take using the piezo electric stage. The increased translation speed of the galvanometric scanning mirrors makes it feasible to produce mesoscale structures (one micron to one centimetre). Mesoscale structures are required to pattern the tens or hundreds of neurons for producing coordinated networks of neurons *in vitro*.

Optical Dose = Dwell Time x Laser Power

Figure 34 Equation of optical dose which is proportional to the dwell time and the laser power.

The scanning area of the mirrors is limited by the field of view of the objective (300 micron^2) for the 25 times magnification objective. The field of view is limited by the necessity of having a high numerical aperture capable of spatially focusing the laser sufficiently to exceed the threshold intensity for two-photon absorption to occur at the focal point of the laser. Large area structures or arrays can be split into sections, corresponding to the relevant positions of the coarse microscope stage, using the software package of the Nanoscribe system, *Describe*. Each section is capable of fitting into an individual field of view of the objective enabling it to be built using the galvanometric scanning mirrors, which is important when building large structures for time efficiency. During fabrication each section is built individually and then another section is stitched on by translating the coarse microscope stage, which has a total translational area of 1 centimetre squared. If one section shadows the path of the laser whilst building a subsequent laser then the laser power can be reduced preventing the two

photon absorption threshold of photon intensity to be reached, at the focal spot of the laser, and polymerisation being initiated. Alternatively, the diffraction of the beam by the shadowing structure can heat the resin causing bubbles and explosions. To prevent shadowing effects by previously fabricated sections a 15 degree angle should be used rather than a direct vertical split to avoid interacting the structure interacting with the beam. The 15 angle slightly decreases the size of the sections the structure is split into but can improve the integration of adjacent sections, reducing any weaknesses due to seams. The automated fabrication of multiple build volumes is dependent on the subsequent section of the structure being automatically positioned on the substrate surface. The automatic positioning onto the substrate surface is facilitated by the automated interface finder, another key advantage of the Nanoscribe GT.

The automated interface find is a key feature of the Nanoscribe as it allows for accurate positioning of the focal spot on the surface enabling the automated fabrication of multiple samples, structures or the sections of a single large structure. It is important to ensure that a structure is built directly on the substrate surface so that it is not partially buried beneath the surface nor fabricated away from substrate. If fabricated away from the substrate the structure is likely to move during fabrication or get washed away during development. The Nanoscribe's automated interface finder is more reliable and much faster than the manual approach used on the custom rig, focussing on a fiducial mark on the substrate. The manual approach involves scoring the coverslip substrate with a diamond pen and locating it with a ten times magnification objective. The objective is then exchanged for the 100 times magnification objective used for initiating the polymerisation. The first major difficulty is bringing the fiducial mark into the field of view of the 100 times objective (<200 micron^2), this allows for coarse focusing of the objective onto the substrate surface using the manual focus wheel and visual assessing the focus using the rig's fiducial camera. The next challenge is bringing the focal spot of the laser slightly below the surface of the substrate. Focusing just beneath the surface is achieved through trial and error by manually opening and closing the shutter and adjusting the height of the substrate using the piezo electric stage to determine the highest stage Z value which allows for polymerisation but

does not result in the structure floating away into the resin. This value represents the height at which the focal spot of the beam has moved from slightly below the substrate surface, where no polymerisation occurs, to just above the surface where polymerisation occurs, and the resultant structure is anchored to the substrate. Although it is possible to manually focus onto the substrate the automated approach of the Nanoscribe not only improves researcher efficiency but allows the device to automatically fabricate multiple samples and stitch build volumes together to produce larger structures.

The Nanoscribe GT finds the substrate using an automated interface finder based on a retroreflection alignment system. The interface finder allows the focal point of the laser to be positioned accurately within 10s of nanometers on the substrate surface. The autofocus on the Nanoscribe is based on projecting a grating of light, in a similar wavelength to the femtosecond laser, onto the substrate and then imaging the reflection of the grating onto a couple charged device (CCD) camera tilted at 45 degrees to the image plane of the retroreflected grating. The microscope stage is then scanned in the Z axis, using the stepper motors of the microscope body, until the most focused grating image is read off the centre of the CCD chip. The most focused reflection of the grating will be produced when the grating is being imaged directly onto the refractive index interface between the glass and the resin, hence the name automated interface finder.

There are a number of advantages bestowed by the automatic interface finder which greatly increases the applicability of two photon polymerisation for the patterning of neurons *in vitro* and for many other scenarios. Automatic positioning of the focal spot on the substrate greatly decreases the difficulty and time taken to produce a sample. The automated interface finder in combination with the coarse microscope stage can navigate automatically and build on the surface of ten samples facilitating, autonomous, production of multiple samples from a single build file. With a single structure taking around an hour to complete an overnight build can be set up to produce ten identical structures without any time expenditure on behalf of the researcher as well as maximising the number

of research projects a single machine is capable of supporting. The automated interface finder does have impose some material constraints due to the necessity of having a significant refractive index mismatch between the substrate surface and the resin intended for polymerisation. This can be overcome by coating the substrate with a thin (<100 nanometre) coating of indium tin oxide, introducing a refractive index mismatch at the substrate surface. By facilitating batch production, the stitching of build volumes and the precise anchoring of the structure to the substrate the automated interface finder is one of the most important features of the Nanoscribe when compared with the custom rig initially used in this thesis.

3.2.2 Dip-in vs standard writing configuration on the Nanoscribe

There are two sample configurations available with the Nanoscribe GT, *standard* and *dip-in* (Figure 34). Aberrations can be caused by passing through highly mismatched refractive index interfaces, such as that between the air and the lens of the high numerical aperture objective mounted on the Nanoscribe. To avoid these aberrations, a layer of immersion oil is commonly used to fill the space between the glass coverslip and the objective lens. This approach is implemented in the standard configuration of the Nanoscribe GT. The standard configuration has limitations in three dimensional fabrication as the beam has to pass through previously built layers which causes structural distortion, limiting the fabrication height to approximately 40 micron. To build structures higher than 40 micron and take advantage of the 300 micron piezo electric z translation and 8cm of coarse microscope translation, Dip-in configuration can be implemented.

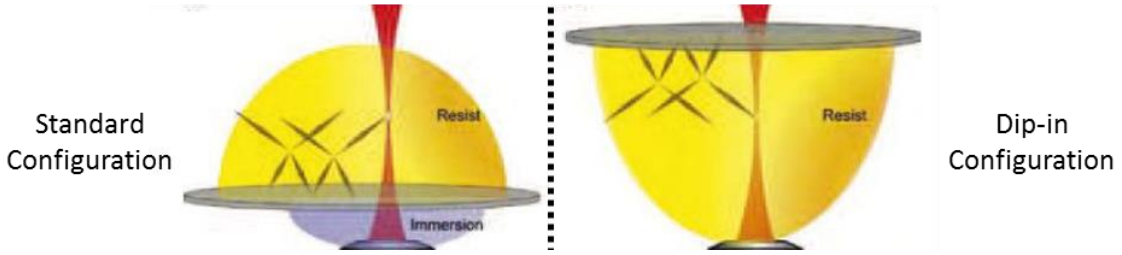


Figure 35 Standard and dip-in orientations for direct laser writing.

Left: The standard configuration involves dipping the objective into immersion oil and irradiating the resist through the substrate with the piezo stage moving the substrate down to add layers. In this configuration, the beam passes through lower layers when exposing upper layers. Passing through the lower levels can lead to refraction of the beam, reducing the power in the upper layers causing them to be defective and at a certain height preventing polymerisation (~40-50 micron).

Right: The dip-in configuration involves dipping the objective directly into the resist and moving the piezo stage up to add layers. This approach avoids irradiating through previously built structures but requires the resist to be matched to the refractive index of the objective. Additionally, the resin should not cause any damage to the objective, i.e. by corroding the objective's coating or leaving dried resin on the surface. To facilitate the automated interface finder a layer of indium tin oxide should be deposited on the surface to introduce a refractive mismatch at the substrate surface.

The dip-in configuration (Figure 35) overcomes this issue by building on the underside of the substrate which involves replacing the immersion oil with a resin which has the same refractive index as the microscope objective. When using a resist which has a similar refractive index to glass and building on a glass substrate there is no effective refractive index mismatch between the resin and the substrate, making the automatic interface finder defunct. As previously mentioned, this can be overcome by coating a glass substrate with indium tin oxide provides a slight refractive index mismatch so as to provide a significant refractive index mismatch at the substrate surface the operation of the automated interface finder. In the later stages of this thesis a 25 times objective with an adjustable cuff, which compensates for refractive index mismatch between the glass objective, was procured. This adjustable cuff allowed the use of water based resins in dip-in mode, although only for short periods of time prior to the resin dehydrating. In summary, the dip-In configuration is required to facilitate the fabrication of structures greater than 40 micron in height and having an adjustable objective cuff allows for a larger range of resins to be used in dip-in mode.

3.2.3 Computer assisted design and manufacture

When designing the microstructures two main considerations were made. Primarily the structure had to be a stable so the strength versus speed of fabrication was the major compromise with direct laser writing microscale three dimensional structures. Secondly the structure was intended to pattern the cells effectively over several weeks, confining cell bodies, guiding the growth of projections and isolating the microculture from the surrounding support culture. These considerations were incorporated into the initial design using the computer aided design package spaceclaim (ANSYS ltd) which was iteratively revised after the production of structures and the characterisation of cells cultured in the presence of the microstructures. The CAD file (.stl) was then converted into the format that could instruct the machine, known as *general writing language (.gwl,)* by the software *Describe* (Photonics Proffesional). This conversion involved three main stages all of which are common to other additive manufacturing processes. Initially the structure was meshed to provide a coordinate map, secondly the layer thickness, or slicing distance, was set based on the z-height of the polymerisation voxel and approximately halved to ensure significant overlap of subsequent layers. The line spacing between each scanned laser line was set as was the design and density of the scaffold filling the core of the structure.

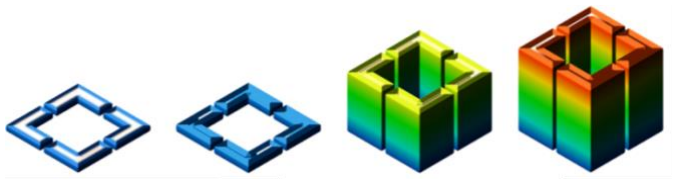


Figure 36 Describe simulation depicting exposed volume at four time points during the build of a single unit of the grid structure for patterning neurons in vitro.

The first image depicts the outline of the first layer of the structure 0.5 seconds. The second image is at 1 seconds into the build towards the end of the second layer. The centre of the layer is being filled in with hatches perpendicular to the outline. The third image at 10 seconds shows the structure three quarters finished. The final image shows the structure at 14s. At 14s the top layer the is almost filled. Build time simulated on a scan speed of 17.5 millimetres per second and line and layer spacing of 500nm.

Defining the line spacing of the structure was key for optimising the speed to strength compromise as it determined the total volume scanned. Parameters which vary this total volume are the thickness of the solid base and the walls of the shell, as well as the spacing and thickness of the walls and floors of the scaffold which fills the inner volume of the structure. The parameters for line spacing and layer thickness are dependent on the build parameters which effects the size of the polymerisation voxel, the scan speed and the laser power.

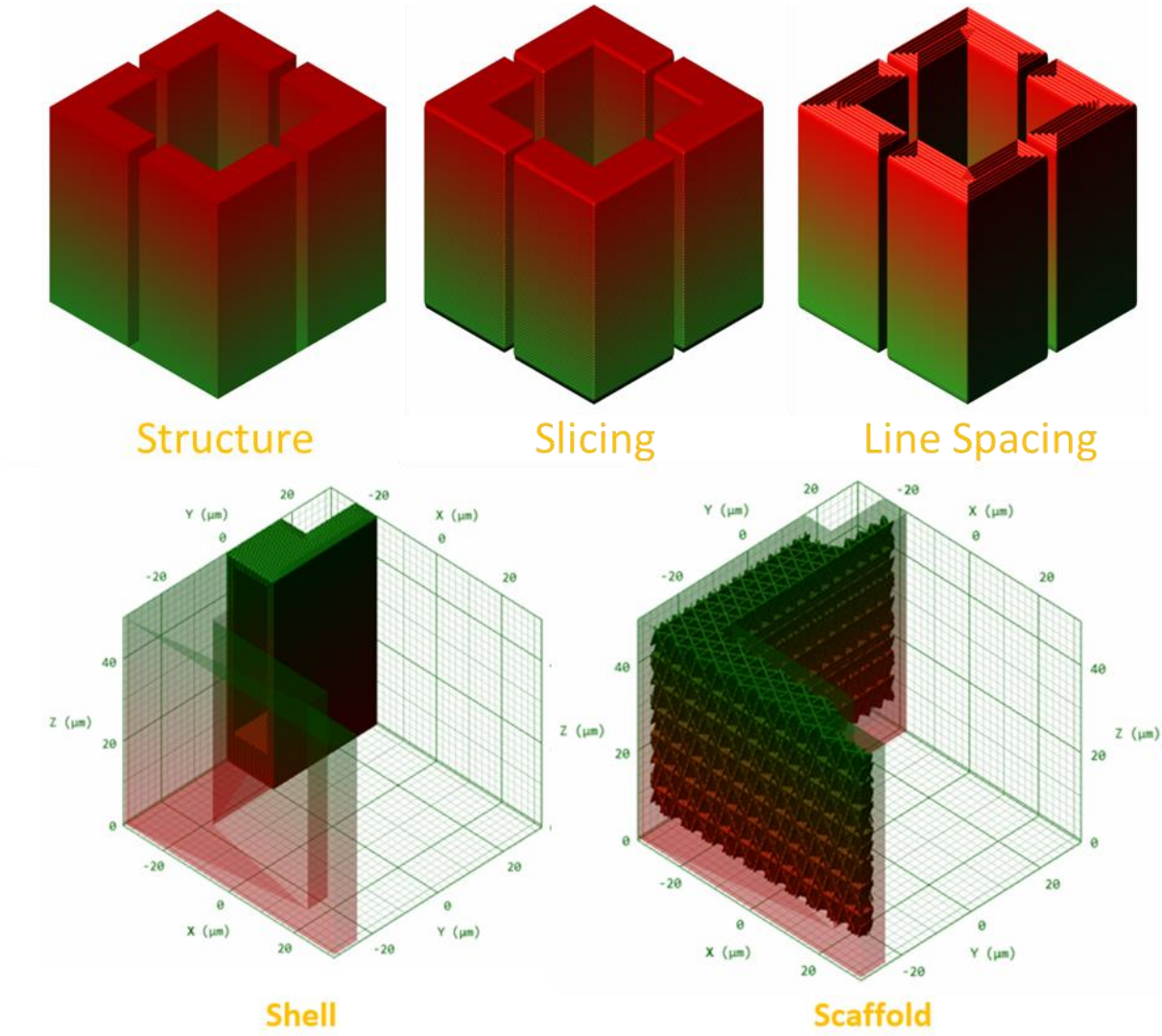


Figure 37 Preparing a file for use on the Nanoscribe: Layer thickness, line spacing, shell thickness and scaffold density.

The first image, from left to right, shows the original CAD file. The second image shows the structure sliced with spacing of 0.5 micron. The third image shows the structure with a line spacing of 0.5 micron. Bottom Left image shows the thickness of the shell and the base of the structure. Bottom right structure shows the scaffold core of the microstructure.

To produce structures greater than the microscope objective's maximum field of view, ~160 micron squared, it is necessary to *stitch* build volumes together. This is done in the last stage of the *Describe* software by *splitting* the whole object into separate build volumes. The stitching of the individual build volumes is performed by the coarse microscope stage of the Nanoscribe GT which can lead to inaccurate placement and therefore mismatching of the stitched parts. If the structures are designed with this stitching in mind whilst still in the computer assisted design package, then joints and overlaps can be designed into the structure to reduce the impact of mismatching (Figure 38). Prototyping a part of an object speeds up the optimisation of build parameters as whole structures often have lengthy build times. This is especially efficient when there is a repeat unit such as the individual grid compartments below. This modular approach also allowed for rapid adaptation of the structure design, and subsequently the network topology, without having to draw a new design in CAD.

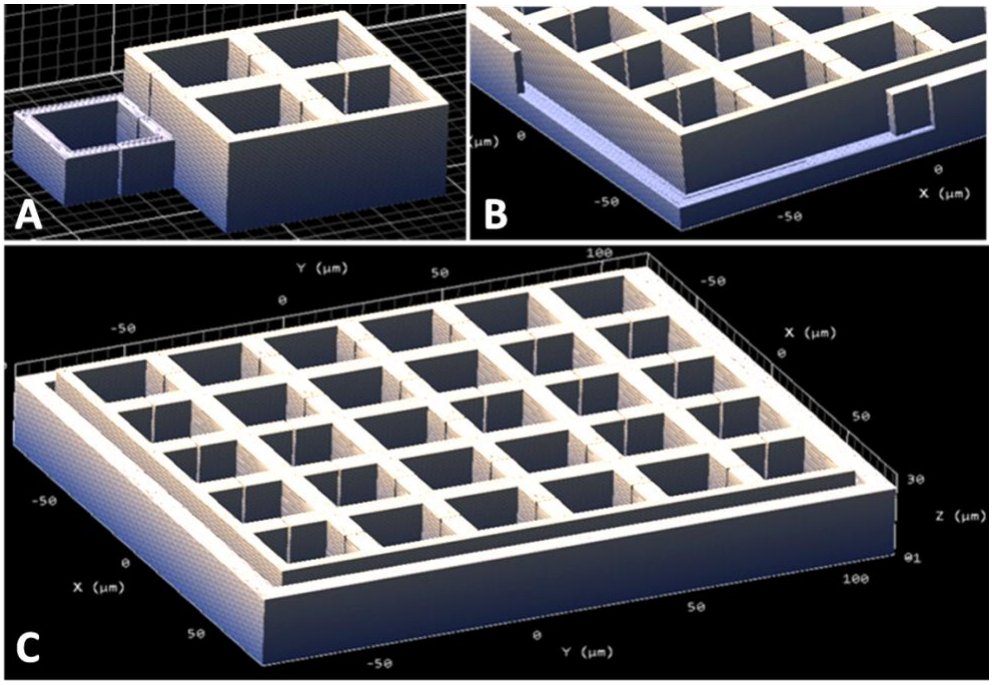


Figure 38 Describe simulation direct laser writing process and build.

A) One half built, and four complete compartments connected by thin passages forming a spiral. B) A corner of the outer wall being built with jigsaw joints connecting it to the other outer wall sections. C) Finished build with the spiral pathway of thin passages starting form the back corner in the top right of the image and finishing in the centre.

3.3 Experimental

3.3.1 Ormocomp substrate preparation

22 x 22 Millimetre no. 1.5 glass coverslips (Menzal-Glasser, Agar Scientific) were cleaned with acetone and isopropanol and subsequently dried under a nitrogen stream. For both dip-in and standard configurations OrmoComp (MicroChem Limited) was dropcast onto the substrate and heated at 80 degrees Celsius for 5 minutes. The substrates were then loaded onto the sample holder, in the dip-In configuration the OrmoComp drop was placed face down whereas in the standard configuration the resin was face up and a drop of emersion oil was placed on the bottom side. To prevent the automated interface finder focussing on the interface between the air and the top surface of the glass, during dip-in mode, a drop of oil was placed on the top of the substrate. For long builds, especially on multiple samples, an 18 x 18 millimetres squared No. 1.5 coverslip (Sigma Aldrich) was placed on top of the oil to trap it, preventing it sliding off during translation of the stage. To find an acceptable set of parameters for writing text, the scan speed was slowly reduced whilst keeping laser power fixed at 100 percent.

3.3.2 Ormocomp substrate preparation

After building had completed, and the sample holder removed from the stage, the samples were taken off the sample holder. OrmoComp microstructures were first developed according to the protocol provided by Microchem. The samples were baked at 80 degrees Celsius for 3 minutes then washed in OrmoDev (Microchem Limited) which is comprised of 50:50 (vol:vol) isopropanol and methylpentanone to dissolve the unpolymerized OrmoComp. The development involved post-exposure heating of the sample to 80 degrees for five minutes to relax the intermolecular bonds helping the material to dissolve in the developer, OrmoDev. The samples were then rinsed in isopropanol and dried with a nitrogen stream and placed in a sterile oven to hard bake at 160 degrees Celsius for 3 hours. As this approach led to poor cell adhesion and viability, the development process was made more thorough. In the revised development protocol, the samples were removed from the

hotplate and immersed in the same OrmoDev developer solution for 5 minutes but thrice instead of once. The substrates were subsequently washed three times in isopropanol, again instead of once, before being dried with nitrogen stream. Finally, the substrates were baked overnight at 37 degrees Celsius for hard baking as well as in order to remove excess toxic residues and sterilise the sample.

3.3.3 Optimisation sweeps

To identify the optimal processing parameters for producing Ormocomp Microstructures a set of parameter sweeps were performed on a sample structure to facilitate rapid optimisation of processing parameters through parameter sweep arrays. The sample structure was the base unit of a modular grid structure designed for patterning neurons on a microelectrode array. Each unit in the grid is built individually which minimises shadowing effects and allows for rapid reconfiguration of the neurite path. These modular grid compartments have the same pitch (30 micron) as a high-density microelectrode array so that each unit of the grid can confine a single soma to a single electrode contact pad. The central 20 micron^2 of each unit is hollow to allow a neuronal soma (~10 micron-16 micron) to adhere to the compartment floor. The channels interlinking the compartments were designed to allow neurites, axons and dendrites, to pass whilst confining soma. Due to the limitations of nuclear deformation somas are unable to pass though gaps of less than 3 micron so the channels width was set at 2 micron. Grid units with various combinations of neurite channels were designed and the unit with all four channels was selected as the test structure for optimising build parameters. This design was selected as it has the slenderest components.

3.3.4 Scanning electron microscopy

After development and a preliminary examination on a light microscope to screen for major defects the samples were coated with a gold thin film using a Q50T sputter coater from Quorom Technologies Ltd. The sputter coater was automatic requiring the user to select the correct target material for the coating and the length of time for it to be deposited, in this case gold for 30 seconds. Although the thickness of the film can be specified it was not required in this case. The samples were then placed

on a tilt and rotate stage in a Hitatchi TM3030 table-top Scanning Electron Microscopy SEM. The tilt was set to approximately 45 degrees. The structure was located on the sample at 30x magnification and then imaged using a 15kV beam. Magnifications used for imaging varied from 300 times to 5000 times magnification for several arrays of structures to individual units respectively.

3.4 Results

A sample design was made compatible with both sculpting neurons and rapid optimisation of the two photon polymerisation process and the resultant CAD file was meshed, sliced and hatched to give a Z series of XY scanning coordinates which made up the three dimensional structure. Four different build files were produced each with different line spacing ranging from 200 nanometre to 500 nanometre. Increasing the distance between lines can decreased the time taken to produce the structure (Figure 39). Increasing the line spacing also produced a less dense and therefore less structurally stable structure as visible in the plan views in Figure 39. Dense structures can be produced with larger line spacing if larger powers are used to increase the size of the polymerisation volume. Increasing the polymerisation volume, however, leads to a loss of resolution and minimum feature size. The smallest feature size of thesis, the neurite channel (2 micron wide), is not pushing the limits of the resolution of the machine (~300-600 nanometre) allowing for higher power values and larger line spacing to be employed. Sweeping through different combinations of line spacing, laser power and scan speed allows for build time and structure stability to be optimised.

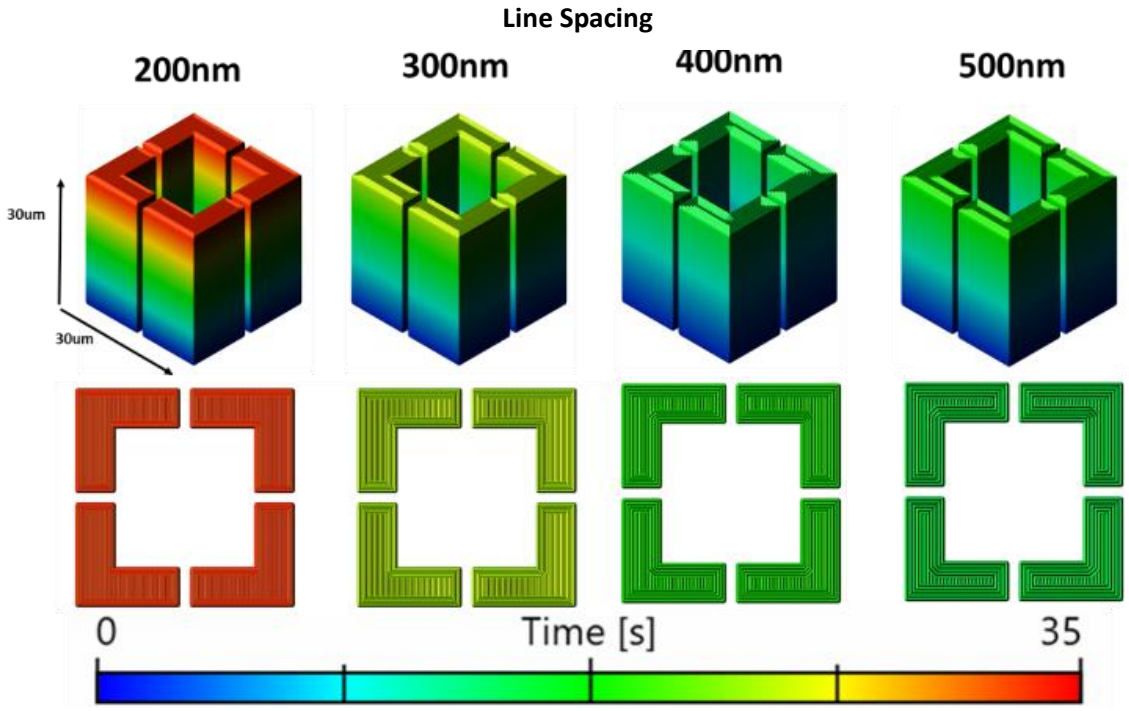


Figure 39 Describe simulation of four identical designs with different line spacing.

The colour gradient infers how long each build file will take to build. Doubling the line spacing halves the build time, red to green shows increasing time.

A *for* loop was used to generate a two-dimensional array with scan speed increasing down the Y axis and laser power increasing in the X axis (Figure 36). Each unit was separated by 100 micron to minimise the effect of neighbouring structures producing bubbles and explosions of the resin due to vaporisation and overheating. The processing parameters used to create each structure, the scan speed and the laser power, were then written under each structure using the "write text" function of the Nanoscribe. The parameter sweep array was generated for each of the different line spacing build files. Initially a coarse array was performed to identify the rough processing window and then a second array was produced with finer parameter increments with the total range restricted within the rough processing window. After the file had been run on the Nanoscribe the structures were developed using the same process optimised for neural adhesion in the previous Chapter. After development, the structures were sputter coated in gold and imaged using a table top scanning electron microscope (Hitachi TM3030). The structures were then qualitatively classed from 0 to 6 depending on their visual

appearance in the scanning electron micrographs (Figure 40). A colour map was then generated based on the class of the structure at that position in the processing parameter array. The information in the colour maps was summarised and presented in histograms to allow easy comparison between the processing windows of different line spacing files.



Figure 40 Scanning electron micrographs of the different classes of microstructures produced by the parameter sweep array.

At the lowest optical doses nothing was visible, or a dark smear was visible with no details discernible from the original file (0 and 1 class, not shown. Nothing is visible for 0 and 1 is a smudge). At higher optical doses collapsed microstructures were produced (2 and 3). The first self-supporting class of structures, 4th, have thin walls and wide channels when compared to the original design. The closest match to the original design is the 5th class of the microstructures. The 6th class of structure is roughly in the 30 micron squared area of the intended microstructure but is otherwise unrecognisable.

A structure qualified as 0 when there was no sign that any structure had ever been present. A class 1 was awarded to structures that appeared as a dark smudge that represented very little Z elevation but some visible signs of polymerisation. Class 2 showed a bright colouration showing it had achieved a significant Z height but was totally collapsed whereas class 3, although collapsed, would have a clear hollow interior. Structures were classed as a 4 if they appeared as an under-formed version of the original file, whereas close to perfect structures were classed as a 5. If the resultant structure appeared as an amorphous blob, then it was classed as a 6. A class 6 is normally because of too much power being applied to the material causing it to vaporise, further leading to explosions and aberrant polymerisation. A class 6 will also be the outcome of a structure which builds in a region which is obscured by bubbles, produced through excessive heating and vaporisation, from a neighbouring structure (2 micron-50 micron). Explosions are also caused by the presence of contaminants as they

absorb the infrared energy of the laser, transducing it rapidly into heat energy which causes the resin to vaporise. The various manifestations of the structures produced at different parameter combinations were classified based on their fidelity to the original design to identify the processing window of the material (Figure 40).

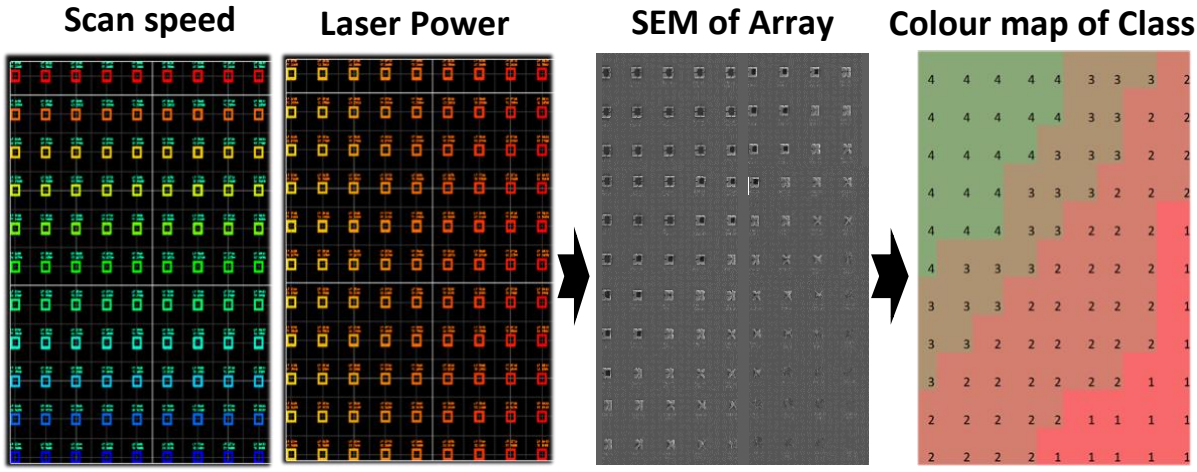


Figure 41 Parameter optimisation Sweep work flow.
Initially an imbedded for loop is used to generate an array of the sample structure. The first two images, from left, are describe simulations showing how the scan speed increases in the Y axis and laser power increases in the X axis. The resultant array of microstructure was then characterised by SEM (Centre). The structures were then categorised based on the fidelity to the original design. The rankings were then used to produce a colour map to show the parameter windows which produced high quality structures (Right).

One of the classes of structures, 6, was produced by vaporisation of the resin leading to an explosion and aberrant uncontrolled polymerisation. An explosion, which can be caused by excess power or the presence of a contaminant, produces bubbles which in turn disturb the beam path causing more explosions. Bubbles which are irradiated by the laser absorb the infrared energy causing them to expand with every exposure. As the bubbles grow, they are more likely to disturb other parts of the build. During the parameter sweep optimisation array bubbles sometimes grew to such a size that they would disturb the production of neighbouring structures, leading to no polymerisation in a region which would normally have class 6s. The top left corner of the 200 nanometre line spacing build file parameter sweep optimisation array, far left in Figure 42, has many class 6s but also many class 0s.

This mix of 0s and 6s is likely due to the large bubbles which were formed during the explosive production of class 6s preventing the polymerisation of neighbouring structures. The presence of a bubble also interferes with the automated interface finder meaning that some structures end up being built not in contact with the substrate. Structures not built on the substrate will be washed away during the development procedure or even during the building of the file.

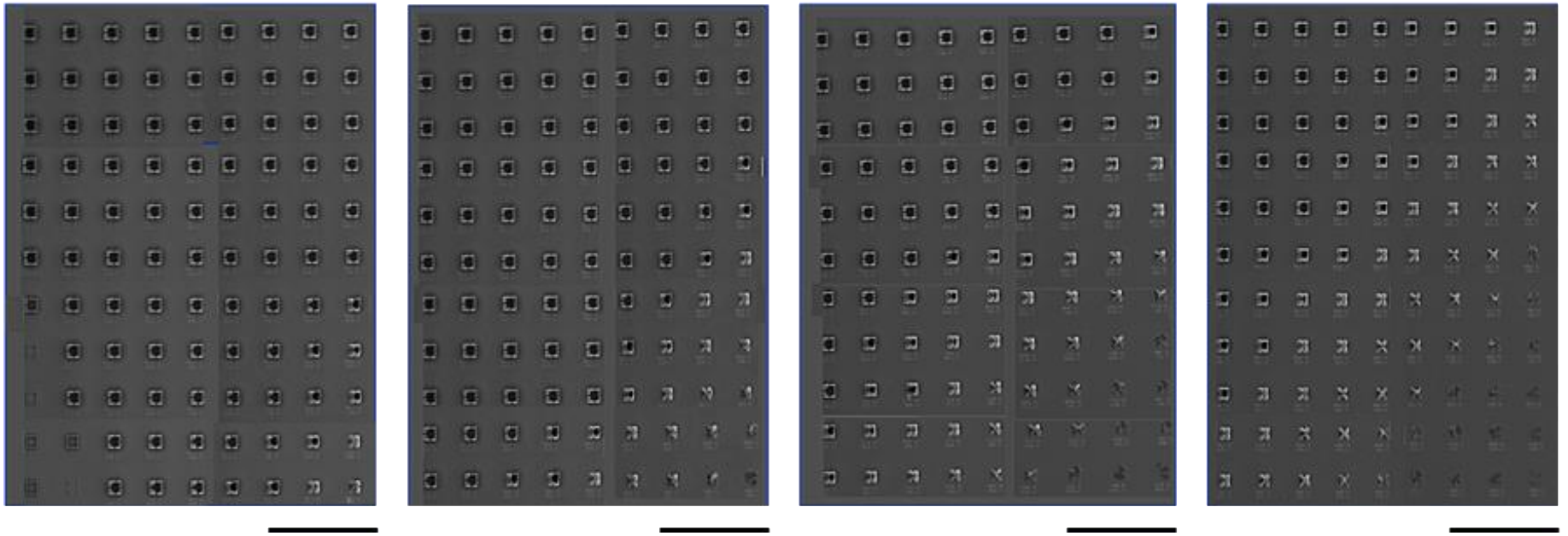


Figure 42 Scanning electron micrograph of an optimisation array.

From left to right the line spacing increases from 200 nanometre to 600 nanometre. Note how at both the beginning and end of the array the structures appear faded or collapsed. On the left this due to an overly high optical dose being used for that line spacing, 200 nanometre. This causes the material to vaporise, producing bubbles which then interferes with the beam leading to more explosions and bubble formation. On the right side the opposite is the case. Not enough energy is being delivered to polymerise the material sufficiently making the structure unstable. This effect is reduced when the line spacing is small. Scale bar 200 micron.

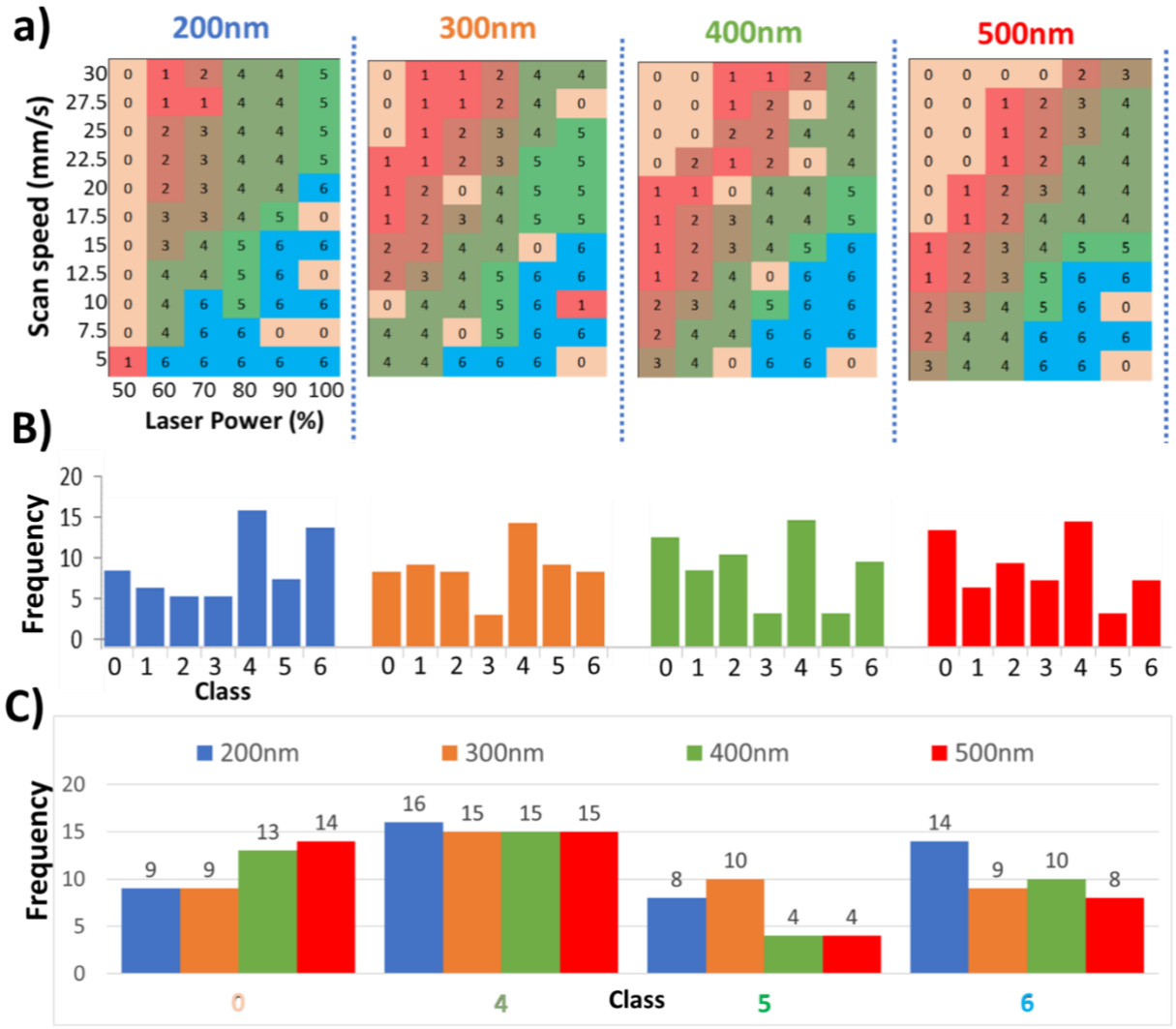


Figure 43 Coarse parameter sweep optimisation array.

A) ***The first parameter sweep was used to identify a coarse processing window for good to perfect (4-5) microstructures. It is apparent that the processing window shrinks as the hatching spacing increases. The majority of good to perfect structures, for all of the line spacings, was between 15 millimetres per second and 30 millimetres per second and between 80 and 100 percent laser power. B) Histogram representing the distribution of different class structures produced by each line spacing file. Each histogram summarises the colour map directly above in A). C) Histogram comparing how many of each class were produced by the different line spacing build files. Not how the wider line spacings, 400 nanometre and 500 nanometre produced more zeros, this highlights the role of the field effect where proximal laser scans can cause polymerisation even if a single beam would be insufficient to exceed the polymerisation threshold. The opposite effect can be seen in the class 5 structures were there is half as many produced by the wider, 400-500 nanometre, line spacing files. Interestingly the same number of class fours were produced by all files, suggesting the under-formed version of the structure is much easier to produce than the final structure.***

Initially a coarse array was generated to identify the rough processing window of OrmoComp. The coarse window swept from 60 percent to 100 percent laser power increasing by 10 percent each step and the scan speeds tested went from 5 millimetres per second to 30 millimetres per second step 2.5 micron per second. At 50 percent laser power all of the line spacing build files produced very little polymerisation, mainly creating structures which were in class 0 or 1. The only reasonable structures at 50 percent power were produced at the very lowest scan speeds, 5 millimetres per second or 7.5 millimetres per second (Figure 43, A). This confirms that the energy threshold for achieving polymerisation is determined by both laser power and scan speed, described above as the optical dose.

Class 5 structures were not produced with anything less than 80 percent of the laser power and still required fairly slow scanning speeds of 10 millimetres per second to 12.5 millimetres per second. When the laser power was at 90 percent and 100 percent, class 5 structures could be produced at much faster speeds. The maximum speed capable of producing class 5 structures decreased with increased line spacing. For example, at 100 percent, the 200 nanometres line spacing file produced a class 5 at 30 millimetres per second whereas the 500 nanometres line spacing file top speed for a class 5 was 15 millimetres per second. The role of scan speed in determining the class confirms that it is not simply Laser Power but again it is the optical dose which determines the dimensions of the polymerisation volume. This can be partially explained by the field effect which causes polymerisation in regions just outside of the focal point which overlap with the fringe of an adjacent laser scan's focal spots. The field effect is due to difffusion of radicals and intermediates between adjacent scan lines altering polymerisation connetics, particurly at the boundry of the two volumes.

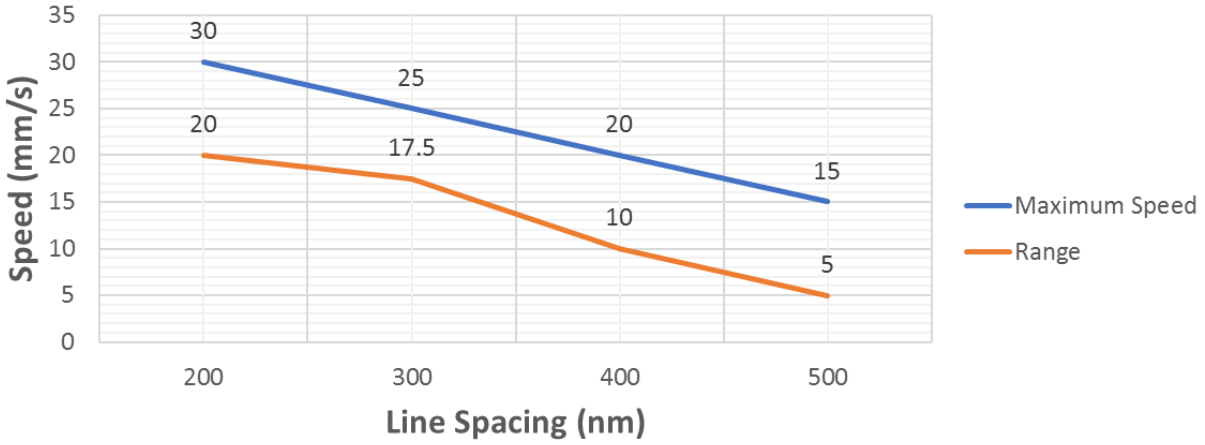


Figure 44 Maximum speed and Processing range depending on line spacing

The range of the processing window is primarily determined by the maximum speed as the lowest speed was 10 millimetres per second for all line spacing files, except one structure built with 300 nanometres line spacing.

All the line spacing files produced their first class 5 with scan speed at 10 millimetres per second and laser power at 80 percent, except for the 300 nanometre spacing file which produced a class 5 structure at 7.5 millimetres per second at 80 percent laser power. As the 200 nanometre line spacing file produces class 5 structures at the highest speed it therefore also has the broadest processing window, followed closely by the 300 nanometre line spacing file (Figure 44). This is reflected by the increased total number of class 5 structures produced by the two smaller line spacing files, 300 nanometre and 200 nanometre, in comparison to the larger line spacing files (Figure 43, C). The 200 nanometre file may produce a class 5 structure at the fastest scan speed, but it is not necessarily the quickest file to build as it has more than twice as many lines to scan per layer. To more accurately identify which file and parameter combination can produce a class 5 structure in the shortest possible time a finer resolved parameter array was performed.

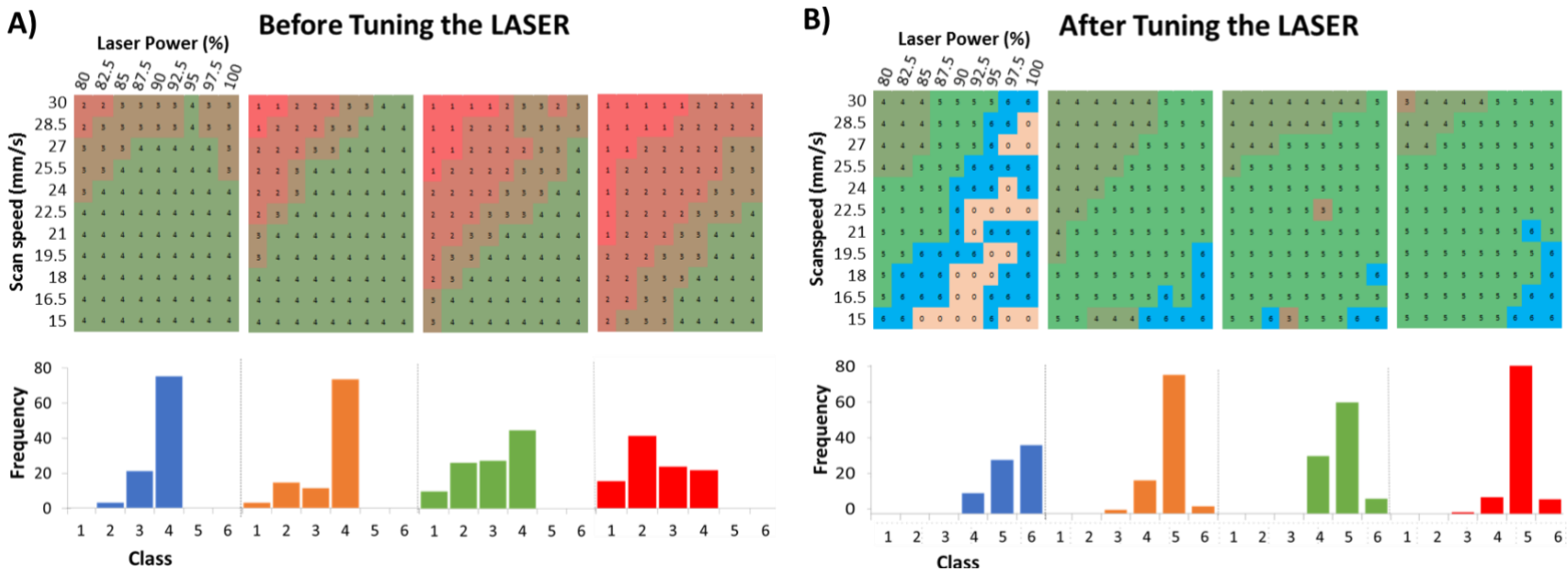


Figure 45 High resolution parameter sweep optimisation array.

Colour map and histogram of a high resolution parameter sweep optimisation array, before and after the laser was retuned. The scan speed ranges from 15 millimetres per second to 30 millimetres per second step 1.5 millimetres per second. The laser power ranges from 80 percent to 100 percent step 2.5 percent . Before the laser was retuned no structures produced were in class 5. As there is only structures in class 1-4 and no structures in class 5-6 it is likely that there is insufficient power to produce the perfect class 5 or create an explosive class 6. These results were in contrast to the coarse array which had been done about 4 weeks before. The discrepancy in the coarse and high-resolution parameter sweeps prompted the service engineer to be called upon to retune the Laser. The second colour map shows the same parameter array but after the laser had been returned to maximum power. The retuning of the laser led to a much larger proportion of the structures produced to be in the class 5 category. The 200 nanometres line spacing file now has the smallest processing window as the amount of energy deposited in any volume in a given time is higher due to the close proximity of the individual line scans. 400 nanometres and 500 nanometres line spacing primarily produced structures in class 5. That after tuning the laser and increasing the power that the polymerisation volume is now between 400nm-500 nanometres diameter. Although this is likely, it is difficult to judge the extent to which the polymerisation is influenced by the field effect from adjacent laser scans.

The high-resolution parameter sweep was performed across the rough processing window identified by the coarse parameter sweep. The rough processing window ranged from 15 millimetres per second to 30 millimetres per second scan speed and 80 percent to 100 percent laser power. The high-resolution array swept through this window at scan speed increments of 1.5 millimetres per second and laser power increments of 2.5 percent. The first attempt at the high-resolution parameter sweep did not produce any class 5 structures (Figure 45, A) but primarily produced class 4 structures. At lower powers and faster speeds, smaller optical doses, a significant proportion of the structures produced were only in classes 1-3. These findings inferred that the power was too low to produce class 5 structures which were incongruent with the findings from the coarse processing window. The high resolution parameter sweep was initially performed one month after the coarse processing window had been performed. A status report from the machine confirmed that the power output of the laser had dropped to approximately 80 percent of the normal operating power. A service engineer was subsequently called to retune the laser and the high-resolution array repeated.

After the laser was retuned repeating the high resolution optimisation array produced rather different results. All the different line spacing files produced structures that were in class 5. Producing many class 5 structures is in closer agreement with the findings of the initial coarse parameter sweep although there were still some discrepancies. When the 200 nanometres line spacing file had been fabricated using 100 percent laser power a class 5 structures had been produced, if the speed was 22.5 millimetres per second or above. The same file in the high-resolution array produced class 6 structures even at the fastest scan speed used, 30 millimetres per second. This suggests that the laser was now operating at a higher power than had been originally used for the coarse parameter sweep. The increase in power is not only apparent in the shrinking of the processing window for the 200 nanometres line spacing file but also in the broadening of the process window of the 400 nanometres and 500 nanometres line spacing files (Figure 45). In the post-tuning parameter sweep optimisation array it was possible to produce a class 5 structure with the most rapid combination of parameters tested, a 500 nanometres line spacing file built at 30 millimetres per second from. In

contrast the maximum speed the 500 nanometres line spacing file produced in the coarse parameter sweep was only 15 millimetres per second. The instability of the laser indicates a need for regular recalibration of the parameters used for any build files, even when using the same material. An alternative to recalibrating the build file's parameters would be regular retuning of the laser.

In context of the higher laser power it may be possible to produce class 5 structures from build files with line spacing greater than 500 nanometres, further reducing the fabrication time. Build files with line spacing greater than 500 nanometres would be rendered unusable as the laser power decreases over time. The 500 nanometres build file at 30 millimetres per second and 100 percent laser power was selected as the parameter combination to use for building the microstructures for patterning the neurons. As the 500 nanometres line spacing file produced class 5 structures with laser power from 90 percent to 100 percent a small decrease in power will not affect the quality of the structures produced. The total build time for a 500 nanometres line spacing build file at 30 millimetres per second is 7 seconds. As there is always a short delay of 2-3 seconds between structures the total build time for a single unit within a larger structure is ~10 seconds. Even the largest structures used to pattern neurons in the following Chapter consisted of 440 units, covering about 2 millimetres squared would take just over an hour to fabricate. Using a modular design allowed for the fabrication of a single unit to be optimised efficiently for both design fidelity and fabrication speed by building arrays of the unit with various scan speeds, laser powers and line spacings.

3.5 Discussion

This experimental Chapter aimed to optimise the two photon polymerisation of OrmoComp microstructures for design fidelity and fabrication speed. The first objective of this Chapter was to produce a modular design, allowing for a single unit to be optimised for a larger structure. The optimisation sweep was used to maximise the speed of fabrication without sacrificing mechanical stability or design fidelity the build parameters optimised included line spacing, scan speed and laser power. Being able to build at faster speeds than the custom rig allowed for larger structures to be produced in a reasonable time, ~1-2 hours per array. These are the largest structures used to pattern the growth of an *in vitro* neurons than previous attempts to do so using two photon polymerisation[19,20,96,152].

The first of objective of this chapter was to produce a modular design which allowed for rapid optimisation and redesigning. Having a modular design which could be broken down to a single unit greatly accelerated the optimisation of the design and build parameters by decreasing the time taken to scan through a sweep of building parameters. The modular design also helped avoid swelling and other post-development defects such as small gaps which have been seen observed in Chapter 2 and in previous attempts at patterning neurons using two photon polymerisation [19]. The modular design also facilitated easy reconfiguration of the units making up the structure allowing different patterns to be produced from the same optimised base units with minimal redesigning. This approach avoids redoing in the initial CAD and CAM steps, e.g. designing the structure and converting it into a laser scanning regime, when altering the growth pattern of the network. This is a more flexible approach than earlier attempts at high resolution patterning of neurons using two photon polymerisation[19,20]. It is therefore apparent that this approach is then also more flexible than laborious three dimensional photolithography processes[17]. Manually programming different configurations of grid units to produce new pattern geometries is; however, currently time consuming and lacks usability (see appendix: Describe Fabrication Codes) and therefore is not yet well suited to facilitating the

adaptation of patten geometry. A graphic user interface could be developed to facilitate this rapid adapation, removing the need for the time consuming coding. This would be an essential step in ensuring that the technique was an accessable technique for electrophysiology researchers.

The second objective of this chapter was to perform parameter sweeps to optimise the speed whilst ensuring the best possible fidelity between design and the fabricated microstructure. Initially the line spacing of the laser scan regime was varied to produced, demonstrating that a wider line spacing of 500 nanometers was over 30% faster than line spacing of 200 nanometers. Determining the line spacing is necessary when optimising a new material due to variations in the polymerisation volume and the field effect, the influence of an adjacent line scans one each other's polymerisation volume. These variations are influenced by the resin's polymerisation kinetics, optical properties and the photochemical properties of the photoinitiator. All of the above are subject to ongoing research in the field to continue improving the efficiency and qualities of existing materials as well as widen the library of materials available for two photon polymerisation.

Sweeps of scan speed and line spacing were then performed to determine optimal combination for each of the designs with different line spacings. Optimisation sweeps revealed a scan speed of 30,000 micron per second, 100% laser power and 500 nanometer line spacing was an optimal combination. However, this was only the case after the laser was retuned, prior to the retuning the optimal parameters were 27,000 micron per second, 100% laser power and 400 nanometer line spacing. This allowed for millimetre sized arrays to be produced in a matter of hours. Being able to produce much larger structures, both in terms of height and area, will allow for the largest, two photon polymerised microstructures to be used to coordinate the growth of the neurons *in vitro*[19,20,152] to be characterised in the following Chapter. The increased size of the structures allows for the control of the entire population of neurons which would be present on a microelectrode array. The dedicated hardware and software of the Nanoscribe GT (Photonics Professional ltd), the only commercially produced two photon polymerisation system, greatly increased the speed of fabrication and usability

in comparison to previous attempts using custom built rigs, such as in Chapter 2, or in the literature[19,20,93]. The influence of different microstructures on the growth of *in vitro* neural cultures will be characterised in the next Chapter.

Optimising power and scan speed not just for new materials but also new designs due to variations in structural stability based on mechanical design. Repeating optimisation sweeps regularly also ensures you are always optimising this compromise between speed and quality and avoids building sub-optimal structures due to inherent, normally decreasing, fluctuations in laser power. Considering the laser scanning regime and the mechanical properties of the design can help to maximise this compromise. Optimising designs for maximising a design's inherent mechanical properties whilst minimising build time or material usage for other additive manufacturing processes is well established[153]. Finite element analysis of the structure can facilitate the topology optimisation of design which would be beneficial to two photon polymerisation due to the slow build times and the increasing need for applications crossing into the mesoscale and therefore requiring longer build times. This need for mesoscale patterning is well recognised in tissue engineering and exemplified in the patterning of neurons *in vitro* where areas of several millimetres squared need to be patterned in structures 100s of micron high.

In summary the modular design, the optimisation sweeps, and the advancements offered by the Nanoscribe GT have facilitated the production of mesoscale structures for patterning neurons. These structures can cover a millimetre squared, with a Z height of seventy micron high, in under an hour at the speeds higher than reported in the literature. This advancement in speed also increased researcher efficiency and volume of cell cultures which could be patterned with reliably repeatable structures as well as produce larger two photon polymerised structures for pattern neurons than previously performed[19,20,152]. The speed and modular design also allowed for the neurite path to be relatively easy to be reprogrammed although the addition of a relatively simple graphic user interface would make the process facile. As a facile way of reprogramming the structures which pattern neurons

this modular design could provide an accessible platform for neurophysiologists and neurobiologist to investigate the role of basic network topology in the neural network dynamics on *in vitro.* The influence of the microstructure's design on the patterning of neurons will be characterised in the subsequent Chapter.

4 Characterising the growth of neurons cultured on microstructured substrates.

4.1 Overview

Patterning neurons *in vitro* on microelectrode arrays promises to improve the reproducibility and complexity of *in vitro* neural interfaces, producing better platforms for investigating neural network dynamics. Primary rat hippocampal neurons were cultured on substrates functionalised with different designs of microstructures built out of OrmoComp using two photon polymerisation. The different designs' efficacy at coordinating the structural topology of neural cultures was assessed initially using phase contrast microscopy. The functional topology of the network was assessed using dynamic calcium imaging and the structural topology more closely characterised using scanning electron microscopy (SEM) and fluorescence microscopy.

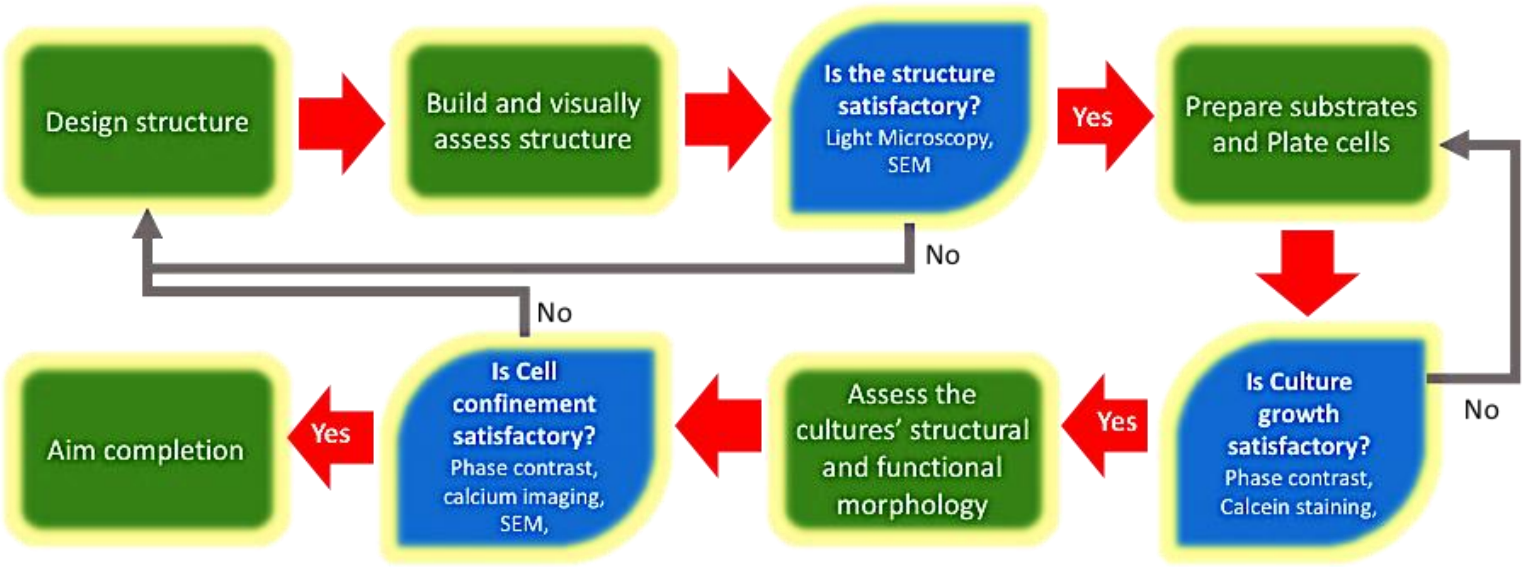


Figure 46 Workflow aiming to pattern neurons using two photon polymerised microstructures. Red arrows indicate normal progress with grey arrows indicating data informing alterations to previous steps.

The process of producing OrmoComp microstructures for patterning neurons was performed with three sequential feedback loops (Figure 46). Each feedback loop used specific characterisation tools to determine the suitability or efficacy of the protocol or design used. The first feedback step was to determine, via bright field microscopy, if the design produced a structure of sufficient structural stability to undergo the development process. Once a stable structure and build file had been produced the structures were then prepared for cell culture according to the protocol developed in the Second Chapter on substrate preparation. The samples were plated with dissociated embryonic rat hippocampal cells and the sample was grown for up to 4 weeks and monitored regularly using phase contrast microscopy. If the culture was observed ignoring the presence of the microstructure then the microstructure was redesigned to improve the influence of the structure on the growth of the culture. When the phase contrast images of a certain design suggested that the microstructures were coordinating the growth of the culture, the functional topology was then characterised using dynamic calcium imaging. As the functional topology seemed to differ from that observed in the phase contrast microscopy further structural characterisation was performed using fluorescence microscopy and SEM. Although the patterning efficacy was improved a proportion of smaller neurites grew over the top of the walls. Interestingly the neurites which grew over the walls were often influenced by the shape of the structure leading to a network growing in a regulated manner in three dimensions. Characterising the growth of neurons on microstructures can be difficult to interpret, highlighting the need for multiple forms of characterisation. Although the topology was never fully constrained by the microstructure it was heavily influenced by the presence of the microstructures. Importantly, soma aggregation appeared to be inhibited by the presence of the microstructures and the guidance effect on the neurites is comparable to any reported in the literature so far [11,19].

4.2 Methodology

4.2.1 Designs for patterning neurons.

Several designs were produced to test the effect of design on coordinating the growth of an *in vitro* neural culture. The designs were made iteratively, with the findings from the previous design informing the subsequent design. The first design, the hexagonal design, comprised of a tessellated hexagonal compartments which have a 2 micron channel connecting each unit to 4 out of 6 adjacent units (Figure 47). The walls of the hexagonal compartment were 3 micron high and 4 micron thick. The hexagonal array was enclosed within a 10 micron high and 20 micron thick wall. To prevent the formation of gaps in the outer wall, at the seams of adjacent build volumes, the wall is divided into sections which are joined via jigsaw joints. All the designs were sliced into 5 micron layers and line spacing was set to 5 micron as per the findings in the previous chapter on the optimisation of OrmoComp two photon polymerisation.

The second design, the high density microelectrode array (HD MEA) design produced was built to fit onto a microelectrode array with 10 micron diameter contact pads, space at 50 micron (Figure 48). The walls were built to a height of 25 micron, higher than the hexagonal arrays, to further constrain the growth of the neurites. A spiral path of 2 micron wide channels connects adjacent compartments of the grid-like array. The top rim of each compartment is chamfered to encourage seed neurons to land on the surface of the compartment rather than on the top surface of the wall. A thin outer wall was used as an additional barrier to the surrounding microculture. Each unit of the design is built individually allowing for rapid reprogramming of the configuration of channels in the design as well as avoiding the need for splitting and stitching of the structure which can lead to defects and gaps. Gaps are particularly an issue when patterning neurons as the neurites and cell bodies can fit through gaps of less than 500 nanometre and 3 micron respectively.

The third design, also built modularly like the HD MEA design, has 40 micron high walls and 30 micron squared compartments but and covered an area of 500 micron squared, the large area array (Figure

49). A border of pyramidal units surrounded the central structure as an extra barrier from the surrounding culture that would also encourage cells to land on either side rather than on the barrier. Another two layers of conventional units were surrounded the pyramidal layer as further separation. The two outer layers were formed of units shaped into u-turns with the intention of allowing neurites from the macro culture to enter and then be guided in the opposite direction, back to the macroculture. To demonstrate the rapid reconfiguration the modular approach facilitates, a second large area was also produced (Figure 58).

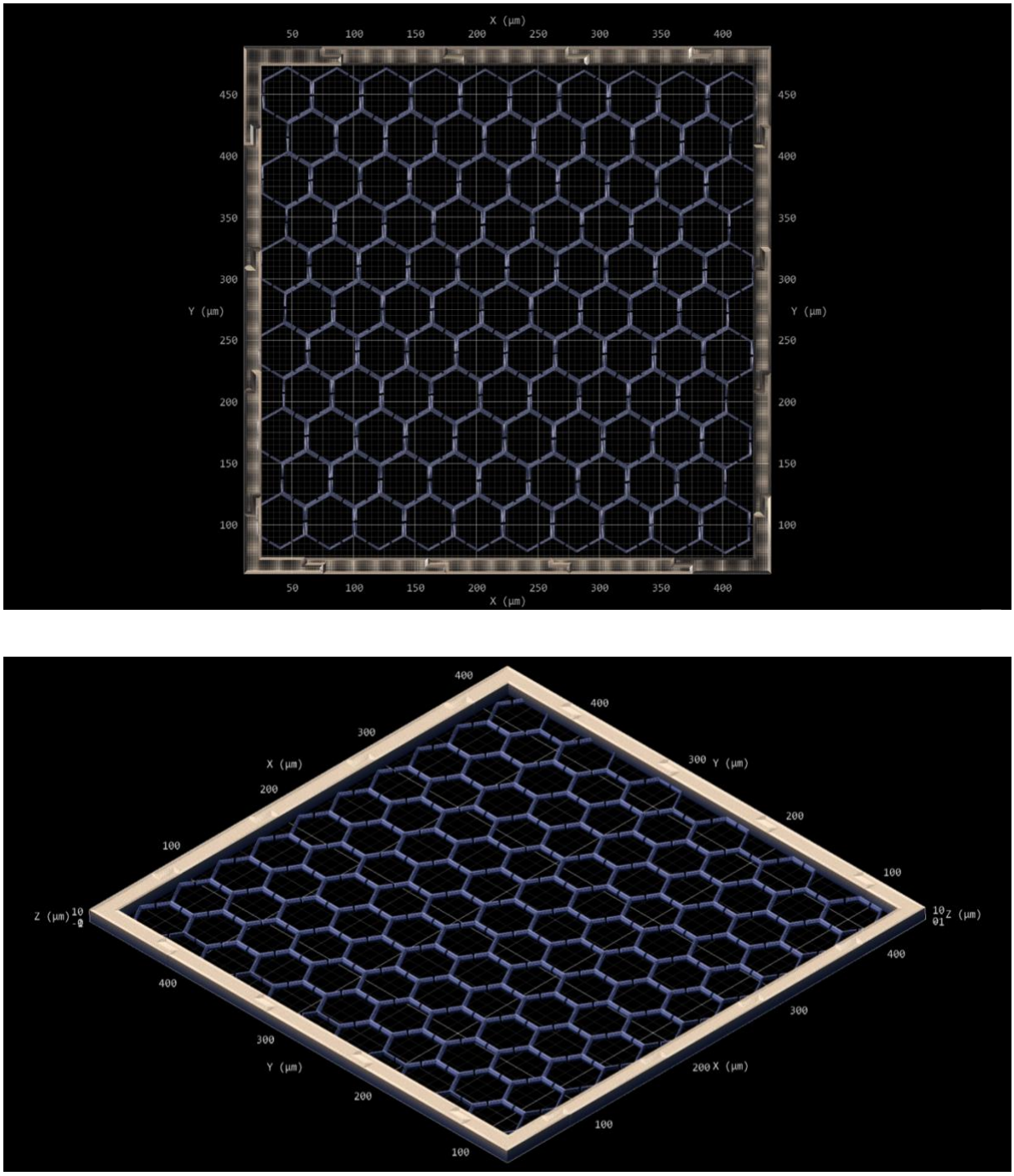


Figure 47 Hexagonal design

Top image: The array covers an area of 450 micron squared. The hexagonal units have a width of 40 micron and walls 4 micron thick. Each unit is connected to 4 out of 6 adjacent compartments via a 2 micron wide channel. The outer wall is 20 micron thick and 10 micron high

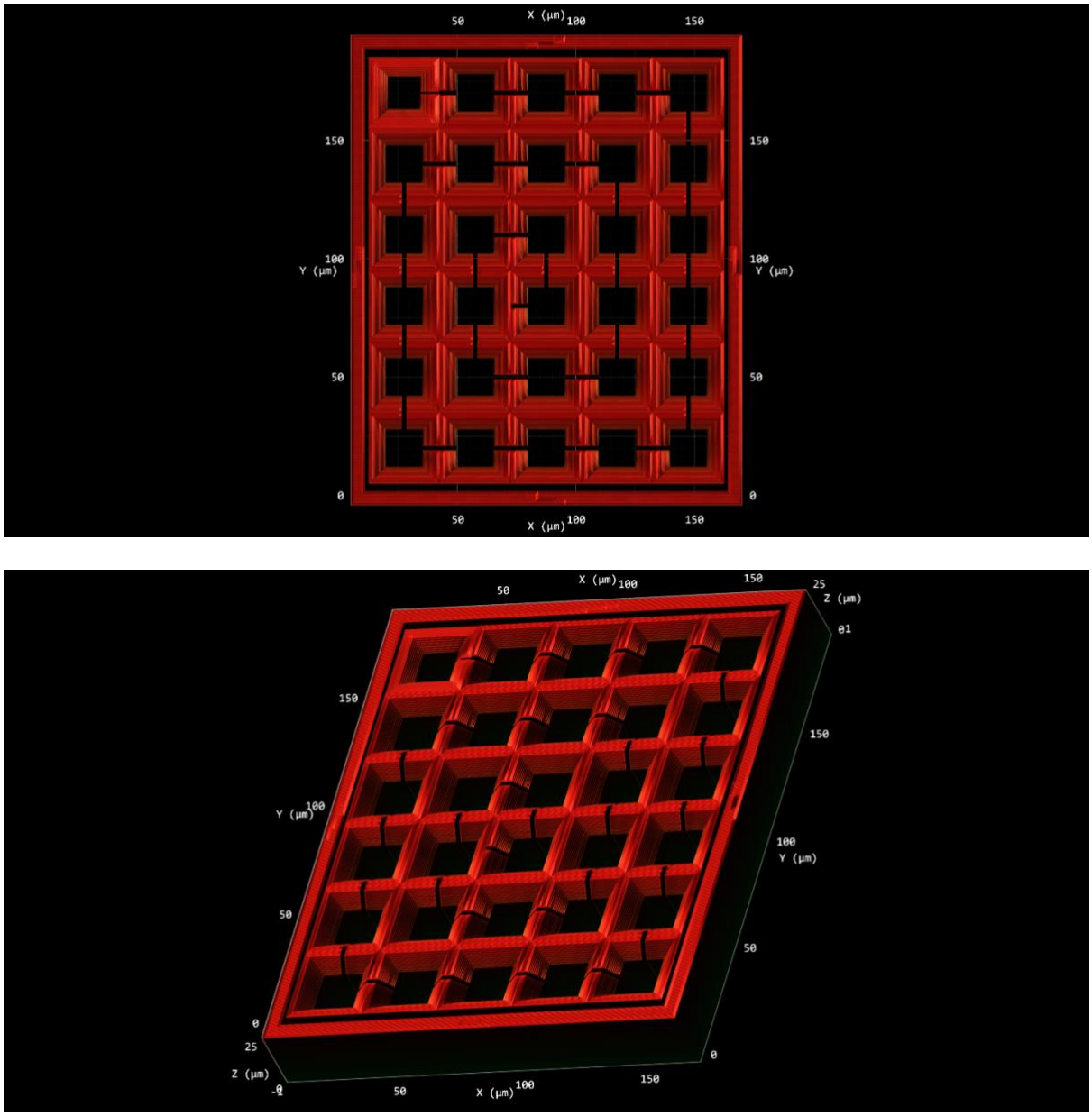


Figure 48 High definition microelectrode array design

Top image shows plan view of the high definition microelectrode array design. Each unit is 30 micron squared, based on the pitch of electrode pads on a high definition microelectrode array. The total array of 5 by 6 units makes the total grid area 150 micron by 180 micron. The surrounding 6 micron thick outer wall, and two micron space, makes the total floor print 176 micron by 196 micron. The channels connecting adjacent units of the grid are two micron wide and arranged to allow only a single spiral path through the grid.

Bottom image shows three dimensional view of the high definition microelectrode array design. Height of all walls is 25 micron high. This height was used after initial attempts to pattern neurons with the with the hex array failed to contain the cell bodies and neurites and the higher outer wall had appeared more effective. The chamfered rim of each unit is to decrease the probability of a neuron cell body land and adhering to the top of the wall during seeding.

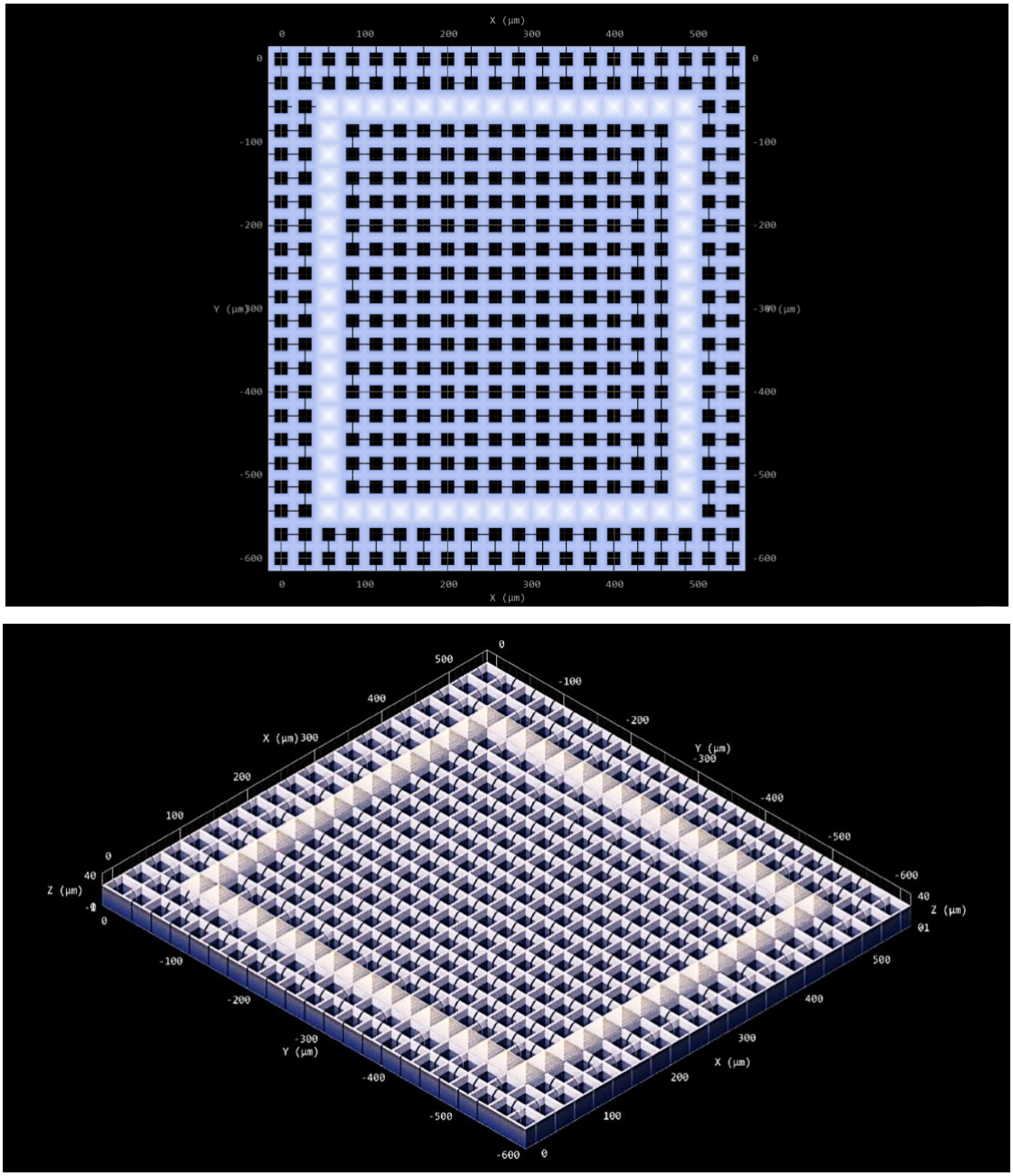


Figure 49 Describe simulation of large area array

Top image shows plan view of the large area array. Each unit is 30 micron squared and 40 micron high. The total array covers an area of 540 micron by 600 micron. The two micro channels connecting adjacent units of the grid are two micron wide and arranged to allow only a single zig-zagging path through the grid that forms a loop. A border of pyramidal units intended to act as a barrier for cells landing or neurites growing. Surrounding the pyramidal layer is another two layer of nits which form blocks of four that make a u -turn intended to divert the neurites from the microculture away from the cells growing inside the structure.

Bottom Image, three dimensional view of the simulated structure showing the pyramidal border jutting 10 micron proud of the other units.

4.2.2 Calcein-Acetomethyl Staining

The intensity of fluorescent emission from certain fluorophores can be very sensitive to the concentration of calcium. This sensitivity to calcium concentration is often due to the fluorophore being attached to a calcium chelater. The non-fluorescent acetomethylated derivative of calcein, Calcein-AM, can cross into the cell membrane where esterases remove the acetomethyl group, which facilitated the molecule crossing the cell membrane. Within the cell the acetomethyl group is cleaved by intracellular esterases which exposes a divalent cation chelation site. The binding of the cation, e.g. calcium or magnesium, leads to an increase in fluorescent emission. The now fluorescent molecule remains trapped within the cell where it fluoresces upon excitation of light at a wavelength of 495 nanometre. As the molecule can only fluoresce from within living cells it can provide a useful method of short term imaging neurons to determine the presence of living cells in a culture. The imaging is limited to short term imaging as the fluorescent form of the dye will undergo photobleaching producing free radicals in the cytosol which are cytotoxic.

4.2.3 Calcium Imaging

The propagation of an action potential results in an influx of calcium ions into the cytosol of a neuron, primarily at the presynaptic bulb. This calcium influx stimulates the vesicular release of neurotransmitters into the synaptic cleft to stimulate the next neuron. By incubating excitable cells with calcium sensitive fluorophores it is also possible to image the activity of the cells. The activity is imaged by monitoring the fluorescent intensity emission over time which is related to the fluctuating intracellular calcium concentration. The technique can be used to infer an order of activation as part of characterising the functional topology of the neural network [18].

4.3 Experimental

4.3.1 Cell dissection, dissociation and seeding

The cell culture and surface treatment protocols used were the same as in the Second Chapter on substrate treatment optimisation. To achieve higher concentrations of neurons within the fabricated microstructures 1 microlitre of the original high concentration cell suspension (~1 million cells per millilitre) was pipetted over the structures whilst the standard cell suspension was adhering. After the cells were plated on the coverslips, they were cultured in a 5 percent humidified CO_2 atmosphere at 37 degrees Celsius except when being imaged with phase contrast microscopy.

4.3.2 Calcein staining and imaging

When staining cells it is best to cause as little perturbation to their physiochemical environment. To minimise the impact of the solution's osmolarity on the culture 100 microlitre of the culture media was removed and used to dissolve a 1 micrograms aliquot of the calcein-AM. After a brief vortex the calcein-AM infused culture media was returned to the culture well plate and left to incubate for one hour. Then, without washing, the sample was imaged using the Fluorescein isethionate (FITC) filter cube, excitation waveband of 467-498 nanometres and emission waveband of 513-556 nanometres (Nikon Eclipse Ti- U) . The sample does not need washing as the extracellular Calcein-AM had not had the AM group removed and therefore does not produce background fluorescence.

4.3.3 Dynamic Calcium Imaging

All dynamic calcium imaging was undertaken after fourteen days *in vitro* as up until this point the culture is still establishing synapses and electrical activity. A 200 microlitre aliquot of media was taken from the sample intended for imaging and tested the osmolarity of the solution using a single sample osmometer (Advanced Instruments). A sterile solution of extracellular solution (ECS), a standard solution used in patch clamping experiments, was adjusted to the correct osmolarity as the cell media through the addition of sucrose. 5 micrograms of the calcium dye, Fluo-4, was thawed and diluted in

1 millilitre of the osmolarity adjusted ECS, the cells were then left to incubate for 2 minutes. The ECS was then removed and the cells were immersed in media. The stained culture was then placed on a Nikon Eclipse Ti-Universal upright microscope and imaged through a 40 times magnification objective and phase contrast imaging was used to locate a microstructure on the substrate. The culture was then illuminated by a white light LED and imaged through a FITC filter cube for 180 milliseconds at 12 frames per second. The camera used was an electron multiplying charged coupled device also known as an EMCCD. The electron multiplier register boosts the signal before the output amplifier adds any readout noise. This allows for improved sensitivity even at the high speeds that dynamic calcium imaging demands.

The pixels of each frame represent the fluorescent intensity proportional to the concentration of calcium. The boundaries of each soma were highlighted manually and the raw signal for each cell created by averaging the intensity of all pixels within the boundary at every time point. Bleaching causes the signal to slope off, but this was corrected for by performing a centred running minima analysis by dividing every intensity value by the minimum intensity value within the surrounding 20 second period of values.

4.3.4 Scanning Electron Microscopy

The samples were dehydrated using ethanol. The ethanol was applied gently by pipetting the ethanol across the substrate so as not to disturb the neurons adhered to the substrate sample. The sample was first removed from the well plate. The tips of two p1000 pipettes placed into the layer of media remaining on the substrate. Whilst one pipette is slowly ejected of ethanol the other pipette draws the cell media, and ejected ethanol, across the substrate and into the tip.

4.4 Results

A series of designs were fabricated on the Nanoscribe GT, treated with the substrate treatment protocol for Ormocomp microstructures developed in the first experimental Chapter and subsequently seeded with primary rat neurons. Each culture's growth in relation to the microstructure was monitored using phase contrast microscopy and the findings were used to adapt the design until a structure appeared to successfully control a neural culture's topology. The first design was a hexagonal grid surrounded by an outer wall, 8 micron high, to keep the neurons within the structure separated from the cells outside the structure (Figure 50). The hexagons, 3 micron high, that tessellate to make the grid have a small channel, 2 micron wide, in five of the six walls. One of these channels was always blocked by the non-channel wall of an adjacent hexagon. The purpose of the channels was to allow neurites to pass through whilst the walls of the hexagons constrained the migration of the soma.

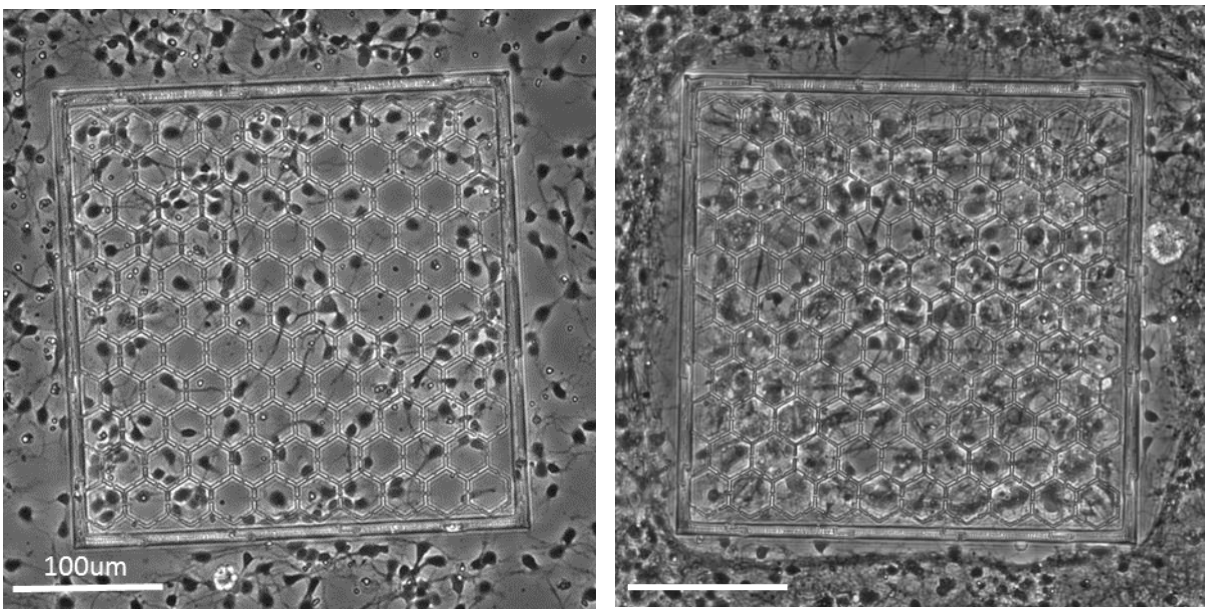


Figure 50 Hexagonal array surrounded by outer wall.

Top left image shows Describe Simulation of the entire design whilst top left shows a close up of one corner of the array. The array is surrounded by an 8 micron high wall intended to isolate a microculture growing within the microstructure from the surrounding macroculture. The internal walls are 3 micron high with 2 micron wide gaps linking each compartment of the structure. Bottom: phase contrast images of culture at 5 (left) and 28 (right) days. Note the alignment of neurites at day 5 and the dense build-up of neurites at the outer wall at day 28. Scale Ba: 100 micron.

Although the neurites show a preference for growing through the gaps in the inner walls at first, visible by the prevalence of parallel neurites within the structure (Figure 50, bottom left), neurites are also visible crossing over the walls. As the culture matured the neurites increasingly grew over the 3 micron high walls. The structure is also surrounded by an 8 micron wide and ten micron high wall. Heavy aggregation and fasciculation of the surrounding macroculture is visible proximal to the outer wall with many of the fascicles growing in parallel to the wall, visible as a dense cable in the bottom of the image and by the small space separating the outer culture and the outer walls around the majority of the structure (Figure 50, bottom right). This observation suggested that the outer wall was restricting the growth of the macroculture into the microculture residing within the microstructure more so than the inner walls were restricting growth between units of the grid. This effect is emphasised when comparing these cultures to hexagonal arrays without outer walls (Figure 51). When no outer wall is present the distribution of neurons seems to remain less uniform within the structure and the is no build-up of neurites around microstructure. The difference between the inner and out walls amounted to a difference of 5 micron in height and 4 micron in width. Increasing the height and width of the structures may therefore improve the containment of the neurons.

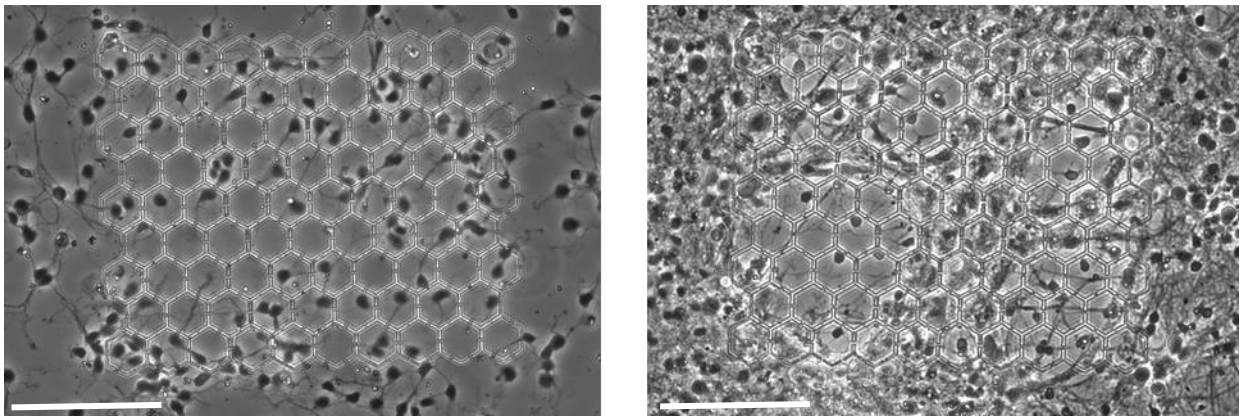


Figure 51 Hexagonal array without outer walls.

Regions with few cells to begin with are slowly infiltrated whereas more populated regions become rapidly denser in neurites this could be due to a neurotropic effect where the more cell dense regions produce larger amounts of a neurotrophic factor guiding neurites towards it. There is no visible build-up of neurites around the microstructure. Scale bars 100 micron.

The gaps between each of the internal compartment s of the microstructure were two micron wide. As the nuclei of most mammalian cells are unable to deform to a have a cross sectional area of less than three micron squared the two micron gap was intended to prevent the migration of neuronal soma from one compartment to the next. It was observed that cells could squeeze through such gaps and also that many soma did successfully change compartment (Figure 52). This is possible as the cross sectional area of the gap was greatly increased due the low walls, only 2 micron high, essentially giving the cell extra headspace to squeeze through the gap. As with the other observations from the hexagonal arrays this indicates that higher internal walls may provide better constraint of soma migration and overall better control of the culture's growth.

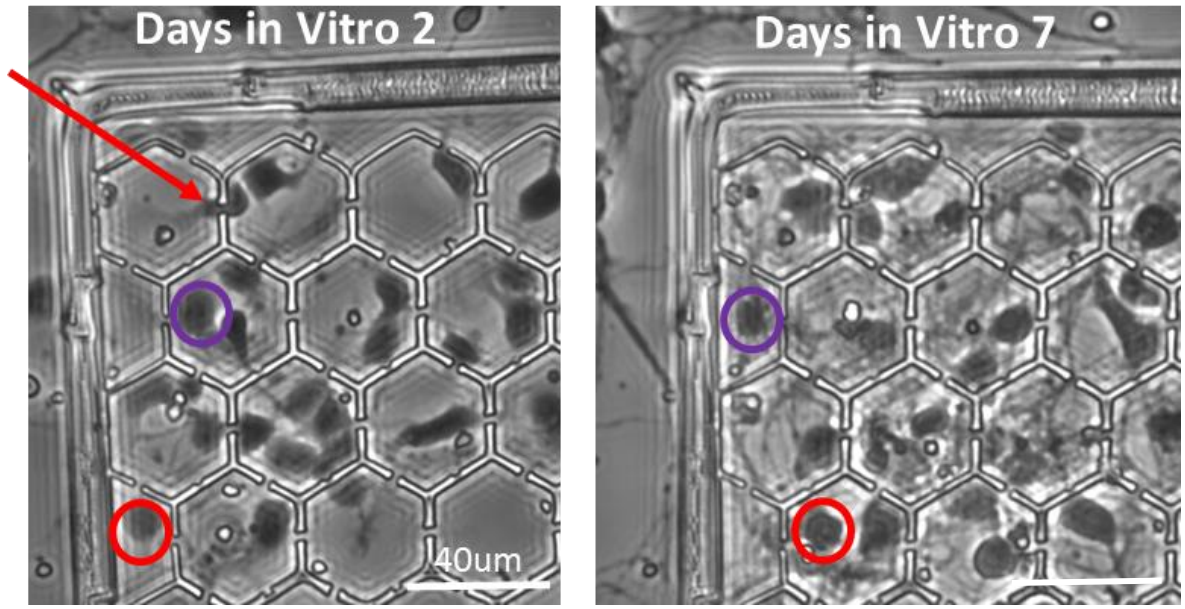


Figure 52 Cells moving between the internal compartments of the hexagonal microstructure.

Cell can be seen squeezing through the gap in the wall (red arrow). Cells switch grids, possible to more equally distribute themselves. (Purple and Red labelled cells). Scale Bar: 40 micron.

To ensure neuron soma remain in compartments and neurites do not grow over separating walls the next design of structures were designed with walls 25 microns high. The new structures were also designed to have only one path interconnecting all the units of the grid to provide the single longest route for a signal to propagate through a network patterned by the structure in preparation for

calcium imaging experiments. The units of the grid were 30 micron apart to facilitate alignment to a high density microelectrode array, with one electrode in each unit. The channel gap was also decreased from 2 micron to 1 micron with the intention of reducing the ability of the neuronal soma to squeeze from one unit to another. The thickness of the separating walls was also increased to avoid producing overly slender walls which would likely be damaged during development as shown previously with OrmoComp microstructures[19].

According to the phase contrast images the cultures grown in the HD array microstructure appear to grow with much more fidelity to the designated path than in the hexagonal microstructures, visible by the spiralling of neurites through the microstructured grid (Figure 52). The area of each compartment however was reduced which led to reduction in the total number of cells in each microstructure as well as a decrease in the occupancy of the microstructure. The occupancy of each microstructure unit, which is ideally one cell per unit, averaged at about one cell in every third unit (Figure 46). To increase the number of occupied units 1 microlitre of a highly concentrated cell suspension solution, at one million cells per millilitre, was directly pipetted on top of a structure once it had already been plated with cells in the standard drop cast method used in the initial experiments. This approach filled almost all the units, with only a few units of the grid unoccupied, however the number of cells per unit also increased. More than one cell in each unit is not desirable as it moves away from the one electrode to one cell interfacing resolution. The increased population per unit is probably due to the overall increased density on the substrate but also enhanced due to the tendency of cells to aggregate when in high density solutions. As the phase contrast imaging demonstrated good pattern fidelity for the HD array microstructures calcium imaging was undertaken to ascertain whether the functional topology resembled that of the intended design.

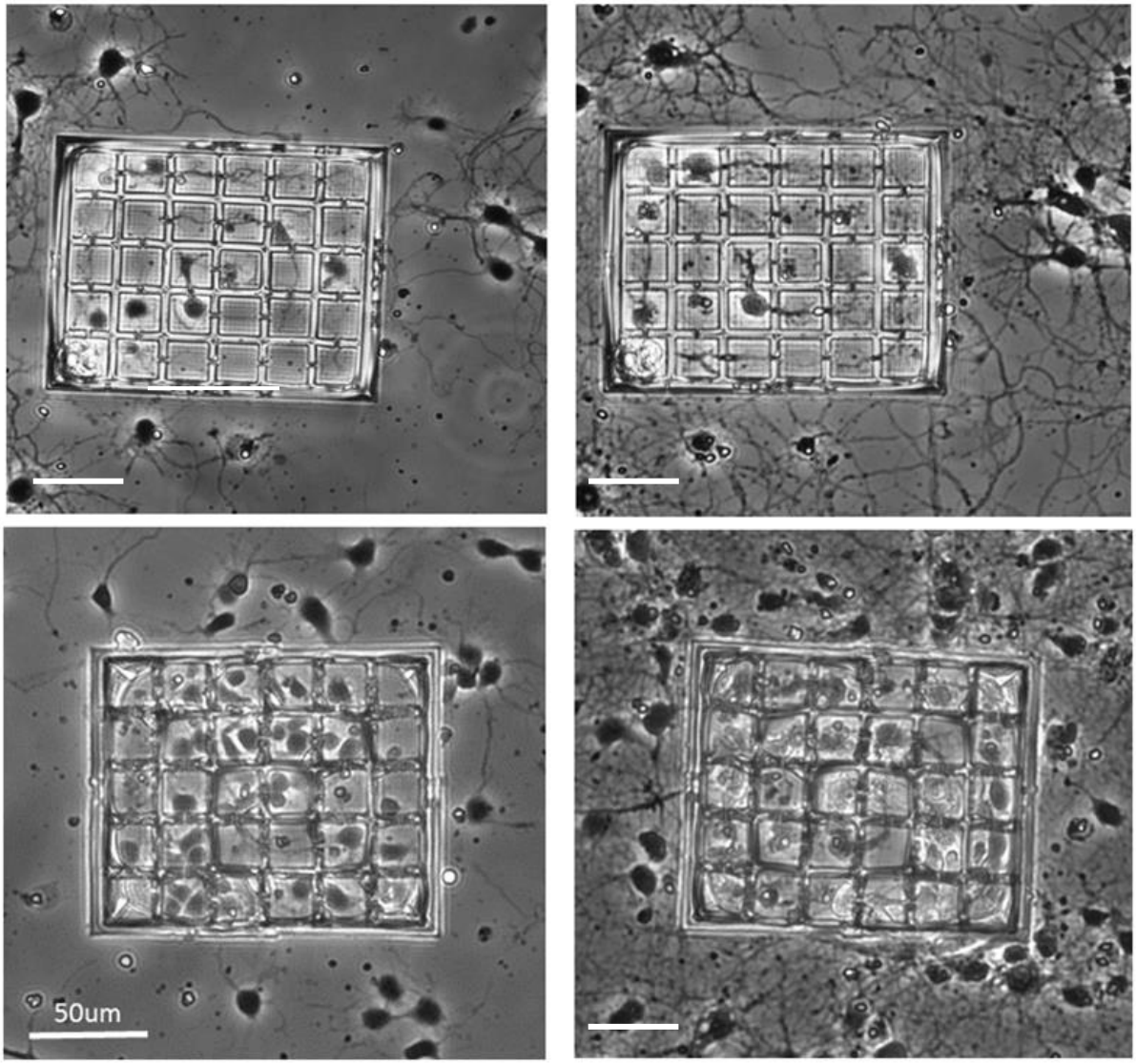


Figure 53 Array designed to fit on a high density microelectrode 5 x 6 array.

Top image: Describe simulation of the structure designed to fit to high density microelectrode array. Middle: Phase contrast micrographs of the same culture at 5 (left) and 28 (right) days in vitro. In both images the cell soma are in the same place and the neurites within the structure appear to mainly pass through the channels intended for them. Bottom: Microstructures designed for high density microelectrode array plated at twice the normal density. (left) 2 days in vitro, (right) 28 days in vitro. Note how although almost all the units in the grid are occupied many of them have 2 or often 3 cells per unit. The high occupancy makes the path of the neurites too difficult to discern. Interestingly neurons seem to migrate towards the structure, increasing the density of cells at the border of the microstructure. Scale Bar: 50 micron.

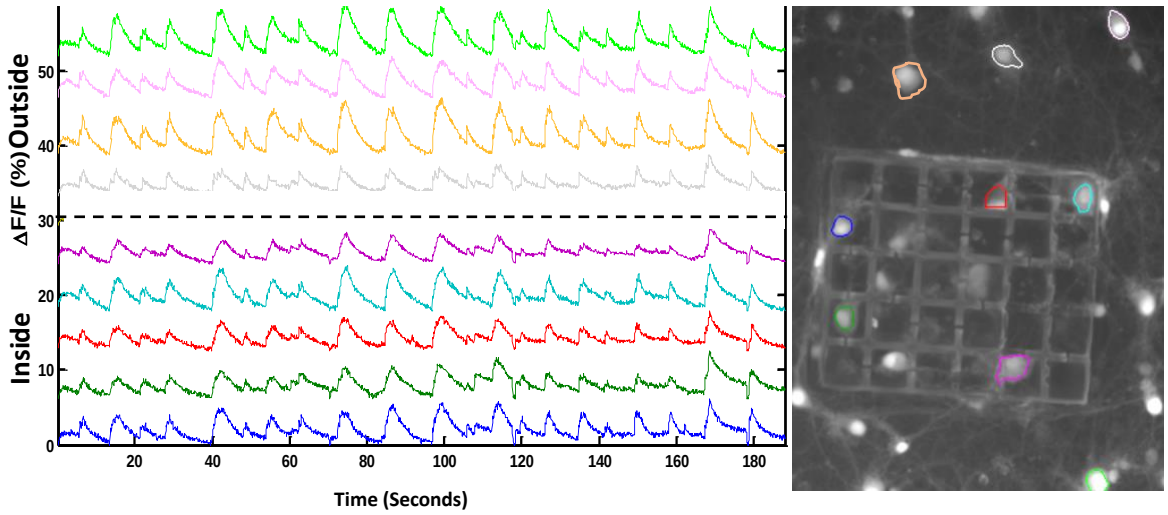


Figure 54 Extracted traces from calcium imaging of neurons cultured on direct laser written microstructures.

Each trace represents the normalised activity of each demarked region of interest, coloured rings on image. The top four traces are outside the structure and the other five are within the structure. Note how both cells inside and outside the structure are active and how the whole culture, both inside and outside the microstructure. fire synchronously.

Calcium imaging, performed according to the protocol described in the experimental section of this chapter, was able to determine that electrically active cells were present both inside the microstructure and in the surrounding macroculture. Cell soma were identified using a circle fitting function and are visible in the left-hand image by the coloured circles (Figure 54). Each coloured line refers to the normalised intensity variations in the corresponding coloured 2D area on the fluorescent intensity image. Synchronous bursting of cells both inside and outside the structures was observed (Figure 54) suggesting the two cultures were not only both active but functionally connected to each other. This differed with the phase contrast data which had suggested that the microstructure was sequestering the cells occupying the microstructure. The fluorescence intensity image from the calcium stain although difficult to discern, suggested some neurites may have crossed over the barriers (Figure 54, top right corner next to the turquoise). The interconnectivity of the neurons inside and outside of the structure prompted further characterisation of the structural topology of the networks grown in microstructures. This was performed by further fluorescence microscopy and SEM and will be detailed at the end of this Chapter.

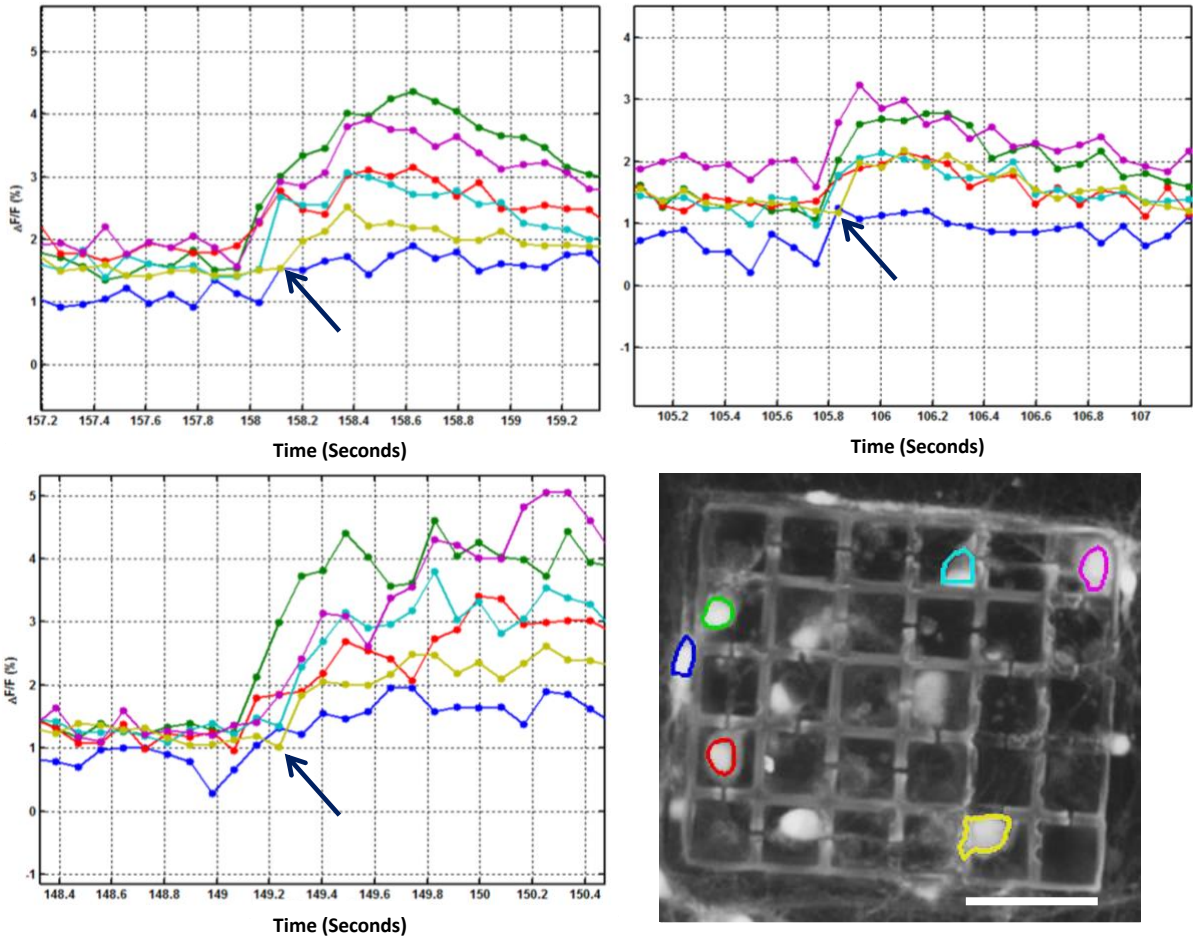


Figure 55 Delayed onset of calcium wave of neurons positioned further inside the grid.

Calcium traces from of neurons cultured in HD MEA grid microstructure. The 3 traces are close ups of individual events from the traces recorded above. Note the yellow trace is delayed by approximately one sample point, 200 milliseconds. The blue trace shows most variability in activation order and is outside the structure. This may suggest that the structure has acted to reduce the total number of connections reaching the neurons in the structure, therefore limiting the possible stimulation regimes that could lead to depolarisation. Scale bar 80 micron.

Despite the interconnectivity with the outer macroculture the internal microculture appeared to have a detectable order in the firing of neurons which was related to their position in the microstructured grid. Figure 54 shows close ups of three individual peaking events in the trace with the yellow trace repeatedly peaking later than the other cells within the structure shown. This suggests that the other cells depolarise first and subsequently activate the yellow circled cell. Cells deeper in the structure than the yellow cell appear quiescent; they do not depolarise into an action potential. Cells between

the yellow cell and the cell at the very centre of the spiral do show some low level activity (Figure 56, red and green). This activity is similar to the activity of the quiescent cells outside the structure suggesting that they are receiving some synaptic input but not enough to trigger an action potential. The cell at the very centre of the spiral however shows significantly less activity than the other quiescent cells, which may be because the only cells stimulating it are its two neighbours (Red and Green) which although show some activity do not peak into an action potential which would stimulate the central cell. It is possible however that the quiescent cells are actually not neurons, possibly astroglia, and this would explain the lack of activity. Determining the cell type could be done using immunohistochemical staining post-culturing.

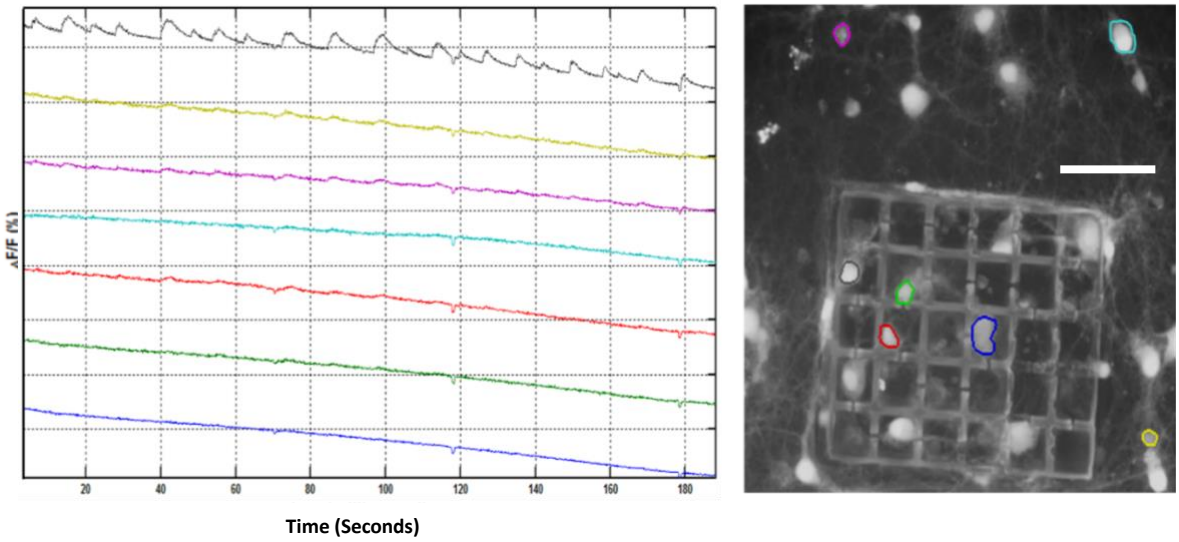


Figure 56 Comparison of quiescent cell traces.

Top trace shows an active cell for comparison. The majority of cells including the red and the green show a very low level of synchronised activity. The bottom blue line shows distinctively less signal, suggesting that residing deeper in the structure the leads to less functional connections and less activity. Scale bar: 80 micron.

Calcium imaging revealed synchronous firing of cells both inside and outside the structure indicating functional connectivity between the microculture and the surrounding macroculture. Upon closer examination of the calcium the cells within the structure appear to have an order of activation reflecting their position within the structure. To better characterise the structural topology of cultures

grown in these microstructures a combination of calcein staining and scanning electron microscopy were undertaken. The additional structural characterisation was performed on two different larger arrays to demonstrate how the technique can be rapidly scaled up and the configuration of the pattern changed. These larger structures, although mainly just a larger array of the HD MEA design, incorporated additional grid units in u-turn configuration forming a border around the edge of the structure. These U-shaped channels were intended to prevent aggregation directly next to the structure and to divert neurites away from the structure rather than attempting to directly repel them. Although the U turn channel produced U turns in the growth of the neurites some neurites can be seen growing on from the U turn to grow over the pyramid border (Figure 57). To see if a further increase of height would better restrict the neurite growth the walls of this structure were made to 40 micron in height.

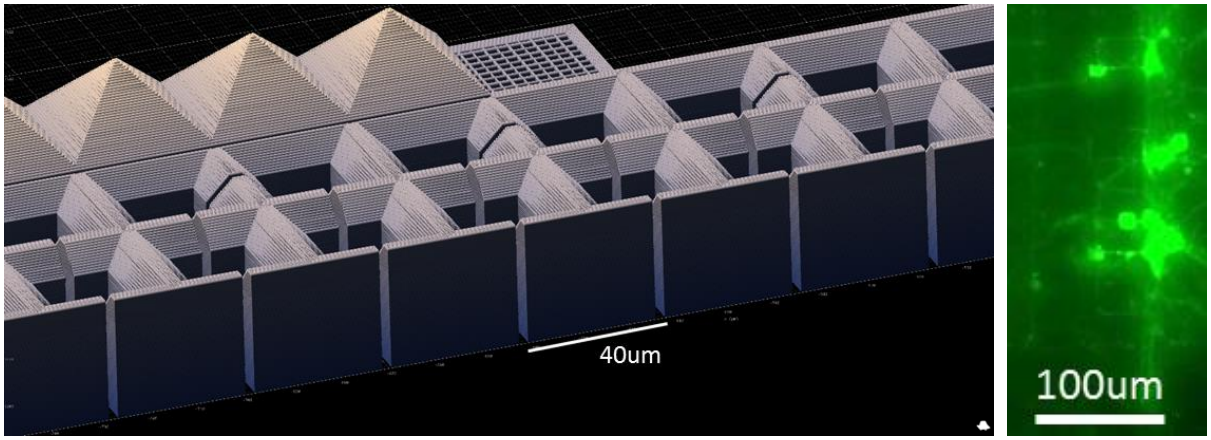


Figure 57 The power of suggestion: Diverting neurites instead of containing them.

Left: Describe simulation of a portion of the outer boundary of the microstructure design. The pyramid shaped boundary intended to prevent cells landing and adhering to those regions, they are also used to block out units in the grid. The pyramids are the tallest structures fabricated at 70 micron. The u-turn shaped path laid out by the other boundary units is intended to divert neurites headed for the structure away from the cells occupy the structure. The internal mesh is visible within a partially constructed pyramid which forms part of the boundary. Right: Fluorescence intensity image of calcein stained culture growing at the u-turn and pyramid boundary. Although the neurites follow the u-turn some of them grow through the gaps between adjacent pyramid border units.

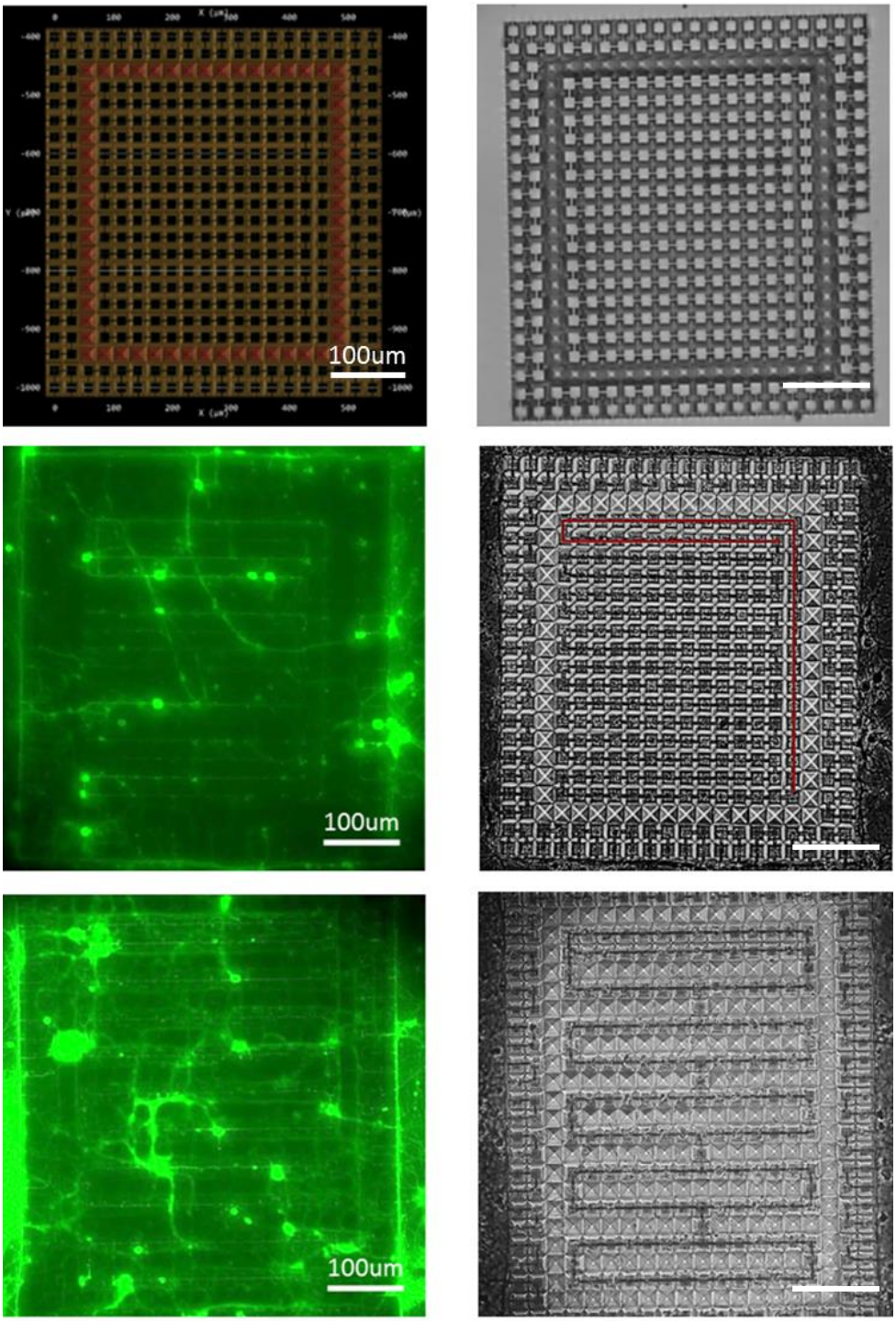


Figure 58 Calcein-AM and phase contrast images of large area microstructures for patterning neurites.

Top left: Describe simulation of build file of zig-zag microstructure. Top right: Brightfield image of microstructure before cells. Mid left: False colour fluorescence intensity image of calcein stained culture in zig-zag microstructures imaged at two weeks in vitro. Mid right: Phase contrast image of culture in zig-zag microstructure Bottom left: Phase contrast image of looping structure with culture imaged at four weeks in vitro. (Bottom right) False colour fluorescence intensity image of calcein stained culture. Scale bar: 100 micron.

The higher walls of the larger structures somewhat obscured the growth of neurites through the structure when observed using phase contrast microscopy. When compared to an unoccupied structure it was possible to see a black cord of neurites running through the entire structure (Figure 58), although this is clearer when manually shifting the focus of the microscope. The shape of the culture within the structure was further revealed with the use of calcein staining and fluorescence microscopy. The calcein image of the zig-zag structure after 14 days (Figure 58, middle left) show about ten cells occupying the structure and spreading their neurites though the channel path. The growth of the neurites through the patterned channels has high fidelity to the intended path, at least at the focal plane approximately corresponding to the substrate surface. It is, however, also clear from the out of focus neurites in the image that some neurites grow over the walls of the microstructure. Most of the neurites growing over the structure appear to be smaller in the fluorescence image. In a scanning electron micrograph a similar relationship is visible with large neurites growing through the channels of the grid whilst multiple smaller neurites grow over the structure. Interestingly it appears as though there are sometimes two layers of neurites, some closely adhered to the substrate surface with others suspended across grid units with adhesion points at the channels linking grid units[154].

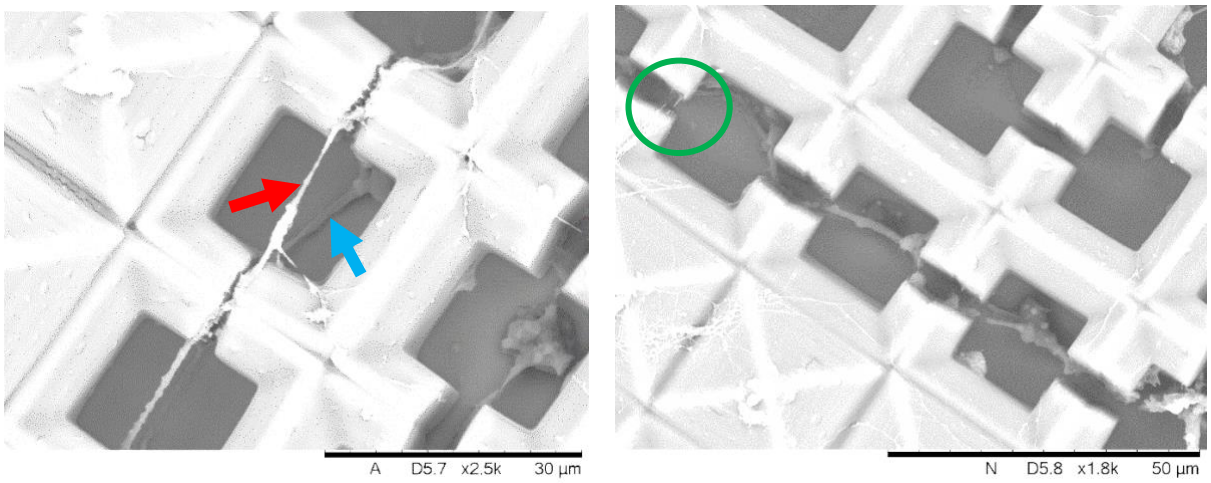


Figure 59 SEM of neural processes passing through the channels in the grid.

The larger processes seem to primarily pass through the channels whilst smaller processes pass over the walls. Interestingly the neurites seem to be both close to the substrate surface (red arrow) and suspended between two channels (blue arrow). Smaller processes can be seen to be bridging the gaps across a single channel (green circle).

In the calcein image of the zig-zag structure a large fascicle can be seen sectioning off the top right corner of the structure. Although this appears to have grown right over the structure there is a possibility that it is a connection that formed around the edge of the structure and once formed detached from the surface to shorten the total length of connection. This is a process observed in the developing nervous system *in vivo* for minimising the distance an action potential has to be propagated, therefore decreasing the metabolic load and propagation time[58,61]. In the fluorescent image of the other looping pattern (Figure 58, bottom left) it is possible to see the in focus tight thin track of neurites following the loop determined by the structure. Dominating this image however are the out of focus tracks which seem to run around the top of the walls of the grid units. Although not the intention of the original design this phenomenon eludes to the ability of the microstructure to effectively coordinate the growth of a three dimensional network of neurons using two photon-polymerised microstructures. This effect was further illustrated by some of the scanning electron micrographs taken of the culture where it can be clearly seen that neurites are growing round the edge of the grid units and even form a synapse at the apex of one of the tapered walls (Figure 60).

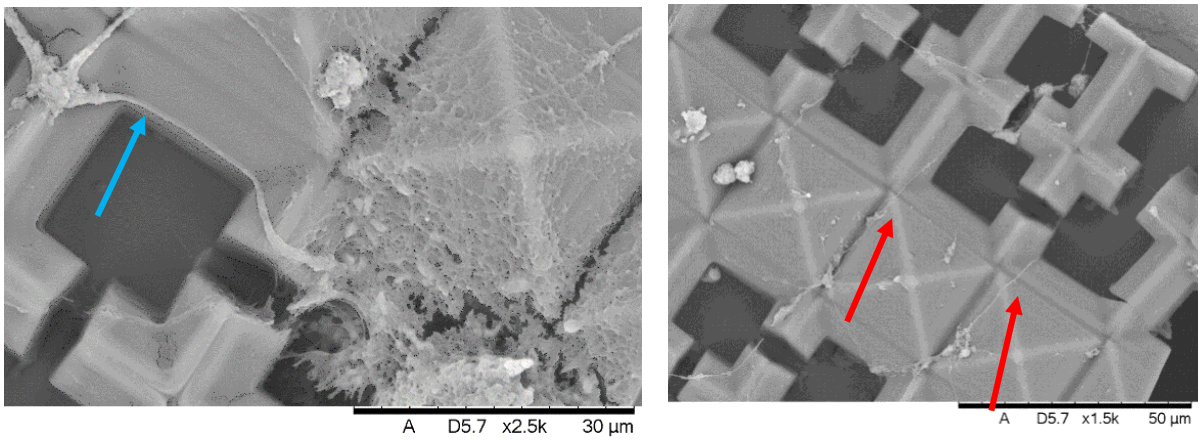


Figure 60 Neurites aligning on a second level.

These SEMs show neurites growing on the OrmoComp microstructures and following the topographic features such as the rim of the units in the grid (Blue arrow). The image on left the also shows several neurites meeting at the apex of a wall and forming a structure which resembles a synapse. The image on the right shows small neurites breaching the pyramidal wall at grooves and corners, in a somewhat parallel fashion to each other (Red arrows).

To determine the feasibility of aligning the microstructures to a micro electrode array a micro electrode array with one hundred micron electrode spacing and 30 micron electrode pad diameter was used as a substrate for two photon polymerisation of OrmoComp. An adapter plate for the sample holder was printed using an ObJet inkjet three dimensional printer (Stratasys). This allowed for the microelectrode array to be inserted into the Nanoscribe and approximately centred. As the holder is not precision manufactured the centre point of the MEA varied each time and as such had to be manually determined by using the Nanoscribe's fiducial camera to zero the job file coordinates in the Describe software. The alignment process worked sufficiently well to position the microelectrode in the centre of a square chamber, as shown in Figure 41. The structure suffered severe defects due to excess heat caused by the gold microelectrodes (Multichannel systems) absorbing infrared light from the laser and heating the resin to the point of vaporisation. The vaporisation leads to explosion craters forming the structure as well as bubbles forming and blocking or deflecting the laser leading to whole regions of the structure not receiving enough power to polymerise or being polymerised off of the substrate. The difficulty of integrating the microelectrode arrays available with the two photon polymerisation process prevented patterned cultures being produced on micro electrode arrays.

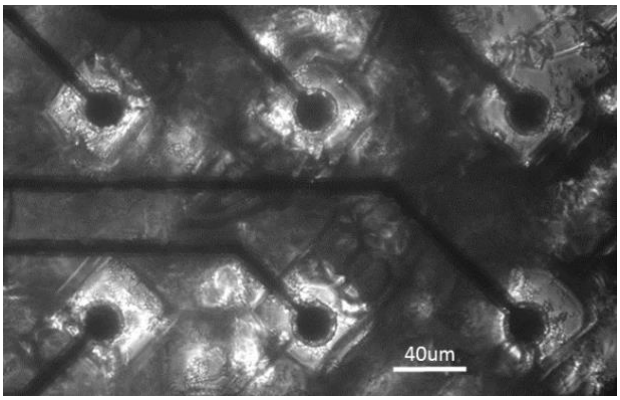


Figure 61 Aligning microstructures to multielectrode array.

It was possible to position electrodes in the centre of each soma chamber however the gold electrodes absorbed the infrared laser energy and converted it to heat, boiling the resin and creating bubbles. These bubbles then interfered with the laser causing majors defects in the microstructure as well as some fabrication issue such as some of the structure delaminating from the top left corner.

4.5 Discussion

In this chapter the growth of neural cultures cultured in the presence of a variety of two photon polymerised was characterised. The growth was monitored using phase contrast microscopy initially to inform design iterations. The main adaptation was to increase the height and thickness of walls to further prevent the overgrowth of neurites. When the phase contrast microscopy inferred that the structural topology of the neural network was constrained to the path of the microstructure characterisation of the functional topology using calcium imaging was performed. An order of activation, dependent on the situation of each neuron within the microstructure, was observed. Synchronous activity was seen in neurons both inside and outside the microstructure suggesting the internal culture had not been fully isolated from the microculture growing outside the microstructure. Further characterisation of the structural topology using fluorescence microscopy and scanning electron microscopy revealed that some neurites were indeed growing over some of the walls, particularly in corners and gaps in the pyramidal wall (Figure 60).

The first geometries used, the hexagonal grid structure, influenced the orientation of the initial outgrowth of neurites (Figure 50) but failed to constrain soma to a single compartment. Despite the initial influence on the culture's growth it was observed that soma changed compartments and that neurites grew over the barriers in a matter of days (Figure 52). The gap between compartments was 2 micron wide to prevent a neurons' nucleus squeezing through, however the low height of the walls, 3 micron, may have allowed the neurons to cross the barrier as the gap as the wall presented a T cross section that, due to the lack of a top horizontal barrier, provided a cross sectional area large enough for the somas to pass over. The 8 micron high outer wall appeared to present more of a barrier to the neurites suggesting that an increase in the internal wall height might improve the effectivity of the growth restriction. The presence of an outer wall surrounding the hexagonal grid, when compared to samples without an outer wall (Figure 51) seemed to reduce fasciculation and aggregation within the grid, improving the influence of the hexagonal grid on the culture (Figure 50). Due to the outer walls

reducing the number of connections with the surrounding culture a decrease in the forces the culture exerts upon itself as it attempts to shorten neuronal connections. As mentioned in the introduction and the Second Chapter on surface modifications, reducing fasciculation and aggregation on MEAs is key to effectively patterning neurons *in vitro* and interrogating *in vitro* neural network dynamics.

The square grid arrays with 30 micron high walls appeared to restrict the growth and migration of both neurites and soma (Figure 53). This suggested that the height or aspect ratio of the walls was key to the level of influence the structure exerted on the neurite. The neurites turned tight corners and u-turns within the structures implying that the presence of the microstructures was the dominant force influencing the growth of the neurites and that they are capable of imposing radical changes in direction. The initial seeding protocol saw only around 5 or 6 cells occupying the structure, approximately 16 percent occupancy. To increase occupancy a high-density cell suspension of ~1 million cells per millilitre were pipetted approximately above the microstructures after the initial drop had been placed. This was successful in increasing the occupancy to 90 percent, but this led to more than 1 neuron, 2 or 3, occupying each compartment, preventing the one to one interfacing required for neural network dynamic investigations. Additionally, the increased height of the piled cells may be more likely to promote fasciculation and aggregation or soma migrating out of compartments with walls a single neuron would not be able to cross. Ideally these microstructures would be coupled with a cell placement technology that would ensure one cell per electrode compartment such as micropipetting[17], inkjet printing[155], or optical tweezers[156].

The level of influence on *in vitro* neuronal topology is much higher than previous attempts using two photon polymerisation, both in terms of pattern fidelity, precision of coordination and scale of patterning (Figure 32)[20,116,152]. There is, however, still outgrowth of neurites over the walls of the microstructure as demonstrated by the dynamic calcium imaging, fluorescence microscopy and scanning electron micrographs (Figure 60, Figure 58). This overgrowth was clearly particularly evident in the phase contrast micrographs taken of the cultures and even in the fluorescent micrographs the

extent of this is over growth can be missed as the overgrowth is out of the focus plane normally being imaged, the substrate surface (Figure 62, Right). This is important to consider in order to avoid the creation of an artefact when making claims about the efficacy of certain techniques used to control neural network topology. Although the microstructures are clearly influencing the topology of the network the calcium imaging data shows that the activity of the neurons is far from definitively restricted by the microstructure containing it. This is apparent with another previous attempt to pattern neurons, the NeuroArray, which claimed to restrict soma to individual compartments and control functional network topology. Close examination of the fluorescent images of the NeuroArray shows that there are soma which are not compartmentalised by the patterning stencil (Figure 62, left). To confirm if all the neuron soma were confined to the holes in the PDMS template the culture could be stained with a nuclear stain such as DAPI and fluorescently imaged.

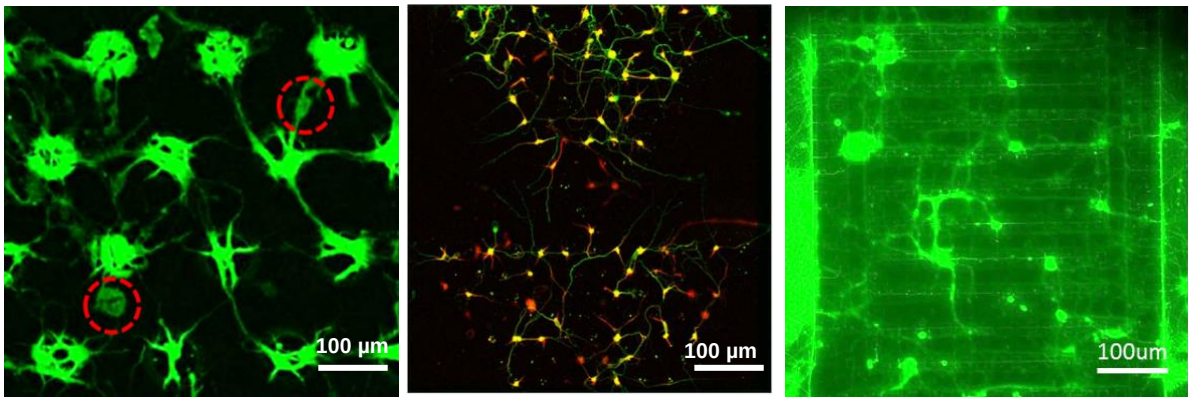


Figure 62 Growing out of the intended pattern visible in fluorescent micrographs of patterned neurons.
Left: Fluorescent micrograph of immunohistochemically stained neurons growing in Neuroarray. Note the out of focus fluorescent in partially spherical shapes, highlighted with red ring, possibly indicating the presence of neuronal Soma on the surface of the PDMS stencil. Contrast and brightness enhance to emphasise the presence of out of focus cells. [18]***. Centre: The Neuroarray claimed to control functional network topology and promote signal propagation by organising the neurons in a triangular configuration. This image already shows overgrowth of the structure and was taken at only five days in vitro. By the time the culture is electrically active at fourteen days in vitro it is unlikely that the culture will appear to have high fidelity to the pattern. Right: Fluorescent micrograph of neuronal cultures after twenty eight days in vitro. Note how the out of focus neurites trace the upper surface of the microstructure to form a neuronal network pattern on two levels.***

The claim that the NeuroArray controls the functional network topology based on dynamic calcium imaging data is also misleading as it is paired with an image of a culture at only five days *in vitro*, before the culture was electrically active (Figure 62, centre). As apparent from the looping microstructure culture (Figure 62, Right), by twenty eight days *in vitro* the amount of neurite outgrowth is extensive. Interestingly the overgrowth of the structure primarily follows the form of the upper surface of the microstructure, in effect making two levels of patterned neurons. This indicates that attempting to pattern neurons in a two-dimensional format is counter intuitive as the neurons will exploit the patterning microstructure as a scaffold to grow into a three dimensional cultured network. Additionally a three dimensional network would be a more valid model for neural network dynamics as *in vivo* neural networks are generally three-dimensional. Various attempts have been made to make three dimensional neural cultures however most rely on optical interfacing techniques, the drawbacks of which are discussed in the introduction section.

The lack of high resolution three dimensional microelectrode arrays currently restricts *in vitro* neural interfaces to two dimensions although this paradigm is being challenged by advances in microelectrode fabrication and the use of optogenetic and fluorescent imaging techniques [157]. Integrating microelectrodes into the growth substrate would be an approach to allow for neurons to be interfaced with in three dimensions and exploit the tendency of cultures neurons to grow in a coordinated way on three dimensional substrates. Although some basic two-dimensional conductive structures have been produced using two photon reduction there are several challenges facing the production of three dimensional integrated microelectronics using two photon fabrication. Multimaterial two photon fabrication is currently not a standardised process and will be a key development in unlocking the potential of two photon fabrication in applications bioelectronic applications such as neuron biosensors. One issue with producing multi-material microstructures containing metals is the absorption of heat energy by the metal microstructures causing vaporisation of a polymer resin as observed in the deformed structure in Figure 61. This is similar to the reflection of the laser by the gold microelectrode tracks on the microelectrode array which prevented the

structures developed in this thesis being fabricated on the microelectrode array. It may be possible to avoid this issue by using microelectrodes made of conductive polymers or a metal which reflects infrared energy with less efficiency than gold. An alternative would be to use an insulator layer which has been doped with a dyes to absorb the laser energy before it reaches the reflective surface.

Being unable to combine gold surfaces with two photon polymerisation microstructures prevented combining the gold selective cRGDfC coating, developed in Chapter 2, with the microstructural patterning. This was unfortunate as the preliminary attempts to promote adhesion of the neurons to gold using the cRGDfC molecule had been promising. As neither mechanical or chemical patterning has previously been able to definitively coordinate the growth of neurons *in vitro* it was hypothesised that a combinatorial approach may have more success but, due to the issue of printing on an MEA, this hypothesis remains untested. Two photon absorption can also be used to conjugate molecules to an existing polymer structure[118]. Thiolated RGD motifs, such as the cRGDfC used in this thesis, can be covalently bonded to acrylate groups additions with great efficiency[145], allowing the distribution of cRGD molecules to be patterned selectively using two photon absorption. Other bioactive molecules other than cell adhesion peptides could also be conjugated to the matrix such as guidance molecules, e.g. ephrins, and growth factors [63,64,104,129,158]. Producing spatially defined patterns of such biomolecules could facilitate a homogenous multipotent cell culture differentiating into complex hetereogenous tissue. In the case of neuron biosensors this would allow for the important interactions of glia and neurons to be observed and neuromodulation to be introduced using neuromodulatory neurons. Most of these photoconjugation techniques have been demonstrated on hydrogel substrates as they allow for diffusion of the bioactive moieties throughout the structure.

The two photon polymerised microstructures produced in this thesis were shown to influence, although not definitively control, the structural and functional topology of an *in vitro* neural culture to a greater extent than previous attempts[19,20,152]. Further work is required to combine substrate selective surface chemistry and two photon polymerised microstructures due to the problem of

vaporisation when printing directly onto an MEA. Future work should focus on exploiting sophisticated three dimensional microfabrication and micro-functionalisation techniques to produce both three dimensional electrode arrays and organised neural architecture. Producing three dimensional organised *in vitro* cultures could have huge impacts for understanding neural networking dynamics and informing learning algorithms.

5 Production of pH sensitive Hydrogel fluorescent microsensors

5.1 Overview

Microfluidic chambers offer automated control over the soluble milieu of the cell culture environment. For neurobiological experiments microfluidic chambers can be used to deliver drugs or expose the culture cell to gradients of growth factors [52]. As the volume the cells are cultured in gets increasingly smaller there is a need to monitor physiochemical variables non-destructively, and in real time, as the volume in the chamber is too small for traditional monitoring methods. A key physiochemical variable in cell culture is pH. This experimental Chapter aimed to produce, using two photon polymerisation, microstructures capable of non-destructively monitoring pH through the incorporation of pH sensitive fluorophores. A hydrophilic polymer polyethylene glycol diacrylate (PEGDA) was used as the resin to be two photon polymerised into a support for the pH sensor resin. As a hydrogel PEDA is capable of facilitating efficient liquid exchange between the sensor dyes and the aqueous analytes[159]. PEGDA was specifically chosen because it has been successfully two photon polymerised[117] and has been patterned on substrates for cultured neurons[160]. The first attempts to polymerise PEGDA using a commercially available photoinitiator required too much power to initiate polymerisation leading to vaporisation of the material without any visible signs of precise polymerisation. Improving the sensitivity of the PEGDA to the two photon polymerisation process was achieved by synthesising a photoinitiator designed specifically for two photon polymerisation. The photoinitiator was synthesised by an aldol condensation performed as described in Liska 2014 and facilitated the efficient two photon polymerisation of a PEGDA:PETA based resin. The microstructures produced with the PEGDA:PETA formulation, once immersed in water, underwent major swelling leading to deformation and delamination. To reduce the swelling the PEGDA was polymerised in 50 percent water. To polymerise the resin in water a second water soluble photoinitiator, E2CK, was synthesised by collaborator Johnathon Moore according to a published protocol [161]. Polymerising in the presence of water greatly reduced the swelling and deformation but

delamination might still occur if the samples were rinsed or disturbed. To further prevent the delamination of the microstructures from the substrates they were coated with trimethoxypropylsilyl methacrylate (TMSMA). The TMSMA forms a silane bond with the glass substrate which allowed the hydrogel microstructures to form covalent bonds methacrylate groups protruding from the substrate surface.

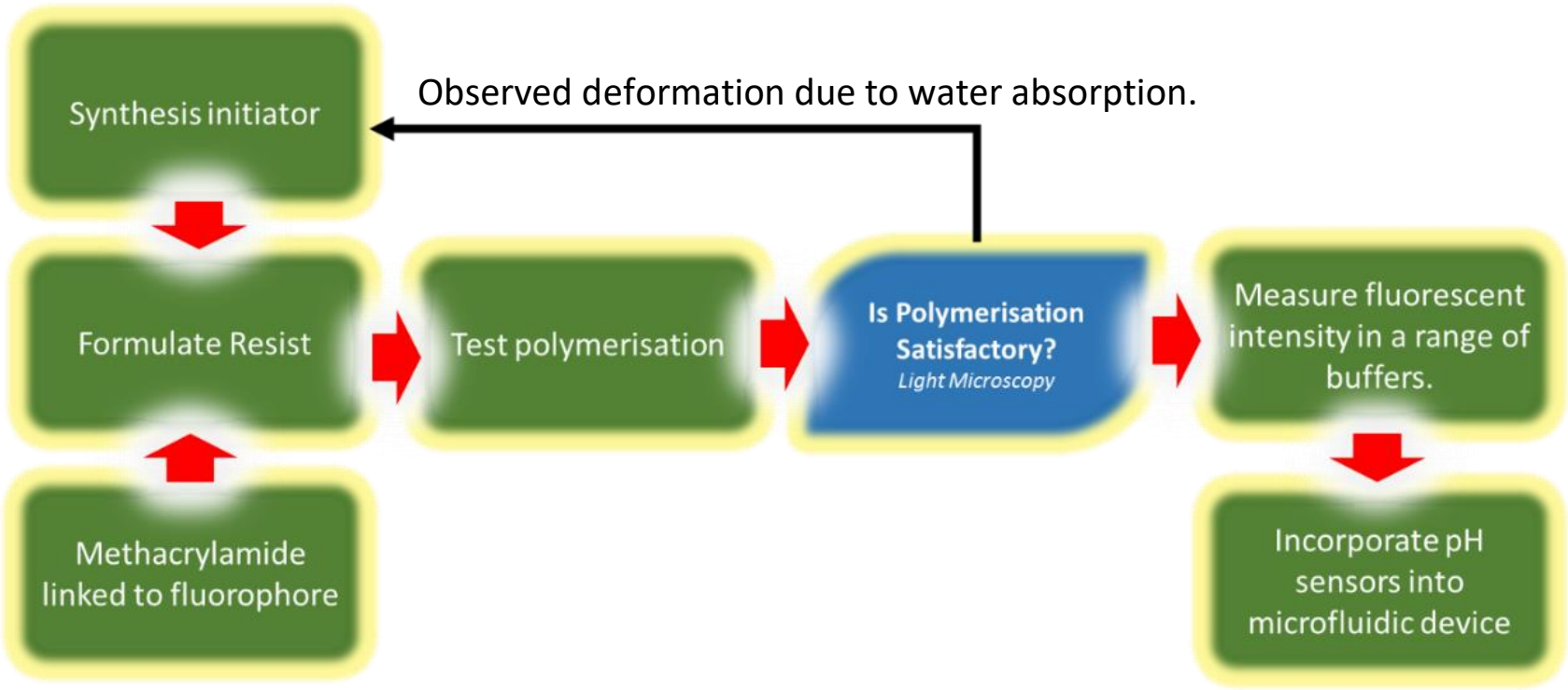


Figure 63 Overview of direct laser written pH sensor development.

Initially the constituents of the resist, the photoinitiator and the fluorescent dyes were synthesised. The PEGDA based resists were then polymerised and the structures assessed for quality using light microscopy. Microstructures of the PEGDA:PETA resist underwent major deformations due to swelling once immersed in water. A second photoinitiator which was water soluble was synthesised and the second water- based formulation did not undergo deformation due to swelling. Fluorescent intensity images were then taken of the microstructures in a range of different pH buffered solutions. The sensor dye measurement was divided by the reference dye measurement so variations in dye concentration did not affect the measurements. The calibration curve confirmed that changes in pH could be ratiometrically detected using the microstructures. The pH sensors were later incorporated into microfluidic device to demonstrate the compatibility of two photon polymerisation with microfluidics.

The pH sensing was performed ratiometrically using two dyes, one whose fluorescent emission intensity was sensitive to pH, FAM-D, and another fluorophore which was insensitive to pH, TAMRA- D. The insensitive dye provides a reference value to compensate for heterogenous distribution of the dyes in the microstructure. The two-photon polymerised PEGDA microstructures containing the two fluorophores were then fluorescently imaged in a range of pH buffers and a calibration curve constructed to successfully demonstrate the microstructures ability to measure pH. As a preliminary demonstration of biocompatibility dissociated neurons were cultured in the presence of the pH sensitive microstructures. The culture adhered to the substrate, even in very close proximity to the structure and showed no sign significant adverse symptoms of being due to the presence of the photoinitiator. The pH sensors were polymerised inside a microfluidic device successfully however any structural channel components were damaged during development. The components were probably unable to withstand the shear force, an unaligned force pushing the body in one direction, when the resin was rinsed out of the channel. Despite being unable to produce structural microfluidic components using the pH sensitive resist the pH sensors had a physiologically relevant sensitivity, good initial biocompatibility and simple structures suitable for sensing applications, such as arrays of dots, easily incorporated into a microfluidic chamber.

5.2 Methodology

5.2.1 Two photon photoinitiation

The crux of two-photon polymerisation is the transduction of electromagnetic energy, the laser beam, into chemical energy, commonly free radicals but sometimes other charged entities such as cations. The molecule responsible for this is the photoinitiator. There are several key attributes which make a molecule an efficient two-photon photoinitiator. The first is having a high two-photon cross section at the wavelength of light being used for excitation. The second desirable attribute is a high quantum efficiency. The quantum efficiency describes the probability that an absorbed photon leads to the generation of reactive species such as a free radical. The absorbed photons excite an electron to a

singlet state. A probabilistic event known as intersystem crossing then occurs which leads to the singlet state moving to a triplet state. In the case of fluorophores this process leads to bleaching. The triplet state is unstable and is rapidly followed by the transfer of the charge to another point in the molecule, leading to the generation of a free radical. It is believed that it is the efficiency of the charge transfer across the molecule which is the strongest determinant of quantum efficiency[162].

As the quantum efficiency, and therefore the efficiency of the charge transfer, is critical to efficient photoinitiation developing an understanding of the relationship between a molecule's structure and its photochemical properties is critical to the development of new photoinitiators. It is considered that coplanar molecules with long conjugated pi bridges have increased charge separation properties which facilitate efficient intramolecular charge transfer[162]. The water soluble photoinitiator (2E,6E)-2,6-Bis(4-(dimethylamino)benzylidene)-4-methylcyclo- hexanone, named 3e in the original papaer[162], was selected as it had shown the widest range of scan speed and laser power settings, or largest processing window, capable of producing a good quality range of out of a family of cycloketone based photoinitiators with various acceptors and donors. Although 3e has a broad processing window and a desirable two photon cross section and quantum efficiency the downstream polymerisation propagation kinetics can also make a photoinitiator incompatible with certain monomers. One basic but key property of the photoinitiator is its solubility in the desired medium. To improve the solubility of a family of cycloketone based photoinitiators, the family of molecules was functionalised with carboxylic acid salts[162]. The water soluble initiator could then be used to efficiently polymerise PEGDA in an aqueous environment.

5.2.2 Self assembled monolayer for promoting adhesion

To ensure that the gel-based microstructures adhered to the glass substrate the properties of the glass surface must be modified. A common method for modifying the properties of a surface is using molecules which self-assemble into monolayers when in contact with certain substrates and under certain conditions[88]. Self-assembled monolayers (SAMs) have a distinct bipolar structure, with two

different functional groups at each end of the molecule often linked by an alkyl chain (Figure 64). One functional group has a high affinity for the substrate surface and is referred to as the head group. The high affinity is responsible for the orientation of the molecule on the surface (Figure 64). The alkyl chain interacts with the alkyl chain of adjacent molecules with Van der Waals forces (Figure 64) increasing the density of the monolayer, creating a lawn of molecules which helps ensure the methacrylate molecules are presented away from the substrate. The methacrylate groups are then viable sites for the covalent binding of PEGDA molecules during photopolymerisation. As the length of the alkyl chain determines the strength of the Van der Vaals forces longer chains have denser more crystalline structures[163]. The density of molecules in a SAM is very high, around one molecule per twenty angstroms although this varies with the molecule, making a more uniform coating than the more random uncontrolled polypeptide coated surface. The functional group at the other end of the alkyl chain, the tail group, forms a uniform coating conveying its functionality to the surface[88].

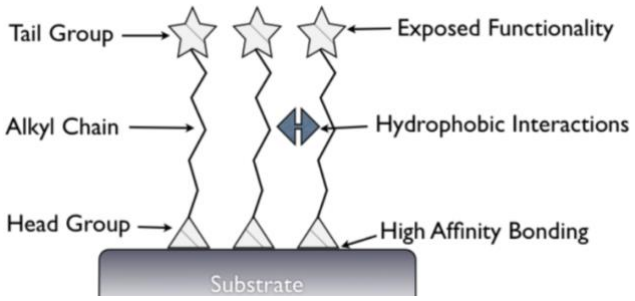


Figure 64 Schematic demonstrating the bipolar structure of a self-assembled monolayer.
The Head group of the molecule binds with high affinity to the substrate. The alkyl chain which links the head and the tail group then interact and align to form a lawn of parallel molecules. The head group is now exposed conveying its functionality and physiochemical properties to the substrate surface.

As a glass substrate was the target of the head group a silane was used, due to their greater stability the silanes used in this thesis were alkoxy silanes rather than halide silanes. Silanes undergo a condensation reaction, forming a silanol bond, when they come into contact with the hydroxyl groups present on the activated glass surface. The silane's alkoxy groups are then displaced by hydroxyl groups on the surface forming -Si-O-Si- and an alcohol molecule. The tail group in this case is a methacrylate group which can form a covalent bond with the polyethylene glycol diacrylate molecules

as they undergo two photon polymerisation. Other SAMs can be used to modify the wettability of the surface[88]. Increasing the wettability of a substrate favours the adsorption of natured proteins to the surface, as the proteins is exterior is comprised of charged groups[164]. A surface with lower wettability may interact with the hydrophobic core of a protein causing it to denature[87].

5.3 Experimental

5.3.1 6-Bis(4-(dimethylamino)benzylidene)-4-methylcyclo- hexanone synthesis

2984 milligrams of benzaldehyde (Sigma)(moles= 20 millimoles; Molarity=149 grams per mole) was mixed with 1122 micrograms of cycloketone (Sigma)(Moles= 10mmol; 112 grams per mole) in 30 millilitres of ethanol. Using a pressure equalised dropping funnel NaOH (Sigma)(10 millimolar) was added dropwise (3 millilitres). The reaction was stirred at room temperature and pressure until the benzaldehyde was completely consumed, approximately 12 hours, the reaction was monitored using aluminium backed thin layer chromatography plates (Cole Palmer) in chloroform (Sigma) and developed in potassium manganate (Sigma). The reaction was then diluted with 200 millilitres of chloroform (Sigma) and washed thrice with 75 millilitres of saturated ammonium chloride solution (Sigma). The combined organic phases were then dried over magnesium sulphate (Sigma) and filtered. The product was then purified using ethanol (Sigma) recrystallization (300 millilitres, 60 degrees Celsius)

5.3.2 Nuclear Magnetic Resonance

To determine the identity of the final product proton and carbon NMR were performed in deuterated chloroform. Mass spectroscopy was also performed to ensure the product mass matched the desired molecules mass. ^{1}H and ^{13}C NMR spectra were recorded in $CDCl_3$, at ambient temperature using Bruker AV3400 (400 MHz) spectrometer. Data are expressed as chemical shifts in parts per million (ppm) relative to the residual solvent signal of $CDCl_3$ (^{1}H NMR 7.27; ^{13}C NMR 77.0) as the internal standard on the δ scale. The nuclear magnetic resonance was performed by Johnny Moore.

5.3.3 Mass spectrometry

High-resolution mass spectra were obtained using a Bruker MicroTOF mass spectrometer using electrospray ionisation and high-performance liquid chromatography at a flow rate of 700 nanometres per second. The mass spectrometry was performed by Johnny Moore.

5.3.4 PEGDA: PETA resin formulation

The initial attempts to two photon polymerise PEGDA used a 1 percent Irgacure 2959 (Sigma) as a photoinitiator. As Irgacure 2959 was unsuccessfully in initiating the two photon polymerisation of PEGDA so a higher efficiency initiator was synthesised, as described above, of E3, 2,6-Bis(4-(dimethylamino)benzylidene)-4-methylcyclo- hexanone. 10 micrograms of the photoinitiator 3e was dissolved in 100 microlitre of chloroform. 50 micrograms of each of the methacrylamide conjugated fluorophores TAMRA and FAM (TAMRA-MA, FAM-MA) was then added to the 100 microlitre of chloroform/photoinitiator solution. 9.5 grams of PEGDA was weighed into a vial followed by 0.5 grams of PETA. The chloroform solution was then added sequentially to the bulk monomer mix, and the vial was closed and inverted several times to assist with the dissolution of the dyes.

5.3.5 PEGDA: Water resin formulation

10 micrograms of E2CK and 50 micrograms of both TAMRA-MA and FAM-MA were dissolved into 100 microlitres of water. The water was then mixed with 5 grams of PEGDA and another 4.9 grams of water and sonicated for 2 minutes.

5.3.6 Coating of substrate with trimethoxysilylmethacrylate

To ensure that the direct laser written microstructures adhered to the substrate glass coverslips they were coated with trimethoxysilylmethacrylate (TMSMA). 22 millimetre x 22 millimetre no. 1.5 glass coverslips (Menzal-Glasser, Agar Scientific). The coverslips were sonicated for 10mins in 10 percent Decon90 (Decon) in deionised water then rinsed twice in deionised water. The substrates were then dried under a nitrogen stream, sonicated in acetone (Sigma) and then isopropanol (Sigma) and dried

again under a nitrogen stream. The substrates were then placed into a plasma oven which was pumped down to 0.2 millibar then flushed with oxygen and allowed to equilibrate at 2.8 millibar. Using a plasma oven (Deiner Electronic, Pico low pressure system) oxygen plasma was then generated using microwave energy (2.5 gigahertz, 300 milliwatts) for a period of 10 minutes. The plasma cleaned samples were then immersed in a 1 percent solution of TMSMA for 1 hour. After the deposition the substrates were rinsed in anhydrous toluene (Sigma), dried under nitrogen and then rinsed in isopropanol and dried under nitrogen. Finally, the substrates were baked for one hour at 100 degrees Celsius.

5.3.7 Calibration of pH sensors using ratiometric measurements

A pH sensitive microstructure was immersed in a series of pH buffers, rinsed with deionised water in between each buffer. During immersion in each buffer a fluorescence intensity image was taken through a fluorescein isothiocyanate (FITC) filter cube and through a Tetramethylrhodamine (TRITC) filter cube. The emission and excitation wavebands of FITC (Excitation: 450-500 Emission: 510-560) and TRITC (Excitation: 530-557 Emission: 590-650) do not overlap much (Figure 65). The exposure was kept constant for all readings using the same filter. The FITC measurement, pH sensitive dye, was then divided by the TAMRA measurement, reference dye, to give a ratiometric measurement value. This was then plotted against the pH of the immersion buffer to give a standard curve.

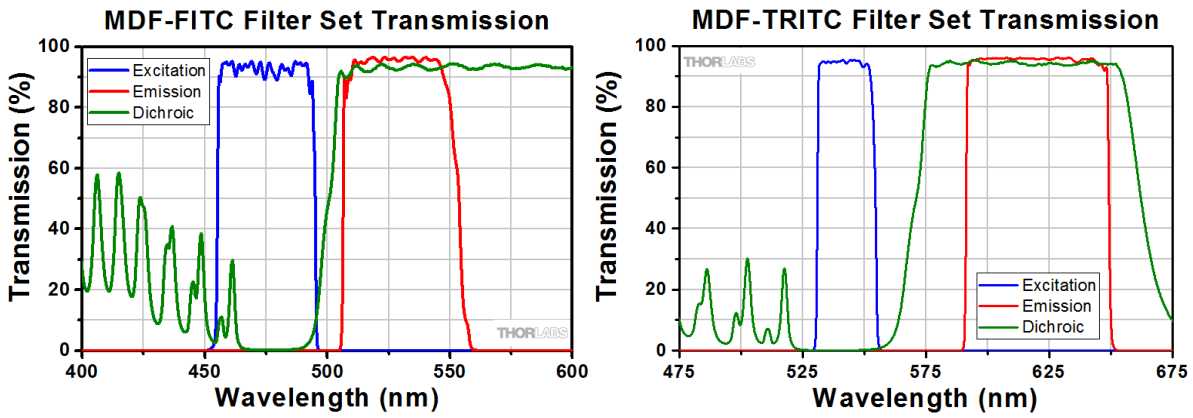


Figure 65 FITC and TRITC filter cube emission and excitation spectra.

5.3.8 Production of tape based microfluidic device.

An indium tin oxide coated glass coverslip provided a refractive index mismatch with the resin to facilitate the function of the automated interface finder. The channel outline was cut into double sided silicon based tape (M3) using a knife cutter (Cameo 3, Silhouette). The height of the channel was determined by the thickness of the tape used, in this case 150 micron. The height was verified by focusing on the top and bottom surfaces of the channel and recording the distance traversed on the microscope Z axis. To cut the tape with the knife cutter it first had to be mounted on a polyethylene backer and then onto the knife cutter's cutting mat. The cutting mat was then loaded onto the knife cutter. A binary, black and white, .tiff file was loaded into the silhouette software to determine the geometry of the pattern to be cut. After the geometry had been cut into the tape the section of the tape which framed the channel geometry was lifted off the polyethylene backing, and the tape lining attached the backing using fine tweezers. The tape cut-out was then placed sticky side down on to the ITO coated glass coverslip. To ensure the tape was placed on the substrate surface with the ITO coating a multimeter, set to measure resistance, was used to detect the conductive layer of ITO. The second lining was then removed, again using the fine tweezers. A PDMS block was then be placed on top of the sticky tape forming a hollow chamber between the ITO coated glass substrate and the PDMS, separated by the layer of thin double-sided sticky tape. Ports were bored out of the PDMS block using a biopsy punch. Once in the UV shielded Nanoscribe room a drop of resin was place on the top of one port. A 1 millilitre syringe was then pressed against the other port and the plunger withdrawn to suck the resin through the chamber.

5.4 Results

To non-destructively measure pH in microvolumes, pH sensitive fluorophores were incorporated in PEGDA microstructures. The first step to achieve this was to successfully polymerise PEGDA using two photon polymerisation. Initial attempts to photopolymerise PEGDA using the custom two photon rig and a commercially available photoinitator, irgacure 2959, required two much power leading to large explosions and bubbles. A photoinitiator, E3, reported to have a large two photon cross section and a high quantum efficiency was synthesised using an aldol condensation as described in the literature [162].

5.4.1 Nuclear Magnetic Resonance

The product of the synthesis was then analysed using carbon and proton nuclear magnetic resonance (NMR). Both carbon and proton NMR corresponded to the spectral information previously published[162] with the exception of a doublet peak at 6.7 parts per mole which appears in the proton NMR spectra as a broad smearing which, when integrated, does correspond to the correct number of protons. This may be due to concentration dependent dimerization effects or protonation of the terminal amino groups leading to stoichiometric rotation inhibition. There was a large peak at 7.29 parts per mole is due to the heavy chloroform used as a solvent. The small carbon peak at 189 parts per mole is characteristic of the single ketone carbon at the centre of the structure. Coupling constants *J* are given in hertz (Hz). Proton NMR: δ (ppm) 7.79 (singlet, 2H), 7.51 (doublet, J = 8.5Hz, 4H), 3.10 (singlet, 12H), 2.94 (m, 4H), 2.48-2.61 (multiple, 2H) 1.86-197 (m, 1H), 1.13 (doublet, J = 5.6Hz). Carbon NMR: δ (ppm) = 189.7, 149.9, 137.4, 132.3, 131.6, 124.3, 111.7, 40.2, 36.8, 29.5, 22.0.

5.4.2 Mass Spectroscopy

The mass to charge ratio detected by the mass spectrometer was detected at 384:1 at 4 delustering potential and the mass to charge ratio of the desired product is 384.

5.4.3 Formulation of PEGDA photoresist

A formulation of PEGDA:PETA was produced with 1 percent of photoinitiator and polymerised on the Nanoscribe. A test structure like those used for neural patterning was produced but after development in water the structure swelled and deformed and some of the structures delaminated despite the substrate having been treated with trimethoxysilyl methacrylate (TMSMA) (Figure 66). Performing the polymerisation in an aqueous solution helps to ensure that the structure will be stable in an aqueous environment as there will be no mass absorption of water into the structure when developed in water. To achieve this a water soluble photoinitiator, sodium 3,39-((((1E,19E)-(5-methyl-2-oxocyclohexane-1,3-diyli- dene)bis(methanylylidene))bis(4,1-phenylene))bis (methylaza- nediyl)) dipropanoate (E2CK), was synthesised in a four step synthesis by collaborator Johnny Moore[161]. A formulation with 1 percent of E2CK was mixed into a PEGDA:H_20 50:50 and polymerised on the Nanoscribe GT. The same test structure used for the PEGDA:PETA formulation was produced using this aqueous resin and the resultant structure showed no signs of swelling or delamination upon development in water. There was however a slight mis-alignment between adjacent sections. This could be reduced by producing each unit of the grid in turn as performed for the microstructures used for patterning neurons. As stable and reproducible PEGDA hydrogel microstructures were successfully fabricated using two photon polymerisation the pH sensitive and insensitive fluorophores for ratiometric pH sensing could now be incorporated.

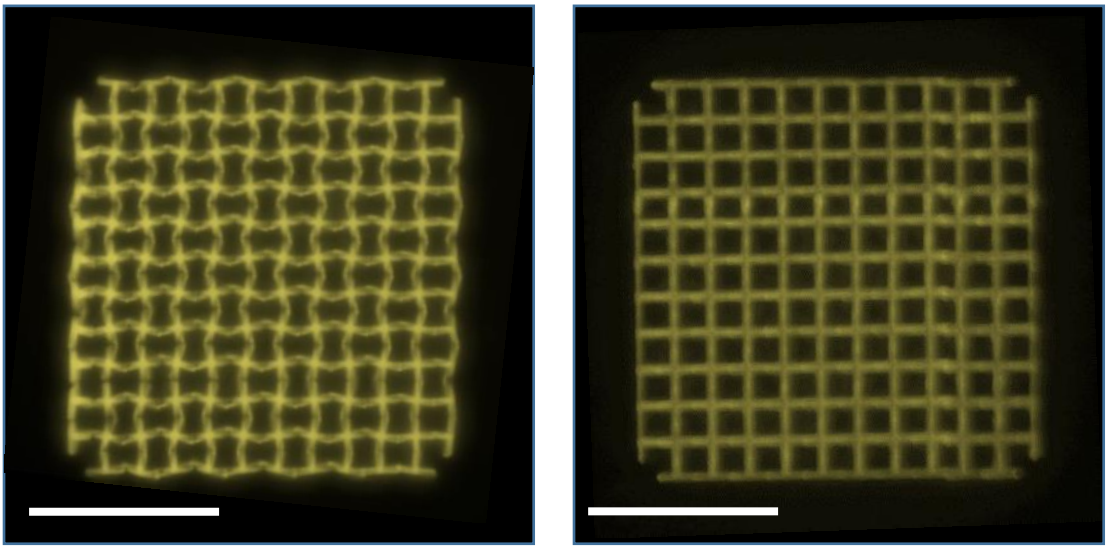


Figure 66 PEGDA:PETA formulation compared to PEGDA:Water.

Left: TRITC fluorescence image of PEGDA:PETA microstructures showing deformation due to swelling of the microstructure once immersed in water. Right: PEGDA:Water resin using water soluble photoinitiator greatly decreases swelling of the microstructure upon addition of preventing deformation of the structure. Scale Bar 150 micron.

5.4.4 Calibration of pH microsensors

The fluorescent dyes TAMRA and FAM, which were previously conjugated to a methacrylamide linker by collaborator Vereen Chauhan [125], were mixed into the PEGDA:PETA solution and polymerised on the Nanoscribe. Slightly higher powers had to be used to achieve the same polymerisation, but the developed microstructures resembled the original designs with only the occasional minor defect. When performing microfabrication outside a cleanroom small amounts of contaminants are to be expected and can lead to minor imperfections. When microstructures were built on glass without the adhesion coating, the entire microstructure delaminated and could be handled with tweezers, not unlike a microtome section. The microstructures where then placed in a range of buffers and fluorescence intensity images were taken through two different filter cubes (FITC and TRITC) with excitation and emission filters matched to the two fluorophores, fluorescein and rhodamine. The readout through the TRITC filter did not vary with any observable trend, providing a reference reading as intended. The fluorescent emission through the FITC filter increased with buffers of increasing pH, as demonstrated by the false colour fluorescence intensity images collated in Figure 67.

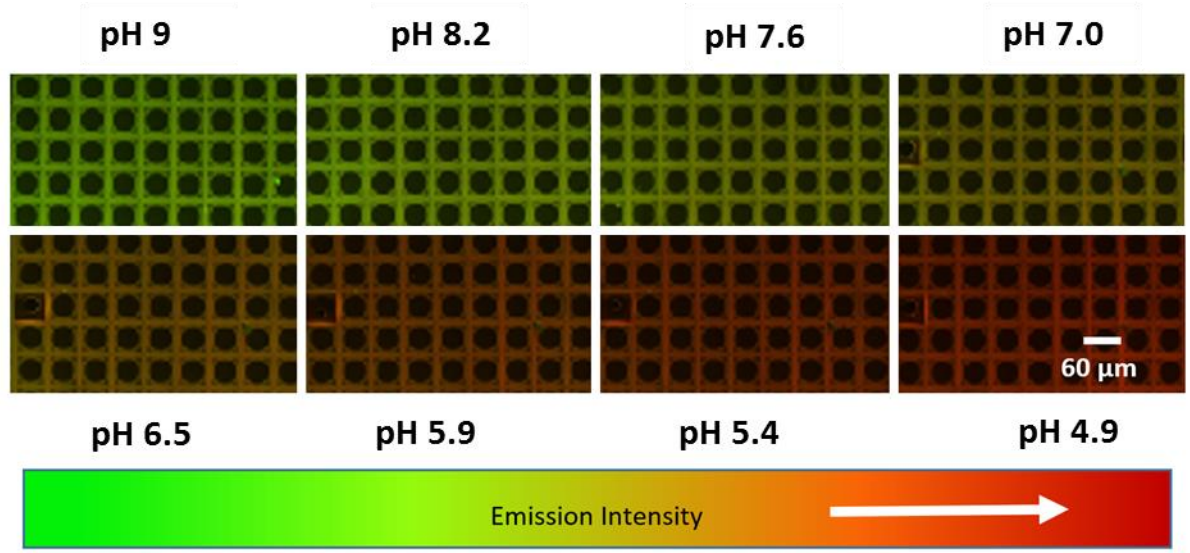


Figure 67 Collage of fluorescent intensity images taken of two photon polymerised hydrogel microstructures in a range of different pH buffers.

The recoloured images represent decreasing ratiometric measurement intensity going from green to red. As this changes happens linearly with decreasing pH it would appear that the sensors are sensitive to changes in pH. The structure fabricated is and array of 50 micron diameter wells.

A standard curve was generated using these two fluorescent intensity measurements, through the FITC and TRITC filter cubes, and demonstrated an almost linear response to increasing pH in the range important for *in vitro* culture of neurons and most other mammalian cells, between pH 6.5 and pH 7.75 (Figure 68). The microstructures demonstrated the ability to detect shifts of 0.25 pH, except between pH 7 and pH 7.25 where the sensitivity was reduced.

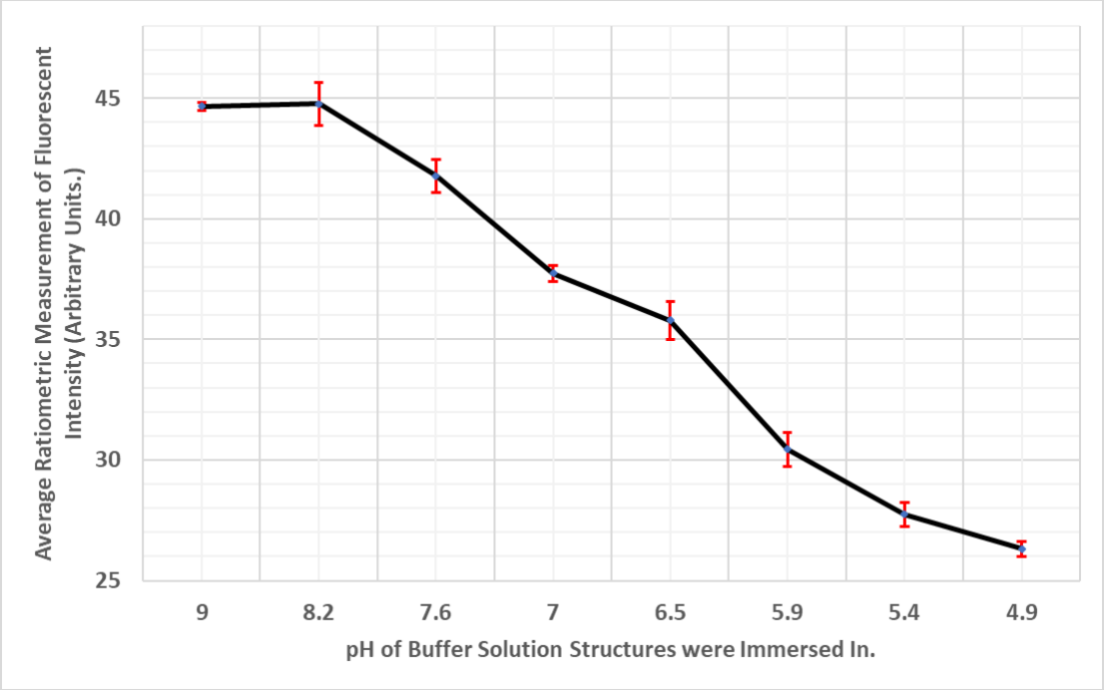


Figure 68 Calibration curve displaying ratiometric measurements of fluorescence intensity in response to a range different pH buffers.

The average of three ratiometric measurements from a two photon polymerised pH sensor was plotted against the pH of the buffer it was immersed in. The standard deviation of the three measurements is apparent is the red error bars. Overall the ratiometric measurement value decreased with pH suggesting the sensors could be used to make measurements of pH. There is, however, no discernible difference between pH 8.2 and pH 9 suggesting these sensors are ineffective at detecting pH above pH 8. Additionally the gradient of the slope pH 5.9 to pH 4.9 is much gentler than from pH 5.9 to pH 8.2 suggesting the sensitivity of detection is lower below pH 6. Taking the error bars into consideration and based on the distances between the data points the calibration graph suggesting that pH can be monitored at a sensitivity of approximately pH 0.2 using these sensors.

To demonstrate the potential applications of these microsensors, proof of concept tests were performed by integrating the microsensors within both microfluidic devices and live cell culture. Primary hippocampal cultures were plated, as according to the protocols described previously in this thesis, in the presence of the fluorescent hydrogel microstructures produced with two photon polymerisation. The resultant cultures were viable and successfully cultured for 4 weeks where they showed no signs of abnormal development, e.g. fasciculation or granulation of neurites. A ratiometric measurement of the culture medium was made, using the calibration curve, after two weeks in culture

to give the value of pH 7.3, in the region of the dominant buffer in the cell media, hydroxyethyl piperazine-ethane-sulfonic acid HEPES, pH 7-7.6. This indicates that the microsensors do not effect the culture in any adverse way and are capable of providing accurate measurements of pH. Quantification of the cytocompatability could be performed using a live-dead stain.

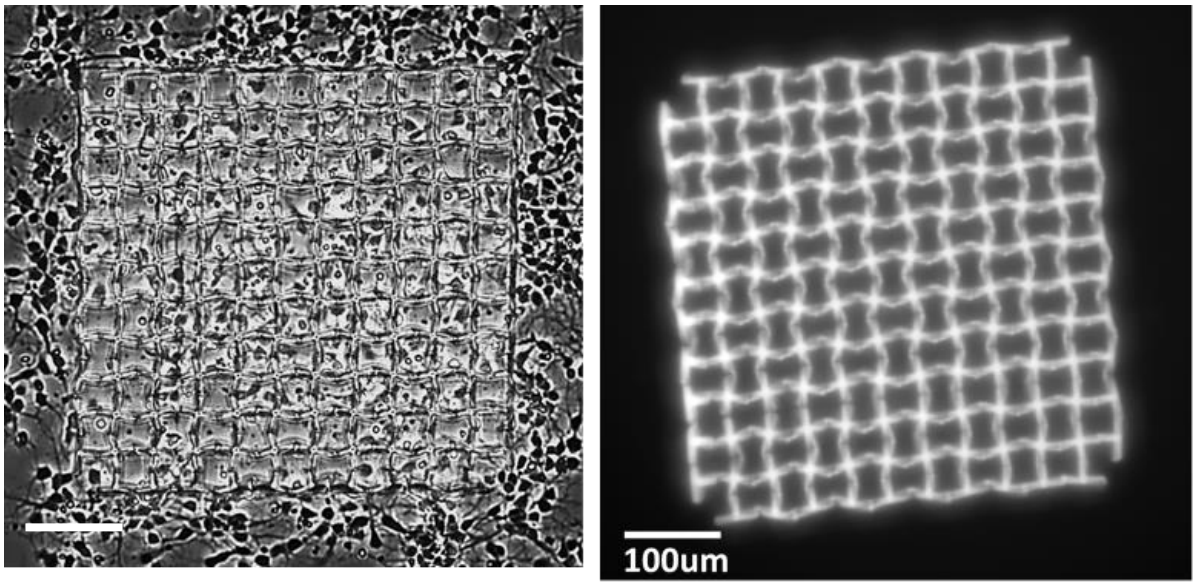


Figure 69 Neurons cultured in the presence pH sensitive microstructures.
Left: Phase contrast image of cells cultured on a grid of pH-sensitive fluorescent hydrogel. Right: Fluorescent intensity image of the same sample. Scale bars 100 micron.

5.4.5 Incorporation of pH microsensors into microfluidic device.

Arrays of micro dots was produced within a microfluidic device built using the tape method described in the experimental section (Figure 70). The array was also produced under the tape suggesting the tape was not fully stuck down allowing some resin under the tape. This also highlights how the tape array was not properly aligned with the channel. As the channel was placed on to the glass substrate by hand it was not precisely aligned to the substrate coordinates. Fluorescence on both walls of the channel is also observed suggesting that some resin stuck to the tape and was not removed during development.

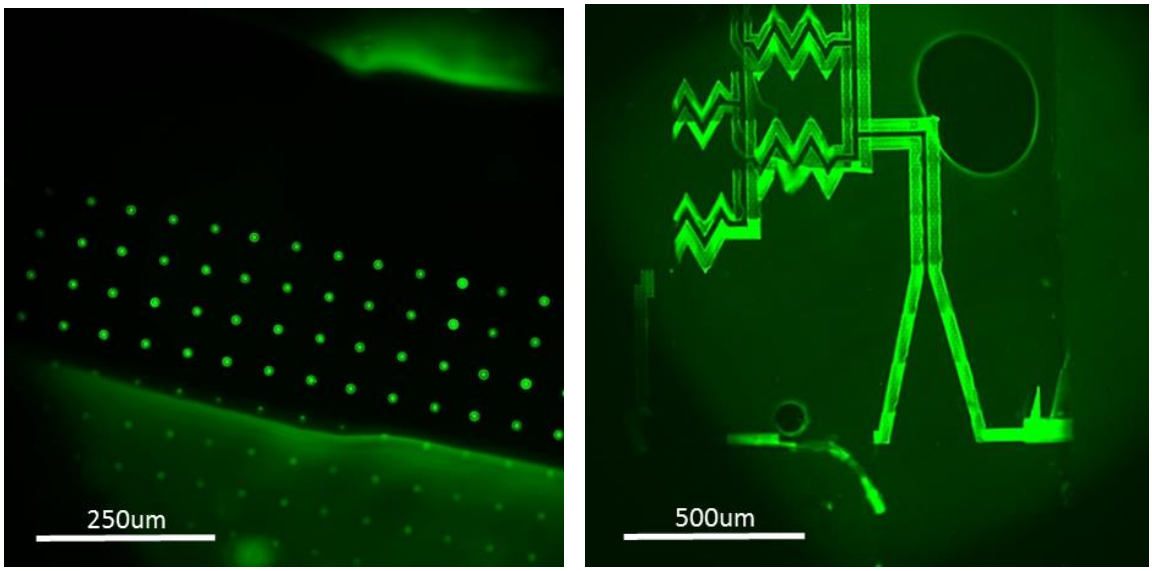


Figure 70 Fluorescent intensity images of two photon polymerised microstructures incorporated into microfluidics channel.

Left: Array of micro dots misaligned to a tape channel. The micro dots under the tape and the fluorescence of the tape reveal the lack of seal between the tape and the glass substrate. Right: The gradient chamber here has broken during development. Optimisation of material properties and channel design could allow for structurally sound pH sensitive nanochannels to be fabricated.

Producing the microfluidic chamber using the prototype Toucan inkjet printer, performed by collaborator Ehab Saleh, allowed for improved alignment as the channel could be automatically aligned to the substrate by the printer. This improved alignment is visible in the attempt to incorporate a gradient generating chamber within the microfluidic device (Figure 70). Additionally, the printed chamber did not allow for fabrication under the walls nor trap residual resin. The gradient chamber however did deform in some regions with some sections completely delaminating. This may be due to the structure being unable to withstand the pressure exerted upon it when water was pipetted through the chamber during development. The production of pH microstructures within prefabricated microfluidic devices was successfully demonstrated although further work is required to make fluidic components out of the pH microstructures.

5.5 Discussion

In this section pH sensors were produced and incorporated within a microfluidic device. A formulation capable of producing PEGDA hydrogel microstructures containing pH sensitive dyes using two photon polymerisation was produced through the synthesis of a photoinitiator optimised for two photon polymerisation in aqueous environments (Figure 66). The microstructures were used to produce a calibration curve to a range of buffers, demonstrating their ability to detect pH ratiometrically, in real time and non-destructively. The sensors were successfully incorporated into microfluidic devices however a structural component capable of influencing the flow within the microfluidic device was not successfully due to damage incurred during development.

To enable the polymerisation of PEGDA, a photoinitiator, with both a high two photon cross section and a high quantum yield facilitating efficient radical generation and polymerisation, was synthesised according to the literature[162], see section above on photoinitiator characterisation. To facilitate larger structures that did not swell, deform or delaminate when exposed to water, the two photon polymerisation was carried out in an aqueous environment. This required synthesis of a second photoinitiator which was water soluble whilst retaining the photochemical attributes of the first initiator. Combining PEGDA, water and the water soluble two photon photoinitiator produced a resin capable of efficient two photon polymerisation of PEGDA microstructures. The introduction of the methacrylamide conjugated fluorophores into the formulation did not significantly hamper the polymerisation. To test if the fluorophores were present, and functional, a pH sensing calibration was carried out. The pH sensing ability of the polymerised gels was demonstrated by producing a calibration curve. The calibration curve was produced by taking a series of fluorescent intensity images from the microstructures immersed in a range of buffers.

The calibration curve demonstrated that the microstructures were capable of measuring a change in pH from 7 to 6.75 and can be considered practically applicable for monitoring the acidification of cell culture due to the build-up of carbon dioxide in the culture medium of an air tight cell culture chamber.

Using these hydrogel microstructures to monitor the gas exchange within three dimensional tissue scaffolds would be interesting, although two photon microscopy would be more suitable for this than the conventional widefield fluorescence imaging used in this thesis. If the hydrogel microstructure are to be used to monitor cell culture, they need to be biocompatible. The biocompatibility of the microstructures, and therefore the synthesised photoinitiator, was rudimentarily demonstrated by culturing primary hippocampal neurons on the microstructured substrate. An initial measurement was made of the pH in the presence of the cell culture.

To demonstrate the integrability of the sensors they were incorporated into fully formed microfluidic devices. Two different microstructures were produced inside microfluidic devices, an array of circular spots and a gradient generating channel. Interestingly the array of circular spots was also produced under the edge of the microfluidic device suggesting that the tape was not fully stuck to the substrate and some resin had seeped under it and highlighted the poor alignment between the handmade tape device and the automated two photon polymerisation. The issues with the tape device prompted the move to inkjet printed microfluidic channels which were better sealed and could be accurately registered to the coordinates of the glass coverslip. The gradient chamber structure built inside the inkjet printed microfluidic device was significantly damaged during the development process. The damage during development may be due to the narrow channels causing high pressure.

In future work the damage to the microstructures in the microfluidic chamber could be reduced with more optimisation of the channel design based on fluid dynamic simulations, potentially using a physical modelling software such as COMSOL. Producing pH sensitive microstructures which have stronger mechanical properties may also be possible, potentially through the introduction of cross linkers in the resin. Further structural optimisation of the PEGDA microstructures, such as performed for OrmoComp, may also improve the strength to speed compromise which is essential when producing mechanically stable mesoscale structures using two photon polymerisation. Alternatively,

if a multi-material two photon polymerisation approach was available the pH sensitive hydrogel structures could be supported by a more structurally sound material, for example OrmoComp.

pH sensitive fluorescent hydrogel microstructures were demonstrated to detect pH in a physiologically relevant range and were successfully incorporated into a microfluidic device. Producing microstructures capable of sensing pH using two photon polymerisation, presented in this thesis was made possible by recent developments in the field of two photon polymerisation. The increasing understanding and availability of two photon initiators[117,161,162,165] facilitated the two photon polymerisation of structurally stable pH sensitive microstructures. The pH sensitive microstructures showed initial signs of biocompatibility, in line with previous work incorporating the same dyes in microparticles[126]. Future work could involve incorporating dyes to detect other physiologically relevant variables, e.g. biomolecule concentration, ionic/gas concentration or temperature[166–168]. Progress being made in the field of two photon polymerisation, particularly in photochemistry and rig optimisation, facilitates the techniques' increasing utility in exciting fields such as the development of real time sensors for monitoring physiologically important variables.

6 Conclusion

The goal of this thesis was to utilise two photon polymerisation to solve challenges facing *in vitro* neuron biosensors, more specifically patterning the growth of neurons *in vitro* and detecting pH with two photon polymerised microstructures. The first aim, see Chapter 2, was the development of a substrate treatment protocol that facilitated the adhesion and viability of an *in vitro* neural culture to a substrate functionalised with two photon microstructures built out of OrmoComp. To enable the fabrication of microstructures up to several millimetres squared in a reasonable time span, the two photon polymerisation of OrmoComp was optimised using several build parameter sweeps, Chapter 3. The optimisation was accelerated by the use of a modular design which also allowed for rapid reconfiguration of the design. In Chapter 4, the growth of neurons in response to OrmoComp microstructures was characterised. After several design iterations, the microstructures constrained somas and heavily influenced the growth of neurites. A possible order of activation was observed depending on a cell's location within the HD-Array design. The designs were however unable to definitively constrain connectivity although repeatable patterning of neurons in three dimensions was inadvertently achieved, as demonstrated by dynamic calcium imaging, fluorescent imaging and scanning electron microscopy. PEGDA hydrogel microstructures were successfully polymerised and made capable of ratiometric pH measurements through the incorporation of both pH sensitive and insensitive fluorophores and the pH sensitive microstructures were incorporated into microfluidic devices.

Two substrate treatment protocols were produced, one to facilitate the adhesion of neurons to substrates functionalised with OrmoComp and on to preferentially promote neuronal adhesion to gold electrode pads over silicon oxide or glass. Close adhesion to the surface is important for tight electromagnetic coupling between an electrode and a neuron and ensuring that a neural culture responds to mechanical guidance cues. Good neuronal adhesion on OrmoComp modified substrates was achieved by optimising the development procedure. Preferentially promoting the adhesion of

neurons on gold rather than glass was achieved through the gold selective adsorption of cRGDfC to gold via the thiol residue present on the cysteine molecule in the motif. The presence of the cRGDfC on the gold alone was verified by the use of ToF-SIMS. The cRGDfC promotes adhesion by mimicking an active motif from fibronectin which binds the integrin receptors on the surface of the neurons. Future work patterning the surfaces of three dimensional microstructures to combine mechanical and chemical guidance cues is suggested, such as the use of two photon photoconjugation to pattern biomolecules on existing polymer structures[118].

To facilitate the production of microstructures covering millimetres in area and tens of microns in height the two photon polymerisation of OrmoComp was optimised. A modular design was produced to decrease the time taken per parameter sweep and also facilitate rapid reconfiguration of the neurite path within the structure. The modular design allowed reconfiguration to be performed without additional CAM or CAD steps however the manual coding could be quickened and made more usable with the incorporation of a graphic user face. The Optimal parameters were found to be 500 nanometer line spacing, 30,000 micron per second scan speed and at 100% laser power, however the optimal parameters depended greatly on how recently the laser had been tuned. Fluctuations in the laser power output should be compensated for with regular parameter sweeps. Application of topology optimisation and finite element analysis could be used to further optimise the speed to design fidelity, or structural stability, compromise.

The growth of neurons *in vitro* in response to range of designs produced using two photon polymerisation was characterised both structurally and functionally. The microstructures heavily influenced the growth of the neurites and constrained cell soma to individual compartments, designed to contain an electrode each. An order of activation was possibly observed depending on a cell's position within the microstructure. The culture within the microstructure was, however, connected to the outer culture and some of the neurons within the structure connected between compartments. Although the Nanoscribe was successfully aligned to the microelectrode array the reflection of the

laser from the gold electrode tracks caused explosions in the resin, damaging the structures. This prevented the incorporation of the gold selective surface chemistry protocol developed in the second Chapter. Utilising non-reflective conductive materials for the electrode tracks or doping the insulating layer with dyes are two approaches which could be adopted in the future to enable two photon polymerisation on MEAs. Future work could build on the combination of chemical and mechanical guidance through the using of bioconjugation techniques or multi-material fabrication. Developing three dimensional interfacing technologies, especially a substrate integrated electrode array would enable the naturally three dimensional growth of neurons to be exploited and investigated.

The progress made towards patterning neurons *in vitro* using more sophisticated two photon polymerised microstructures was facilitated by the software and hardware optimisations offered by the Nanoscribe system over custom built in house rigs. Future developments in the production of both two and three dimensional patterned *in vitro* neural cultures will also depend on the development of more sophisticated two photon fabrication devices. This next generation of fabrication devices will be designed with the fabrication of artificial tissues in mind and will allow for multiple bioactive materials and cell types to be patterned at micron resolution, in situ, through the integration of two photon polymerisation, microfluidics and potentially optical trapping.

Incorporation of pH sensitive fluorophores within two photon polymerised PEGDA microstructures allowed for ratiometric pH measurements to be made in a physiologically relevant range. The development of new materials for two photon polymerisation has been facilitated by the development of two photon initiators[117,162,165]. The pH sensor were successfully incorporated into microfluidic devices which can allow for closed loop maintenance of the soluble environment in the microfluidic device which could have important applications in bioprocessing, tissue engineering and drug screening. Further optimisation would be required to make structurally elements of microfluidic channels using this material, this could be achieved by structural optimisation and simulation of the fluidic dynamics within the microfluidic device which damage the structures during development.

These microsensors pave the way for a wider range of dyes sensitive to other physiochemical parameters, such as oxygenation or temperature, which combined with automated gas mixing and micro heating systems could allow for closed loop micro reactors.

The potential of two photon polymerisation to improve the manufacture of neuron biosensors has been demonstrated in this thesis. Further impact on the field of neuron biosensors, and other related tissue engineering fields, will be attained through the continued development of software, hardware and photochemical material processing for two photon polymerisation. The incorporation of three dimensional chemical patterning and multiple cell types will allow for increasingly sophisticated artificial tissues which will become ever more valid models of *in vivo* tissue.

Bibliography

1. Wildanger, D., Rittweger, E., Kastrup, L. & Hell, S. W. STED microscopy with a supercontinuum laser source. *Opt. Express* **16**, 9614–21 (2008).

2. Wollhofen, R., Katzmann, J., Hrelescu, C., Jacak, J. & Klar, T. A. 120 nm resolution and 55 nm structure size in STED-lithography. *Opt. Express* **21**, 10831 (2013).

3. Rettinger, J., Schwarz, S. and Schwarz, W. *Electrophysiology: Basics, Modern Approaches and Applications.* (Springer International Publishing, 2016).

4. Cobb, M. Exorcizing the animal spirits: John Swammerdam on nerve function. *Nat. Rev.* **3**, 395–400 (2002).

5. Verkhratsky, A., Krishtal, O. A. & Petersen, O. H. From Galvani to patch clamp: The development of electrophysiology. *Pflugers Arch. Eur. J. Physiol.* **453**, 233–247 (2006).

6. Walsh, John, S. & Sieu. Of the Electric Property of the Torpedo. In a Letter from John Walsh, Esq; F. R. S. to Benjamin Franklin, Esq; LL.D., F. R. S., Ac. R. Par. Soc. Ext., &c. *Philosopical Trans.* **63**, 461–480 (1773).

7. Galvani, L. De viribus electricitaits in motu musculari. *Commentarius* (1791).

8. Liu, Q., Hu, N., Zhang, F., Zhang, D., Hsia, K. J. & Wang, P. Olfactory epithelium biosensor: Odor discrimination of receptor neurons from a bio-hybrid sensing system. *Biomed. Microdevices* **14**, 1055–1061 (2012).

9. Bhattacharjee, N., Li, N., Keenan, T. M. & Folch, A. A neuron-benign microfluidic gradient generator for studying the response of mammalian neurons towards axon guidance factors. *Integr. Biol. (Camb).* **2**, 669–79 (2010).

10. Kleinfeld, D. Controlled Substrates. *Jounral Neurosci.* 4105 (1988).

11. Kwiat, M., Elnathan, R., Pevzner, A., Peretz, A., Barak, B., Peretz, H., Ducobni, T., Stein, D., Mittelman, L., Ashery, U. & Patolsky, F. Highly ordered large-scale neuronal networks of individual cells - toward single cell to 3D nanowire intracellular interfaces. *ACS Appl. Mater. Interfaces* **4**, 3542–9 (2012).

12. Harrison, R. G. The cultivation of tissues in extraneous media as a method of morpho-genetic study. *Anat. Rec.* **6**, 181–193 (1912).

13. Weiss, P. Experiments on cell and axon orientation in vitro: The role of colloidal exudates in tissue organization. *J. Exp. Zool.* **100**, 353–386 (1945).

14. Vielmetter, J., Stolze, B., Bonhoeffer, F. & Stuermer, O. In vitro assay to test differential substrate affinities of growing axons and migratory cells. *Exp. Brain Res.* **81**, 283–287 (1990).

15. Britland, S., Perridge, C., Denyer, M., Morgan, H., Curtis, A. & Wilkinson, C. Morphogenetic guidance cues can interact synergistically and hierarchically in steering nerve cell growth. *Exp. Biol. Online* **1**, 1–15 (1996).

16. Campenot, R. B. NGF and the local control of nerve terminal growth. *J. Neurobiol.* **25**, 599–611 (1994).

17. Erickson, J., Tooker, A., Tai, Y. & Pine, J. Caged neuron MEA : A system for long-term investigation of cultured neural network connectivity. **175**, 1–16 (2008).

18. Li, W., Xu, Z., Huang, J., Lin, X., Luo, R., Chen, C. H. & Shi, P. NeuroArray: A universal interface for patterning and interrogating neural circuitry with single cell resolution. *Sci. Rep.* **4**, 1–7 (2014).

19. Turunen, S., Käpylä, E., Lähteenmäki, M., Ylä-Outinen, L., Narkilahti, S. & Kellomäki, M. Direct laser writing of microstructures for the growth guidance of human pluripotent stem cell derived neuronal cells. *Opt. Lasers Eng.* **55**, 197–204 (2014).

20. Marino, A., Ciofani, G., Filippeschi, C., Pellegrino, M., Pellegrini, M., Orsini, P., Pasqualetti, M., Mattoli, V. & Mazzolai, B. Two-Photon Polymerization of Sub-micrometric Patterned Surfaces: Investigation of Cell-Substrate Interactions and Improved Differentiation of Neuron-like Cells. *ACS Appl. Mater. Interfaces* (2013). doi:10.1021/am403895k

21. Christopher, G. F. & Anna, S. L. Microfluidic methods for generating continuous droplet streams. *J. Phys. D. Appl. Phys.* **40**, (2007).

22. Taylor, A., Blurton-Jones, M. & Rhee, S. A microfluidic culture platform for CNS axonal injury, regeneration and transport. *Nat. …* **2**, 599–605 (2005).

23. Kamudzandu, M., Yang, Y., Roach, P. & Fricker, R. A. Efficient alignment of primary CNS neurites using structurally engineered surfaces and biochemical cues. *RSC Adv.* **5**, 22053–22059 (2015).

24. Kanagasabapathi, T. T., Ciliberti, D., Martinoia, S., Wadman, W. J. & Decré, M. M. J. Dual-compartment neurofluidic system for electrophysiological measurements in physically segregated and functionally connected neuronal cell culture. *Front. Neuroeng.* **4**, 13 (2011).

25. Millet, L. J., Stewart, M. E., Sweedler, J. V, Nuzzo, R. G. & Gillette, M. U. Microfluidic devices for culturing primary mammalian neurons at low densities. *Lab Chip* **7**, 987–94 (2007).

26. Prince, M. J., Wu, F., Guo, Y., Gutierrez Robledo, L. M., O'Donnell, M., Sullivan, R. & Yusuf, S. The burden of disease in older people and implications for health policy and practice. *Lancet* **385**, 549–562 (2015).

27. Skierlo, S., Rommer, P. S. & Zettl, U. K. Symptomatic treatment in multiple sclerosis—interim analysis of a nationwide registry. *Acta Neurol. Scand.* **135**, 394–399 (2017).

28. Wundt, W. M. Beiträge zur theorie der sinneswahrnehmung. *CF* **Winter**, (1862).

29. Kolb, B. & Whishaw, I. Q. Fundamentals of Human Neuropsychology. *New York Free. Co.* (1980).

30. Gross, C. G. Early History of Neuroscience. *Encyclopedia of Neuroscience* 843–847 (1987).

31. Yoo, S. S., Talos, I. F., Golby, A. J., Black, P. M. L. & Panych, L. P. Evaluating Requirements for Spatial Resolution of fMRI for Neurosurgical Planning. *Hum. Brain Mapp.* **21**, 34–43 (2004).

32. Cajal, S. R. Y. The Croonian Lecture : La Fine Structure des Centres Nerveux. (1894).

33. Weissman, T. A., Sanes, J. R., Lichtman, J. W. & Livet, J. Generating and Imaging Multicolor Brainbow Mice. 763–770 (2016). doi:10.1101/pdb.top114

34. Lotti, F., Ranieri, F., Vadalà, G., Zollo, L. & Di Pino, G. Invasive intraneural interfaces: Foreign body reaction issues. *Front. Neurosci.* **11**, 1–14 (2017).

35. Kwiat, M., Elnathan, R., Pevzner, A., Peretz, A., Barak, B., Peretz, H., Ducobni, T., Stein, D., Mittelman, L., Ashery, U. & Patolsky, F. Highly Ordered Large-Scale Neuronal Networks of Individual Cells - Toward Single Cell to 3D Nanowire Intracellular Interfaces. *ACS Appl. Mater. Interfaces* 3542–3549 (2012). doi:10.1021/am300602e

36. Yavin, E. & Yavin, Z. Attatchment and Culture of Dissociated Cells from Rat Embryo Cerebral

Hemispheres on Polylysine-coated Strates. *J. Cell Biol.* **62**, 540–546 (1974).

37. Viswam, V., Dragas, J., Shadmani, A., Chen, Y., Stettler, A., Müller, J. & Hierlemann, A. Multi-Functional Microelectrode Array System. 394–396 (2016). doi:10.1109/ISSCC.2016.7418073

38. Marom, A., Mahto, S. K., Shor, E., Tenenbaum-Katan, J., Sznitman, J. & Shoham, S. Microfluidic Chip for Site-Specific Neuropharmacological Treatment and Activity Probing of 3D Neuronal 'Optonet' Cultures. *Adv. Healthc. Mater.* **4**, 1478–1483 (2015).

39. Ito, Daisuke; Komatsu, Takumi; Gohara, K. Measurement of saturation processes in glutamatergic and GABAergic synapse densities during long-term development of cultured rat cortical networks. *Brain Res.* **1534: 22**-**3**, (2013).

40. Maccione, A., Garofalo, M., Nieus, T., Tedesco, M., Berdondini, L. & Martinoia, S. Multiscale functional connectivity estimation on low-density neuronal cultures recorded by high-density CMOS Micro Electrode Arrays. *J. Neurosci. Methods* **207**, 161–171 (2012).

41. Petersen, C. L., Chen, T. P., Ansermino, J. M. & Dumont, G. A. Design and Evaluation of a Low-Cost Smartphone Pulse Oximeter. 16882–16893 (2013). doi:10.3390/s131216882

42. Hochberg, L. R., Bacher, D., Jarosiewicz, B., Masse, N. Y., John, D., Vogel, J., Haddadin, S., Liu, J., Cash, S. S., Donoghue, J. P., Service, D. & Hospital, G. Reach and grasp by people with tetraplegia using a neurally controlled robotic arm. **485**, 372–375 (2013).

43. Zamaleeva, Alsu I., Ilziya R. Sharipova, Rezeda V. Shamagsumova, Alexey N. Ivanov, Gennady A. Evtugyn, Dilara G. Ishmuchametova, and R. F. F. A whole-cell amperometric herbicide biosensor based on magnetically functionalised microalgae and screen-printed electrodes †. *Anal. methods* 509–513 (2011). doi:10.1039/c0ay00627k

44. Masand, S. N., Mignone, L., Zahn, J. D. & Shreiber, D. I. Nanoporous membrane-sealed microfluidic devices for improved cell viability. *Biomed. Microdevices* **13**, 955–61 (2011).

45. Trist, D. G., Cohen, A. & Bye, A. ScienceDirect Clinical pharmacology in neuroscience drug discovery : quo vadis ? *Curr. Opin. Pharmacol.* **14**, 50–53 (2014).

46. Marshak, D. R., Lukas, T. J. & Watterson, D. M. Drug-Protein Interactions: Binding of Chlorpromazine to Calmodulin, Calmodulin Fragments, and Related Calcium Binding Proteins. *Biochemistry* **24**, 144–150 (1985).

47. Giedroc, D. P., Keravis, T. M., James, V., Ling, N. & Jack, N. Functional Properties of Covalent 5-Endorphin Peptide Calmodulin Complexes . Chlorpromazine Binding and Phosphodiesterase Activation. *Biochemistry* 1203–1211 (1985).

48. Nathan, P. J., Phan, K. L., Harmer, C. J., Mehta, M. A. & Bullmore, E. T. ScienceDirect Increasing pharmacological knowledge about human neurological and psychiatric disorders through functional neuroimaging and its application in drug discovery. *Curr. Opin. Pharmacol.* **14**, 54–61 (2014).

49. Hodgkin, A L, Huxley, A. F. A quantitive description of membrane current and its application to nerve excitation. 500–544 (1952).

50. Monica Subashini, M. & Sahoo, S. K. Pulse coupled neural networks and its applications. *Expert Syst. Appl.* **41**, 3965–3974 (2014).

51. Nakamoto, M., Cheng, H. J., Friedman, G. C., McLaughlin, T., Hansen, M. J., Yoon, C. H., O'Leary, D. D. M. & Flanagan, J. G. Topographically specific effects of ELF-1 on retinal axon guidance in vitro and retinal axon mapping in vivo. *Cell* **86**, 755–766 (1996).

52. Wang, J., Ren, L., Li, L., Liu, W., Zhou, J., Yu, W., Tong, D. & Chen, S. Microfluidics: a new cosset for neurobiology. *Lab Chip* **9**, 644–52 (2009).

53. Chung, B. G., Flanagan, L. a, Rhee, S. W., Schwartz, P. H., Lee, A. P., Monuki, E. S. & Jeon, N. L. Human neural stem cell growth and differentiation in a gradient-generating microfluidic device. *Lab Chip* **5**, 401–6 (2005).

54. Croushore, C. A., Supharoek, S., Lee, C. Y., Jakmunee, J. & Sweedler, J. V. Microfluidic Device for the Selective Chemical Stimulation of Neurons and Characterization of Peptide Release with Mass Spectrometry. *Anal. Chem.* 9445–9456 (2012).

55. Geckil, H., Xu, F., Zhang, X., Moon, S. & Demirci, U. Engineering hydrogels as extracellular matrix mimics. *Nanomedicine* **5**, 469–484 (2010).

56. Lledo, P., Gheusi, G. & Vincent, J. Information Processing in the Mammalian Olfactory System. *Physiol. Rev.* **85**, 281–317 (2005).

57. Guthman, E. M. & Vera, J. A Cellular Mechanism for Main and Accessory Olfactory Integration at the Medial Amygdala. *J. Neurosci.* **36**, 2083–2085 (2016).

58. Dickson, B. J. Molecular Mechanisms of Axon Guidance. *Science (80-.).* **298**, 1959–1963 (2002).

59. Wilson, L. & Maden, M. The mechanisms of dorsoventral patterning in the vertebrate neural tube. *Developmental Biology* **282**, 1–13 (2005).

60. Kalil, K. & Dent, E. W. Touch and go: Guidance cues signal to the growth cone cytoskeleton. *Current Opinion in Neurobiology* **15**, 521–526 (2005).

61. Nieto, M. A. Molecular Biology of Axon Guidance. *Neuron* **17**, 1039–1048 (1996).

62. Kochhar, D. M. Limb Development in Mouse Embryos. *Teratology* **7**, 289–298 (1972).

63. Roy, J., Kennedy, T. E. & Costantino, S. Engineered cell culture substrates for axon guidance studies: moving beyond proof of concept. *Lab Chip* **13**, 498–508 (2013).

64. Saik, J. E., Gould, D. J., Keswani, A. H., Dickinson, M. E. & West, J. L. Biomimetic hydrogels with immobilized ephrinA1 for therapeutic angiogenesis. *Biomacromolecules* **12**, 2715–22 (2011).

65. Doering, L. C. *Protocols for neural cell culture: fourth edition*. (2010).

66. Barker, A. T., Jalinous, R. & Freeston, I. L. Non-Invasive Magnetic Stimulation of Human Motor Cortex. *Lancet* **325**, 1106–1107 (1985).

67. Berger, H. Uber das Elektrenkephalogramm des Menschen, 2nd report. *J Psychol Neurol* **40**, 160–179 (1930).

68. Meduna, L. V. Uber experimentelle Campherepilepsie. *Arch. Psychiatr. Nervenkr.* 333–339 (1934).

69. Smith, S. J. M. EEG in the diagnosis, classification, and management of patients with epilepsy. *J. Neurol. Neurosurg. Psychiatry* **76**, ii2-ii7 (2005).

70. Ogawa, S., Lee, T. M., Nayak, A. S. & Glynn, P. Oxygenation-sensitive contrast in magnetic resonance image of rodent brain at high magnetic fields. *Magn. Reson. Med.* **14**, 68–78 (1990).

71. Perin, R. & Markram, H. A Computer-assisted Multi-electrode Patch-clamp System. *J. Vis. Exp.* 1–13 (2013). doi:10.3791/50630

72. Attneave, F., B., M. & Hebb, D. O. The Organization of Behavior; A Neuropsychological Theory.

Am. J. Psychol. **63**, 633 (1950).

73. Baxter, R., Hastings, N., Law, a. & Glass, E. J. . [No Title]. *Animal Genetics* **39**, 561–563 (2008).

74. Nagel, G., Ollig, D., Fuhrmann, M., Kateriya, S., Musti, A. M., Bamberg, E. & Hegemann, P. Channelrhodopsin-1: A light-gated proton channel in green algae. *Science (80-.).* **296**, 2395–2398 (2002).

75. Thomas, C. A., Springer, P. A., Loeb, G. E., Berwald- Netter, Y., And Okun, L. M. A Miniature Electrode Array to Monitor the Bioelectric Activity of Cultured Cells. *Exp. Cell Res.* **74**, 61–66 (1972).

76. Fejtl, M., Stett, A., Nisch, W., Boven, K. & Andreas, M. On Micro-Electrode Array Revival : Its Development , Sophistication of Recording , and Stimulation. 24–38

77. Vitale, F. & Litt, B. Bioelectronics: the promise of leveraging the body's circuitry to treat disease. *Bioelectron. Med.* **1**, 3–7 (2017).

78. Kim, S. & Rieth, L. Integrated wireless neural interface based on the Utah electrode array . Biomed Microdevices electrode array. *Microdevices, Biomed.* (2009). doi:10.1007/s10544-008-9251-y

79. Heer, F., Franks, W., Blau, A., Taschini, S., Ziegler, C., Hierlemann, A. & Baltes, H. CMOS microelectrode array for the monitoring of electrogenic cells. *Biosens. Bioelectron.* **20**, 358–366 (2004).

80. Heer, F., Hafizovic, S., Franks, W., Blau, A., Ziegler, C. & Hierlemann, A. CMOS microelectrode array for bidirectional interaction with neuronal networks. *Solid-State Circuits, IEEE J.* **41**, 1620–1629 (2006).

81. Andersen, R. A., Burdick, J. W., Musallam, S., Pesaran, B. & Cham, J. G. Cognitive neural prosthetics. *Trends in Cognitive Sciences* **8**, 486–493 (2004).

82. Paik, S. J., Park, Y. & Cho, D. I. D. Roughened polysilicon for low impedance microelectrodes in neural probes. *J. Micromechanics Microengineering* **13**, 373–379 (2003).

83. Obien, M. E. J., Deligkaris, K., Bullmann, T. & Bakkum, D. J. Revealing neuronal function through microelectrode array recordings. **8**, 1–30 (2015).

84. Krämer-Albers, E.-M., Fröhlich, D., Kuo, W. P., Frühbeis, C., Sun, J., Zehendner, C. M., Luhmann, H. J., Pinto, S., Toedling, J. & Trotter, J. Multifaceted effects of oligodendroglial exosomes on neurons: impact on neuronal firing rate, signal transduction and gene regulation. *Philos. Trans. R. Soc. B-Biological Sci.* **369**, 13 (2014).

85. Ringer, S. A further Contribution regarding the influence of the different Constituents of the Blood on the Contraction of the Heart. *J. Physiol.* **4**, 29–42 (1883).

86. Khan, S. & Newaz, G. A comprehensive review of surface modification for neural cell adhesion and patterning. *Journal of Biomedical Materials Research - Part A* **93**, 1209–1224 (2010).

87. Schaffner, a E., Barker, J. L., Stenger, D. a & Hickman, J. J. Investigation of the factors necessary for growth of hippocampal neurons in a defined system. *J. Neurosci. Methods* **62**, 111–9 (1995).

88. Ulman, A. Formation and Structure of Self-Assembled Monolayers. *Chem. Rev.* **96**, 1533–1554 (1996).

89. Swindle-Reilly, K. E., Papke, J. B., Kutosky, H. P., Throm, A., Hammer, J. a, Harkins, A. B. & Willits, R. K. The impact of laminin on 3D neurite extension in collagen gels. *J. Neural Eng.* **9**, 046007

(2012).

90. Lanniel, M., Huq, E., Allen, S., Buttery, L., Williams, P. M. & Alexander, M. R. Substrate induced differentiation of human mesenchymal stem cells on hydrogels with modified surface chemistry and controlled modulus. *Soft Matter* **7**, 6501 (2011).

91. Sorribas, H., Padeste, C. & Tiefenauer, L. Photolithographic generation of protein micropatterns for neuron culture applications. *Biomaterials* **23**, 893–900 (2002).

92. Xia, Y., Kim, E., Mrksich, M. & Whitesides, G. M. Microcontact Printing of Alkanethiols on Copper and Its Application in Microfabrication Patterned SAMs of hexadecanethiolate on gold and silver can be used directly as ultrathin resists in selective wet etching to fabricate patterned microstruc- nique , s. *Chem. Mater.* 601–603 (1996).

93. Jun, S. B., Hynd, M. R., Dowell-Mesfin, N., Smith, K. L., Turner, J. N., Shain, W. & Kim, S. J. Low-density neuronal networks cultured using patterned poly-l-lysine on microelectrode arrays. *J. Neurosci. Methods* **160**, 317–26 (2007).

94. Heller, D. a, Garga, V., Kelleher, K. J., Lee, T.-C., Mahbubani, S., Sigworth, L. a, Lee, T. R. & Rea, M. a. Patterned networks of mouse hippocampal neurons on peptide-coated gold surfaces. *Biomaterials* **26**, 883–9 (2005).

95. Scholl, M., Sprössler, C., Denyer, M., Krause, M., Nakajima, K., Maelicke, a, Knoll, W. & Offenhäusser, a. Ordered networks of rat hippocampal neurons attached to silicon oxide surfaces. *J. Neurosci. Methods* **104**, 65–75 (2000).

96. Costantino, S., Heinze, K. G., Martínez, O. E., De Koninck, P. & Wiseman, P. W. Two-photon fluorescent microlithography for live-cell imaging. *Microsc. Res. Tech.* **68**, 272–6 (2005).

97. Geissler, M. & Xia, Y. Patterning: Principles and Some New Developments. *Adv. Mater.* **16**, 1249–1269 (2004).

98. Walter, J., Kern-Veits, B., Huf, J., Stolze, B. & Bonhoeffer, F. Recognition of position-specific properties of tectal cell membranes by retinal axons in vitro. *Development* **101**, 685–96 (1987).

99. Knöll, B., Weinl, C., Nordheim, A. & Bonhoeffer, F. Stripe assay to examine axonal guidance and cell migration. *Nat. Protoc.* **2**, 1216–1224 (2007).

100. Millet, L. J. & Gillette, M. U. New perspectives on neuronal development via microfluidic environments. *Trends Neurosci.* **35**, 752–61 (2012).

101. Andersson, H. & van den Berg, A. Microfabrication and microfluidics for tissue engineering: state of the art and future opportunities. *Lab Chip* **4**, 98–103 (2004).

102. Zhang, Y., Chopp, M., Liu, X. S., Kassis, H., Wang, X., Li, C., An, G. & Zhang, Z. G. MicroRNAs in the Axon Locally Mediate the Effects of Chondroitin Sulfate Proteoglycans and cGMP on Axonal Growth Primary Cortical Neurons Cultured in a. **1**, 1402–1419 (2015).

103. Roth, E. a, Xu, T., Das, M., Gregory, C., Hickman, J. J. & Boland, T. Inkjet printing for high-throughput cell patterning. *Biomaterials* **25**, 3707–15 (2004).

104. Ilkhanizadeh, S., Teixeira, A. I. & Hermanson, O. Inkjet printing of macromolecules on hydrogels to steer neural stem cell differentiation. *Biomaterials* **28**, 3936–43 (2007).

105. Kufelt, O., El-Tamer, A., Sehring, C., Schlie-Wolter, S. & Chichkov, B. N. Hyaluronic Acid Based Materials for Scaffolding via Two-Photon Polymerization. *Biomacromolecules* **15**, 650–9 (2014).

106. Goeppert-mayer, M. Über Elementarakte mit zwei Quantensprüngen, Annal- en der Physik.

273–294. (1931).

107. Spangenberg, A., Hobeika, N. & Stehlin, F. Recent Advances in Two-Photon Stereolithography. (2013).

108. Pao, Y.-H. & Rentzepis, P. M. Multiphoton Absorption and Optical-Harmonic Generation in Highly Absorbing Molecular Crystals. *J. Chem. Phys.* **43**, 1281 (1965).

109. Kawata, S., Sun, H. B., Tanaka, T. & Takada, K. Finer features for functional microdevices. *Nature* **412**, 697–8 (2001).

110. Maruo, S., Nakamura, O. & Kawata, S. Three-dimensional microfabrication with two-photon-absorbed photopolymerization. *Opt. Lett.* **22**, 132–4 (1997).

111. Klein, F., Richter, B., Striebel, T., Franz, C. M., von Freymann, G., Wegener, M. & Bastmeyer, M. Two-component polymer scaffolds for controlled three-dimensional cell culture. *Adv. Mater.* **23**, 1341–5 (2011).

112. Torgersen, J., Qin, X.-H., Li, Z., Ovsianikov, A., Liska, R. & Stampfl, J. Hydrogels for Two-Photon Polymerization: A Toolbox for Mimicking the Extracellular Matrix. *Adv. Funct. Mater.* **23**, 4542–4554 (2013).

113. Engelhardt, S., Hoch, E., Borchers, K., Meyer, W., Krüger, H., Tovar, G. E. M. & Gillner, A. Fabrication of 2D protein microstructures and 3D polymer-protein hybrid microstructures by two-photon polymerization. *Biofabrication* **3**, 025003 (2011).

114. Ovsianikov, A., Deiwick, A., Van Vlierberghe, S., Pflaum, M., Wilhelmi, M., Dubruel, P. & Chichkov, B. Laser Fabrication of 3D Gelatin Scaffolds for the Generation of Bioartificial Tissues. *Materials (Basel).* **4**, 288–299 (2011).

115. Olsen, M. H. Two-photon polymerization of immune cell scaffolds. (2013).

116. Koskela, J. E., Turunen, S., Ylä, L., Narkilahti, S. & Kellomäki, M. Two - photon microfabrication of poly (ethylene glycol) diacrylate and a novel biodegradable photopolymer — comparison of processability for biomedical applications Fabrication setup. (2012). doi:10.1002/pat.2002

117. Nguyen, A. K., Gittard, S. D., Koroleva, A., Schlie, S., Gaidukeviciute, A., Chichkov, B. N. & Narayan, R. J. Two-photon polymerization of polyethylene glycol diacrylate scaffolds with riboflavin and triethanolamine used as a water-soluble photoinitiator. *Regen. Med.* **8**, 725–38 (2013).

118. Deforest, C. A. & Anseth, K. S. photoconjugation and photocleavage reactions. **3**, 925–931 (2011).

119. DeForest, C. a & Anseth, K. S. Photoreversible patterning of biomolecules within click-based hydrogels. *Angew. Chem. Int. Ed. Engl.* **51**, 1816–9 (2012).

120. Kaully, T., Kaufman-Francis, K., Lesman, A. & Levenberg, S. Vascularization—The Conduit to Viable Engineered Tissues. *Tissue Eng. Part B Rev.* **15**, 159–169 (2009).

121. Iseda, K., Kokado, K. & Sada, K. Design and function of smart polymer gels based on ion recognition. *React. Funct. Polym.* **73**, 951–957 (2013).

122. Chu, L., Xie, R. & Ju, X. Stimuli-responsive Membranes: Smart Tools for Controllable Mass-transfer and Separation Processes. *Chinese J. Chem. Eng.* **19**, 891–903 (2011).

123. Balaconis, M. K. & Clark, H. A. Gel Encapsulation of Glucose Nanosensors for Prolonged. **7**, 53–61 (2013).

124. Peppas, N. a, Keys, K. B., Torres-Lugo, M. & Lowman, a M. Poly(ethylene glycol)-containing hydrogels in drug delivery. *J. Control. Release* **62**, 81–7 (1999).

125. Chauhan, V. M., Burnett, G. R. & Aylott, J. W. Dual-fluorophore ratiometric pH nanosensor with tuneable pKa and extended dynamic range. *Analyst* **136**, 1799–801 (2011).

126. Chauhan, V. M., Orsi, G., Brown, A., Pritchard, D. I. & Aylott, J. W. Mapping the pharyngeal and intestinal pH of Caenorhabditis elegans and real-time luminal pH oscillations using extended dynamic range pH-sensitive nanosensors. *ACS Nano* **7**, 5577–5587 (2013).

127. Sarkar, D., Mallick, A., Haldar, B. & Chattopadhyay, N. Ratiometric spectroscopic response of pH sensitive probes: An alternative strategy for multidimensional sensing. *Chem. Phys. Lett.* **484**, 168–172 (2010).

128. Ruoslahti, E. Brain extracellular matrix. *Glycobiology* **6**, 489–492 (1996).

129. Gunn, J. W., Turner, S. D. & Mann, B. K. Adhesive and mechanical properties of hydrogels influence neurite extension. *J. Biomed. Mater. Res. A* **72**, 91–7 (2005).

130. Kloxin, A. M., Tibbitt, M. W. & Anseth, K. S. Synthesis of photodegradable hydrogels as dynamically tunable cell culture platforms. *Nat. Protoc.* **5**, 1867–87 (2010).

131. Kloxin, A. M., Lewis, K. J. R., DeForest, C. a, Seedorf, G., Tibbitt, M. W., Balasubramaniam, V. & Anseth, K. S. Responsive culture platform to examine the influence of microenvironmental geometry on cell function in 3D. *Integr. Biol. (Camb).* **4**, 1540–9 (2012).

132. Langer, R. & Vacanti, J. P. Tissue Engineering. *Science (80-.).* **260**, 920–925 (1993).

133. Hoffman, a S. Hydrogels for biomedical applications. *Ann. N. Y. Acad. Sci.* **944**, 62–73 (2001).

134. Drury, J. L. & Mooney, D. J. Hydrogels for tissue engineering: scaffold design variables and applications. *Biomaterials* **24**, 4337–4351 (2003).

135. Traphagen, S. & Yelick, P. Reclaiming a natural beauty: whole-organ engineering with natural extracellular materials. *Regen. Med.* **4**, 747–758 (2009).

136. Sachlos, E., Reis, N., Ainsley, C., Derby, B. & Czernuszka, J. T. Novel collagen scaffolds with predefined internal morphology made by solid freeform fabrication. **24**, 1487–1497 (2003).

137. Kaech, S., Huang, C.-F. & Banker, G. General considerations for live imaging of developing hippocampal neurons in culture. *Cold Spring Harb. Protoc.* **2012**, 312–8 (2012).

138. Revzin, a, Russell, R. J., Yadavalli, V. K., Koh, W. G., Deister, C., Hile, D. D., Mellott, M. B. & Pishko, M. V. Fabrication of poly(ethylene glycol) hydrogel microstructures using photolithography. *Langmuir* **17**, 5440–7 (2001).

139. Ananthanarayanan, B., Little, L., Schaffer, D. V, Healy, K. E. & Tirrell, M. Neural stem cell adhesion and proliferation on phospholipid bilayers functionalized with RGD peptides. *Biomaterials* **31**, 8706–15 (2010).

140. Patel, P. R., Kiser, R. C., Lu, Y. Y., Fong, E., Ho, W. C., Tirrell, D. a & Grubbs, R. H. Synthesis and cell adhesive properties of linear and cyclic RGD functionalized polynorbornene thin films. *Biomacromolecules* **13**, 2546–53 (2012).

141. Hersel, U., Dahmen, C. & Kessler, H. RGD modified polymers: biomaterials for stimulated cell adhesion and beyond. *Biomaterials* **24**, 4385–4415 (2003).

142. Shi, Y. & Ethell, I. M. Integrins control dendritic spine plasticity in hippocampal neurons through NMDA receptor and Ca2+/calmodulin-dependent protein kinase II-mediated actin

reorganization. *J. Neurosci.* **26**, 1813–22 (2006).

143. Fairbanks, B., Schwartz, M., Bowman, C. & Anseth, K. Photoinitiated polymerization of PEG-diacrylate with lithium phenyl-2, 4, 6-trimethylbenzoylphosphinate: polymerization rate and cytocompatibility. *Biomaterials* **20**, 333–339 (2009).

144. Kaech, S. & Banker, G. Culturing hippocampal neurons. *Nat. Protoc.* **1**, 2406–15 (2006).

145. Elbert, D. L. & Hubbell, J. a. Conjugate addition reactions combined with free-radical cross-linking for the design of materials for tissue engineering. *Biomacromolecules* **2**, 430–41 (2001).

146. Lhoest, J. B., Wagner, M. S., Tidwell, C. D. & Castner, D. G. Characterization of adsorbed protein films by time of flight secondary ion mass spectrometry. *J. Biomed. Mater. Res.* **57**, 432–40 (2001).

147. Albutt, D. J. Surface Chemistry Modification of Glass and Gold for Low Density Neural Cell Culture. (2013).

148. Kankate, L., Turchanin, A. & Gölzhäuser, A. On the release of hydrogen from the S-H groups in the formation of self-assembled monolayers of thiols. *Langmuir* **25**, 10435–8 (2009).

149. Rieth, L., Williams, L. & Caldwell, R. Bilayer Encapsulated Utah Electrode Array Based. *J. Neural Eng.* **11**, 1–23 (2015).

150. Abaddi, M. A.-, Sasso, L., Dimaki, M. & Svendsen, W. E. Microelectronic Engineering Fabrication of 3D nano / microelectrodes via two-photon-polymerization. *Microelectron. Eng.* **98**, 378–381 (2012).

151. Paredes, R. M., Etzler, J. C., Watts, L. T. & Lechleiter, J. D. NIH Public Access. *Imaging* **46**, 143–151 (2009).

152. Koroleva, A., Gill, A. A., Ortega, I., Haycock, J. W., Schlie, S., Gittard, S. D., Chichkov, B. N. & Claeyssens, F. Two-photon polymerization-generated and micromolding-replicated 3D scaffolds for peripheral neural tissue engineering applications. *Biofabrication* **4**, (2012).

153. Clausen, A., Wang, F., Jensen, J. S., Sigmund, O. & Lewis, J. A. Topology Optimized Architectures with Programmable Poisson's Ratio over Large Deformations. *Adv. Mater.* **27**, 5523–5527 (2015).

154. Aebersold, M. J., Dermutz, H., Forró, C., Weydert, S., Thompson-Steckel, G., Vörös, J. & Demkó, L. 'Brains on a chip': Towards engineered neural networks. *TrAC - Trends Anal. Chem.* **78**, 60–69 (2016).

155. Lorber, B., Hsiao, W.-K., Hutchings, I. M. & Martin, K. R. Adult rat retinal ganglion cells and glia can be printed by piezoelectric inkjet printing. *Biofabrication* **6**, 015001 (2014).

156. Zhang, H. & Liu, K. K. Optical tweezers for single cells. *Journal of the Royal Society Interface* **5**, 671–690 (2008).

157. Aregueta-Robles, U. A., Lim, K. S., Martens, P. J., Lovell, N. H., Poole-Warren, L. A. & Green, R. Producing 3D neuronal networks in hydrogels for living bionic device interfaces. *Proc. Annu. Int. Conf. IEEE Eng. Med. Biol. Soc. EMBS* **2015**–**Novem**, 2600–2603 (2015).

158. Wylie, R. G., Ahsan, S., Aizawa, Y., Maxwell, K. L., Morshead, C. M. & Shoichet, M. S. Spatially controlled simultaneous patterning of multiple growth factors in three-dimensional hydrogels. *Nat. Mater.* **10**, 799–806 (2011).

159. Richter, A., Paschew, G., Klatt, S., Lienig, J., Arndt, K. & Adler, H. P. Review on Hydrogel-based

pH Sensors and Microsensors. **c**, 561–581 (2008).

160. Wilson, K., Stancescu, M., Das, M., Rumsey, J. & Hickman, J. Direct patterning of coplanar polyethylene glycol alkylsilane monolayers by deep-ultraviolet photolithography as a general method for high fidelity, long-term cell patterning and culture. *J. Vac. Sci. Technol. B Nanotechnol. Microelectron.* **29**, 21020 (2011).

161. Li, Z., Torgersen, J., Ajami, A., Mühleder, S., Qin, X., Husinsky, W., Holnthoner, W., Ovsianikov, A., Stampfl, J. & Liska, R. Initiation efficiency and cytotoxicity of novel water-soluble two-photon photoinitiators for direct 3D microfabrication of hydrogels. *RSC Adv.* **3**, 15939–15946 (2013).

162. Li, Z., Pucher, N., Cicha, K., Torgersen, J., Ligon, S. C., Ajami, A., Husinsky, W., Rosspeintner, A., Vauthey, E., Naumov, S., Scherzer, T., Stampfl, J. & Liska, R. A straightforward synthesis and structure-activity relationship of highly efficient initiators for two-photon polymerization. *Macromolecules* **46**, 352–361 (2013).

163. San Juan, R. R., Miller, M. S., Ferrato, M.-A. & Carmichael, T. B. Influence of alkyl chain length on the structure of dialkyldithiophosphinic acid self-assembled monolayers on gold. *Langmuir* **28**, 13253–60 (2012).

164. Murugan, R. & Molnar, P. Biomaterial surface patterning of self-assembled monolayers for controlling neuronal cell behaviour. *Int. J. …* **2**, 104–134 (2009).

165. Schafer, K. J., Hales, J. M., Balu, M., Belfield, K. D., Van Stryland, E. W. & Hagan, D. J. Two-photon absorption cross-sections of common photoinitiators. *J. Photochem. Photobiol. A Chem.* **162**, 497–502 (2004).

166. Kocincova, A. S., Borisov, S. M., Krause, C. & Wolfbeis, O. S. Fiber-optic microsensors for simultaneous sensing of oxygen and pH, and of oxygen and temperature. *Anal. Chem.* **79**, 8486–93 (2007).

167. Okamoto, T., Suzuki, T. & Yamamoto, N. Microarray fabrication with covalent attachment of DNA using bubble jet technology. *Nat. Biotechnol.* **18**, 438–41 (2000).

168. Lee, S., Ibey, B. L., Coté, G. L. & Pishko, M. V. Measurement of pH and dissolved oxygen within cell culture media using a hydrogel microarray sensor. *Sensors Actuators B Chem.* **128**, 388–398 (2008).

Websites:

http://www.leica-microsystems.com/science-lab/the-patch-clamp-technique/

Appendix

Nuclear Magnetic Resonance Spectra of Photoinitiator E3

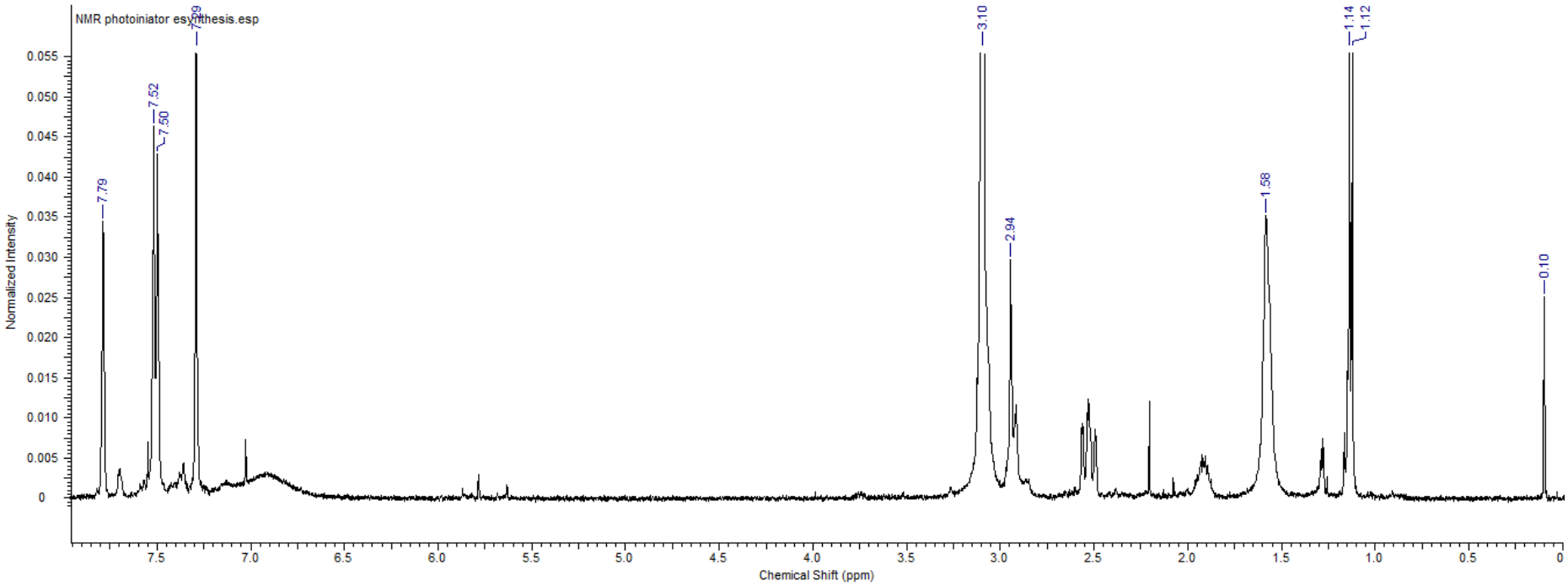


Figure 71 Proton Nuclear Magnetic Resonance Spectra of Photoinitiator E3.

Nuclear magnetic resonance spectra of synthesised photoinitiator 3e demonstrating peaks previously reported form the synthesis of this compound. Proton NMR: δ (ppm) 7.79 (singlet, 2H), 7.51 (doublet, J = 8.5Hz, 4H), 3.10 (singlet, 12H), 2.94 (m, 4H), 2.48-2.61 (multiple, 2H) 1.86-197 (m, 1H), 1.13 (doublet, J = 5.6Hz).

Infrared spectra of Photoinitiator E3

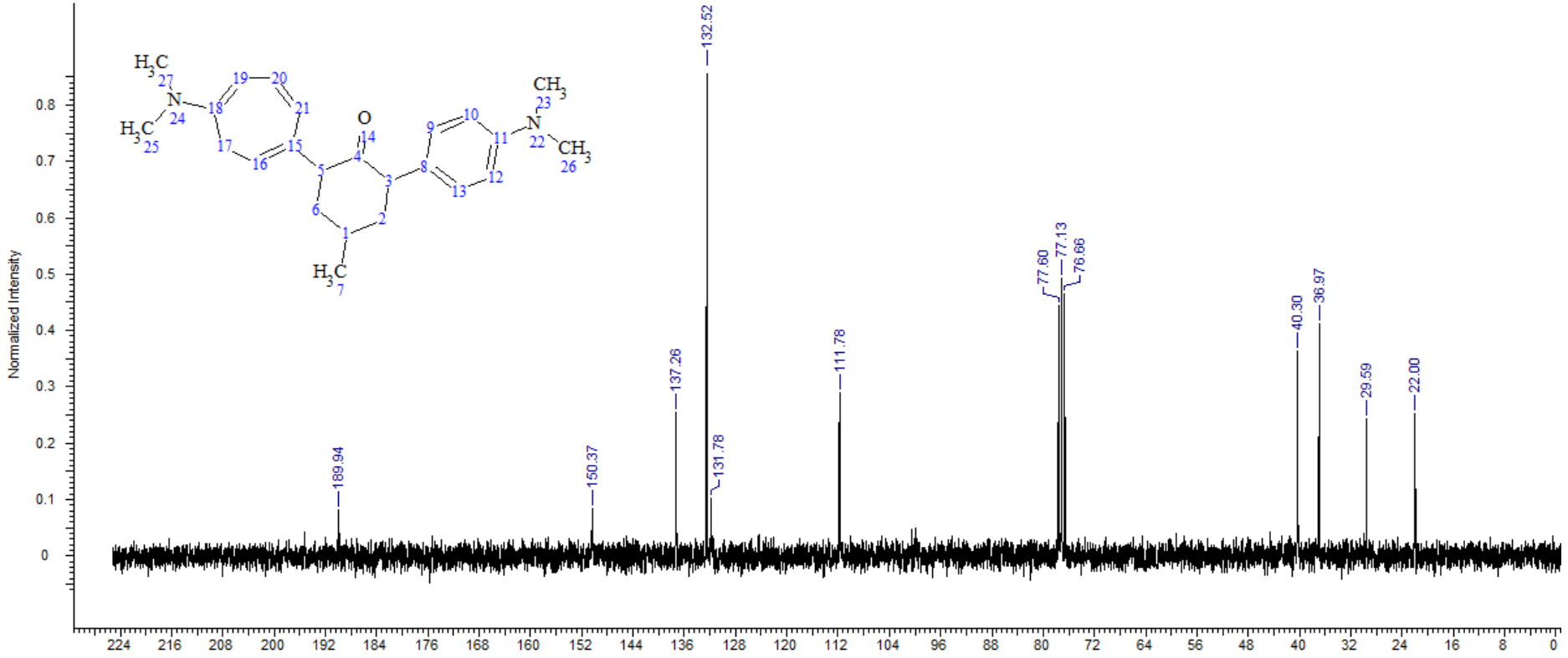


Figure 72 Infrared spectra of synthesised photoinitiator E3.

The infrared spectra accounts for all the bond lengths present within the photoinitiator E3.

Describe fabrication codes

The describe code for building the large area design using a modular approach is shown below. The first 8 lines describe the mode and parameter settings of the build. The subsequent commands are for the placement of various modular unites of the design. Some of the units are deployed in for loops in the code as are multiple repeats of the units per sample.

```
GalvoScanMode
ContinuousMode
PiezoSettlingTime 200
GalvoSettlingTime 2
PowerScaling 1.3
LaserPower 100
ScanSpeed 50000
ResetInterface

movestagex - 870
movestagey 1000

var $nRR = 1
 percent no. of rows of
structures

var $nR = 1
 percent no. of columns of
structures

var $yarray = 1

for $yarray =
1 to $nR step 1

Movestagex -($nRR * 870)
MoveStageY 700

var $Xarray = 1

for $Xarray =
1 to $nRR step 1
MoveStageX 870
movestagey -500
Wait 3
 percent line 1
var $o = 1
for $o = 1 to 10
  Wait 1
  FindInterfaceAt 1
  Include N S_Data.gwl
  MoveStageX 28.5
  Wait 1
  FindInterfaceAt 1
  include N S_data.gwl
  MoveStageX 28.5
end

Movestagey 28.5
MoveStageX -28.5
 percent line 2
var $o = 1
for $o = 1 to 10
  Wait 1
  FindInterfaceAt 1
  Include N W_Data.gwl
  MoveStageX -28.5
  Wait 1
  FindInterfaceAt 1
  include N E_data.gwl
```

```
   MoveStageX -28.5
end

 percent line 3
Movestagey 28.5
MoveStageX 28.5
Wait 1
   FindInterfaceAt 1
   Include E W_Data.gwl
   MoveStageX 28.5

Wait 1
   FindInterfaceAt 1
   Include S W_Data.gwl


Var $b =1

for $b = 1 to 16
   Wait 1
   MoveStageX 28.5
   wait 1
findinterfaceat 1
include border_data.gwl
end

movestagex 28.5
Wait 1
   FindInterfaceAt 1
   Include E S_Data.gwl
   MoveStageX 28.5
Wait 1
   FindInterfaceAt 1
   Include E W_Data.gwl

 percent  line 4
MoveStageY 28.5
Wait 1
   FindInterfaceAt 1
   Include E W_Data.gwl
   MoveStageX -28.5
Wait 1
   FindInterfaceAt 1
   Include N E_Data.gwl
movestagex -28.5
Wait 1
FindInterfaceAt 1
include border_data.gwl
movestagex -28.5
FindInterfaceAt 1

Wait 1
include S W_data.gwl


Var $EW = 1
for $EW = 1 to 12
MoveStageX -28.5
FindInterfaceAt 1
wait 1
include E W_data.gwl
end


MoveStageX -28.5
FindInterfaceAt 1
wait 1
include  E S_data.gwl
movestagex -28.5
FindInterfaceAt 1
Wait 1
include border_data.gwl
movestagex -28.5
Wait 1
   FindInterfaceAt 1
   Include N W_Data.gwl
   MoveStageX -28.5
Wait 1
```

```
   FindInterfaceAt 1
   Include E W_Data.gwl

var $a = 1
for $a = 1 to 6
 percent line 6
MoveStageY 28.5
Wait 1
   FindInterfaceAt 1
   include E W_Data.gwl
   movestagex 28.5
Wait 1
   FindInterfaceAt 1
   Include  S W_Data.gwl
movestagex 28.5
FindInterfaceAt 1
Wait 1
include border_data.gwl
movestagex 28.5
FindInterfaceAt 1
wait 3
include N E_data.gwl

Var $EW = 1
for $EW = 1 to 11
MoveStageX 28.5
FindInterfaceAt 1
wait 1
include E W_data.gwl
end

MoveStageX 28.5
FindInterfaceAt 1
wait 1
include S W_data.gwl
MoveStageX 28.5
FindInterfaceAt 1
wait 1
include N S_data.gwl
MoveStageX 28.5
FindInterfaceAt 1
Wait 1
include border_data.gwl
movestagex 28.5
Wait 1
   FindInterfaceAt 1
   Include E S_Data.gwl
   MoveStageX 28.5
Wait 1
   FindInterfaceAt 1
   include E W_Data.gwl

 percent line 7 after middel
section)
MoveStageY 28.5
Wait 1
   FindInterfaceAt 1
   Include E W_Data.gwl
   MoveStageX -28.5
Wait 1
   FindInterfaceAt 1
   Include N E_Data.gwl
movestagex -28.5
FindInterfaceAt 1
Wait 1
include border_data.gwl
movestagex -28.5
FindInterfaceAt 1
wait 1
include N S_data.gwl
movestagex -28.5
FindInterfaceAt 1
wait 1
include N W_data.gwl
Var $EW = 1
for $EW = 1 to 11
MoveStageX -28.5
FindInterfaceAt 1
```

```
wait 1
include E W_data.gwl
end
MoveStageX -28.5
FindInterfaceAt 1
wait 1
include E S_data.gwl
movestagex -28.5
FindInterfaceAt 1
Wait 1
include border_data.gwl
movestagex -28.5
Wait 1
   FindInterfaceAt 1
   Include N W_Data.gwl
   MoveStageX -28.5

Wait 1
   FindInterfaceAt 1
   Include E W_Data.gwl
end
MoveStageY 28.5
Wait 1
   FindInterfaceAt 1
   include E W_Data.gwl
   movestagex 28.5
```

```
Wait 1
   FindInterfaceAt 1
   Include  S W_Data.gwl
movestagex 28.5
FindInterfaceAt 1
Wait 1
include border_data.gwl
movestagex 28.5
FindInterfaceAt 1
wait 3
include N E_data.gwl


Var $EW = 1
for $EW = 1 to 11
MoveStageX 28.5
FindInterfaceAt 1
wait 1
include E W_data.gwl
end


MoveStageX 28.5
FindInterfaceAt 1
wait 1
include S W_data.gwl
MoveStageX 28.5
FindInterfaceAt 1
```

```
wait 1
include N S_data.gwl
MoveStageX 28.5
FindInterfaceAt 1
Wait 1
include border_data.gwl
movestagex 28.5
Wait 1
   FindInterfaceAt 1
   Include E S_Data.gwl
   MoveStageX 28.5


Wait 1
   FindInterfaceAt 1
   include E W_Data.gwl


 percent line 8 (after middel
section)
MoveStageY 28.5
FindInterfaceAt 1
Wait 1
include E W_data.gwl
MoveStageX -28.5
FindInterfaceAt 1
Wait 1
include N E_data.gwl
```

```
FindInterfaceAt 1
Wait 1
MoveStageX -28.5
include border_data.gwl
MoveStageX -28.5
wait 1
include N S_data.gwl
MoveStageX -28.5
wait 1
include N W_data.gwl

Var $EW = 1
for $EW = 1 to 11
MoveStageX -28.5
FindInterfaceAt 1
wait 1
include E W_data.gwl
end

MoveStageX -28.5
Wait 1
include E S_data.gwl
MoveStageX -28.5
FindInterfaceAt 1
Wait 1
include border_data.gwl
MoveStageX -28.5
FindInterfaceAt 1
Wait 1
include N W_data.gwl
MoveStageX -28.5
FindInterfaceAt 1
Wait 1
include E W_data.gwl
MoveStageY 28.5
FindInterfaceAt 1
Wait 1
include E W_data.gwl
MoveStageX 28.5
FindInterfaceAt 1
Wait 1
include S W_data.gwl
MoveStageX 28.5
FindInterfaceAt 1
Wait 1
include border_data.gwl
MoveStageX 28.5
FindInterfaceAt 1
Wait 1
include N E_data.gwl

Var $EW = 1
for $EW = 1 to 12
MoveStageX 28.5
FindInterfaceAt 1
wait 1
include E W_data.gwl
end

MoveStageX 28.5
FindInterfaceAt 1
Wait 1
include N W_data.gwl
MoveStageX 28.5
FindInterfaceAt 1
Wait 1
include border_data.gwl
MoveStageX 28.5
FindInterfaceAt 1
Wait 1
include E S_data.gwl
MoveStageX 28.5
FindInterfaceAt 1
Wait 1
include E W_data.gwl
MoveStageY 28.5
FindInterfaceAt 1
```

```
Wait 1
include E w_data.gwl
MoveStageX -28.5
FindInterfaceAt 1
Wait 1
include N W_data.gwl
MoveStageX -28.5
Var $EW = 1
for $EW = 1 to 16
FindInterfaceAt 1
wait 1
include border_data.gwl
MoveStageX -28.5
end
FindInterfaceAt 1
Wait 1
include N E_data.gwl
MoveStageX -28.5
FindInterfaceAt 1
Wait 1
include E W_data.gwl
MoveStageY 28.5
var $o = 1
for $o = 1 to 10
  Wait 1
  FindInterfaceAt 1
  Include S W_Data.gwl
  MoveStageX 28.5
  Wait 1
  FindInterfaceAt 1
  include E S_data.gwl
  MoveStageX 28.5
end
Movestagey 28.5
MoveStageX -28.5
var $o = 1
for $o = 1 to 10
  Wait 1
  FindInterfaceAt 1
  Include N S_Data.gwl
  MoveStageX -28.5
  Wait 1
  FindInterfaceAt 1
  include N S_data.gwl
  MoveStageX -28.5
end
end
```

ToF-SIMs positive ion spectra of cRGDfC modified glass and gold substrates.

The total ion mass spectra and any specific ions of interest are presented here for the whole substrate area, the gold region and the glass region. The gold and glass regions were selected as regions of interest based on the ion intensity images of Au and silicon ions which colocalised by the optically visible glass and gold regions. As well as Si+ and Au+ as markers of silicon and gold respectively several organic daughter ions which can be attributed to specific amino acids[146]. The fragments and the their corresponding amino acid are CHS for Cysteine, CH_4N for Glycine, CH_3N_2 for Arginine and $C_8H_{10}N$ for phenylalanine. All the amino acid associated daughter fragment ions were found in the total spectra and the gold region of interest suggesting the cRGDfC had successfully adsorbed to the gold substrate surface. As the glass region of interest had none of the daughter ions corresponding to the amino acids it can be concluded that the CRGDcF did not adsorb to the glass and the adsorption was gold selective.

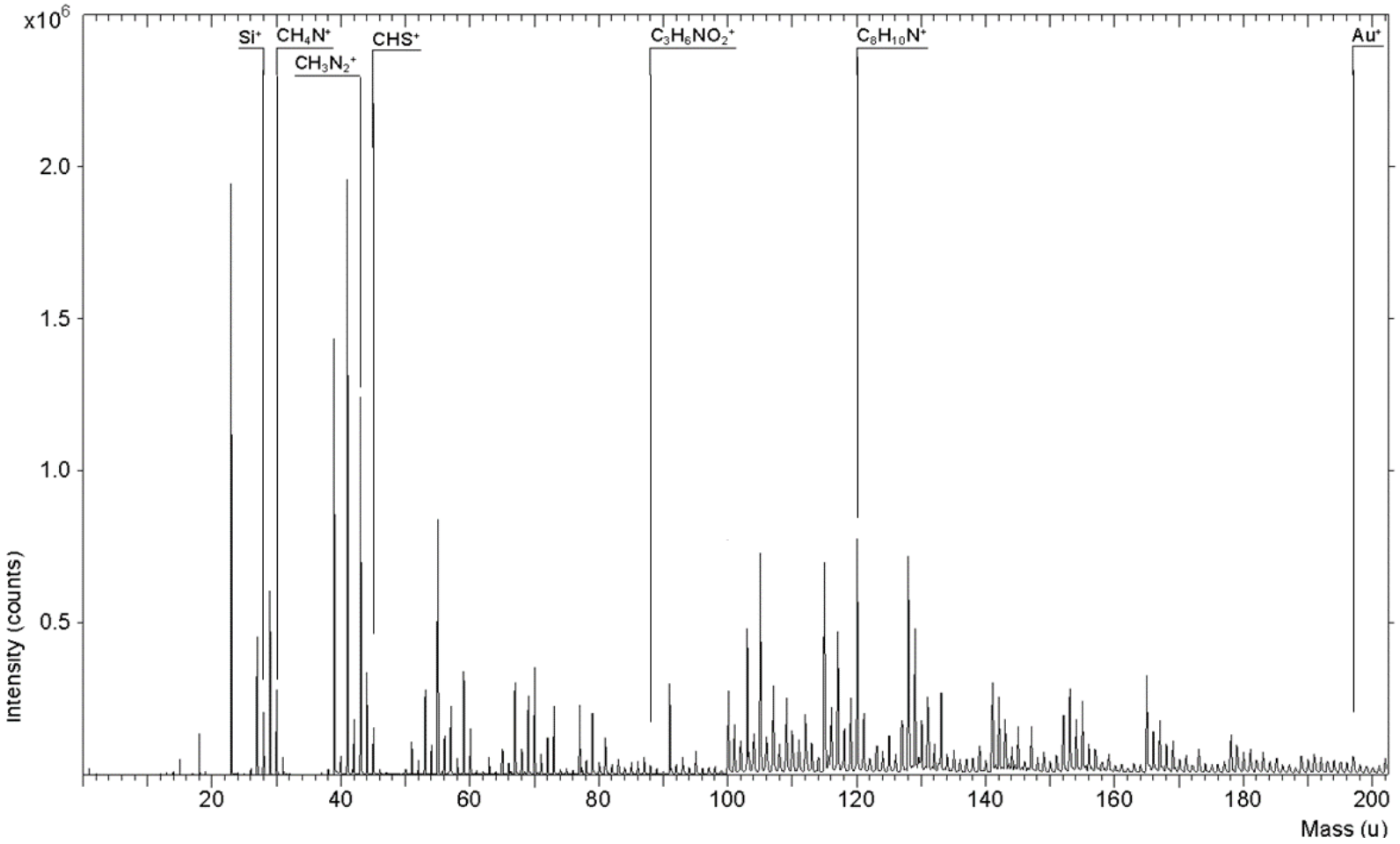


Figure 73 Total Time of Flight secondary positive ion mass spectra of whole area of the cRGDfC modified glass and gold substrates.

The Si+ peak is indicative of the glass substrate whilst the Au+ peak is indicative of the gold coating. Note the presence of the daughter ions of associated with the amino acids from CRGDfC. are present ono the substrate suggesting the cRGDfC has adsorbed to the substrate. The daughter ions are CHS for Cysteine, CH_4N for Glycine, CH_3N_2 for Arginine and C $_8H_{10}N$ for phenylalanine.

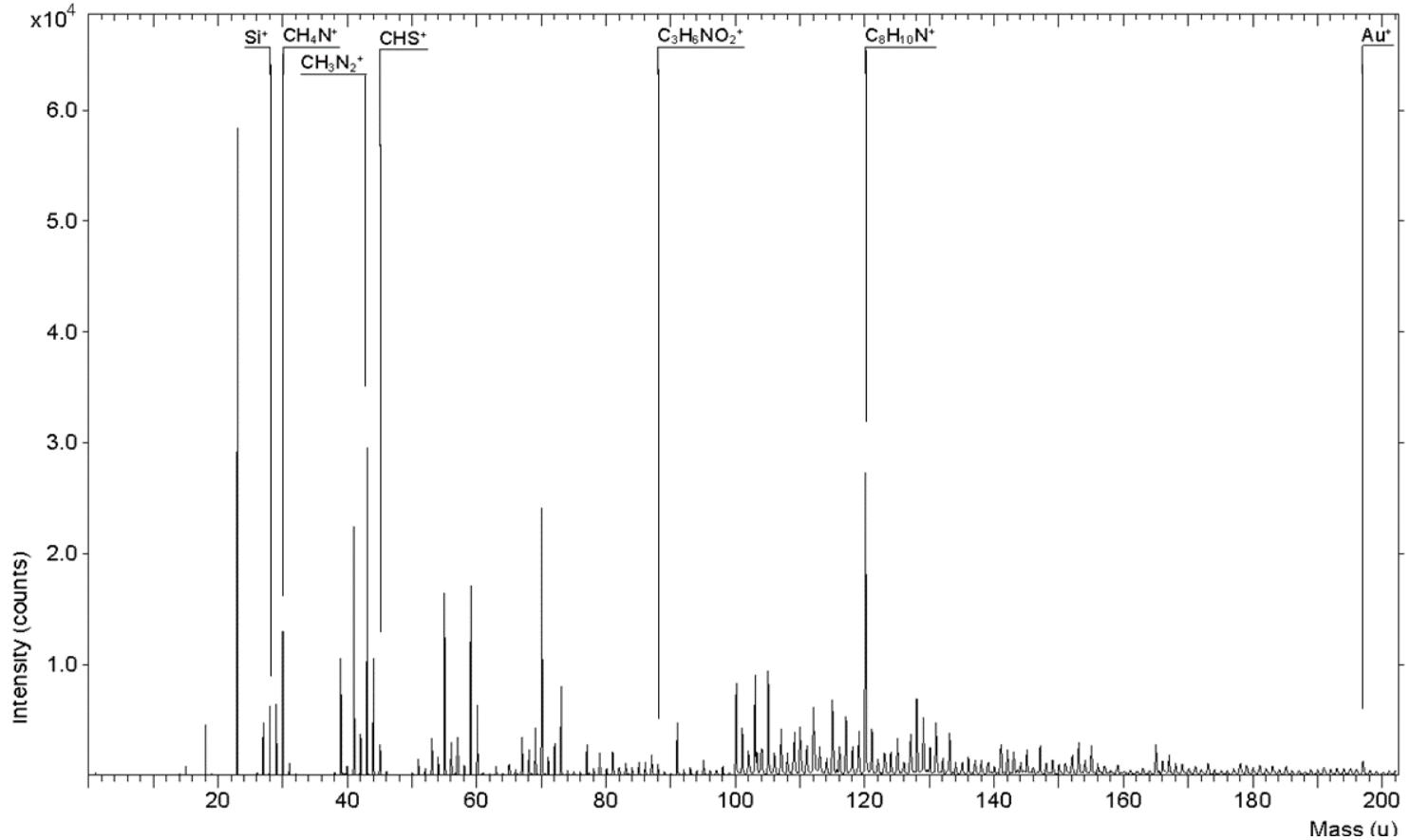


Figure 74 Total Time of Flight secondary positive ion mas spectra of the gold region of the cRGDfC modified glass and gold substrates.

The Si+ peak is indicative of the glass substrate whilst the Au+ peak is indicative of the gold coating. Note the presence of the daughter ions of associated with the amino acids from CRGDfC. Note the presence of the daughter ions of associated with the amino acids from cRGDfC are present on the gold region of interest suggesting the cRGDfC has adsorbed to the gold. The daughter ions are CHS for Cysteine, CH_4N for Glycine, CH_3N_2 for Arginine and $C_8H_{10}N$ for phenylalanine.

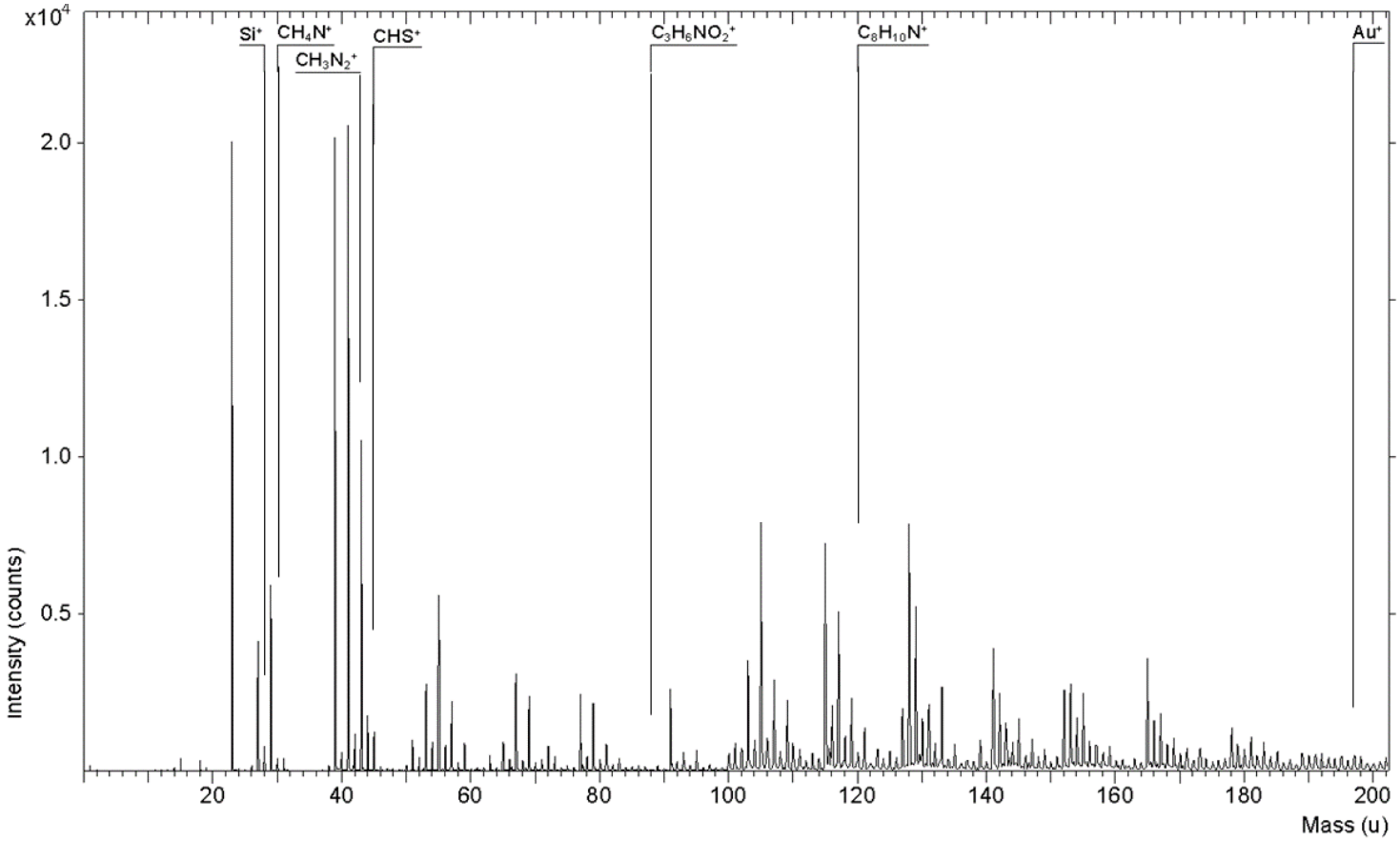


Figure 75 Total Time of Flight secondary positive ion mas spectra of the glass region of the cRGDfC modified glass and gold substrates.

The Si+ peak is indicative of the glass substrate whilst the Au+ peak is indicative of the gold coating. Note the presence of the daughter ions of associated with the amino acids from CRGDfC.

Note the lack of the daughter ions of associated with the amino acids from cRGDfC are present on the glass region of interest suggesting the cRGDfC has not adsorbed to the glass.

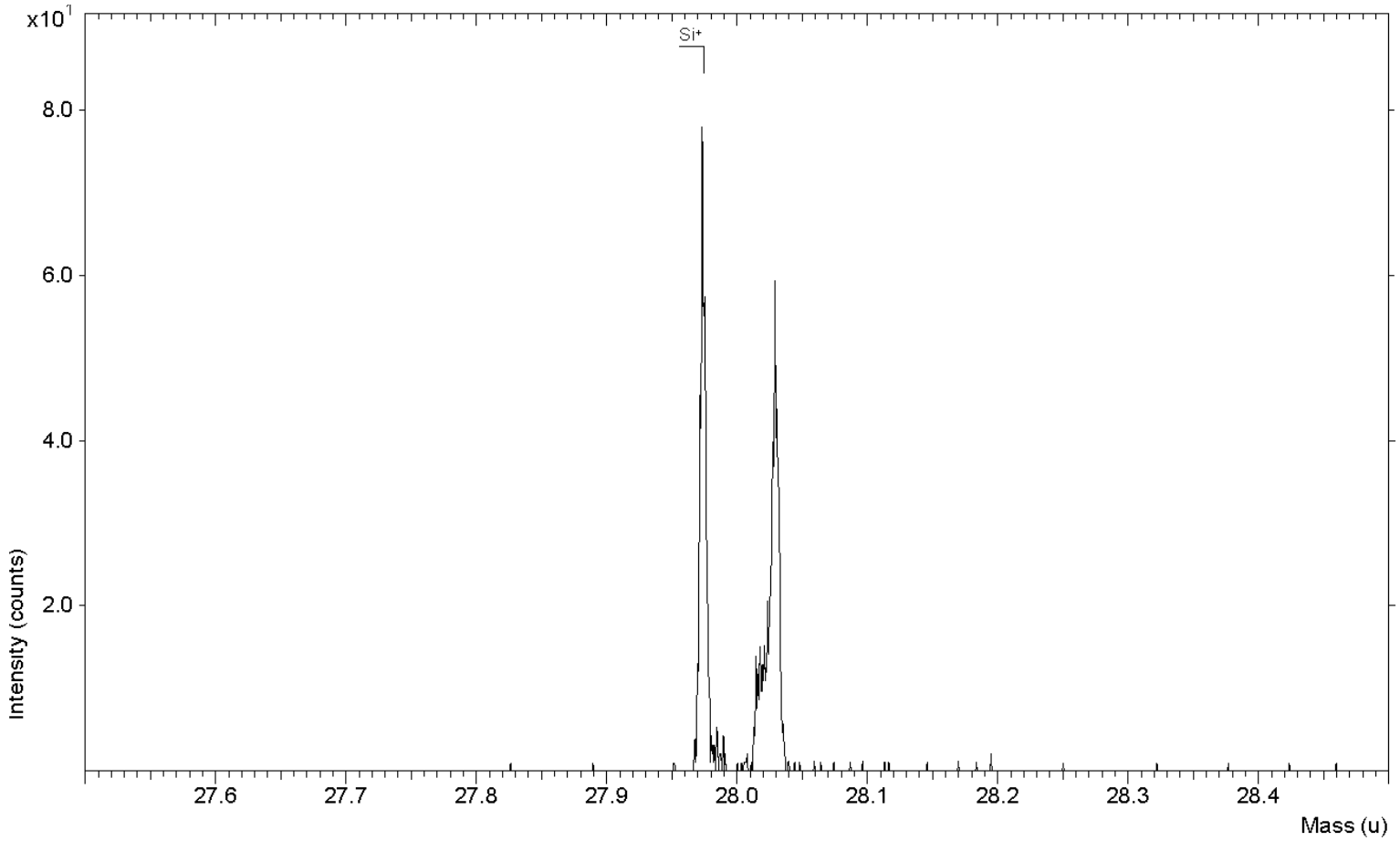


Figure 76 Time of Flight secondary positive ion mass spectra of Si on the whole area of the cRGDfC modified glass and gold substrates.

The whole area of the substrate has a Si+ ions indicative of the glass substrate.

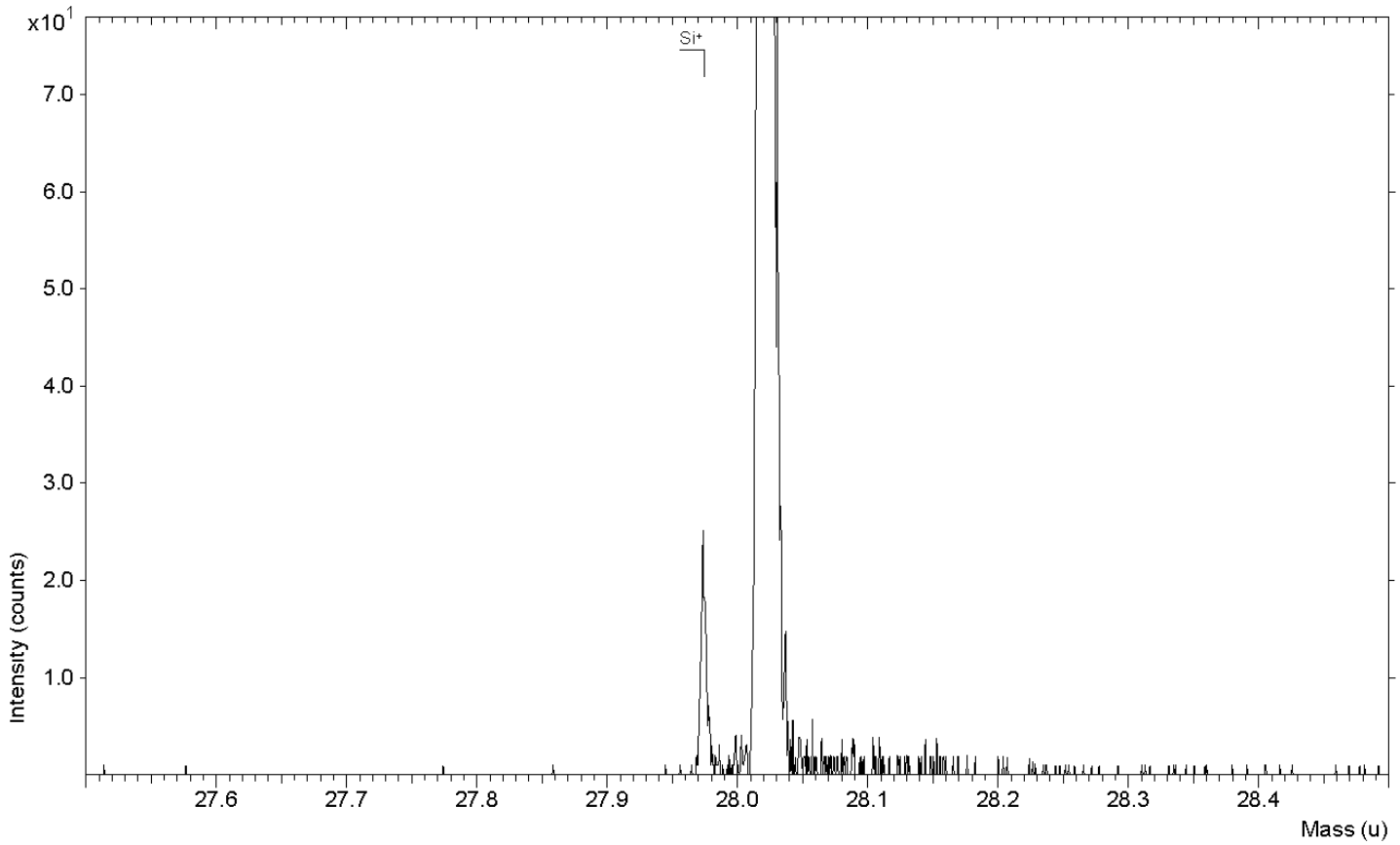


Figure 77 Time of Flight secondary positive ion mass spectra of Si on the gold region of the cRGDfC modified glass and gold substrates

. The gold of the substrate has a small intensity of Si+ ions indicative of the glass substrate that is under the gold coating.

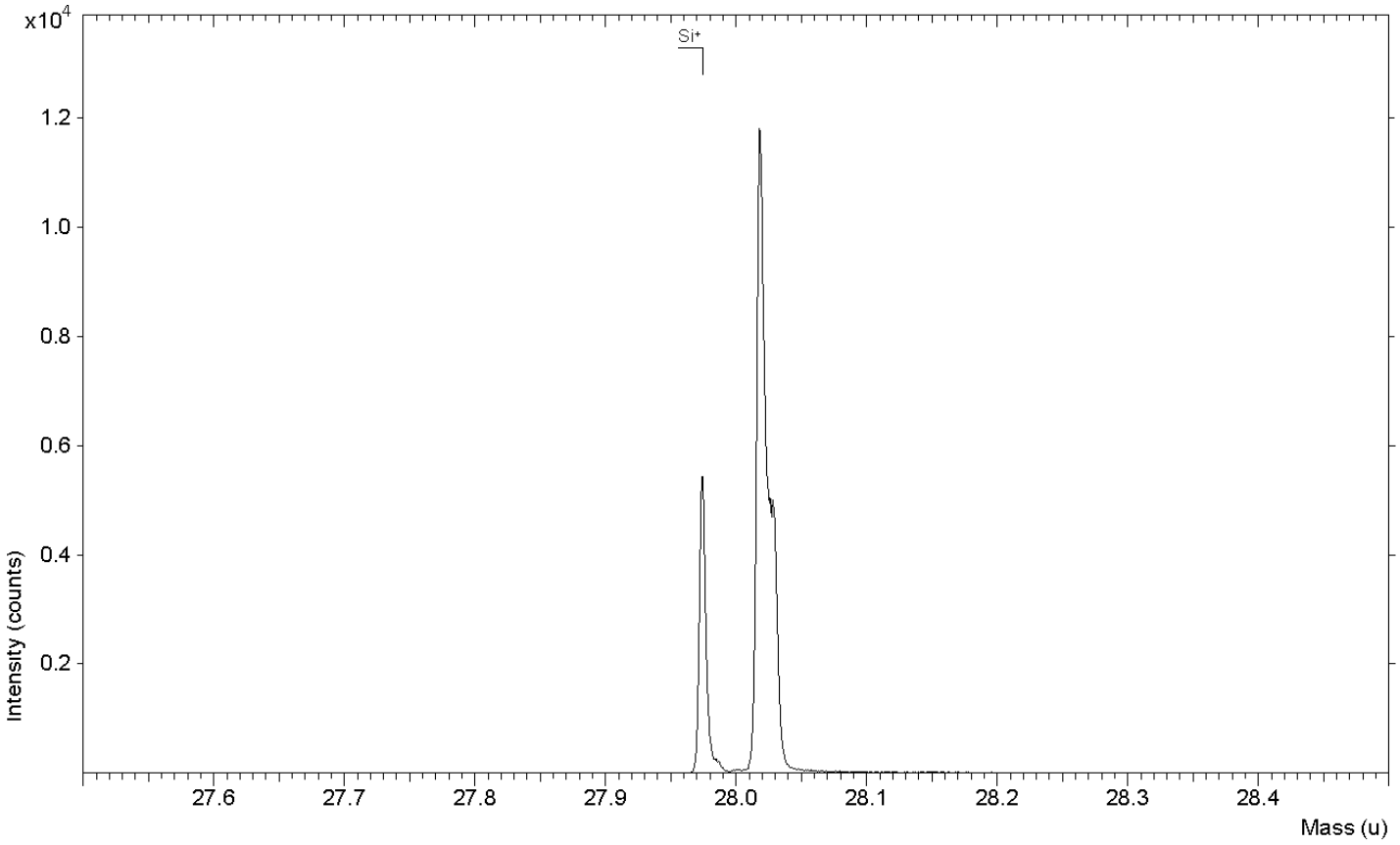


Figure 78 Time of Flight secondary positive ion mass spectra of Si on the glass region of the cRGDfC modified glass and gold substrates

The glass region of the substrate has a high Si+ ion intensity indicative of the glass substrate.

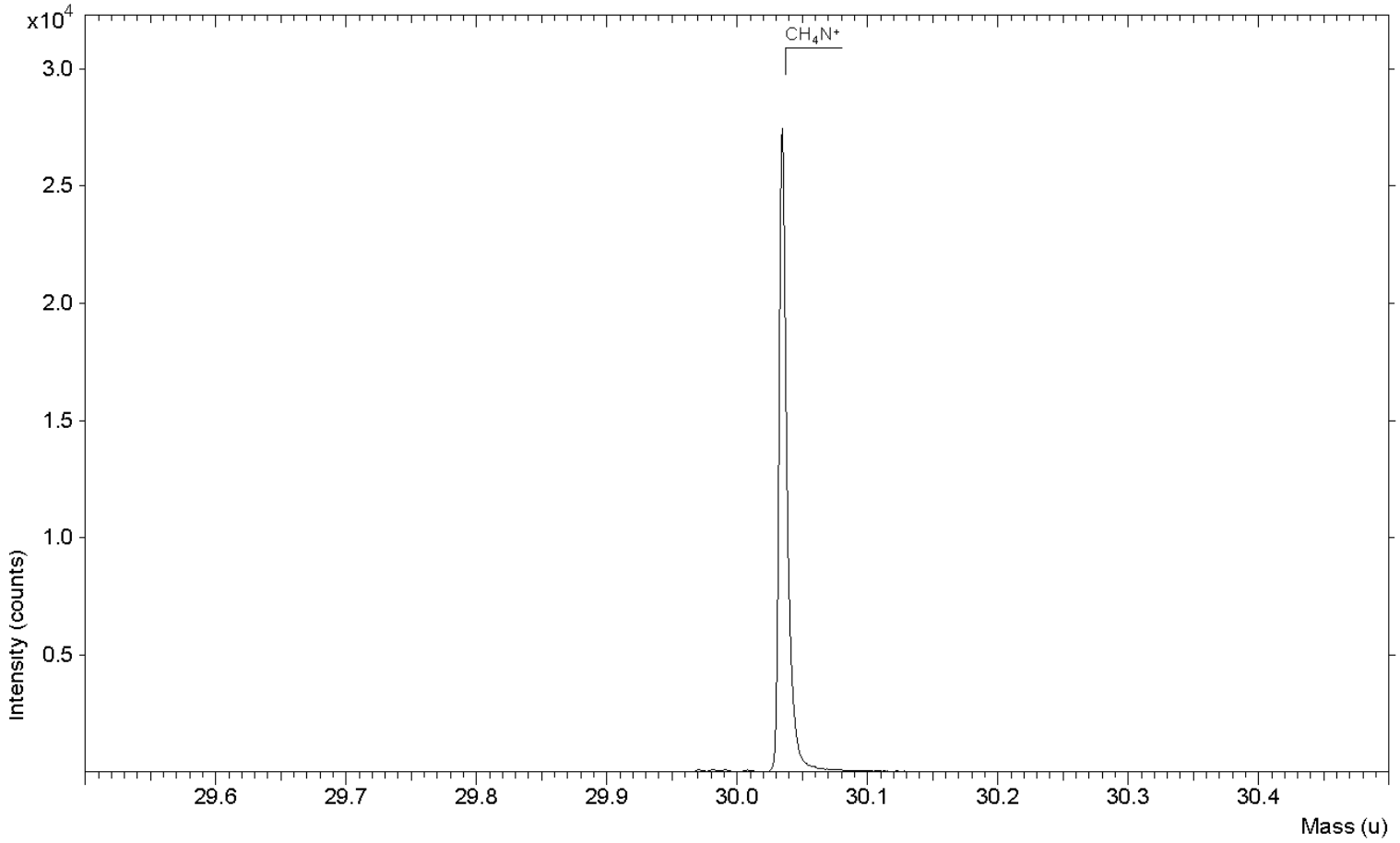


Figure 79 Time of Flight secondary positive ion mass spectra of CH_4N on the whole are of the cRGDfC modified glass and gold substrates.

The whole area of the substrate has a high CH_4N+ ion intensity indicative of the presence of glycine.

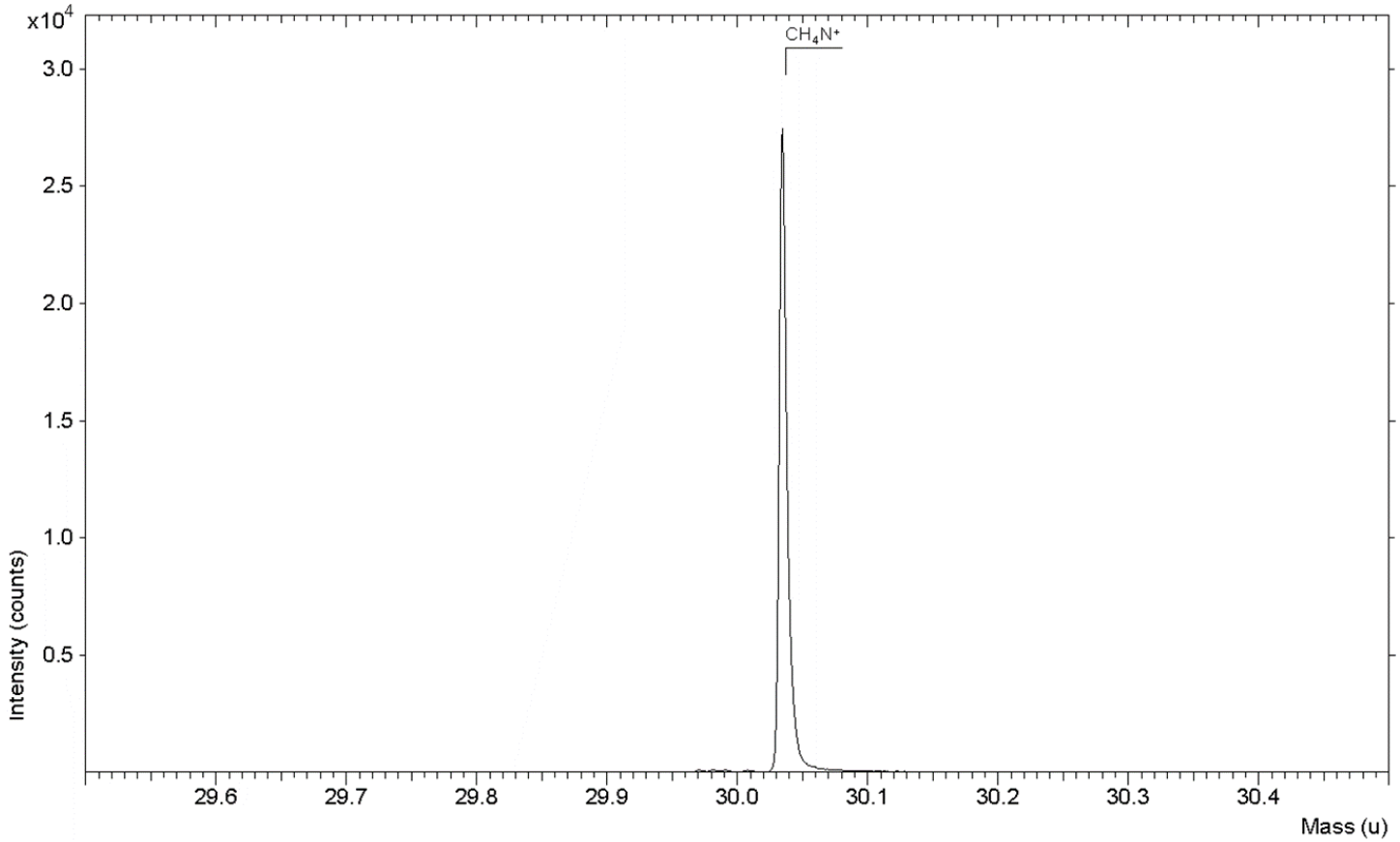


Figure 80 Time of Flight secondary positive ion mass spectra of CH_4N on the gold region of the cRGDfC modified glass and gold substrate.

The gold region of the substrate has a high CH_4N+ ion intensity indicative of the presence of glycine.

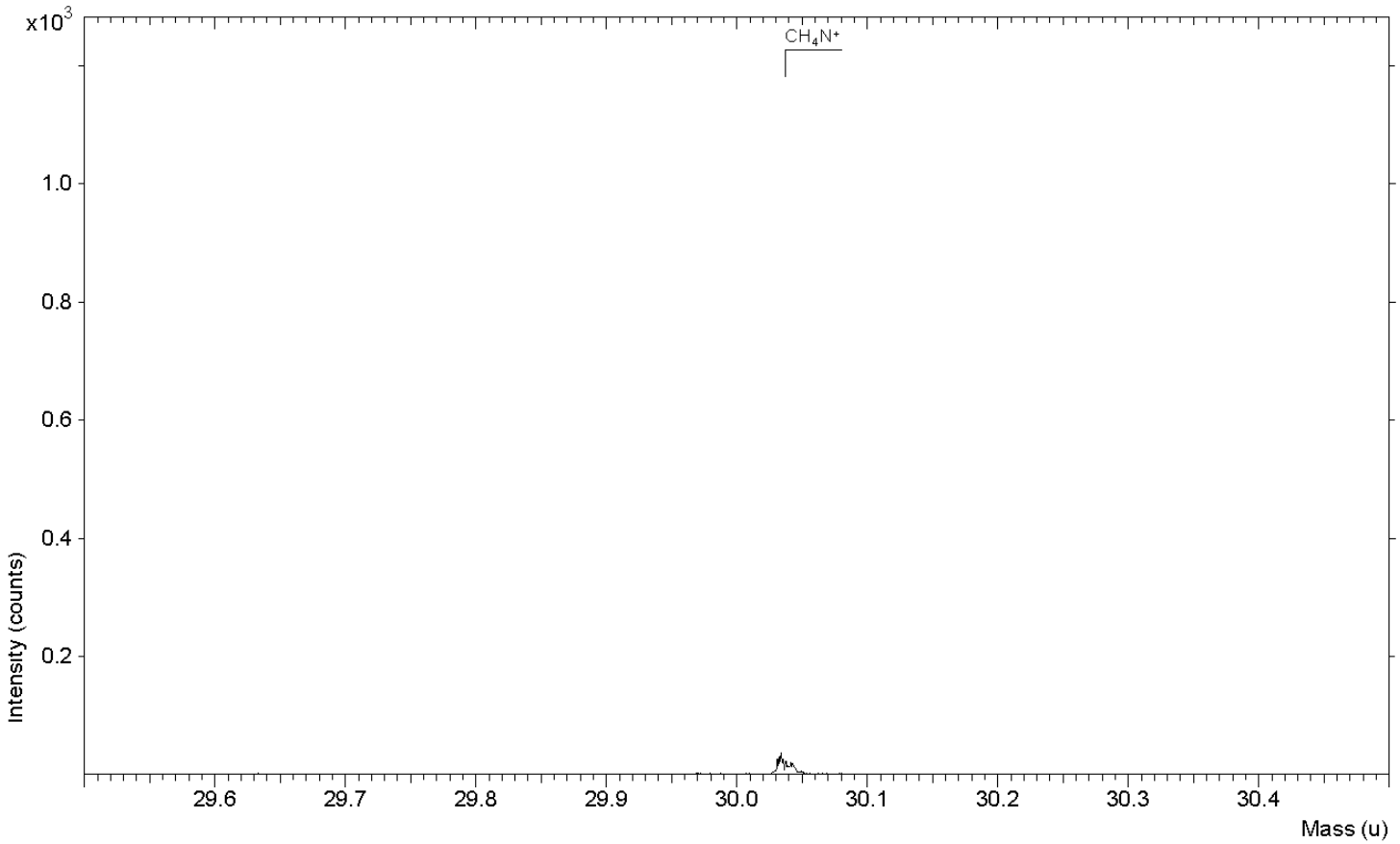


Figure 81 Time of Flight secondary positive ion mass spectra of CH_4N+ on the glass region of the cRGDfC modified glass and gold substrates

The glass region of the substrate has a very low CH_4N+ ion intensity indicative of a lack of glycine.

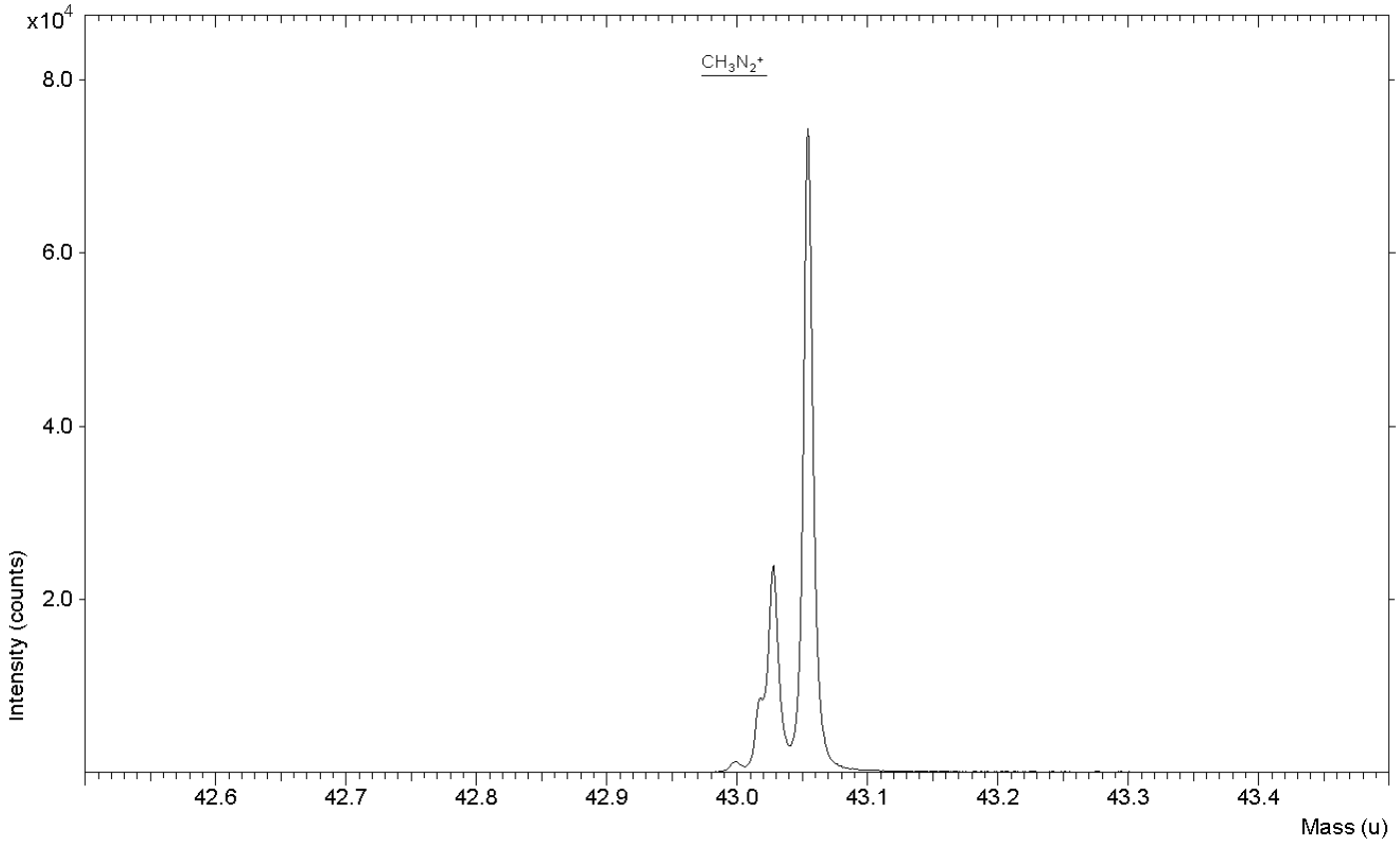


Figure 82 Time of Flight secondary positive ion mass spectra of CH_3N_2+ on the whole area of the cRGDfC modified glass and gold substrates

The whole area of the substrate has a high CH_3N_2+ ion intensity indicative of the presence of arginine.

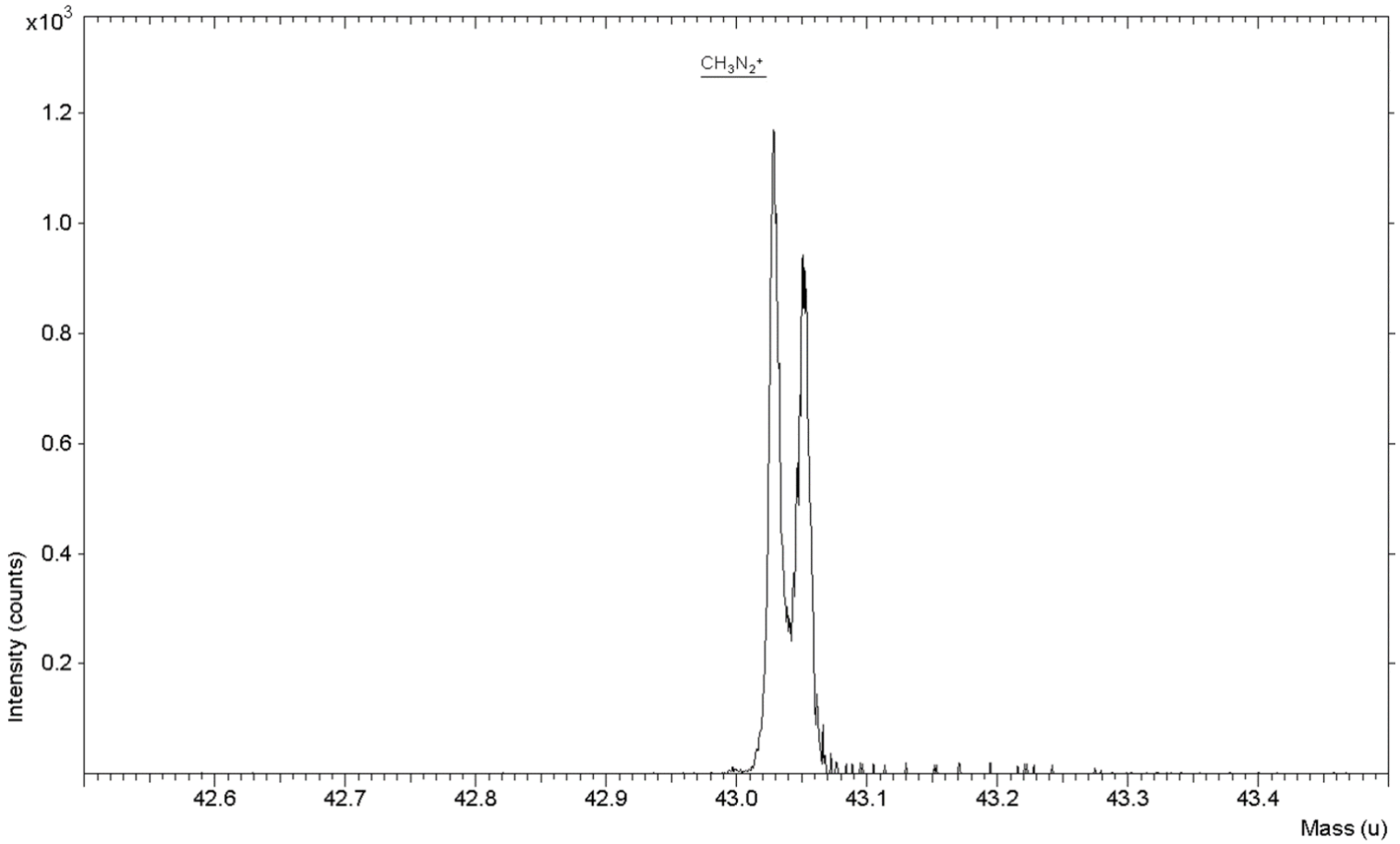


Figure 83 Time of Flight secondary positive ion mass spectra of CH_3N_2+ on the whole area of the cRGDfC modified glass and gold substrates

The gold region of the substrate has a high CH_3N_2+ ion intensity indicative of the presence of arginine.

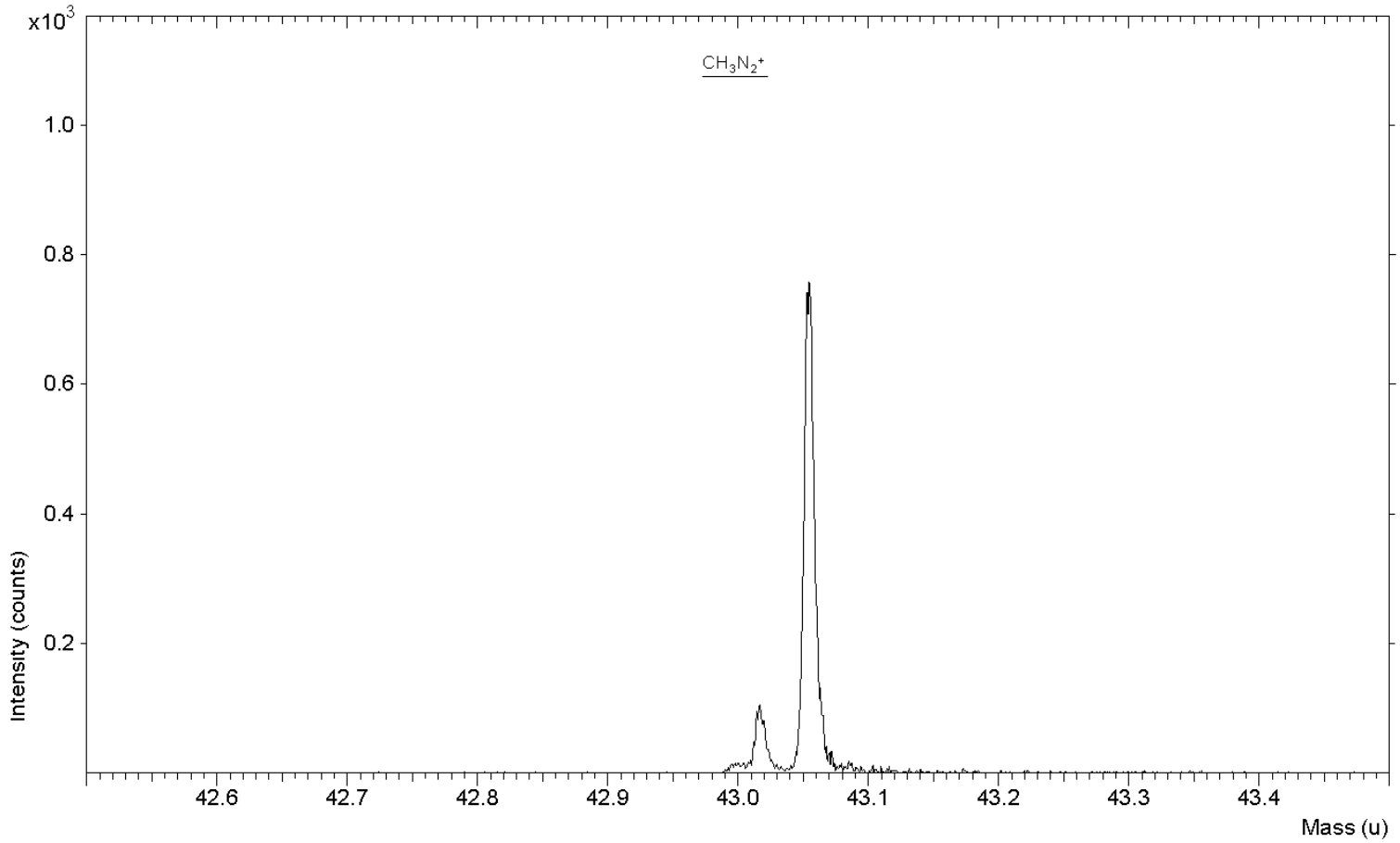


Figure 84 Time of Flight secondary positive ion mass spectra of CH_4N+ on the glass region of the cRGDfC modified glass and gold substrates

The glass region of the substrate has a low CH_3N_2+ ion intensity indicative of the lack of arginine.

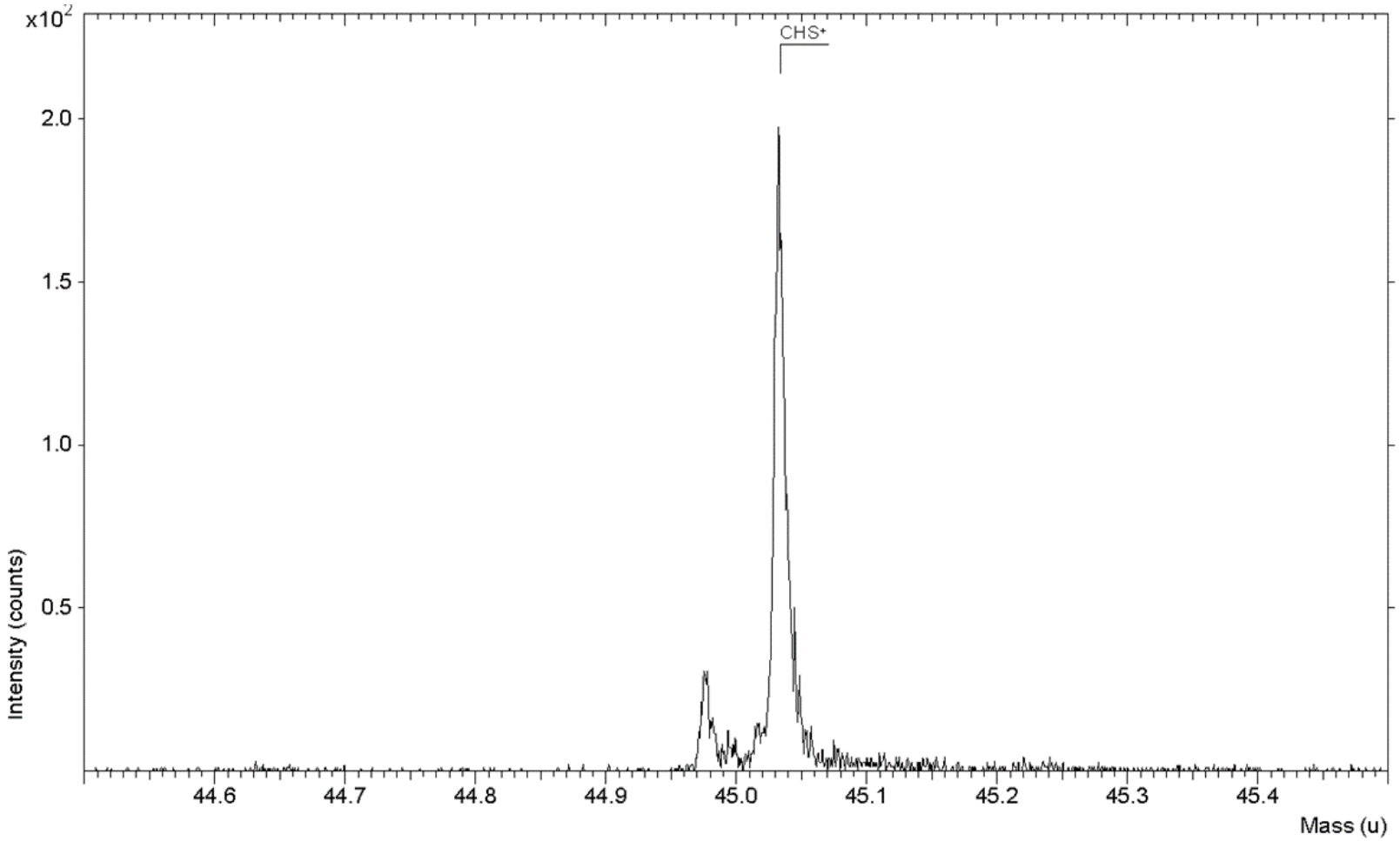


Figure 85 Time of Flight secondary positive ion mass spectra of CHS+ on the gold region of the cRGDfC modified glass and gold substrates

The whole area of the substrate has a high CHS+ ion intensity indicative of the presence of cysteine.

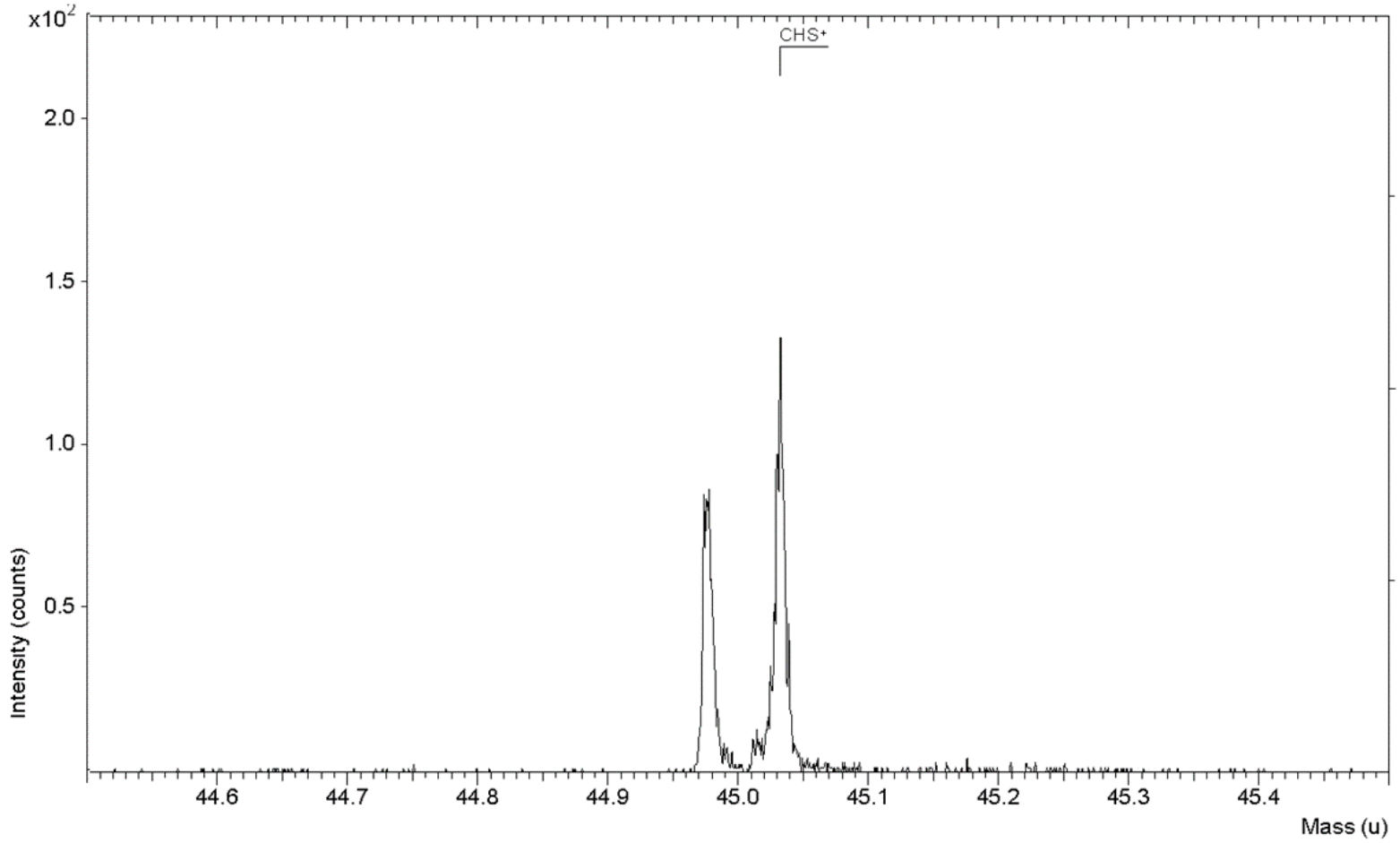


Figure 86 Time of Flight secondary positive ion mass spectra of CHS+ on the glass region of the cRGDfC modified glass and gold substrates

The gold region of the substrate has a high CHS+ ion intensity indicative of the presence of cysteine.

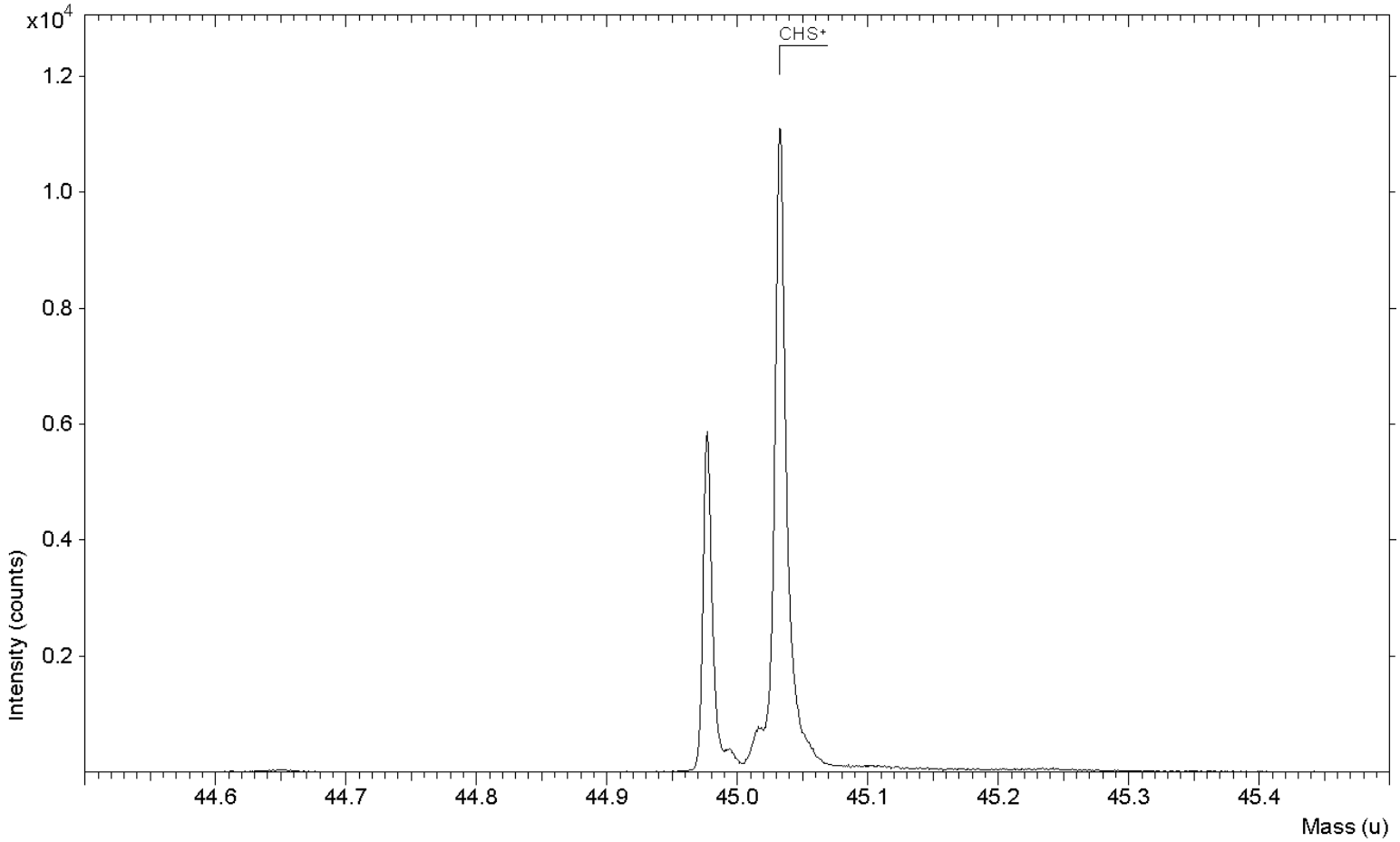


Figure 87 Time of Flight secondary positive ion mass spectra of CHS+ on the whole area of the cRGDfC modified glass and gold substrates.

The glass region of the substrate has a low CHS+ ion intensity indicative of a lack of cysteine.

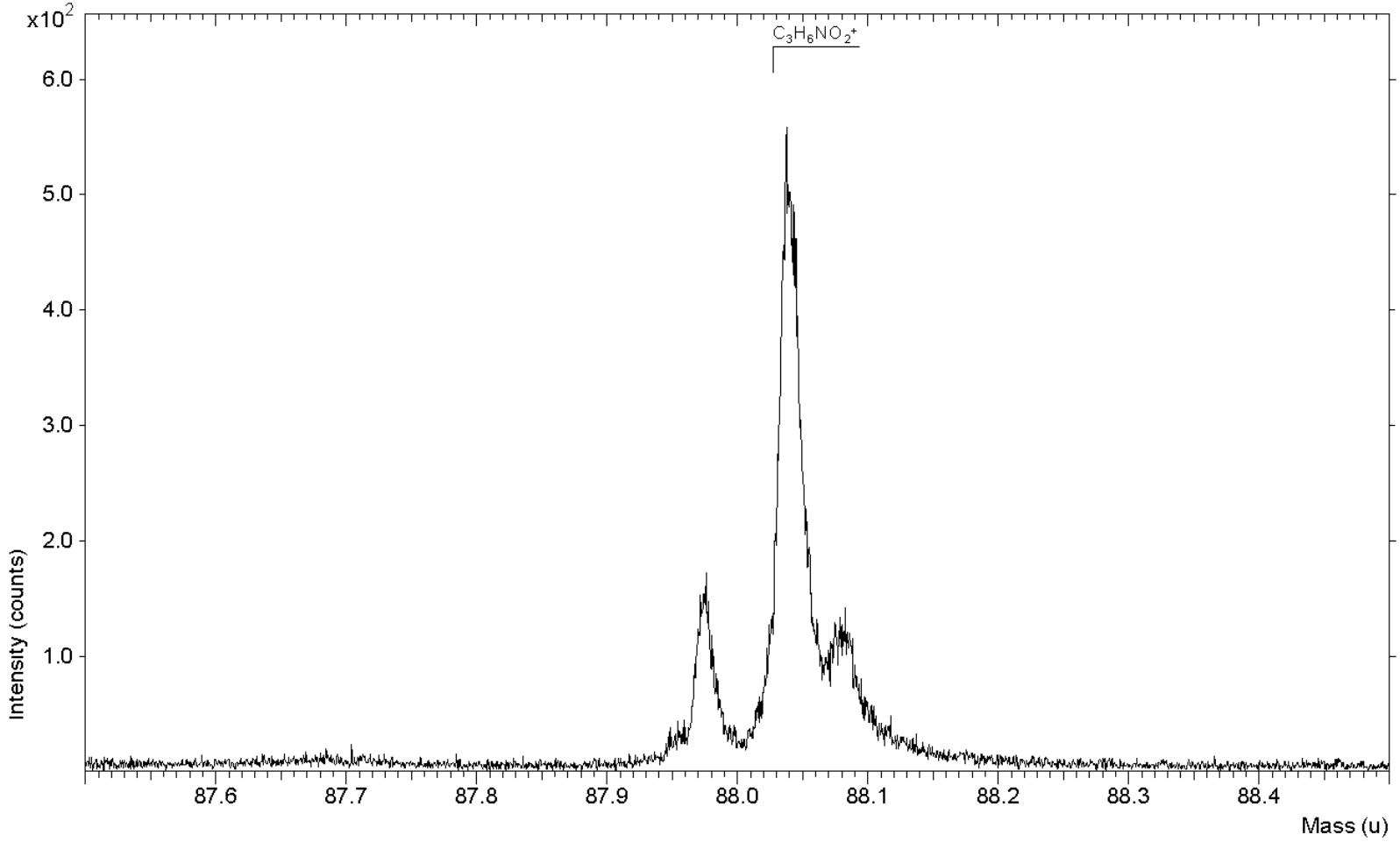


Figure 88 Time of Flight secondary positive ion mass spectra of $C_3H_6NO_2$+ on the whole area of the cRGDfC modified glass and gold substrates

The whole area of the substrate has a high $C_3H_6NO_2$+ ion intensity indicative of the presence of aspartate.

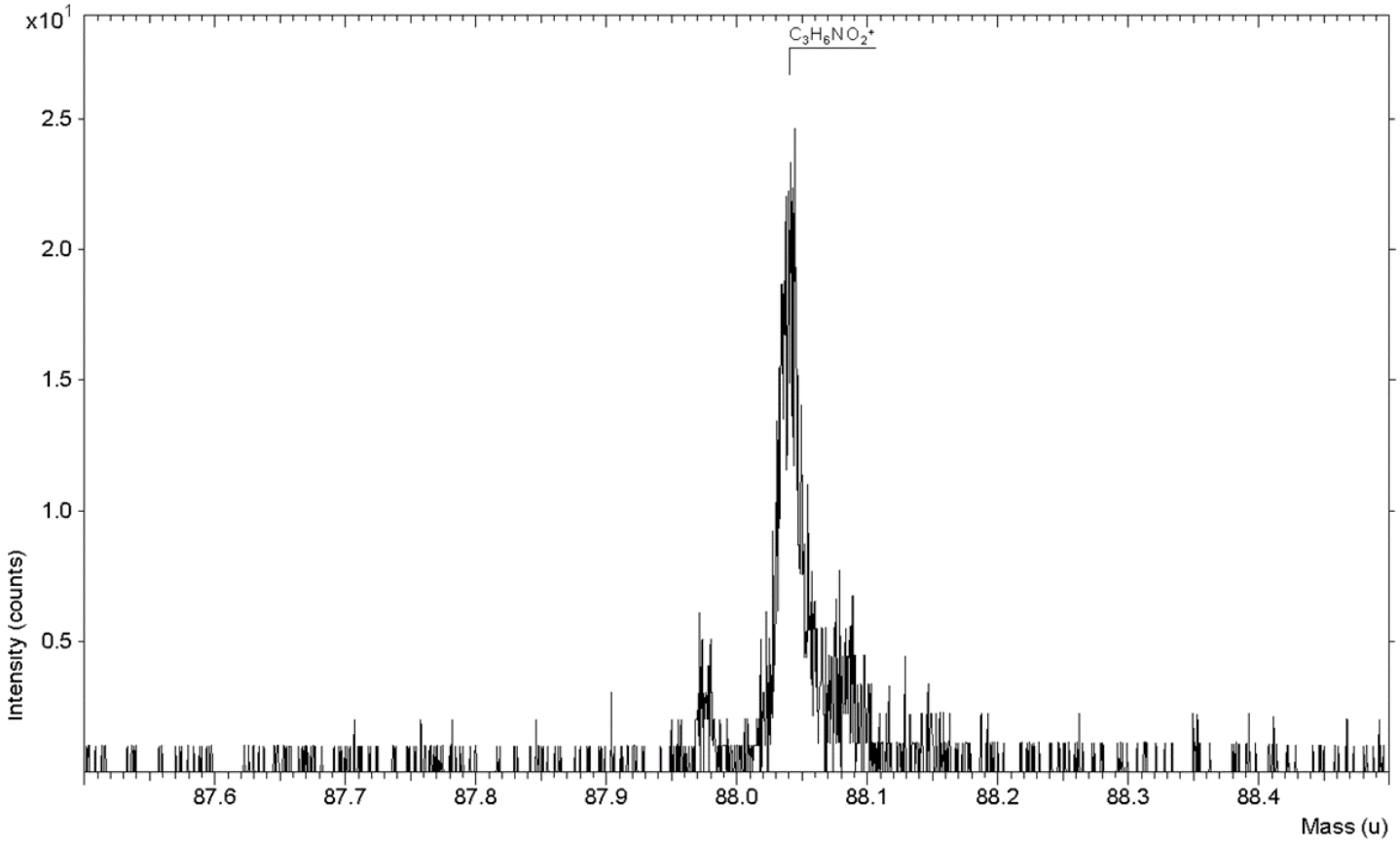


Figure 89 Time of Flight secondary positive ion mass spectra of $C_3H_6NO_2$+ on the gold region of the cRGDfC modified glass and gold substrates

The gold region of the substrate has a high $C_3H_6NO_2$+ ion intensity indicative of the presence of aspartate.

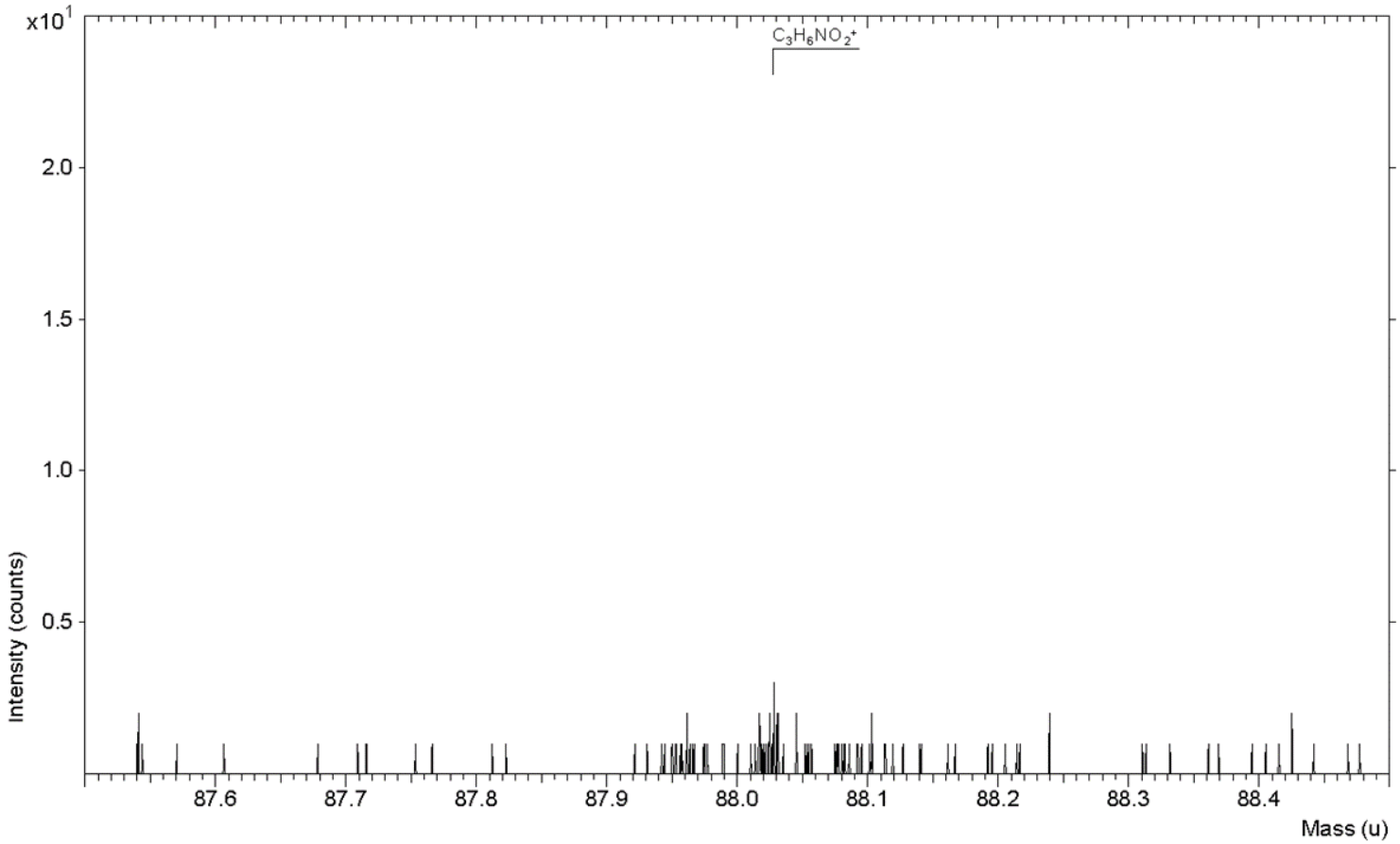


Figure 90 Time of Flight secondary positive ion mass spectra of $C_3H_6NO_2$+ on the glass region of the cRGDfC modified glass and gold substrates

The glass region of the substrate has a high $C_3H_6NO_2$+ ion intensity indicative of a lack of aspartate.

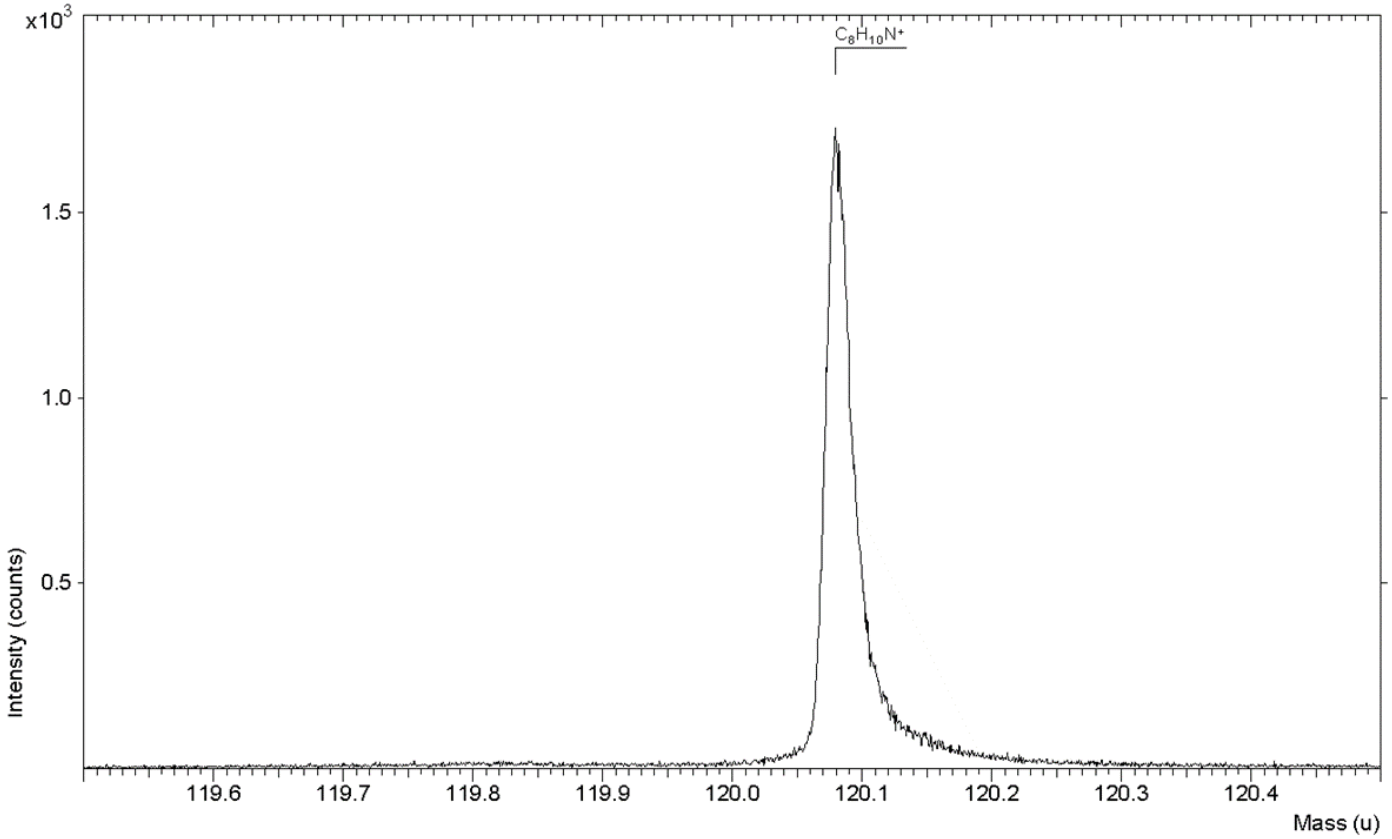


Figure 91 Time of Flight secondary positive ion mass spectra of $C_8H_{10}N^+$ on the whole area of the cRGDfC modified glass and gold substrates

The whole area of the substrate has a high $C_8H_{10}N^+$ ion intensity indicative of the presence of phenylalalnine.

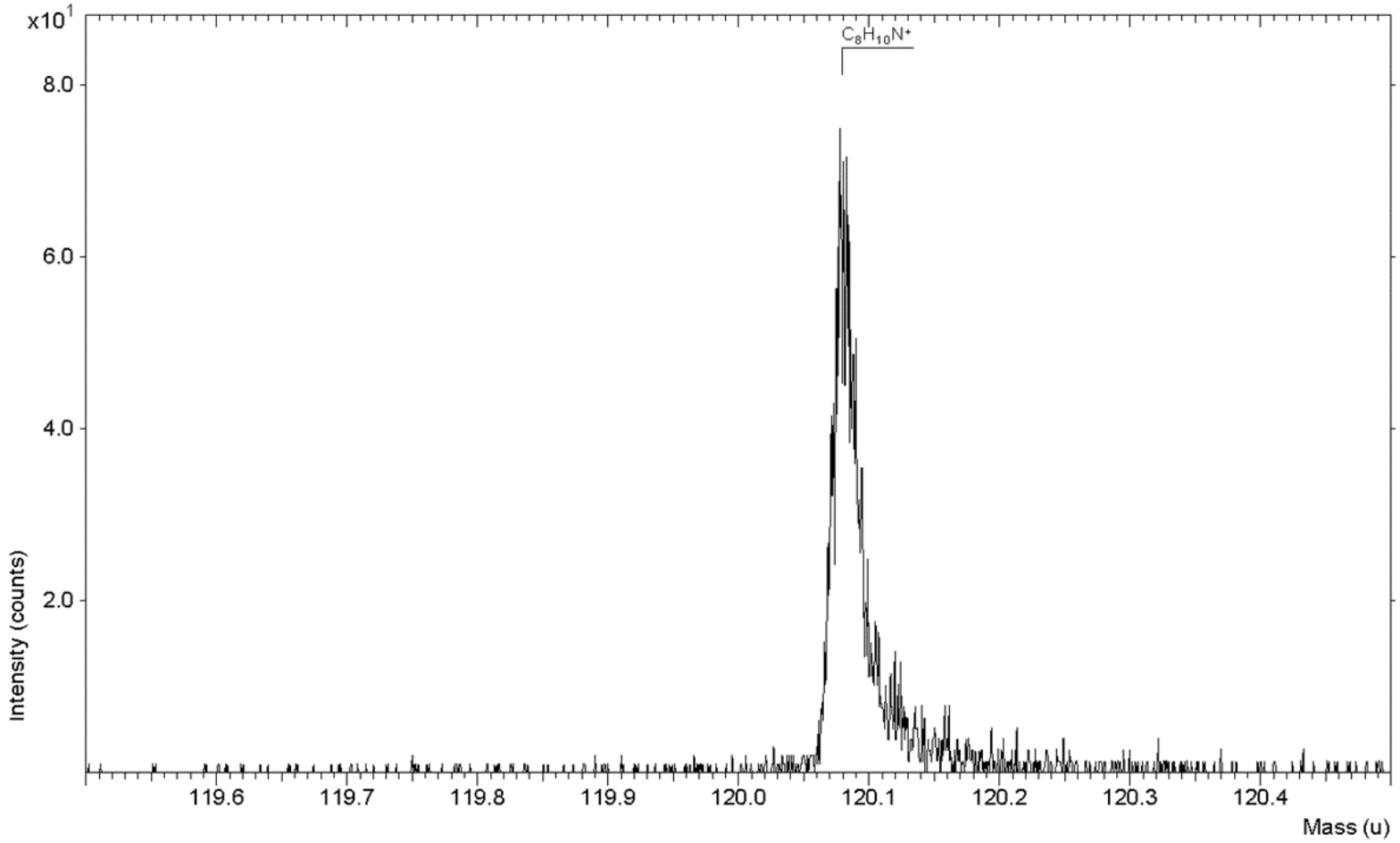


Figure 92 Time of Flight secondary positive ion mass spectra of $C_8H_{10}N+$ on the gold region of the cRGDfC modified glass and gold substrates

The gold region of the substrate has a high $C_8H_{10}N+$ ion intensity indicative of the presence of phenylalanine.

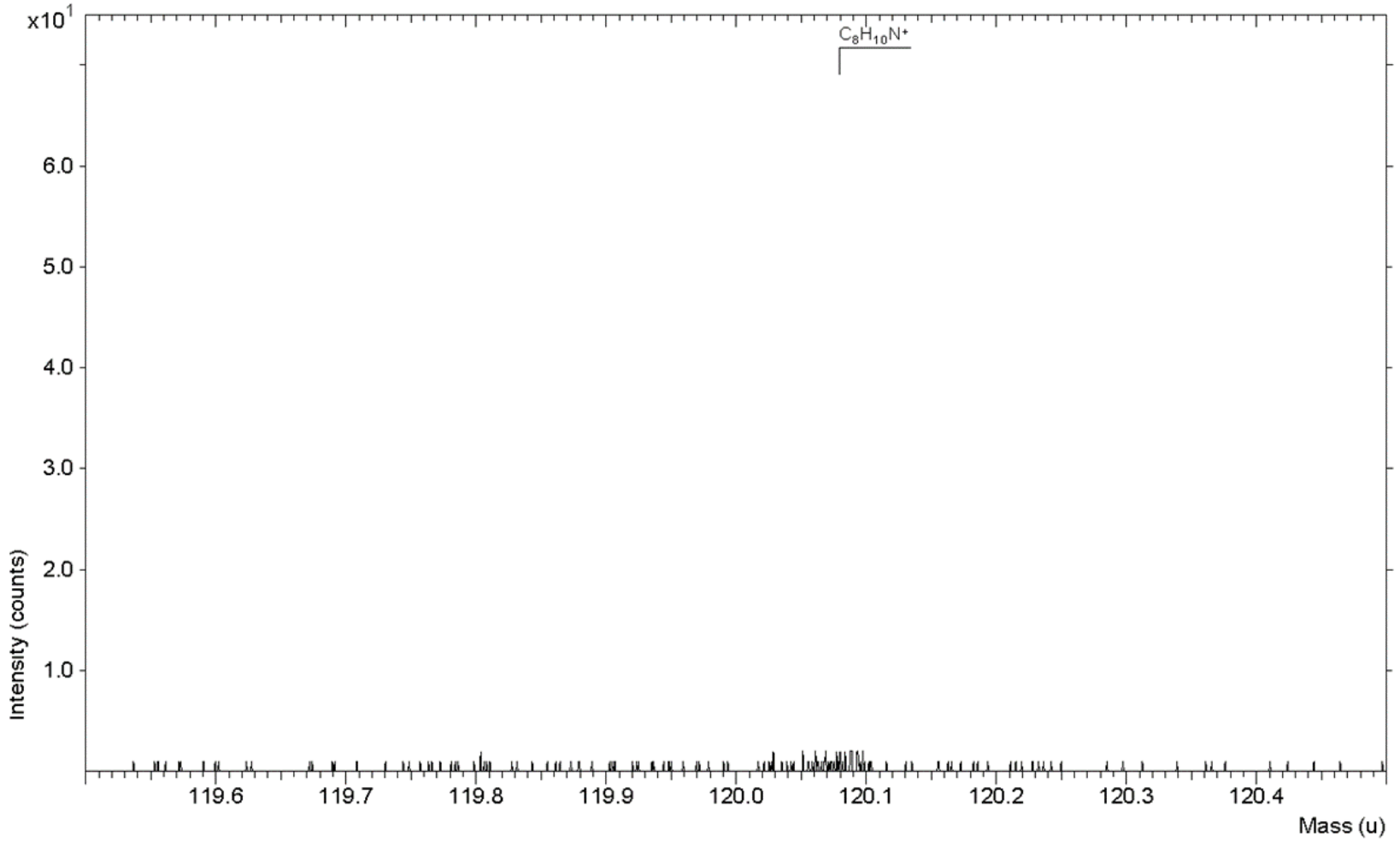


Figure 93 Time of Flight secondary positive ion mass spectra of $C_8H_{10}N+$ on the glass region of the cRGDfC modified glass and gold substrates

The glass region of the substrate has a low $C_8H_{10}N+$ ion intensity indicative of a lack of phenylalalnine.

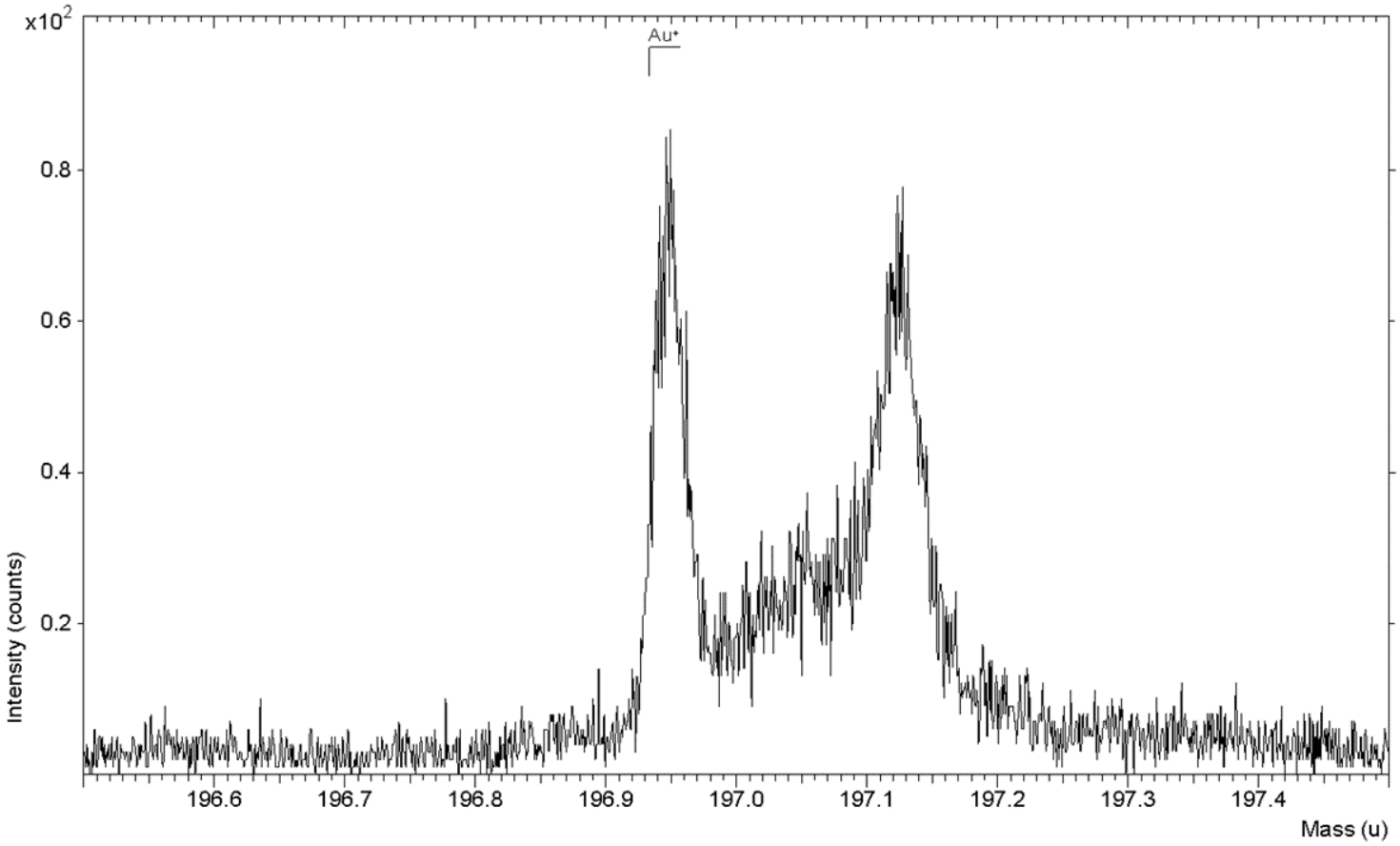


Figure 94 Time of Flight secondary positive ion mass spectra of Au+ on the whole area of the cRGDfC modified glass and gold substrates

The whole area of the substrate has a high Au+ ion intensity indicative of the presence of gold on the substrate.

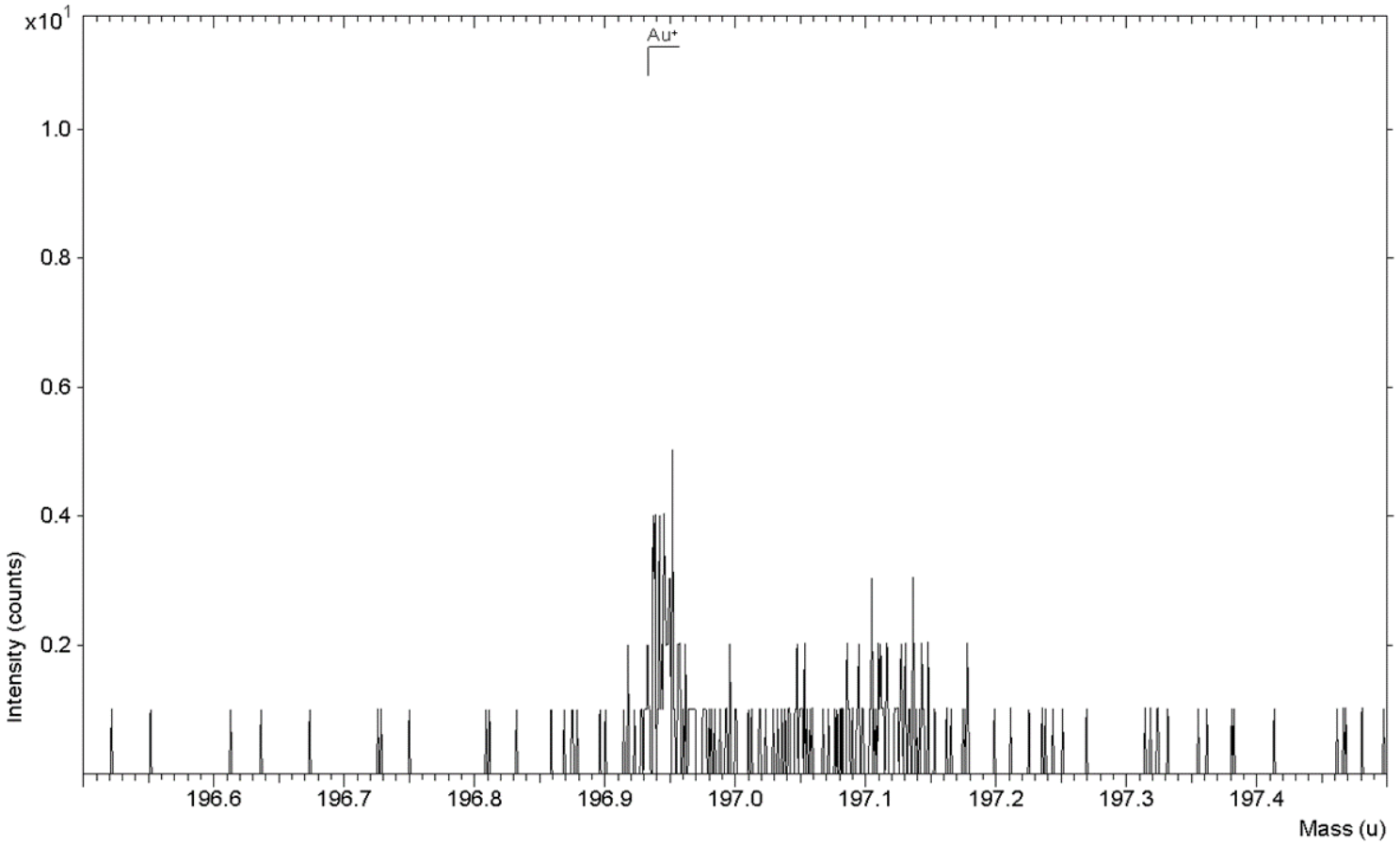


Figure 95 Time of Flight secondary positive ion mass spectra of Au+ on the gold region of the cRGDfC modified glass and gold substrates

The gold region of the substrate has a high Au+ ion intensity indicative of the presence of gold on the substrate.

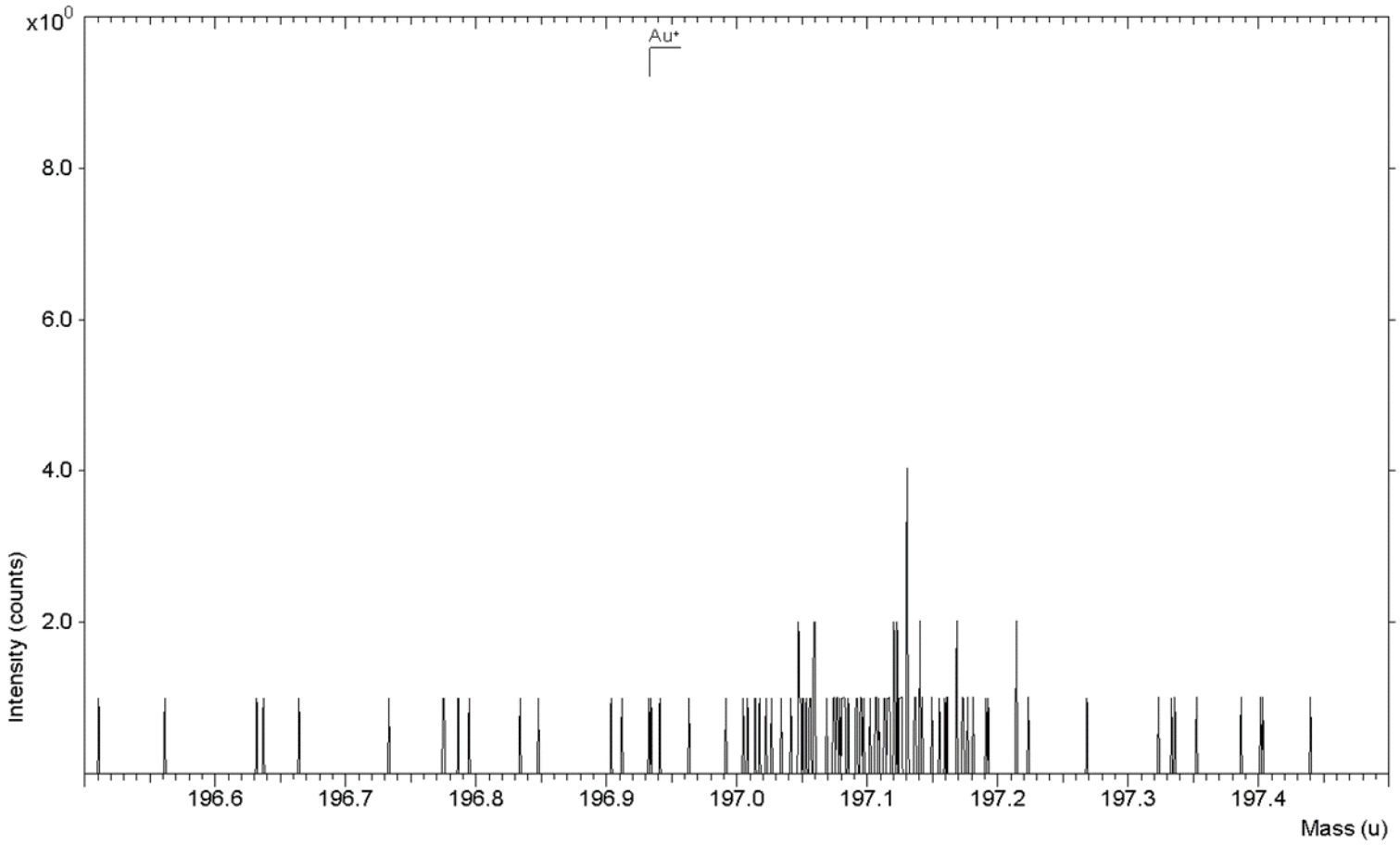


Figure 96 Time of Flight secondary positive ion mass spectra of Au+ on the glass region of the cRGDfC modified glass and gold substrates

The glass region of the substrate has a low Au+ ion intensity indicative of a lack of gold on the glass region.